Universidad de Granada

DEPARTAMENTO DE MINERALOGÍA Y PETROLOGÍA

DESIGN OF READY-TO-USE RENDERING MORTARS FOR USE IN RESTORATION WORK

Tesis Doctoral – PhD thesis –

Anna Arizzi

Abril 2012

Editor: Editorial de la Universidad de Granada
Autor: Anna Arizzi
D.L.: GR 2248-2012
ISBN: 978-84-9028-132-1

DEPARTAMENTO DE MINERALOGÍA Y PETROLOGÍA

Giuseppe Cultrone, Profesor Titular de Universidad, adscrito al Departamento de Mineralogía y Petrología, hace constar:

Que la presente memoria titulada: "DESIGN OF READY-TO-USE RENDERING MORTARS FOR USE IN RESTORATION WORK" ha sido realizada bajo su dirección por la doctoranda Dña. Anna Arizzi y cumple los requisitos necesarios para que su autora pueda optar al grado de Doctora por la Universidad de Granada.

Fdo. Anna Arizzi

VºBº del Director

Fdo. Prof. Giuseppe Cultrone

“L’arte rinnova i popoli e ne rivela la vita...”
(Palermo, frontone del Teatro Massimo)

Agradecimientos

En primer lugar deseo agradecer a mi director de Tesis, el Dr. Giuseppe Cultrone, por la oportunidad que me brindó para poder realizar esta investigación y por su inestimable ayuda, confianza, disponibilidad y apoyo a lo largo de estos años. Sobre todo, le agradezco su trato humano y su interés constante en mi formación científica. *Grazie infinite*.

Agradezco al Departamento de Mineralogía y Petrología por acogerme física y personalmente; en especial a su director, Dr. Miguel Ortega Huertas, por su disponibilidad e interés.

De igual modo, agradezco a todos los profesores del Departamento, en particular al Dr. Eduardo Sebastián Pardo por guiar mis primeros pasos en la investigación de los morteros y por el afecto demostrado, al Dr. Carlos Rodríguez Navarro por su siempre asequible ayuda científica y a la Dra. Carolina Cardell por su amabilidad.

Al programa de Doctorado de Ciencias de la Tierra, en especial a su coordinador, el Dr. Antonio García Casco por su ayuda y dedicación a los estudiantes de Doctorado.

El trabajo descrito en esta Tesis no hubiera sido posible sin la ayuda y el material proporcionado por la empresa ARGOS Derivados del cemento, Prealpa S.L. (Padul, Granada). Deseo agradecer a todo equipo del laboratorio por acogerme como una más entre ellos; en especial, a Eugenio Navarro Torres, por su inestimable ayuda a lo largo de estos años, a Ruben, porque sin él no hubiera podido aplicar mis morteros, a Julio, por sus consejos prácticos y a Miriam, por su amabilidad.

También agradezco al Prof. David Benavente, del departamento de Ciencias de la Tierra y del Medio Ambiente de la Universidad de Alicante, por darme la oportunidad de trabajar esporádicamente en sus laboratorios. Gracias y mil gracias al Dr. Javier Martínez Martínez, por el esfuerzo que ha hecho para entender el maravilloso y a la vez misterioso mundo de los morteros, pero sobre todo por su amistad y afecto.

Gracias a Angela Tate, por la revisión del inglés de este manuscrito.

I would like to thank Prof. Koenraad Van Balen and Prof. Heather Viles, for their hospitality during my two stages at the Catholic University of Leuven and the University of Oxford, respectively. Thanks for giving me the opportunity to work for a short time under your supervision. I would also thank Dr. Roel Hendrickx and Dr. Mona Edwards for their help during my stages at their labs.

A mis compañeros del grupo de "Monumentos": Encarni, por su compañerismo y ayuda científica; Eduardo, por soportar y solucionar mis problemas a diario; Julia, por compartir algo más que el despacho. Gracias, sobre todo, a las personas que ya no forman parte de este grupo: Ana, por ser una persona auténtica y una amiga siempre presente y Maja, por su amistad y por las risas que hemos compartido.

A todo el personal de administración y servicio, en particular Inés, Sandra, Noelia y Jesús, por atenderme siempre con una sonrisa.

A todos mis amigos becarios y doctores, con los que he vivido momentos llenos de alegría y compañerismo dentro y fuera de la Facultad, en particular a Claudio, por su amistad y afecto, Iñaki, por su predisposición a ayudar, a Pedro, mi compañero de Tesis, siempre allí para escucharme y animarme, y a mis compañeros del Máster, en especial a Sandra, por las cervezitas de los jueves. Gracias a todos ellos, la realización de esta Tesis ha sido más fácil.

Grazie mille al Prof. Maurizio Triscari dell'Università di Messina, per la stima avuta nei miei confronti.

Je voudrais remercier mes amis français, Mathieu, Priscille et Sébastien pour son amitié pendant et après mon stage à l'ISTO, avant de commencer cette Thèse. Je n'oublie pas mes premiers pas comme chercheuse avec vous.

Grazie a Claudia, Ambra ed Elvira, le mie amiche di sempre che, da lontano, hanno saputo come starmi vicino. Un affettuoso pensiero va anche a tutte le mie compagnette della "Giovane Ensemble" ed alle mie colleghe, per meglio dire amiche, Catia, Donatella e Letizia. Se sono arrivata fin qui è anche grazie al vostro continuo incoraggiamento.

A Borja, por estar allí, darme confianza y animarme cada vez que me he venido abajo. Gracias por tu comprensión y por hacer que me sienta la mejor.

Mil gracias también a la familia Arias Santiago, por los detalles que siempre tenéis conmigo y por vuestro afecto.

Infine, il più grande e sentito ringraziamento va alla mia famiglia.

Ai miei genitori, perchè la comprensione e l'affetto smisurato che mi dimostrate fanno che io sia una persona migliore.

Ai miei fratelli, per l'amore che mi date senza chiedere niente in cambio.

Alle mie dolcissime cognate e ai miei adorati nipoti, perchè avete fatto della nostra famiglia la perfezione.

Senza l'appoggio di tutti voi non sarei mai potuta arrivare fin qui. GRAZIE!

Contents

List of symbols and abbreviations

Analytical Techniques

EDX, energy dispersive X-ray analysis
ESEM, environmental scanning electron microscopy
FESEM, field emission scanning electron microscopy
HRTEM and **TEM**, high resolution transmission electron microscopy
MIP, mercury intrusion porosimetry
OM, polarized optical microscopy
SAED, selected area electron diffraction
TGA, thermogravimetric analysis
XRD, X-ray diffraction
XRF, X-ray fluorescence

Compounds and Minerals

Al_2O_3, alumina
CAĈH, ($Ca_4Al_2(CO_3)(OH)_{12} \cdot 6H_2O$), calcium alumina carbonate hydrate, or *monocarboaluminate*
CAH, ($CaO\text{-}Al_2O_3\text{-}H_2O$), calcium aluminate hydrate
Ca^{2+}, calcium ion
CaO, calcium oxide, lime
CASH, ($CaO\text{-}Al_2O_3\text{-}SiO_2\text{-}H_2O$), calcium alumina silicate hydrate
CC, ($CaCO_3$), calcite
CH, ($Ca(OH)_2$), calcium hydroxide, portlandite
Cl^-, chloride ion
CO, carbon monoxide
CO_2, carbon dioxide
CS_2, ($2CaO\cdot SiO_2$), di-calcium silicate (*belite*)
CS_3, ($3CaO\cdot SiO_2$), tri-calcium silicate (*alite*)
CSH, ($CaO\text{-}SiO_2\text{-}H_2O$), calcium silicate hydrate
Gyp, ($CaSO_4\cdot H_2O$), calcium sulphate hydrate, gypsum
Et, ($Ca_6Al_2(SO_4)_3(OH)_{12}\cdot 26H_2O$), ettringite
Fe_2O_3, iron oxide
KBr, potassium bromide
MgO, magnesium oxide, periclase
$Mg_5(CO_3)_4(OH)_2\cdot 4H_2O$, hydromagnesite
$Mg(OH)_2$, magnesium hydroxide, brucite
Na^+, sodium ion
Na_2SO_4, sodium sulphate decahydrate, thenardite
$Na_2SO_4\cdot 10H_2O$, sodium sulphate, mirabilite
NO_2, nitrogen dioxide
PM_1 and **PM_{10},** particulate matter
Qtz, quartz
SiO_2, silica

SO_2, sulphure oxide
SO_4^{2-}, sulphate ion
TiO_2, titanium oxide

General abbreviations and parameters

α_s, spatial attenuation of ultrasonic primary wave
A, imbibition coefficient from the mass uptake per surface unit
A_e, maximum amplitude emitted by the transmitter sensor
A_{mx}, maximum amplitude registered by the receptor sensor
B, imbibition coefficient determined from the height of the capillary front
B/A, binder-to-aggregate ratio
c, ultrasonic wave velocity
c_{11}, c_{44}, independent elastic constants of the elastic constant tensor (C) in isotropic media
C_a, absorption coefficient
C_{shr}, shrinkage coefficient
CP, cumulative percent (Fuller' and Bolomey's models)
CPFT, cumulative percent finer than (Dinger's model)
CR, controlled rate
CS, controlled stress
d, particle length
ε, porosity of a wet mixture
E, Young modulus
-ex, external sample
φ, packing density
φ_{dry}, packing density of the dry components
φ_{max} or φ_m, maximum solid concentration
f, empirical constant of Bolomey's model
$\dot{\gamma}$, shear rate
G, rigidity modulus
H, mineral hardness
I_{CD}, carbonation degree index
I_d, drying index
-in, internal sample
ITZ, interfacial transition zone
K, volume (or compressive) modulus
K_h, coefficient of permeability to water liquid, or hydraulic conductivity
K_v, coefficient of permeability to water vapour
n, fineness or distribution modulus
η, viscosity
[η], intrinsic viscosity
l, particle thickness
μ_e, electrophoretic mobility
ν, Poisson's coefficient
v_p^m, propagation velocities within the matrix

v_p^a, propagation velocities within the aggregate
Ω, angular velocity
π, porosity of dry granular component or mixture
P or **p,** primary waves
P_o, open porosity
PSD, pore size distribution
ρ, density
ρ_b, bulk density
ρ_b^*, bulk density after compaction
ρ_s or **ρ,** solid density
ρ_w, water density
r, pore radius
R, reflection coefficient
R_c, compressive resistance
RCP, random close packing fraction
R_f, flexural resistance
RH, relative humidity
RLP, random loose packing fraction
r_p, aspect ratio
S or **s,** secondary wave
SSA, specific surface area
T, temperature
u, voids index
u_w, volumetric water content
$u_{w\ min}$, minimal water content
v_p and **V_p,** propagation velocity of ultrasonic primary wave
v_s and **V_s,** propagation velocity of ultrasonic secondary wave
W/B, water-to-binder ratio
w/c, water-to-cement ratio
WPM, wet packing method
W/T, water content on the total mass of the mix
χ^m, relative volumes of sample matrix
χ^a, relative volumes of sample aggregate
Z, acoustic impedance
ø, diameter of the aggregate grains

Mortar components and names

CL, calcitic dry-hydrated lime
DL, dolomitic dry-hydrated lime
CA, calcareous aggregate with continuous grading
CDA, calcareous aggregate with discontinuous grading
SA, siliceous aggregate with discontinuous grading
WPC, white Portland cement
MK, metakaolin
P, perlite

C, cellulose derivative
R, polycarboxylate
CC, mortar with calcitic lime and calcareous aggregate with continuous grading
CD, mortar with calcitic lime and calcareous aggregate with discontinuous grading
CS, mortar with calcitic lime and siliceous aggregate with discontinuous grading
DC, mortar with dolomitic lime and calcareous aggregate with continuous grading
DS, mortar with dolomitic lime and siliceous aggregate with discontinuous grading
CPC, mortar with calcitic lime, white Portland cement and calcareous aggregate with continuous grading
CCM, mortar with calcitic lime, metakaolin and calcareous aggregate with continuous grading
CCMP, mortar with calcitic lime, metakaolin, calcareous aggregate with continuous grading and perlite
CCMPC, mortar with calcitic lime, metakaolin, calcareous aggregate with continuous grading, perlite and cellulose derivative
CCMPCR and M, mortar with calcitic lime, metakaolin, calcareous aggregate with continuous grading, perlite, cellulose derivative and polycarboxylate

DISEÑO DE MORTEROS DE REVESTIMIENTO PRE-DOSIFICADOS PARA SU APLICACIÓN EN OBRAS DE RESTAURACIÓN

Resumen

Desde el descubrimiento del cemento Portland, hace casi dos siglos, la producción industrial de morteros llevó a entusiasmar a tal punto a arquitectos e ingenieros que el cemento Portland remplazó los morteros tradicionales en la totalidad de las nuevas construcciones. Lamentablemente, esto ocurrió también en los edificios históricos, donde el cemento fue usado irracionalmente como material de restauración. La incompatibilidad del cemento con los materiales de construcción tradicionales ha causado la aceleración de los procesos de deterioro, con daños finales irreversibles en nuestro Patrimonio Arquitectónico y Artístico. Hoy en día los profesionales están demostrando un renovado interés hacia el uso de morteros tradicionales, especialmente en base cal, ya que estos aseguran compatibilidad, adaptabilidad y longevidad. Sin embargo, las técnicas de producción adoptadas en el pasado no se pueden recuperar en la época moderna, ya que hay que tener en cuenta otros requisitos, como tiempos y costes de producción.

Esta Tesis doctoral quiere contribuir a la conservación del Patrimonio Arquitectónico, proporcionando una base para el diseño de nuevos morteros de restauración para revestimientos que se puedan producir y comercializar a nivel industrial. Con este fin, los componentes de los morteros y los métodos de preparación se han seleccionado teniendo en cuenta tanto los requisitos de la restauración, como los de la industria.

Muchas de las técnicas analíticas más empleadas para la caracterización de los morteros se han usado en esta Tesis doctoral:

- Los componentes y morteros se han caracterizado mediante técnicas químicas (fluorescencia de rayos X; cromatografía de iones) y mineralógicas (difracción de rayos X; termogravimetría) y su textura y microestructura se han estudiado mediante microscopía óptica y electrónica de barrido y trasmisión.

- Las propiedades de los morteros en estado fresco se han evaluado mediante métodos estándar (ensayo de consistencia) y no-estándar ("wet packing method"). Además, distintos aparatos reológicos se han usado para caracterizar el comportamiento de las cales hidratadas en suspensión, que está relacionado con la trabajabilidad del mortero.

- Las propiedades físico-mecánicas de los morteros en estado de endurecimiento se han determinado mediante ensayos hídricos (absorción libre de agua y secado; imbibición capilar; conductividad hidráulica; permeabilidad al vapor de agua) y mecánicos. Además, algunas técnicas físico-mecánicas no destructivas y parcialmente destructivas, tales como ultrasonidos y una prensa micro-mecánica, se han utilizado con éxito para la caracterización textural de los morteros.

- Se han diseñado nuevos ensayos de laboratorio para el estudio de la durabilidad de los morteros y de los mecanismos de deterioro inducidos por variaciones de temperatura y humedad, lluvia, ciclos de hielo-deshielo y ataque por sales.

Los componentes iniciales elegidos para esta Tesis han sido: dos cales hidratadas de composición calcítica y dolomítica, dos áridos calcítico y silíceo, dos componentes hidráulicos usados como aditivos y tres adiciones. Las condiciones de curado de baja humedad a las que se han expuesto los morteros durante el estudio han sido decisivas en la selección de los componentes y las dosificaciones finales, tal y como se indica a continuación:

- Las cales calcítica y dolomítica presentan una microestructura muy diferente que influye en su comportamiento en suspensión y, consecuentemente, en la trabajabilidad final de la pasta de mortero, que es mayor cuando se utiliza cal dolomítica. Sin embargo, los morteros de cal dolomítica han mostrado una retracción mucho más alta y peores propiedades durante el endurecimiento, con respecto a los de cal calcítica. Por tanto, el uso de la cal dolomítica en esta Tesis se ha descartado.

- El uso de un árido calcítico o silíceo tiene una influencia directa sobre la cantidad de agua de amasado, así como sobre la porosidad abierta, que era más alta en los morteros con árido calcítico. Sin embargo, se ha observado que el árido calcítico induce una mejora en la microestructura y textura de los morteros durante la carbonatación, por lo que se ha elegido el árido calcítico para esta investigación.

- Dos componentes hidráulicos se han añadido a los morteros: cemento blanco Portland y metacaolín. El primero ha resultado ser un componente perjudicial en la durabilidad de los morteros y su uso se ha definitivamente descartado. El ultimo, en cambio, ha mejorado las propiedades físico-mecánicas de los morteros. Sin embargo, los morteros presentaban aún una alta porosidad, por lo que se ha considerado necesario el uso de adiciones para reducir el contenido en agua.

- La perlita ha permitido disminuir la densidad de los morteros y el contenido en agua y, además, ha aumentado su trabajabilidad. El derivado de celulosa ha reducido la cantidad de agua de amasado y mejorado la capacidad de retención de agua de la cal. Finalmente, el plastificante ha aumentado ligeramente el contenido en agua pero ha mejorado sustancialmente la trabajabilidad de los morteros, favoreciendo la dispersión de las partículas y, por tanto, su reactividad.

- Los estudios realizados han destacado también la importancia de la correcta elección de las proporciones aglomerantes-áridos más apropiadas para morteros de restauración para revestimiento.

Esta Tesis doctoral cumple con los objetivos iniciales propuestos, respecto a la selección de los componentes y dosificaciones más adecuados para el diseño de morteros de revestimiento compatibles y durables. Además, esta Tesis proporciona nuevos conocimientos de los métodos de ensayo y líneas guía para la preparación de morteros de cal.

Introducción y objetivos

En el último siglo muchos edificios históricos han sufrido intervenciones de restauración que se han revelado erróneas debido al uso indiscriminado del cemento Pórtland que ha dado lugar, en numerosos casos, a daños irreparables. El cemento es un material de elevada rigidez y baja permeabilidad y, además, contiene sales solubles, lo que lo hace incompatible con los elementos de mampostería tradicionales (Veniale et al., 2003; Callebaut et al., 2001). El resultado de su uso en el Patrimonio Arquitectónico ha sido contraproducente como lo demuestra la aceleración de los procesos de deterioro que se han desarrollado en los edificios históricos donde este material ha sido aplicado.

Según numerosos estudios científicos, el mortero de cal es el que más se aproxima, por sus propiedades, a los materiales tradicionales de construcción, además de ser el más longevo (Maurenbrecher, 2004; Groot et al., 1999; Cowper, 1927), por lo que su empleo en los procesos de sustitución e integración de materiales históricos deteriorados parece, en definitiva, el más idóneo. El uso del mortero de cal presenta numerosas ventajas respecto al del cemento Portland y de sus derivados. Es un material que permite la "transpiración" de la piedra a la que está unido y, por su composición química, no da lugar a la formación de sustancias inestables y dañinas en las obras de construcción. Además, el lento proceso de carbonatación que caracteriza los morteros de cal produce un aumento gradual de las resistencias mecánicas en el tiempo, reduciendo al mínimo los esfuerzos y las tensiones entre los materiales. Su utilización puede constituir incluso un beneficio para el medio ambiente, porque en el proceso de cocción de la cal se necesitan temperaturas más bajas de las que se alcanzan en la producción de cementos, lo que requiere un menor consumo de combustible. También, desde el punto de vista estético los morteros de cal son más compatibles con los materiales originales: su color blanco y la amplia gama de colores y tonalidades que se pueden conseguir con la adición de pigmentos, hacen que se mantenga el aspecto cromático original del monumento (Rattazzi, 2007). Por estas razones, en los últimos diez años se está reconsiderando y revalorizando el uso del mortero de cal. Desafortunadamente, el prolongado abandono de su uso en la construcción ha llevado a un casi total desconocimiento de las técnicas de fabricación tradicionales, lo que hace difícil la recuperación de la calidad de los productos alcanzada en el pasado con la cal, sobre todo por la falta de mano de obra especializada en el uso de materias primas no "cementicias".

En los últimos años el mundo científico está demostrando un renovado interés hacia el estudio de las propiedades y características de los morteros antiguos, para llegar a un mejor conocimiento de las técnicas de fabricación y métodos de aplicación utilizados en el pasado (Elert et al., 2002). Gracias al avance en el estudio de los morteros, el mundo científico ha logrado convencer a la industria de la necesidad de una diferenciación de los materiales en función de su utilización, sobre todo cuando está en

juego la salvaguardia del Patrimonio Histórico y Monumental, fomentando así el interés hacia la producción de otros productos más adecuados y "tradicionales". Por otra parte, en el ámbito de la construcción actual, no sería posible recuperar del todo las viejas metodologías de construcción, ya que éstas resultan muchas veces incompatibles con los requisitos de la industria moderna, entre ellos costes de producción y tiempos de ejecución. Además, no existe una normativa referida a la fabricación de morteros de cal sino que se debe hacer referencia a normas adecuadas a cementos y hormigones. La falta de una estandarización de todos los parámetros que influyen en las prestaciones de este material, hace complicada su reproducción a nivel industrial, sobre todo por la polivalencia funcional y constructiva del mortero de cal.

Una de las consecuencias principales de la producción industrial de morteros es el abandono de los morteros artesanales (UNE-EN 998-2, 2004) en favor de morteros en forma de polvo seco, en los cuales el árido y la cal (también en forma de polvo seco) están homogéneamente mezclados y listos para ser utilizados. Si por un lado la producción de morteros en polvo conlleva algunas ventajas, tanto en la elaboración (garantía y control de calidad) como en la obra (rapidez de amasado y ningún desperdicio del producto) (Boletín AFAM, 2003), por otro lado ésta supone el uso de materiales de menor calidad con respecto a los empleados tradicionalmente.

Por ejemplo, la cal hidratada en polvo no tiene las excelentes propiedades reológicas de las cales en pasta (Rodríguez-Navarro et al., 2005; Ruiz Agudo y Rodríguez Navarro, 2010), por lo que con esta cal no se pueden obtener morteros de elevada plasticidad y reactividad (Cazalla et al., 2000) a no ser que se añadan aditivos. A pesar de la superioridad de la pasta de cal, la cal hidratada en polvo es actualmente la más utilizada en la fabricación de morteros, debido a sus bajos costes de producción y comercialización y a la facilidad y rapidez de su uso.

El objetivo principal de esta Tesis Doctoral es la elaboración de nuevos morteros de restauración en base cal que se puedan producir a nivel industrial y comercializar en forma de polvo seco, para su aplicación final como morteros de revestimiento en edificios históricos y modernos.

Para alcanzar este objetivo ha sido necesario lograr también los siguientes objetivos parciales:

- seleccionar los componentes más compatibles y las proporciones más adecuadas para morteros de revoco;
- considerar nuevos métodos para la evaluación de la calidad de los morteros de cal en estado fresco y en proceso de endurecimiento;
- evaluar la durabilidad de morteros de cal para revoco, mediante la realización de nuevos ensayos de laboratorio.

• *Requisitos de la investigación*

En los últimos años, muchos han sido los intentos de diseñar nuevos morteros de restauración que se puedan comercializar a nivel industrial. Sin embargo, la mayoría de los productos existentes en el mercado son morteros hidráulicos o aéreos que tienen añadido cemento Portland. Algunos estudios (Marie-Victoire and Bromblet, 1999; Jornet et al., 2010) han demostrado que estos productos se caracterizan por mayores resistencias mecánicas y menor porosidad capilar y permeabilidad al vapor de agua comparado con los materiales tradicionales. Por estas razones, no se puede reprochar a los restauradores y arquitectos su indecisión acerca de la preferencia de estos morteros a los tradicionales, preparados in-situ.

Sin embargo, no es imposible producir industrialmente morteros de restauración de buena calidad, siempre y cuando se respecten algunos aspectos básicos que tienen en cuenta tanto los requisitos generales de la producción industrial como los más específicos de la restauración:

a) en primer lugar, el mortero de restauración debe ser compatible con los demás elementos de mampostería. Esto puede asegurarse mediante una cuidadosa selección de los componentes de los morteros;

b) en segundo lugar, es necesario establecer cuales son las características requeridas en el mortero, en función de su utilización. En el caso de morteros de revestimiento las principales son (Groot, 2010; Hughes, 2010):

- moderada tendencia a la retracción;
- adherencia y flexibilidad suficientes para seguir los movimientos de mampostería;
- baja absorción capilar;
- elevada permeabilidad al vapor de agua;
- alta resistencia a ciclos de hielo-deshielo;
- color y textura compatibles con los objetivos definidos para la restauración.

c) en tercer lugar, hay que tener en cuenta que las características antes mencionadas pueden variar una vez aplicadas, dependiendo de los materiales con los que el mortero está en contacto. Por ejemplo, un mismo mortero de revestimiento puede presentar diferentes grados de retracción y adherencia si aplicado sobre soportes con diferente capacidad de absorción de agua.

d) Finalmente, las características de un mortero también dependen de las condiciones climáticas a las que está expuesto, por lo que es necesario diseñar los morteros en función del lugar donde se aplicará.

Por último, existen otros aspectos que es necesario tener en cuenta a la hora de diseñar un mortero de restauración que sea producido a nivel industrial:

e) Como se ha comentado anteriormente, la cal seleccionada debe ser en forma de polvo seco, debido a la incompatibilidad de la pasta de

cal con la forma industrial de producir y suministrar los morteros (en estado seco);

f) También relacionado con la anterior condición, existen métodos de elaboración que están obligatoriamente descartados en un proceso industrial. Uno de ellos es el amasado de la cal con agua antes de mezclarla con los demás componentes, que permite alcanzar una mayor plasticidad de la pasta de mortero (Burnell, 1990). A pesar de que este procedimiento sería mejor, la producción industrial prevé la mezcla simultánea de todos los componentes con el agua (cuya cantidad está indicada en la ficha técnica del producto).

Una vez tenidas en cuenta estas restricciones, es aún posible diseñar un mortero de restauración pre-dosificados que a la vez cumpla con los requisitos de compatibilidad y longevidad establecidos para morteros de restauración y posea las características requeridas en un mortero de revestimiento. Y es sobre la base de estas exigencias que se ha desarrollado esta Tesis Doctoral.

• *Esquema de la investigación*

Esta tesis doctoral consta de cuatro partes principales que resumo a continuación:

- PARTE I: Selección de los componentes más adecuados para la elaboración de morteros de restauración, mediante el estudio de la micro-estructura y propiedades reológicas de cales calcítica y dolomítica (*capítulo I.1*) y la caracterización mineralógica, textural y físico-mecánica de morteros elaborados con cales calcítica y dolomítica y áridos calcítico y silíceo (*capítulos I.2, I.3, I.4* y *I.5*). En este apartado se estudia, en particular, la influencia de la mineralogía, granulometría y textura del árido en las propiedades de los morteros y la evolución de estas propiedades durante el proceso de carbonatación (*capítulos I.3, I.4* y *I.5*). Además, se investiga la eficacia de técnicas no- o parcialmente destructivas para la caracterización textural de morteros de cal (capítulos I.4 y I.5).

- PARTE II: Aplicación de métodos estándar y no-estándar para una correcta elaboración de morteros de cal. En este apartado se hace hincapié en los problemas debidos a la falta de una normativa específica para morteros de cal (*capítulo II.1*).

- PARTE III: Utilización de distintos tipos de aditivos para disminuir la cantidad de agua de amasado, con el objetivo principal de reducir la retracción de los morteros de cal. En este apartado se realiza un estudio de la compatibilidad químico-mineralógica, textural y físico-mecánica de los aditivos con los componentes principales de los morteros (*capítulos III.1* y *III.2*).

- PARTE IV: Estudio de la durabilidad de los morteros de cal, mediante la evaluación de su comportamiento frente al agua (*capítulo IV.1*) y de su respuesta ante ensayos de envejecimiento específicos para morteros de

revestimiento aplicados en zonas de baja humedad y amplias oscilaciones térmicas (*capítulo IV.2*). En este último capítulo se estudian los principales factores (absorción capilar de agua, cristalización de sales, niebla salina, hielo-deshielo) que provocan el deterioro de morteros de revestimiento.

Materiales y métodos

• *Materiales utilizados*

Aglomerantes

Cal calcitíca apagada (CL): (CL 90-S; UNE-EN 459-1, 2002) fabricada por la empresa ANCASA, del grupo CALCINOR (Sevilla) y proporcionada por la empresa ARGOS Derivados del cemento S.L. (Padul, Granada);

Cal dolomítica apagada (DL): (DL 85-S; UNE-EN 459-1, 2002) producida en los Estados Unidos y proporcionada por LHOIST-Recherche et Développement S.A. (Nivelles, Bélgica).

Cemento Portland blanco (WPC): tipo BL II/A-LL 52,5 R (UNE-EN 197-1, 2000), fabricado por CEMEX comercial (Valencia) y proporcionado por ARGOS Derivados del cemento. Este aglomerante se ha utilizado en una cantidad del 25% en peso en sustitución de la cal en la elaboración de algunos de los morteros diseñados en esta tesis.

Áridos

Árido silíceo (SA): es un árido granular natural (UNE-EN 13139, 2003) de granulometría comprendida entre 0,1 y 0,5 mm y procedente de Arcos de la Frontera (SIBELCO, Cádiz) y proporcionado por ARGOS Derivados del cemento.

Árido calcítico (CA): es un árido de machaqueo (UNE-EN 13139, 2003) de granulometría comprendida entre 0,063 y 1,5 mm. Este árido está formado por una mezcla de tres áridos calcíticos de distinta granulometría fabricados a partir de la misma caliza con alto grado de pureza y elevada blancura, procedentes de una cantera de la provincia de Granada y proporcionados por ARGOS Derivados del cemento.

Aditivos

Metacaolín (MK): es una arcilla calcinada, clasificada como CLASS N POZZOLAN (ASTM C618-08), fabricada por BURGESS PIGMENT COMPANY (Estados Unidos) y proporcionada por ARGOS Derivados del cemento. Este componente se ha usado en sustitución del 10-20% en peso de la cal en la elaboración de algunos de los morteros diseñados en esta Tesis.

Perlita (P): es una perlita expandida, usada como adición en algunos morteros con la función de aligerante. Su nombre es Otaperl 0/1-TR, producida por Otavi Iberica Slu y proporcionada por ARGOS Derivados del Cemento.

Derivado de celulosa (C): es una metilhidroxietilcelulosa, usada como adición en algunos morteros con la función de retenedor de agua. Su

nombre es Tylose MHS 10012 P6, producida por SE Tylose GmbH&CO.KG (Alemania) y proporcionada por ARGOS Derivados del Cemento.

Policarboxilato (R): es un policarboxilato de cadenas largas, usado como adición en algunos morteros con la función de plastificante. Su nombre es Rheomix GT205 MA, producido por BASF Chemical Company y proporcionado por ARGOS Derivados del Cemento.

- ## *Elaboración de los morteros*

La fabricación de las probetas de mortero se ha efectuado siguiendo las normativas UNE-EN 1015-2 (1999) y UNE-EN 1015-11 (1999). Sin embargo, en algunas etapas de la elaboración se han aplicado las modificaciones propuestas por Cazalla (2002). La preparación de las probetas ha constado de cinco etapas principales:

1) mezcla de los componentes (los componentes se mezclan primero en seco y luego con agua);
2) amasado (90 s en amasadora);
3) enmoldado (en moldes normalizados de 4×4×16 cm);
4) desmoldado (después de 7 días);
5) conservación de las probetas en cámara de curado a T = 20 ± 5 ºC y HR = 60 ± 5% durante 28 días.

Todos estos procesos se llevaron a cabo en los laboratorios de la empresa ARGOS.

- ## *Caracterización física de componentes y morteros*

- *Determinación de la granulometría de los áridos*: se ha realizado con una tamizadora mecánica siguiendo las indicaciones de la norma UNE EN 933-2 (1996).

- *Determinación de la granulometría de las cales*: se ha realizado con un medidor de tamaño de partículas GALAI CIS-1.

- *Determinación de la movilidad electroforética y potencial-Z*: se ha realizado mediante el método Smoluchowski (1903), usando un instrumento Malvern Zetasizer 2000 (del Dpto. de Física Aplicada, Universidad de Granada).

- *Determinación de la densidad de partículas*: se ha realizado mediante picnómetro (en el Dpto. de Ingeniería Civil de la Universidad Católica de Lovaina, Bélgica), según el estándar ASTM D 854-92 (1993).

- *Determinación de los valores de RLP y RCP y la densidad de empaquetamiento*: se ha realizado según los métodos de Shapiro and Probestein (1992) y Wong and Kwan (2007).

- *Determinación de la superficie específica y volumen de microporos*: se ha realizado mediante la técnica de Adsorción de N_2 (Micromeritics 3000 Tristar) y según los métodos de Brunauer-Emmet-Teller (BET) (1938) y Barret–Joyner–Halenda (BJH) (1951).

- *Análisis reológicos*: se han realizado mediante un viscosímetro Viskomat PC y un reómetro Brookfield, en procedimiento de velocidad (CR) y esfuerzo (CS) controlados.

- *Determinación de la consistencia*: se ha realizado mediante el método de la mesa de sacudidas, UNE EN 1015-3 (1999).
- *Determinación de la retracción*: se ha realizado con el equipo SWG-H-400 (de ARGOS Derivados del Cemento) y midiendo la variación dimensional de las probetas a lo largo del tiempo.

- ***Caracterización químico-mineralógica y petrográfica de componentes y morteros***

- *Análisis químicos*: se han realizado mediante las técnicas de fluorescencia de rayos X (espectrómetro Bruker S4 Pioneer) y cromatografía de iones (Dionex IC DX500 (de la Escuela de Geografía y Ambiente de la Universidad de Oxford, Reino Unido).
- *Análisis mineralógicos*: se han realizado mediante las técnicas de difracción de rayos X (difractómetros Philips PW-1710 y Panalytical X'Pert PRO MPD) y termogravimetría (Shimadzu TGA-50H).
- *Estudio petrográfico*: se ha realizado mediante microscopía óptica (Olympus BX-60) y electrónica (FESEM, Carl Zeiss Leo-Gemini 1530; HRTEM, Philips CM20+EDAX; ESEM, Philips Quanta 400).
- *Caracterización del sistema poroso*: se ha realizado mediante las técnicas de porosimetría de intrusión de Hg (Micromeritics Autopore III 9410) y adsorción de N_2 (Micromeritics 3000 Tristar).
- *Determinación de las propiedades hídricas*: se ha realizado mediante ensayos de absorción, desorción, capilaridad, conductividad hidráulica y permeabilidad al vapor de agua.
- *Determinación de la resistencia a flexión y compresión*: se ha realizado mediante dos tipos de prensa hidráulica, una INCOTECNIC-Matest (de ARGOS Derivados del cemento) y una Instron 4411 (del Dpto. de Ciencias de la Tierra y del Ambiente, Alicante).
- *Medida de propagación de ultrasonidos*: mediante un equipo Panametrics HV Pulser/Receiver 5058 PR acoplado a un Tektronix TDS 3012B.

- ***Estudio de la durabilidad de morteros***

- *Ensayos de envejecimiento acelerado*: se han realizado mediante una cámara climática Sanyo-FE 300H/MP/R20 (de la Escuela de Geografía y Ambiente de la Universidad de Oxford, Reino Unido), en las que se han establecido variaciones de temperatura, humedad relativa y luz, y se han simulado condiciones de lluvia, absorción de sales y niebla salina.

Resultados y discusión

PARTE I: Cales y áridos: estudio de su influencia en las propiedades de los morteros en estado de endurecimiento y evaluación inicial de las proporciones más adecuadas.

- ***Capítulo I.1: Diferencias en las propiedades reológicas de suspensiones de cal calcítica y dolomítica: influencia de las características de las partículas e implicaciones prácticas en la fabricación de morteros de cal.***

Arizzi A., Hendrickx R., Cultrone G., Van Balen K.
Materiales de Construcción (2012)
DOI 10.3989/mc.2011.00311

El estudio de las propiedades reológicas de suspensiones de cal es una herramienta muy útil para evaluar la trabajabilidad de morteros de cal. En este trabajo se ha estudiado el comportamiento en suspensión de dos cales hidratadas, de composición calcítica y dolomítica, mediante dos tipos de reómetros con geometría y modalidades distintas de medida. Los resultados obtenidos se han interpretado teniendo en cuenta las diferencias en la microestructura y las propiedades de superficie de las partículas en suspensión. Las partículas de cal calcítica están formadas por aglomerados angulares y polidispersos y, una vez dispersadas en agua, presentan un comportamiento tixotrópico. Por su parte, la cal dolomítica está formada por nanopartículas y pequeños agregados redondeados y muestra en suspensión un pronunciado comportamiento plástico. Esta importante diferencia entre las dos cales explica la preferencia tradicional hacia morteros de cal dolomítica para aplicaciones en revocos.

- ***Capítulo I.2: Diferencias en el comportamiento de morteros de cal calcítica y dolomítica curados en condiciones de baja humedad: relación entre las propiedades texturales y físico-mecánicas.***

Arizzi A., Cultrone G.
Enviado a *Cement and Concrete Research*
(aceptado)

En este trabajo se han investigado las diferencias en la textura, mineralogía y propiedades hídricas y mecánicas de morteros preparados con cales apagadas en polvo de composición calcítica y dolomítica. En particular se ha estudiado la influencia en estas propiedades de la microestructura de la cal y de las condiciones de curado de los morteros. Se ha examinado, además, el efecto del uso de dos áridos distintos (uno granular de composición silícea y otro de machaqueo de composición

calcítica). Los resultados muestran que el uso de la cal dolomítica no es recomendable si los morteros están aplicados en zonas secas, ya que en estas condiciones se generan muchas fisuras de retracción y no se obtiene una mejora de la resistencia de los morteros. Además, los morteros de cal dolomítica presentan un sistema poroso que empeora el comportamiento hídrico. En cambio, los morteros de cal calcítica presentan un mayor grado de carbonatación y mejores propiedades físico-mecánicas. Finalmente, el uso de un árido calcítico es preferible porque genera una mejor cohesión en el mortero.

- ***Capítulo I.3: Cambios microestructurales y evolución de las propiedades físico-mecánicas de morteros de cal aérea debido a la carbonatación. Influencia de la mineralogía y morfología del árido.***

Arizzi A., Cultrone G.
Enviado a *Quarterly Journal of Engineering Geology and Hydrogeology*

Este estudio se ha centrado en investigar la influencia de la mineralogía y morfología del árido en las propiedades microstructurales y macroscópicas de morteros de cal aérea. Se ha intentado también comprender el papel del árido en el proceso de carbonatación. Para esto, morteros preparados con dos tipos de árido (calcítico y silíceo) se han curado durante dos años en condiciones estándar y se han estudiado a distintos intervalos de tiempo mediante análisis texturales y mineralógicos, así como a través de ensayos hídricos y físico-mecánicos. Los resultados muestran que las diferencias en las propiedades iniciales del mortero dependen de la morfología del árido, que también afecta a la evolución de las características del mortero. Se ha encontrado también que el árido calcítico induce una mayor carbonatación y mejores propiedades texturales y físico-mecánicas que el árido silíceo, y esto se debe especialmente a las diferencias de composición y textura entre los dos tipos de áridos.

- ***Capítulo I.4: Propagación de los ultrasonidos en morteros de cal aérea: una herramienta útil y alternativa para la caracterización textural.***

Arizzi A., Martínez-Martínez J., Cultrone G.
Enviado a *Materials and Structures*
(en revisión)

La caracterización textural detallada de morteros de cal resulta una tarea difícil cuando el muestreo está limitado (por ejemplo, en edificios históricos). En estas situaciones, técnicas no-destructivas como los ultrasonidos representan una eficaz alternativa, debido a su amplia posibilidad de aplicación. En este trabajo se ha estudiado la respuesta de la velocidad de propagación (v_p) y la atenuación espacial (α_s) de los ultrasonidos en morteros de cal con diferentes proporciones cal-árido,

cantidad de agua, mineralogía y granulometría del árido y grado de carbonatación. Los resultados muestran que los principales parámetros texturales que controlan v_p y α_s son la porosidad y el grado de carbonatación de los morteros. La primera está relacionada con la cantidad de agua de amasado, mientras que el segundo depende de la edad del mortero. Se han obtenido dos ecuaciones empíricas para evaluar la porosidad y el grado de carbonatación de los morteros mediante las medidas de propagación de los ultrasonidos, estableciendo así el primer paso para la caracterización de la textura de morteros de cal en un futuro mediante técnicas no-destructivas. Estos resultados se han corroborado mediante microscopía óptica y electrónica de barrido, difracción de rayos X y análisis de porosimetría de inyección de mercurio.

- ***Capítulo I.5: Evolución de las propiedades mecánicas de morteros de cal aérea durante el proceso de carbonatación.***

Arizzi A., Martínez-Martínez J., Cultrone G., Benavente D.
Key Engineering Materials, 465 (2011) 483-486.

El mortero de cal es uno de los materiales de construcción más antiguos y longevos. Se caracteriza por una lenta carbonatación durante la cual el $Ca(OH)_2$ reacciona con el CO_2 presente en el aire para formar calcita, dando lugar a un material más compacto y más fuerte. Este proceso tiene lugar desde la superficie hacia el interior del material y está condicionado por las condiciones de reacción. El objetivo de este estudio es cuantificar los incrementos de resistencia y elasticidad de distintos morteros de cal en relación a su grado de carbonatación. Para esto, se han elaborado seis tipos de morteros con diferentes proporciones cal-árido y con áridos de mineralogía y granulometría distintas. Para seguir el proceso de carbonatación se han realizado estudios mineralógicos y texturales. Cada mortero ha sido sometido a compresión uniaxial después de 15, 28 y 60 días desde la elaboración. Para diferenciar el comportamiento mecánico de las partes externas e internas de los morteros, dos micro-probetas (10×10×10 mm) se han obtenido de los primeros 10 mm y del interior de cada paralelepípedo. Los resultados muestran que los incrementos de resistencia y, en particular, del módulo elástico están asociados al proceso de carbonatación, pero varían en función de la composición y compacidad de los morteros.

- ***Conclusiones parciales***

En esta parte de la Tesis se ha alcanzado un conocimiento detallado de la microestructura de las cales, de las características texturales de los áridos y de las características mineralógicas y texturales y propiedades físico-mecánicas de los morteros.

En particular, se ha encontrado que la cal dolomítica en polvo confiere una mayor plasticidad a las pastas de cal con respecto a la cal calcítica. Esta diferencia de comportamiento en suspensión entre las dos cales está relacionada con su micro- y nanoestructura. Este estudio sugiere que se

obtienen morteros más trabajables con la cal dolomítica (*capítulo I.1*). De ese modo, se puede pensar que los morteros de cal dolomítica presentan también mejores propiedades en estado endurecido con respecto a los morteros de cal calcítica.

Sin embargo, el estudio de las propiedades de los morteros de cal calcítica y dolomítica en estado endurecido muestran resultados contradictorios respecto a la preferencia de una cal o de otra (*capítulo I.2*). En efecto, los morteros de cal dolomítica, aunque muestran una mejor trabajabilidad en estado fresco, no mantienen esta ventaja sobre los morteros de cal calcítica durante el endurecimiento.

Probablemente, la razón principal de esta diferencia se debe a las condiciones de curado a las cuales los morteros fueron expuestos durante la fase de endurecimiento. En este estudio, se han considerado condiciones secas (T = 20 ºC; HR = 60%), ya que el objetivo principal de esta Tesis es el diseño de morteros de revestimiento que se puedan aplicar en zonas secas o de baja humedad. De acuerdo con este objetivo, el uso de la cal calcítica se ha mantenido mientras que el de la cal dolomítica ha sido descartado. Sin embargo, el uso de morteros de cal dolomítica no debería descartarse en zonas de alta humedad.

El proceso de carbonatación de los morteros se ha estudiado durante dos años desde su elaboración (*capítulos I.3* y *I.4*). De acuerdo con la mayoría de investigaciones sobre la carbonatación, se ha confirmado que la trasformación de la portlandita en calcita es un proceso muy lento en los morteros de cal aérea. Nuestros resultados muestran que la carbonatación ocurre principalmente durante los dos primeros meses de vida de los morteros y después continúa a una velocidad mucho menor.

Para evaluar y cuantificar la carbonatación en el tiempo se han usado tres parámetros: el grado de carbonatación (I_{CD}) (*capítulos I.3* y *I.4*) y la velocidad de propagación (V_p) y atenuación espacial (α_s) de los ultrasonidos en los morteros. En particular, se ha observado una relación directa entre los valores de I_{CD} y V_p, ya que el último refleja los cambios de mineralogía en los morteros (*capítulo I.4*).

Otro factor que influye en los parámetros ultrasónicos y mecánicos es el sistema poroso de los morteros en el que a su vez influye la cantidad de agua de amasado (*capítulos I.4* y *I.5*). Este resultado representa el primer paso para la caracterización textural de los morteros mediante técnicas no o parcialmente destructivas, como los ultrasonidos y los ensayos de mini-compresión.

Se han encontrado resultados concordantes con respecto a la selección del árido (*capítulos I.2*, *I.3*, *I.4* y *I.5*). La preferencia se ha dado al árido calcítico, que da lugar a un mayor grado de carbonatación y mejores cohesión entre árido y matriz, compacidad y resistencias de los morteros, debido a una similitud de composición y textura entre los componentes de los morteros elaborados con este árido.

La selección de la proporción cal-árido más adecuada será considerada también en los capítulos siguientes, ya que en esta parte de la Tesis no se

ha encontrado una satisfactoria relación entre el contenido en árido y las propiedades de los morteros.

PARTE II: Métodos estándar y no estándar: estudio de su adaptabilidad a morteros de cal aérea.

• *Capítulo II.1: Comparación de distintos métodos para determinar la densidad de empaquetamiento de mezclas granulares frescas. Fracaso de su aplicación en los morteros de cal.*

Arizzi A., Cultrone G.
Enviado a *Cement and Concrete Composites*
(en revisión)

La densidad de empaquetamiento es uno de los factores que más influyen en la calidad de morteros en estado fresco. Existen métodos estándar para su determinación de forma directa e indirecta, pero en la mayoría de los casos estos métodos no dan una estimación realista de la porosidad (o contenido en espacios vacíos). En este trabajo se ha utilizado el método llamado "wet packing method" recientemente desarrollado por Wong y Kwan (2008), con el objetivo de determinar la proporción agua-cal a la que se alcanza el empaquetamiento en morteros de cal con distintas proporciones cal-árido. Para apoyar la validez de este método, los datos se han comparados con los obtenidos midiendo la densidad aparente de los componentes en estado seco, con y sin compactación, y la consistencia de las pastas de morteros, mediante el método estándar de la mesa de sacudidas. Después, para comprobar la fiabilidad del "wet packing method", es decir, para confirmar si los morteros preparados con este método presentan buenas propiedades una vez endurecidos, sus propiedades mineralógicas, texturales y mecánicas se han estudiado después de dos y seis meses de carbonatación. Los resultados han mostrado que, aunque el "wet packing method" parece ser más realista que la mayoría de los estándares usados para determinar el contenido en poros y alcanzar una óptima trabajabilidad en mezclas granulares, este método sigue sin ser el más adecuado para la elaboración de morteros de cal aérea con buenas propiedades en estado fresco y endurecido.

• *Conclusiones parciales*

Ninguno de los métodos estudiados en esta parte de la tesis se puede considerar totalmente adecuado para el diseño de morteros de restauración de cal. Sin embargo, este estudio lleva a consideraciones importantes que se describen a continuación.

En primer lugar, esta investigación ha mostrado que para establecer la correcta cantidad de agua a utilizar en los morteros, es mejor aplicar

métodos que determinan sus características, como densidad y contenido en aire, cuando los morteros están en estado fresco.

En segundo lugar, se ha descubierto que la escasa adaptabilidad del ensayo de consistencia a morteros de cal se debe principalmente a que el intervalo de valores de escurrimiento establecido en el estándar resulta incorrecto para este tipo de morteros. Por tanto, es importante definir un nuevo intervalo de valores que se aplique a los morteros de cal para su correcta elaboración. Por ejemplo, en el *capítulo II.1*, para mezclas bien empaquetadas de cal y árido se ha encontrado un intervalo de escurrimiento aproximativo entre 140 y 170 mm, que es más estrecho que el establecido en la normativa para morteros de cemento (140-200 mm).

Finalmente, el método "wet packing method" no se ha adoptado en los estudios siguientes de esta Tesis, a pesar de ser el más adecuado para evaluar la densidad de empaquetamiento de mezclas de morteros de cal aérea. La razón es que en los morteros elaborados con este método se ha observado un sistema poroso discontinuo (entre la superficie y el interior) que no puede ser beneficioso para la calidad final del mortero.

PARTE III: Aditivos y adiciones: estudio de su influencia en las propiedades de los morteros en estado de endurecimiento y evaluación de las proporciones más adecuadas.

- ***Capítulo III.1: Efectos negativos del uso de cemento Portland blanco como aditivo en morteros de cal aérea: un estudio químico, mineralógico y físico-mecánico.***

Arizzi A., Cultrone G.
Capítulo del libro *Bricks and Mortars Research,*
ISBN: 978-1-61942-927-7

Recientemente se está reconsiderando el estudio del mortero de cal, ya que este material presenta una elevada compatibilidad con los materiales de construcción del Patrimonio Arquitectónico. Por otro lado, el escaso conocimiento de las técnicas de fabricación y de los métodos de aplicación utilizados en el pasado, además de los largos tiempos de endurecimiento del mortero de cal, han obligado investigadores y restauradores a usar otros aglomerantes (como cemento y puzolanas) juntos con la cal, con el fin de reducir los inconvenientes de este material. El uso del cemento Portland como aditivo en morteros de cal parece ser una fácil alternativa en la producción industrial de morteros de restauración.

En este trabajo, se han comparado las características químico-mineralógicas y físico-mecánicas de morteros preparados con cal calcítica y árido calcítico, con las de morteros en los cuales el cemento Portland blanco se ha usado en sustitución de un 25% en peso de cal. Este estudio

muestra que los morteros preparados con cemento Portland no proporcionan resultados satisfactorios después de dos meses de curado. De acuerdo con los datos mineralógicos y los análisis porosimétricos no se han observado mejoras con la adición de cemento. En efecto, aunque el porcentaje de cemento añadido ha reducido la retracción que muestran los morteros de cal, este componente no ha mejorado sus propiedades mecánicas e hídricas. Aún más importante, el cemento ha causado la formación de ettringita que ha provocado la aparición de fisuras en las probetas de mortero.

Este estudio demuestra que el uso del cemento Portland blanco, aunque solo como aditivo en morteros de cal, puede perjudicar la longevidad de los materiales que lo rodean.

- ***Capítulo III.2: Morteros de cal aérea con un aditivo puzolánico y distintas adiciones: un estudio mineralógico, textural y físico-mecánico.***

Arizzi A., Cultrone G.
Construction and Building Materials
31 (2012) 135-143

Este trabajo trata los efectos inducidos por un árido aligerante y agentes reductores y retenedores de agua en las propiedades de morteros en estado endurecido, donde la cal aérea está remplazada por un 10% y un 20% de metacaolín. Además, se ha investigado la influencia de distintas proporciones cal-árido (1:3,1:4,1:6,1:9 en peso). Se ha encontrado una estrecha relación entre el contenido de metacaolín y las propiedades físico-mecánicas (resistencia a compresión y sistema poroso) de los morteros. Este estudio es muy útil ya que permite establecer las proporciones adecuadas de aditivos y adiciones que se utilizan en morteros de cal aérea diseñados para obras de restauración.

- ***Conclusiones parciales***

La idea de usar un cemento Portland blanco como aditivos en morteros de cal ha sido descartada, ya que este material ha demostrado tener un efecto negativo en la durabilidad de los morteros. A pesar de haber sido eficaz en reducir la retracción, su uso no se puede contemplar en el diseño de morteros de restauración (*capítulo III.1*).

Por otro lado, un importante avance se ha conseguido con la investigación presentada en el *capítulo III.2*.

En primer lugar, se ha observado que el contenido de metacaolín influye de manera importante tanto en el sistema poroso como en las propiedades mecánicas de los morteros. Cuando su proporción es del 20% en peso de la cal, se obtienen morteros con resistencias y porosidades elevadas. Ya que estas características son inadecuadas para morteros de

revestimiento, solo la proporción del 10% se ha mantenido en los siguientes estudios, mientras que la proporción del 20% se ha descartado.

En segundo lugar, el uso simultáneo de diversas adiciones ha resultado ser una forma eficaz de reducir el contenido en agua y, consecuentemente, la porosidad. Además, esto ha sido posible con una pequeña cantidad de adiciones (solo el 2% del total). De esta forma, la composición del mortero es todavía muy parecida a la de la mezcla de cal, metacaolín y árido, lo que es beneficioso desde el punto de vista de la compatibilidad.

PARTE IV: La durabilidad de los morteros: estudio de su comportamiento como morteros de revestimiento.

• *Capítulo IV.1: Propiedades hídricas y retracción plástica en morteros de cal aérea: evaluación de su calidad como morteros de revestimiento.*

Arizzi A., Cultrone G.
Enviado a *Journal of Cultural Heritage*

El agua (en su estado solido, líquido y vapor) es uno de los factores principales que causan el deterioro de los materiales. Por tanto, es fundamental estudiar el comportamiento de los morteros frente al agua, para poder evaluar la calidad y durabilidad de un mortero de revestimiento, y así asegurar su función protectiva en la mampostería. Los morteros estudiados han sido elaborados con una cal calcítica hidratada, un árido calcítico, una puzolana, un árido aligerante, un agente retenedor de agua y un plastificante. El efecto de diferentes proporciones aglomerante-árido se ha estudiado a través de ensayos de absorción de agua por inmersión total, secado, capilaridad y permeabilidad al agua y al vapor de agua. Otro aspecto que se ha considerado en la evaluación de la calidad de los morteros ha sido la retracción plástica, que se ha medido a través de un aparato no-estandarizado. Se ha encontrado que los morteros con más alto contenido de cal absorben una mayor cantidad de agua, mientras que los morteros con mayor proporción de árido muestran un secado más rápido y valores más altos de permeabilidad al agua y al vapor de agua. Tanto el comportamiento hídrico, como los valores de retracción, se han interpretado teniendo en cuenta las diferencias en la microestructura y sistema poroso de los morteros.

- *Capítulo IV.2: Estudio experimental de la durabilidad de morteros de cal utilizados para el revestimiento de edificios históricos.*

Arizzi A., Viles H., Cultrone G.
Construction and Building Materials
28 (2012) 807-818

Para obtener un mortero de revoco con la mejor durabilidad, se han diseñado cuatro ensayos de envejecimiento acelerado que miran a simular los movimientos del agua, la formación de hielo y la cristalización de sales en el interior de morteros de cal expuestos a un rango de temperatura y humedad extremo pero, al mismo tiempo, realista. Se ha encontrado que la respuesta de cada mezcla de mortero es diferente en relación al mecanismo y agente de deterioro. Estos resultados sugieren que, para proporcionar datos útiles, tanto el enfoque del ensayo experimental como el tipo de mortero estudiado deben ser adaptados a la particular circunstancia en la que el mortero será aplicado.

• *Conclusiones parciales*

En esta parte final de la Tesis se ha conseguido un mejor conocimiento de las propiedades de los morteros durante el endurecimiento.

La evaluación de las propiedades hídricas ha sido crucial para entender más en detalle la susceptibilidad de estos materiales al deterioro causado por el agua. En particular, el estudio realizado en el capítulo IV.1 ha permitido seleccionar la proporción aglomerante-árido más adecuada en términos de comportamiento hídrico.

Al mismo tiempo, la medida de la retracción plástica ha permitido comprender los factores que influyen en la reducción del volumen de los morteros debida a la evaporación del agua, los cuales no están relacionados solo con los contenidos en agua y cal. Sin embargo, hay que tener presente que la retracción medida sobre muestras de laboratorio no puede corresponder exactamente a la experimentada por los morteros una vez expuesto a las condiciones ambientales. Además, la capacidad de succión del soporte, que afecta la formación de fisuras, no se ha considerado en este tipo de medida. Por tanto, los valores de retracción determinados mediante el aparato usado deben tomarse simplemente para propósitos comparativos.

Finalmente, en el *capítulo IV.2* se ha obtenido un profundo conocimiento de los factores que afectan la durabilidad de los cuatro morteros finales diseñados en esta Tesis. A través de este estudio, ha sido también posible seleccionar el mortero de mayor durabilidad. Sin embargo, la selección de la proporción aglomerante-árido más adecuada debe ser realizada sobre la base de lo que se ha encontrado en los dos estudios de esta última parte de la Tesis.

Conclusiones

• *Conclusiones generales*

Esta Tesis doctoral se ha realizado con el objetivo principal de diseñar morteros de revoco para su uso en edificios antiguos y modernos. Para esto, esta investigación ha abordado algunos de los aspectos más importantes del diseño de morteros de restauración:

1) la selección de los componentes de los morteros, como por ejemplo aglomerantes, áridos y aditivos, que cumplan con el requisito de compatibilidad y sean apropiados para intervenciones de restauración;
2) la selección de las dosificaciones correctas, en cuanto a contenido en agua y aditivos y proporción aglomerante-árido, para diseñar morteros con óptimas propiedades en estado fresco y endurecido;
3) la selección de métodos de elaboración, curado y estudio apropiados para obtener una caracterización precisa y exhaustiva de los morteros.

Los resultados principales y las conclusiones parciales de esta investigación se han comentado en los apartados precedentes (*cf. Resultados y Discusión*). Las conclusiones generales que se pueden sacar de esta Tesis se comentan a continuación.

Los componentes de los morteros

Los morteros de cal dolomítica han mostrado una mejor trabajabilidad, debida a la mayor capacidad de retención de agua de las partículas de la cal dolomítica y al comportamiento plástico que ésta manifiesta en suspensión. No obstante, el uso de la cal calcítica en morteros expuestos a condiciones de curado de baja humedad ha producido un mayor grado de carbonatación y mejores propiedades mecánicas. Sin embargo, en la práctica, hay que tener en cuenta que la calidad de los morteros de cal dolomítica puede ser mejorada manteniendo húmeda la superficie del revestimiento.

El tipo de árido influye notablemente en las propiedades texturales de los morteros y en su evolución durante el endurecimiento. El uso de un árido silíceo ha dado lugar a morteros frágiles, a causa de la escasa compacidad y el bajo grado de carbonatación alcanzados. Por otro lado, el uso de un árido calcítico ha producido una mayor cohesión y mejores resistencias mecánicas. Además, el árido calcítico ha favorecido la carbonatación de la cal calcítica, gracias a una similitud en la composición de estos materiales.

El uso del cemento Portland blanco en morteros de cal ha producido daños irreversibles cuando los morteros estaban en contacto con agua. Esto indica que el cemento Portland blanco es un material perjudicial para los materiales de fábrica tradicionales y, por esto, su empleo en intervenciones de restauración debe ser descartado, de la misma forma que el cemento Portland gris.

La adición de metacaolín es sin duda un método mejor de mejorar la calidad y durabilidad de los morteros de cal aérea. Sin embargo, el

incremento de la resistencias mecánicas y el efecto del metakaolin en el sistema poroso ocurren en diferentes grados, dependiendo de la cantidad de metakaolin añadida. Por ello, es importante controlar su contenido según las propiedades finales que se requieren. Las condiciones de curado han influido también en el resultado de la presencia del metakaolin, tal y como se comentará a continuación.

La inclusión de adiciones ha mejorado notablemente las propiedades de los morteros de cal en estado fresco, ya que han actuado disminuyendo el contenido de agua de amasado y la densidad del mortero. Sin embargo, estas adiciones no han modificado las características mineralógicas y micro-estructurales de los morteros. La perlita, de hecho, no ha manifestado el débil carácter hidráulico esperado, probablemente por las condiciones de baja humedad a los que los morteros estaban expuestos. El derivado de celulosa y el policarboxilato han mejorado la capacidad de retención de agua y la dispersión de las partículas de cal, respectivamente. Como consecuencia, también la reactividad de la cal hacia el CO_2 ha aumentado.

Las dosificaciones de los morteros

Para la elaboración de los morteros compuestos exclusivamente por cal y árido se han necesitado grandes cantidades de agua de amasado. Esto ha resultado en una elevada retracción durante el secado y en una alta porosidad durante y una vez terminado el endurecimiento de los morteros. La cantidad de agua de amasado se ha intentado reducir de dos formas: aplicando métodos de preparación no-estandardizados y usando algunas adiciones específicas. En definitiva, el uso de adiciones se ha revelado el método mejor para disminuir el contenido en agua y la porosidad de los morteros, especialmente si se tiene en cuenta que la cantidad total de adiciones empleadas no supera el 2% sobre el peso del mortero. Sin embargo, en algunas situaciones específicas, (por ejemplo, en verano) la cantidad del agente retenedor de agua debería ser aumentada para contrarrestar con más eficacia la retracción.

Las propiedades de los morteros han mostrado diferentes respuestas en función de la cantidad de metacaolín añadida. Para morteros de revoco, la proporción de metacaolín más apropiada ha resultado ser el 10% sobre el peso total del mortero, ya que ésta da lugar a cambios moderados de las resistencias mecánicas y de la porosidad.

Las proporciones aglomerante-árido han influenciado en gran medida el comportamiento hídrico y mecánico de los morteros. En general, los morteros con elevados contenidos de cal (proporciones de 1:3 y 1:4 en peso) han mostrado un mayor absorción de agua por inmersión y capilaridad y bajas resistencias mecánicas, como era de esperar. Sin embargo, la mejora de las propiedades mecánicas debida al incremento del contenido en árido alcanza un límite después del cual mayores proporciones de árido dan lugar a una perdida de compacidad y resistencias (como ocurre en el mortero de proporción 1:9). Esto se debe principalmente a una escasa cohesión en la interfaz entre los granos de

áridos y la matriz. Por la misma razón, en los morteros con mayor proporción de árido (1:6 y 1:9 en peso) se han medido valores más alto de conductividad hidráulica, permeabilidad al vapor de agua y retracción plástica. Además, se han obtenido diferentes respuestas a los ensayos de durabilidad en función de la proporción aglomerante-árido. En conclusión, las proporciones con menor y mayor contenido de árido (1:3 y 1:9 en peso) deben descartarse para morteros de revestimiento, ya que la primera ha dado lugar a una porosidad y absorción de agua demasiado elevadas, mientras que la segunda ha producido una cohesión muy baja y un fuerte deterioro superficial. De acuerdo con los requisitos específicos establecidos para morteros de revestimiento, el mortero con proporción aglomerante-árido de 1:6 sin duda ha mostrado las propiedades más adecuadas:

- El contenido en agua usado para la elaboración de este mortero ha sido entre los más bajos (21.5 % sobre el peso total), así como la porosidad (P_o~31%) y la absorción de agua (C_a~7.95 g/min$^{1/2}$ and A~0.03 g/cm^{2}min$^{1/2}$). El valor de permeabilidad de agua obtenido es parecido en todos los morteros y, en éste, es inferior de sólo un 0.4 (K_v~2.69 g/m^{2}h) respecto al más alto.
- Este mortero presenta los valores más altos de resistencias mecánicas (R_f~1.86 MPa and R_c~3.63 MPa), sin ser demasiado resistente para un mortero de revestimiento y, al mismo tiempo, de restauración.
- También ha mostrado cierta resistencia al deterioro causado por la absorción capilar de sales y por los ciclos de hielo-deshielo y sólo un lígero deterioro superficial debido a la deposición superficial de sales.
- Por último, el grado de carbonatación de este mortero ha sido entre los más altos después de la exposición a las condiciones ambientales establecidas durante los ensayos de durabilidad.

Métodos de preparación, curado y ensayo

Todos los estándares para morteros de cemento ha mostrado ciertas lagunas cuando se han aplicado a morteros de cal aérea. Uno de los aspectos más controvertidos que se han abordado en esta Tesis doctoral es la forma de elegir el contenido más adecuado de agua de amasado. En particular, los valores de consistencia indicados en el estándar UNE EN 1015-3:1999 han resultado ser inapropiados para los morteros de cal diseñados, por los que se ha establecido un nuevo rango de flujo (entre 120 y 150 mm aproximadamente).

Las condiciones de curado de baja humedad elegidas para esta Tesis han influenciado notablemente la calidad final de los morteros. Los morteros de cal dolomítica han mostrado una retracción plástica muy importante bajo estas condiciones, con la consecuencia de que sus propiedades finales han sido empeoradas de forma irreversible. Por la misma razón, no se ha producido una completa hidratación de las fases

reactivas del metacaolín; esto, sin embargo, es una ventaja para la calidad de los morteros, ya que se han producido solo un lígero incremento de las resistencias mecánicas. De la misma forma, la perlita no ha mostrado su potencial carácter hidráulico.

La técnica de ultrasonidos ha resultado ser más útil de lo esperado. En efecto, esta técnica se ha empleado no sólo para medir los parámetros dinámico-mecánico de los morteros, sino también como herramienta adicional para caracterizar la textura de los morteros durante el endurecimiento. Se han encontrado resultados concordantes a través de las técnicas analíticas destructivas más comunes, como difracción de rayos X, microscopía electrónica y porosimetría de mercurio, y la técnica no destructiva de los ultrasonidos. Además, el estudio de los morteros mediante ultrasonidos ha sido crucial para comprender la importancia del contenido en agua sobre la microestructura de los morteros de cal.

El diseño de nuevos ensayos de laboratorio para el estudio de la durabilidad de revocos ha contribuido a un conocimiento más detallado de los mecanismos de deterioro que ocurren en este tipo de mortero. La metodología diseñada, en las que se establecen particulares condiciones ambientales, agentes de deterioro, forma y tamaño de las muestras, puede tomarse como referencia para evaluar la longevidad de morteros que se van a aplicar en otras áreas con clima parecido o más suave. Además, este estudio puede facilitar la elección de las dosificaciones de árido más apropiadas, de acuerdo con la función principal que el mortero va a ejercer en la mampostería.

- ## *Contribuciones originales*

Esta Tesis doctoral lleva a un gran avance en el campo de investigación de los morteros de cal y, al mismo tiempo, contribuye a la sobrevivencia de nuestro Patrimonio Arquitectónico, con el diseño de adecuados morteros de restauración. La originalidad de este trabajo de investigación está en el tentativo de encontrar una solución a la falta de morteros compatibles y durables que se requieren para evitar los daños provocados al Patrimonio Arquitectónico, así como a la gran demanda de morteros pre-dosificados, debida a los bajos costes y tiempos de producción y a la facilidad de uso de morteros producidos y comercializados a nivel industrial. Esta Tesis ha abordado con éxito la difícil tarea de asegurar una beneficiosa combinación entre los requisitos de la industria y de la restauración, y los resultados obtenidos representan un punto de inicio para investigaciones similares.

- ## *Futuras perspectivas de trabajo*

Múltiples son las posibilidades para ulteriores investigaciones; en particular, las pautas propuestas en esta Tesis para el diseño de morteros de restauración deberían ser validadas en una base más amplia. Por ejemplo:

- Deberían adoptarse condiciones de curado de elevada humedad para investigar su influencia en las propiedades finales de los morteros.

En estas condiciones, deberían estudiarse el grado de retracción de los morteros de cal dolomítica, el resultado de los procesos de hidratación y carbonatación en los morteros de cal con metacaolín y el carácter hidráulico de la perlita, con el objetivo de verificar las hipótesis hechas.

- Deberían considerarse también cales hidráulicas naturales (NHL), especialmente para el diseño de morteros que van a aplicarse en zonas de alta humedad.
- Para mejorar ulteriormente la calidad de los morteros, deberían ensayarse más tipos de adiciones. En particular, se deberían considerar adiciones naturales, orgánicas e inorgánicas, cómo almidón, jugo y mucílago de Nopal, fibras y tierras diatomáceas, entre otras.
- La aplicación de los métodos de ensayo a una variedad más amplia de morteros proporcionaría un conocimiento más detallado de sus límites y, sobre esta basis, se podrían desarrollar nuevos estándares más específicos para morteros de cal aérea.
- Las ecuaciones empíricas obtenidas para evaluar la porosidad y el grado de carbonatación de los morteros debería validarse mediante el desarrollo de un modelo micro-mecánico basado sobre los datos de ultrasonidos.

Finalmente, el estudio a largo plazo e in-situ de los revocos diseñados en esta Tesis completaría esta investigación y proporcionaría un mejor conocimiento de la calidad y durabilidad de estos morteros.

Referencias

ASTM D854-92 (1993). Standard test method for specific gravity of soils. ASTM International Standards Worldwide, Pennsylvania (USA).

Barret E.P., Joyner L-J., Halenda P. The determination of pore volume and area distributions in porous substances. I. Computations from nitrogen isotherms. J. Am. Chem. Soc., 73 (1951), 373-380.

Boletín AFAM. Morteros. Guía General. (2003).

Brunauer S., Emmett P.H., Teller J. Adsorption of gases in multimolecular layers. J. Am. Chem. Soc., 60 (1938), 309.

Burnell G.R. Rudimentary Treatise on Limes, Cements, Mortars, Concretes, Mastics, Plastering, Etc. Ed. London G. Weale (1900).

Callebaut K., Elsen J., Van Balen K., Viaene W. Nineteenth century hydraulic restauration mortars in the Saint Michael's Church (Leuven, Belgium). Natural hydraulic lime or cement? Cem Concr Res 31 (2001) 397-403.

Cazalla O., Rodríguez-Navarro C., Sebastián E., Cultrone G., De La Torre M. J. Aging of Lime Putty : Effects on traditional Lime Mortar Carbonation. J Am Ceram Soc 83 (5) (2000) 1070-1076.

Cowper A.D. Lime and Lime mortars. Donhead Ed. (1927), reprinted by Building Research Establishment Ltd. In 1998.

Elert K., Rodriguez-Navarro C., Sebastián Pardo E., Hansen E., Cazalla O. Lime mortars for the conservation of historic buildings. Studies in conservation 47 (2002) 62-75.

Groot C., Bartos P., Hughes J. Historic mortars: characteristics and test concluding summary and state of the art. International Workshop on Historic Mortars, Paisley (UK) (1999).

Groot C.J.W.P. Performance and repair requirements for renders and plasters. International Workshop on "Repair mortars for historic masonry". RILEM TC 203-RHM, Prague (2010).

Hughes J.J. The role of mortar in masonry: an introduction to requirements for the design of repair mortars. International Workshop on "Repair mortars for historic masonry". RILEM TC 203-RHM, Prague (2010).

Jornet A., Mosca C., Cavallo G., Corredig G. Comparison between traditional, lime based, and industrial, dry mortars. Proceedings of the 2nd Historic Mortars Conference, Prague (2010).

Marie-Victoire E., Bromblet P. A new generation of cement based renderings : an alternative to traditional lime based mortars? International Workshop on "Historic Mortars: Characteristics and Tests". RILEM TC-167COM, University of Paisley, Scotland (1999).

Maurenbrecher A.H.P. Mortars for repair of traditional masonry. Practice Periodical on Structural Design and Construction 9 (2) (2004) 62-65.

Rattazzi A. Conosci il grassello di calce? $Ca(OH)_2$ + H_2O. Origine, produzione e impiego del grassello di calce in architettura, nell'arte e nel restauro. Ed. Edicom Monfalcone (2007).

Rodríguez-Navarro C., Ruiz Agudo E., Ortega-Huertas M., Hansen E. Nanostructure and irreversible colloidal behaviour of $Ca(OH)_2$: implication in Cultural Heritage Conservation. Langmuir, 21 (2005) 24.

Ruiz Agudo E., Rodríguez Navarro C. Microstructure and rheology of lime putty Langmuir 26 (6) (2010) 3868–3877.

UNE EN 197-1 (2000). Cemento. Parte 1: Composición, especificaciones y criterios de conformidad para los cementos comunes. AENOR, Madrid.

UNE EN 459-1 (2002). Cales para la construcción. Parte 1: Definiciones, especificaciones y criterios de conformidad. AENOR, Madrid.

UNE EN 933-2 (1996). Tests for geometrical properties of aggregates - Part 2: Determination of particle size distribution - Test sieves, nominal size of apertures. AENOR, Madrid.

UNE-EN 998-2. Especificaciones de los morteros para albañilería. Parte 2: Morteros para albañilería. AENOR, Madrid (2004).

UNE-EN 1015-3 (1998). Métodos de ensayo de los morteros para albanileria. Parte 3: Determinación de la consistencia del mortero fresco (por la mesa de sacudidas). AENOR, Madrid.

UNE-EN 13139 (2003). Áridos para morteros. AENOR, Madrid.

Shapiro A.P., Probstein R.F. Random packings of spheres and fluidity limits of monodisperse and bidisperse suspensions. Phys. Rev. Lett. 68 (9) (1992), 1422-1425.

Veniale F., Setti M., Rodriguez-Navarro C., Lodola S., Palestra W., Busetto A. Thaumasite as decay product of cement mortar in brick masonry of a church near Venice. Cem Concr Compos 25 (2003) 1123-1129.

Von Smoluchowski M. Bull. Int. Acad. Sci. (1903), 184.

Wong H.H.C., Kwan A.K.H. Packing density of cementitious materials: part 1-measurement using a wet packing method. Mater. Struct. 41 (4) (2008), 689-701.

DISEGNO DI MALTE DA INTONACO PRE-DOSIFICATE PER LA LORO APPLICAZIONE IN INTERVENTI DI RESTAURO

Riassunto

Sin dalla sua scoperta, quasi due secoli fa, l'uso del cemento Portland ha generato un entusiasmo tra architetti ed ingegneri tale da preferirlo alle malte tradizionali in tutte le nuove costruzioni. Purtroppo però, questo è accaduto anche negli edifici storici, nei quali il cemento è stato usato in modo irrazionale come materiale da restauro. L'incompatibilità del cemento con i materiali da costruzione tradizionali ha portato ad un'accelerazione dei processi di degrado, con danni finali irreversibili al nostro Patrimonio Architettonico ed Artistico. Oggigiorno i professionisti della costruzione stanno dimostrando un rinnovato interesse verso l'uso di malte tradizionali, soprattutto di calce, poiché esse garantiscono compatibilità, adattabilità e durevolezza. Ciò nonostante, le tecniche di produzione che si adottavano in passato non possono essere recuperate in epoca moderna, poiché è necessario prendere in considerazione altri requisiti, come ad esempio i costi ed i tempi di produzione.

Questa Tesi di dottorato intende contribuire alla conservazione del Patrimonio Architettonico, fornendo una base per il disegno di nuove malte da intonaco per il restauro, che si possano produrre e distribuire a livello industriale. A tal proposito, i componenti delle malte ed i metodi di preparazione sono stati selezionati considerando i requisiti della restaurazione, così come quelli del settore industriale.

Molte delle tecniche analitiche che si usano comunemente per la caratterizzazione delle malte sono state usate in questa Tesi di dottorato:

- I componenti e le malte sono stati studiati mediante tecniche chimiche (fluorescenza a raggi X; cromatografia ionica) e mineralogiche (diffrazione a raggi X; termogravimetria), mentre la tessitura e la microstruttura sono state caratterizzate mediante microscopia ottica (OM) ed elettronica a scansione (FESEM; ESEM) ed a trasmissione (HRTEM).

- Le proprietà delle malte allo stato fresco, cioè una volta miscelate con acqua, sono state determinate mediante metodi standard (come il test di consistenza) e non ("wet packing method"). Inoltre, sono stati usati diversi reometri per caratterizzare il comportamento delle calci spente in sospensione. Tale comportamento è connesso con la lavorabilità della malta.

- Le proprietà fisiche e meccaniche delle malte durante il consolidamento sono state caratterizzate mediante test idrici (assorbimento libero d'acqua ed asciugamento; risalita capillare; conduttività idraulica; permeabilità all'acqua ed al vapore acqueo) e meccanici. Inoltre, sono state usate tecniche fisico-meccaniche non- e semi-distruttive, come gli ultrasuoni ed una pressa micromeccanica, per caratterizzare la tessitura delle malte.

- Sono stati progettati nuovi test di laboratorio per lo studio della durevolezza delle malte e dei meccanismi di degrado provocati da variazioni igrotermiche, pioggia, cicli di gelo-disgelo ed attacco da parte dei sali solubili.

I componenti iniziali scelti per questa Tesi sono stati: due calci spente in polvere, una di composizione calcitica e l'altra dolomitica, due inerti, uno calcitico ed uno siliceo, due componenti idraulici come additivi ed, infine, tre tipi di addizioni. Le condizioni di conservazione di bassa umidità alle quali sono state esposte le malte durante la ricerca sono state decisive nella scelta dei componenti e delle dosi finali, come viene indicato di seguito:

- Le calci calcitica e dolomitica presentano una microstruttura molto diversa che influisce nel loro comportamento in sospensione e, di conseguenza, nella lavorabilità finale della malta fresca, che è stata migliore quando si è impiegata una calce dolomitica. Tuttavia, le malte con calce dolomitica hanno mostrato un restringimento maggiore e delle peggiori proprietà durante la fase di consolidamento rispetto a quelle con calce calcitica. Per questo motivo, l'uso della calce dolomitica in questa ricerca è stato scartato.

- L'uso di un inerte calcitico o siliceo influisce direttamente sulla quantità d'acqua necessaria per la miscela, così come sulla porosità aperta, che è stata più alta nelle malte con inerte calcitico. Ciò nonostante, è stato osservato che l'inerte calcitico migliora la microstruttura e la tessitura delle malte durante la carbonatazione, perciò quest'inerte è stato preferito alla silice.

- Nelle malte sono stati aggiunti anche due componenti idraulici: un cemento Portland bianco e un metacaolino. Il primo componente si è dimostrato nocivo per la durevolezza delle malte, per cui il suo uso è stato definitivamente scartato. Il secondo, invece, ha migliorato le proprietà fisico-meccaniche delle malte. Tuttavia, le malte presentavano ancora una porosità troppo alta, per cui si è considerato necessario l'uso di addizioni che riducono la quantità d'acqua.

- La perlite ha favorito la diminuzione della densità delle malte e della quantità d'acqua ed, inoltre, ha aumentato la loro lavorabilità. Il derivato di cellulosa ha ridotto la quantità d'acqua ed ha migliorato la capacità di ritenzione d'acqua da parte della calce. Infine, il plastificante ha aumentato leggermente la quantità d'acqua ma ha migliorato notevolmente la lavorabilità delle malte, favorendo la dispersione delle particelle di calce e quindi la loro reattività.

- Gli studi realizzati hanno anche messo in rilievo l'importanza della giusta scelta delle proporzioni agglomerante-inerte più adatte per intonaci da restauro.

Questa Tesi di dottorato centra gli obiettivi iniziali proposti, riguardo alla selezione dei componenti e le dosi più appropriate per il disegno di malte da intonaco compatibili e, allo stesso tempo, durevoli. Inoltre, questa Tesi fornisce nuove conoscenze sui metodi di analisi e nuove linee guida per la preparazione di malte di calce.

Summary

Since the invention of Portland cement, almost two centuries ago, the industrial production of mortars led to the diffusion of such an enthusiasm among architects and engineers that the Portland cement replaced the traditional mortars in the totality of new fabrics. Regrettably, this occurred also in old buildings, in which cement was irrationally used as repair material. The incompatibility of cement with the traditional building materials resulted in the acceleration of the decay processes, with final, irreversible damages to our architectural and artistic heritage. Professionals are now demonstrating a renewed interest towards the use of traditional mortars, especially lime-based ones, because they ensure compatibility, suitability and longevity. However, the manufacturing techniques adopted in the past cannot be recovered in modern times, since other requirements, such as manufacturing costs and times must be taken into account.

This PhD thesis aims to contribute to the preservation of our architectural heritage, by providing the basis for the design of new repair rendering mortars that can be produced and marketed on an industrial scale. To this purpose, mortars components and preparation methods were selected by taking into account both restoration and industry requirements.

Most of the common analytical techniques for mortars characterization were used to develop this research:

- Components and mortars have been characterized by means of chemical (X-ray fluorescence; ion chromatography) and mineralogical (X-ray diffraction; thermogravimetry) techniques and their texture and microstructure have been studied by means of optical, scanning and transmission electron microscopies.
- Mortars performances in the fresh state were assessed by means of standardized (flow test) and no-standardized ("wet packing method") methods. Furthermore, different rheological devices have been used to characterize the behaviour of the dry hydrated limes in suspension, which is related to the mortar workability.
- Mortars physical-mechanical properties in the hardening state were determined by performing hydric tests (free water absorption and drying; capillary uptake; hydraulic conductivity; water vapour permeability) and mechanical assays. Moreover, physical-mechanical no- and low- destructive techniques, such as ultrasounds and a micromechanical press, were also successfully used for the textural characterization of mortars.
- New specific laboratory tests were designed to study the durability of mortars and the mechanisms of decay induced by temperature and humidity variations, rain, freeze-thaw cycles and salt attack.

The initial components selected in this thesis were: two dry hydrated limes of calcitic and dolomitic composition, calcareous and siliceous

aggregates with continuous and discontinuous grading, two hydraulic components used as additives and three admixtures. The dry curing conditions to which mortars were exposed during the study have been crucial in the selection of the most suitable components and dosages for repair rendering mortars, which are indicated below:

- Calcitic and dolomitic dry hydrated limes have a very different microstructure that influences their behaviour in suspension and, consequently, the final workability of the mortar paste, which is higher when using the dolomitic lime. However, the dolomitic mortars showed a much higher shrinkage and worse performances during hardening than the calcitic ones. Therefore the use of the dolomitic lime was discarded in this research.
- The use of a calcareous or siliceous aggregate have a direct influence upon the amount of kneading water needed, then the initial open porosity, which was higher in mortars with the calcareous aggregate. However, it has been observed that the calcareous aggregate induced a better improvement of mortar microstructure and texture during carbonation, then the preference towards this aggregate.
- Two hydraulic components were added to mortars: white Portland cement and metakaolin. The former turned out to be a deleterious component for mortar durability and its use was definitively discarded. The latter, on the contrary, improved the physical-mechanical properties of mortars. However, mortars still presented a high porosity, so that different admixtures were used to reduce the water content.
- Perlite enabled to reduce the mortar density and water content and improve the workability. A cellulose derivative enabled to further reduce the amount of kneading water and to increase the water-retention capacity of the lime. Finally, a superplasticiser increases slightly the water content but it improves the workability of mortars, by favouring the dispersion of lime particles, therefore, their reactivity.
- The studies performed also highlighted how to assess the most suitable binder-to-aggregate proportions for repair rendering mortars.

This PhD thesis accomplishes the objectives initially proposed, regarding the selection of suitable components and dosages for the design of compatible and durable repair rendering mortars. Furthermore, it provides new insights into the testing methods and useful guidelines for the preparation of aerial lime-based mortars.

1. INTRODUCTION

1.1. General Introduction

1.1.1 Subject of the Research

During the last few decades the use of lime has been gradually reassessed in the field of architectural heritage. After almost a century, during which the use of lime has declined in favour of Portland cement, lime mortar is now generally accepted as being the most suitable type of mortar for repair interventions. Nevertheless, the prolonged abandonment of its use has led to a loss of knowledge about the traditional manufacturing techniques involved, with the consequence that recovering the quality achieved with lime in the past is a difficult challenge.

By means of recent research carried out into construction materials employed in historic buildings, we have reached a deeper understanding of the compositional characteristics and performances of the lime mortars used in the past. The hardening processes occurring in lime mortars, together with the mechanisms and variables that determine them, have been investigated, revealing the influence of all these parameters on the final quality of the mortar [1].

Thanks to recent advances in the study of lime mortars the scientific world is managing to convince industry that it is necessary to distinguish between materials according to their use, especially when our historic and artistic heritage is at stake. In this way, the production of more suitable "traditional" mortars is being encouraged. The production of repair mortars, however, presents a considerable task for industry because of a series of aspects that hinder a faithful re-establishment of the materials available in the past. In modern times, the output of an industrial process is reflected not only in the quality of the products involved but also, and above all, in manufacturing times and costs. Furthermore, there are no standards referring to the production of lime mortars and this makes their reproduction more complicated at an industrial level, especially bearing in mind the functional and constructive versatility of lime mortars. All these aspects have a direct influence upon the outcome of both the industrial process and restoration work.

In spite of these problems, ready-to-use repair mortar finds itself in ever-increasing demand. Within this context, the subject of this thesis is to design rendering mortars that can be produced and marketed on an industrial scale and at the same time applied as repair materials in historic buildings. This means that both industrial and repair requirements must be taken into consideration for the development of these new materials.

1.1.2 Objectives of the Research

The main objectives of this thesis are:

- to select the most compatible components and suitable proportions for repair rendering mortars;

- to consider new methods for assessing the quality of fresh aerial-lime-based mortars and their hardening processes;

- to gauge the durability of rendering mortars by conducting new laboratory tests;

The final aim of these studies has been to design ready-to-use repair mortars for rendering purposes.

1.1.3 Problems and Limits of the Research

In recent decades there have been many attempts to produce industrial repair mortars, as demonstrated by the wide amount of ready-to-use repair mortars available on the market. As proved by different researchers [2,3] and as indicated in some technical specifications, these products are mostly hydraulic and, in some cases, aerial mortars containing small amounts of cement. These mortars generally have higher compressive and flexural strengths, lower capillary porosity and water absorption and are more resistant to water-vapour transmission compared to traditional lime mortars [3]. For these reasons most restorers still prefer traditional mortars, prepared *in-situ*, to ready-to-use ones.

Only lately have we begun to be truly aware of the damage caused by the use of mortars made with Portland cement, which is basically an industrial building material that has also been used indiscriminately in repairing architectural heritage, and is still being used as a secondary component in repair mortars. In fact it is difficult to conceive of any kind of close relationship between "industrial production", which always seems to entail "mass production" and the smaller, more specialised needs of the restoration of old buildings and monuments.

Thence the questions:

Is it possible to produce a mortar to repair any type of historic building regardless of the wide variety of building materials and techniques originally employed in their construction? And will this mortar always fulfil the specific requirements of suitability and compatibility?

The answer to these questions may well turn out to be affirmative, even if with some reservations concerning the initial assumptions made, as commented upon more fully below:

a) The first step in the design of any type of repair mortar is to establish the basic requirements that the material must meet. Thus, studies carried out into the deterioration of masonry structures clearly stress the importance of the compatibility between the repair material and the original masonry.

"Compatible is defined as: not causing any damage (in a broad sense, ranging from technical to aesthetical and historical) to the existing fabric and being as durable as possible under that condition" [4].

When the original materials are unknown, as is the case with a general rendering repair mortar, compatibility is ensured firstly by selecting

mortar components that are harmless to the original masonry such as aerial or hydraulic lime without cement, dolomite-free aggregate, chloride-free additives, materials that do not release soluble salts and so on.

b) Secondly, it is fundamental to achieve specific characteristics in the mortar according to its intended function in the masonry (in this case rendering, *cf.* Section 1.2.2).

c) In relation to point b, it is important to consider that the substrate (stone, brick, concrete etc.) should also play a role in the final performance of the mortar. For example, the same render may shrink by different degrees when applied to substrates with different suction characteristics and this might require a mortar with high water-retention capacity.

d) Finally, to design a repair mortar the climatic conditions to which the mortar will be exposed (*e.g.* dry, low-moisture, high-moisture) must be taken into account. From a certain point of view this limits the application of any one type of mortar everywhere in the world. Nevertheless, this condition is crucial for the design of durable mortars.

Hughes's statement [5] about repair actions and mortar specifications can be regarded as a summary of these points:

"A mortar repair action can be classified by the function of the mortar, constrained by the typology of the masonry itself and influenced by the choice of binder type".

In the specific case of this research, the main objective of which is to design a dry, ready-to–mix, rendering mortar, there are further aspects that need to be commented upon with regard to the limits set by industrial production:

e) In relation to point a, the binders selected in this thesis are dry hydrated aerial limes. Despite the superiority of lime putty (lime as a paste) compared to the dry hydrated one (*cf.* Section 1.2.3), the former has had to be discarded in this research since it is incompatible with supplying ready-to-use mortars as dry powder.

f) As far as this last consideration is concerned, there are preparation methods that could not be adopted in this research either. One of these concerns the way of mixing mortar components: as a general rule, it is better to reduce the lime to a paste, *i.e.* to mix it with water, before adding other ingredients such as the aggregate [6]. In spite of this, industrial production requires the dry components (lime, aggregate and additions) to be mixed simultaneously and the water to be added later on site in the quantity set out in the technical specifications.

In spite of these limits, the employment of ready-to-use mortars entails important advantages compared to traditional ones, such as a guarantee and quality control of the components and easier application. Moreover, it is also important to point out that the performance of ready-to-use mortars cannot be influenced by any subjective criterion on the mason's part, so that potential "personal" mistakes during mixing are greatly reduced.

1.1.4 Outline of the Research

This thesis is divided into four main parts, included in the Results and Discussion chapter (Chapter 3), the contents of which in summary are as follows:

PART I: An assessment of the compatibility and suitability of limes and aggregates in repair mortars.

- *Chapter I.1*: A study of the relationship between the microstructure of lime and its rheological properties in suspension. A comparison between two dry, hydrated limes. one calcitic and the other dolomitic.
- *Chapter I.2*: A study of the performances during the hardening of calcitic and dolomitic lime mortars cured under dry conditions.
- *Chapter I.3*: A two-year study of the carbonation process in aerial lime-based mortars made with calcareous and siliceous aggregates. The relationship between the mineralogy and morphology of the aggregate and degree of carbonation and the properties of mortars during hardening.
- *Chapter I.4*: A textural characterization using ultrasound techniques of the carbonation process in aerial lime-based mortars made with calcareous and siliceous aggregates.
- *Chapter I.5*: A mechanical characterization using a micro-mechanical press of the carbonation process in aerial lime-based mortars made with calcareous and siliceous aggregate.

PART II: An assessment of the suitability of test methods.

- *Chapter II.1*: A study of the suitability of standardized and non-standardized methods for the correct mixing of aerial lime-based mortars.

PART III: An assessment of the compatibility and suitability of additions in lime-based mortars.

- *Chapter III.1*: A study of the compatibility of a white Portland cement added to an aerial lime-based mortar.
- *Chapter III.2*: A study of the mineralogical, textural and physical-mechanical modifications induced by the use of metakaolin and different admixtures in aerial lime-based mortars. Selection of the most suitable additions and proportions for rendering purposes.

PART IV: An assessment of the durability of rendering repair mortars.

- *Chapter IV.1*: A study of the hydric behaviour and plastic shrinkage of mortars designed for rendering purposes.
- *Chapter IV.2*: An experimental durability study of mortars designed for rendering purposes.

1.2. The design of repair mortars: history, state of the art and general requirements

With hindsight many of the repair works carried out on architectural heritage during the last century have been erroneous. Portland cement, used indiscriminately in the majority of deteriorated historic buildings, has led to highly regrettable, irreparable damage. Nowadays restoration works must fulfil three basic requirements that have become the focal point for restorers, architects and engineering-designers: sustainability, compatibility and longevity. Looking back, the only material that accomplishes these requirements is without doubt lime [7-9].

The following sections define the basis from which the present research has been developed by dealing with some of the general aspects surrounding the design of lime-based repair mortars, and rendering mortars in particular, and more specific features such as their limits, requirements, materials and properties.

1.2.1 Standards concerning mortars and problems involved in their application to repair mortars

The first known regulations concerning construction materials and techniques are contained in Vitruvius's multi-volume work *De Architectura libri decem* (Ten Books on Architecture). This complete, detailed handbook represents the only remaining record of the Romans' approach to architecture, and much of it is still valid today.

In modern times, tests methods for the manufacture and quality control of mortars are specified in the European (EN) and North American (ASTM) standards. The test methods in these standards are classified according to the state of the mortar (*i.e.* fresh or hardened) but not according to its final function (structural, grouting, pointing, flooring, rendering, plastering etc.) and they refer mainly to industrial mortars in which a hydraulic binder (cement) is used. More specific guidance on the testing and design of repair mortars is to be found in the RILEM recommendations. These publications provide considerable support for restorers, architects and researchers working in the field of architectural heritage conservation. Nevertheless, the scientific community still relies completely upon the EN and ASTM standards for the assessment of repair mortar properties. This has led, on the one hand, to a notable homogeneity of methods arising within different countries. On the other hand, many inconsistencies have derived from the application of these test standards to lime-based repair mortars due mainly to the fact that most of the equipment and methods used, ranges of values suggested, curing conditions established and proportions provided turn out to be incompatible with repair lime-based mortars. These aspects can make the results meaningless, unless they are merely assumed for comparative purposes.

To overcome these limits it is feasible to adopt some modifications of the standards that comply more closely with the specific mortar in question [10,11].

In Spain, the *Asociación Nacional de Fabricantes de Morteros* (AFAM) (the National Association of Mortar Manufacturers) has published a guide [12] that tackles the general aspects of the study and manufacture of mortars in order to encourage its correct use. Although this handbook provides practical and useful skills for architects and masons, it still deals with cement mortars, with the consequence that it does not completely fill the gap existing between industry and restoration.

1.2.2 Rendering mortars

Rendering is the practice of covering a wall or a building façade with one or more layers of mortar (Fig. 1). Being the layer most exposed to weathering agents such as water, salts, pollutants and so on, renders are considered to be "sacrificial layers" that fulfil a protective function towards the substrate and the whole masonry of stone, brick, concrete, adobe or the like [13-16].

Figure 1 *Examples of renders in modern and ancient buildings.*

In many cases, a render is a finishing or decoration layer (Fig. 2) but it never has a structural function [17]. As the external layer of a building, a render also plays an important role in the energy balance of the building itself [18].

Figure 2 *Examples of decorated renders.*

Environmental conditions during rendering must also be born in mind; for example:

- rendering should not be undertaken in the rain and any surface already rendered must be covered with plastic sheeting;
- rendering is not to be recommended in very hot or windy conditions and if it is done the surface must be wetted down to avoid rapid drying.

Generally, the recommended temperature range for rendering applications is between 5ºC and 30ºC [19].

Rendering can be done in one or more layers, the thicknesses of which generally range from 1 to 2 centimetres [19], although under certain circumstances very thin or thick coats have been applied since ancient times [14]. When two layers are applied it is important to ensure that the first layer is completely dry before applying the second one (Fig. 3).

Figure 3 *Examples of bad rendering: the second layer has been applied before the first one was completely dry and this has produced large, irregular spots that alter the final colour.*

The aggregate dosage varies according to the proximity to the surface. In the initial layers, *i.e.* those closest to the substrate, a "lean" mortar, with a higher aggregate content, is recommended, whilst in the final layers it is better to apply a "fat" mortar, with lower aggregate content. In this way the more resistant first layers are able to withstand the shrinkage undergone by the final ones [20]. The render is often applied on a polyester mesh, which ensures better adhesion between the substrate and the render (Fig. 4a) [19]. The render can be finished off in many different ways: trowelled (Fig. 4b), smoothed, sculpted (Fig. 4c), sponged, dragged and so on, according to the final visual aspect required.

Figure 4 *Example of render application on a polyester mesh (a) and renders with trowelled (b) and sculpted (c) finishes.*

Lime-based rendering mortars are often characterized by high plastic shrinkage, that is to say, a reduction in volume caused by a rapid drying, with the corresponding formation of fissures (Fig. 6), a phenomenon which is increased by the presence of an aerial lime, by an extensive surface exposed to the air and, eventually, by high temperatures. By using the right amount of water it is possible to reduce shrinkage and improve the mechanical properties of a mortar. According to Burnell [6]:

"All limes lose two-fifths of their strength if mixed with too much water. It is then better to wet the materials to be used and to employ a stiff mortar,

than to follow the course usually adopted by masons and bricklayers of using very soft fluid mortar".

The general technical requirements established by Groot [14] for repair renders and plasters are:

- not to damage the existing substrate, which implies compatibility;
- not to be stronger than any existing old mortars;
- to be flexible enough to spread and fill lacunae;
- to adhere well to the masonry;
- to have a low tendency to shrink;
- to resist local adverse environmental conditions as much as possible.

Thus, the specific technical requirements for a render are [14]:

- moderate capillary water absorption;
- high vapour transmission [5];
- some degree of surface hardness;
- low amounts of released salts;
- good resistance to soluble salts;
- good resistance to freeze-thaw cycles;
- colour and texture compatibility with the objectives defined for the intervention.

1.2.3 Lime

The properties of a mortar are controlled mainly by the binder and then by the aggregate and additions used. This means that by using one or another binder it is possible to obtain mortars that meet different requirements and functions. Lime has been the binder of preference in the majority of construction works undertaken by man over the last five thousand years. Throughout this long period its use has spread to most civilizations across most of Europe, America, North Africa and West Asia. Evidence for the practice of burning limestone to produce lime goes back to 2450 B.C. [21]. But, despite this, little information about lime exists today because of the rapid abandonment of traditional lime mortars and their replacement by industrially manufactured, hydraulic mortars after the invention of Portland cement in 1824. The reduction of manufacturing costs and times achieved thanks to the standardization of Portland cement encouraged its rapid diffusion through the world of industrial construction and, regrettably to architectural heritage as well [22,23] (Fig. 5). Fortunately, over the last 50 years the constructive value of lime is being reconsidered and a big effort is being made to recover our knowledge about its use.

Nowadays masons prefer aerial to hydraulic lime for repair works, especially for rendering and plastering, in spite of its high water needs and the fairly slow setting [24]. One of the reasons for this preference is the improvement in workability and increase in workable time when using aerial lime. The inclusion of this lime in renders ensures a mortar with high vapour transmission, medium water penetration and freeze-thaw resistance and low thermal dilatation and strength [5]. Moreover, from the aesthetic point of view aerial lime is the most compatible with the original

materials: its neutral colour and the wide range of colours and shades that can be obtained with the addition of pigments ensure the preservation of the original colour of the masonry [25].

Figure 5 *Examples of bad restorations, in which Portland cement (indicated by the arrows) has been used.*

Even if its use is currently limited, lime putty is still the most suitable raw material for rendering as well as implementing decorative techniques such as stucco, lime painting and painting al fresco [20,25]. Lime putty has been produced since ancient times by storing the lime under water for many years. It has been found that this type of aging causes micro-structural modifications in portlandite crystals that lead to an increase in the specific surface area and an improvement in its rheological properties [26]. This has a positive effect upon the carbonation process and consequently the final properties of the mortar [27]. Dry hydrated limes, on the other hand, do not show the same excellent rheological properties as lime putty [28], because they are characterized by iso-oriented crystal agglomerates that give rise to an increase in particle size and a concomitant decrease in their specific surface area [29].

In spite of the superiority of lime putty, dry hydrated lime is nowadays the most widely used product in the making of mortars since it is easier and cheaper to produce. Moreover, the lime standardization process guarantees uniformity of composition and controls the presence of impurities in the lime. Standard EN 459 [30] lays down the specifications for each type of lime, classified mainly according to their chemical composition (*i.e.* content in CaO, MgO, SO_3 etc.) and state (slaked or otherwise). In the near future standard EN 459 [30] is to be reviewed and a new group of standardized limes will be taken into account: formulated limes (FLs). This group includes aerial limes mixed with natural hydraulic

lime (NHLs), possibly with pozzolanic, organic and/or mineral additives, among others. Nevertheless, as explained by Middendorf et al. [31], little is known about the properties of the fresh and hardened states of mortars prepared with these types of lime.

Recently, a traditional mortar made with quicklime, known as "hot lime mortar" has been re-considered for restoration work. This kind of mortar is produced by means of a method dating back to ancient Greece [32] and consists of mixing the aggregate with quicklime prior to slaking. Hot lime mortars are extremely workable due to the high water-retention capacity of the paste, as well as having a very compact microstructure, low porosity and far fewer shrinkage fissures compared to normal lime mortars. Moreover, these mortars contain a large number of not interconnected round pores, resulting in high resistance to freeze-thaw cycles [33]. The most crucial aspects of hot lime mortars are their high plasticity and applicability even during the hardest winter months. Despite these advantages, it is evident that hot lime mortars cannot be produced industrially, because of both the preparation method and the long maturation periods required for these mortars [34].

1.2.4 Aggregate

The aggregate is a mortar's "skeleton"; it gives it its mechanical properties and, more importantly in the case of a render, confers volume stability to the mixture, thus reducing plastic shrinkage. It is widely recognized that the characteristics of the aggregate, such as mineralogy, form and grading, have an influence on the mortar's properties (workability, flow ability, compressive strength, porosity, water absorption and permeability) in both its fresh and hardened state [35-37]. Thus, for example, the form and grading of the aggregate influence the packing of the mass. In a well-packed aggregate, voids between particles of the same size are filled by smaller particles and this provides greater compactness. The presence of a fine fraction plays an important role in the packing of the aggregate. According to Romagnoli and Rivasi [38], a mixture is densely packed when it contains a higher percentage of fine than coarse or medium-sized grains. Moreover, they also observed that mixtures of fine and coarse sands give a higher density compared to mixtures of medium and coarse sands, because of the proximity of these two latter sizes. Venkatarama and Gupta [37], on the other hand, observed that mortars made with fine sands showed a high drying shrinkage and a reduction in tensile bond and compressive strength compared with mortars made of coarse and medium sands, which required less water during their preparation.

The properties of fine sand, including particle shape, surface area, grading, roughness, sphericity and volume, do indeed influence the water content. Westerholm et al. [39] observed that aggregates with an angular shape, rough surface (crushed sands) and large surface area need more water than round aggregates with a smoother surface (natural sands). The characteristics of fine sands also influence the mortar's rheological

properties, such as its workability and fluidity when fresh. In particular, an increase in the fineness of sand and in the mortar's fines content influences its yield stress, that is,the stress required for the mass to flow, whilst the shape of the particles influences its plastic viscosity [40,41], which increases when crushed sands instead of natural sands are used [39]. Furthermore, the use of coarse aggregates seems to favour the formation of voids, especially between the matrix and the grains, which increases the rate of water absorption. Consequently it is essential to choose the correct sand grading in the design of mortars.

Since the beginning of the XX century many models for mixtures with maximum packing density have been proposed but for the most part these theoretical models have proved to be unrealistic when compared to real systems [42]. Feret [43] was one of the first researchers to conduct studies into aggregate mixtures for concretes; he suggested that maximum compactness in concretes is achieved when coarse and fine particles are mixed, excluding medium sizes. In spite of this suggested discontinuous distribution, Fuller and Thompson [44] found that continuous granulometric curves provided more workable concretes with higher mechanical strengths. The distribution proposed by Fuller and Thompson, known as Fuller's method, contains a mixture of dispersions in which all particles are exactly the same size [45]. A similar approach was adopted by Furnas [46] but his work was not directed toward any specific material. Simultaneously, Andreasen and Andersen [47] came up with another packing model based on continuous distribution. The authors described a system in which all particle sizes were represented. Some years later Dinger [45] verified that the continuous approach proposed by Andreasen and Andersen was correct and at the same time found a relationship between Andreasen's and Furnas' packing theories. Hence, he modified these two models and constructed a new one that described the particle-size distribution of aggregates in greater detail.

Among the many ideal granulometric curves proposed, and probably the most widely accepted for concretes, is that of Bolomey [48]. This model represents a modification of Fuller and Thompson's theory: it includes a higher content of fines and the shape factor in the calculation of particle packing to improve the workability of the mass when fresh.

Nowadays the aggregate grading and fines content to be used in mortars and concrete have been standardized in the current norm [49-51], although there is still some confusion about the most suitable granulometric theory that should be applied to achieve optimum aggregate packing. Indeed, differences of opinion are still to be found concerning the advisability or not of using continuous or discontinuous granulometric curves [38,52].

1.2.5 The use of pozzolans in mortars

Aerial lime does not always guarantee durability, especially in moist climates, coastal areas or dry climates with high levels of pollution, which cause damage by acid attack, with the consequence that the use of aerial-lime mortars with some level of hydraulicity is advisable [17].

Studies of ancient mortars have revealed that the addition of small amounts of hydraulic components such as pozzolans, fly ashes, silica fumes, calcined clays, brick pebbles or dust to lime mortar was an efficacious way of improving its mechanical strength, permeability to water and durability as well as cohesion between the matrix and the aggregate [14,53-56]. Such hydraulic components were also employed for decorative purposes [14]. The Romans were also aware of the advantage of using pozzolanic components in mortars for improving their durability. They discovered that the addition of a volcanic brown material proceeding from the city of Pozzuoli in Naples, the so-called *pulvis puteolana*, allowed calcium hydroxide to be fixed under water, thus originating solid, insoluble, resistant mortars that they called *opus caementicium*. We still have many examples of the ample range of construction ability that the Romans were capable of thanks to the use of lime and pozzolans, among which are aqueducts, bridges, dams, theatres, amphitheatres, public baths and so on. The dome of the Pantheon (27-25 B.C) in Rome (Fig. 6) is perhaps one of the most magnificent results of the Romans' architectural capacity, which is, in Stendhal's words,

"Le plus beau reste de l'antiquité romaine c'est sans doute le Panthéon; ce temple a si peu souffert qu'il nous apparaît comme aux Romains" (*)
(*Promenade dans Rome*, 1829)

(*) "The most beautiful relic of Roman times is definitely the Pantheon; this temple had suffered so little that it appears to us in the same way as it did to Romans".

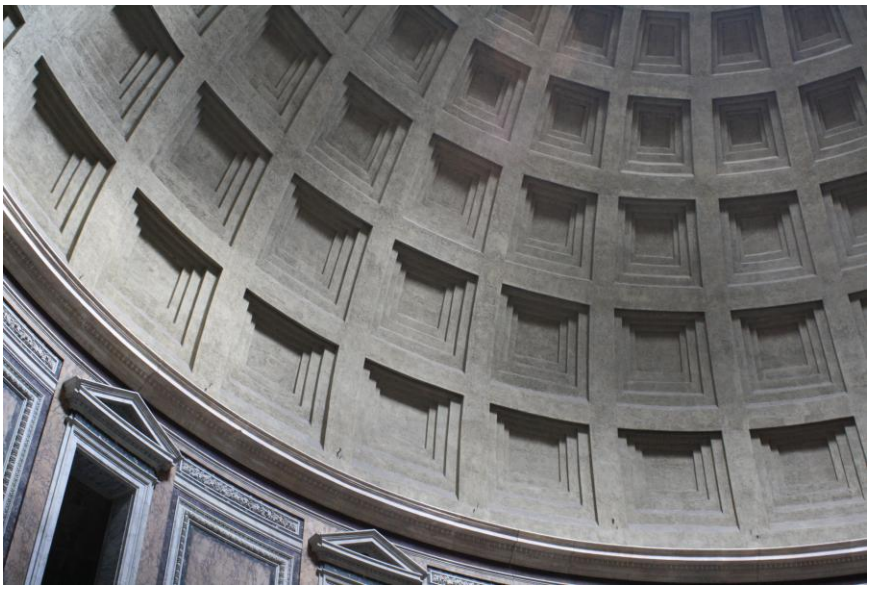

Figure 6 *Photo of the dome of the Pantheon (Rome, Italy).*

The construction of this dome, with a diameter of 43 m, was possible thanks to the use of hydraulic mortars of different composition that contributed to lightening its structure. It still holds the record for being the world's largest unreinforced concrete dome [57].

- ## Metakaolin

Metakaolin is one of the most commonly used pozzolanic materials nowadays, showing as it does a high degree of activity, below that of silica fume but above fly ashes [58]. It derives from the thermal activation of kaolin between 700 and 800ºC, a process that destroys the crystalline structure of clays and yields highly reactive and poorly crystallized phases such as aluminosilicates ($Al_2O_3 \cdot 2SiO_2$). Both mineralogical characteristics of raw kaolin [59] and calcining temperature [60,61] play a role in the reactivity of the metakaolin.

Added to lime pastes, the hydrated phases of metakaolin react with calcium hydroxide, yielding cementitious products, which afford added strength and durability to the mortar. Different phases develop during this reaction depending upon whether the binder is Portland cement or lime [62], the calcium-hydroxide content, water-solid ratio [63], curing temperature and time [64] and chloride content [65].

Several authors [62-64,66-68] have reported that the main hydrated phases formed at room temperature (20ºC) are calcium silicate hydrates ($CaO\text{-}SiO_2\text{-}H_2O$) and calcium-aluminate hydrates C_2ASH_8 ($Ca_2Al(AlSi)O_2(OH)_{10} \cdot 2.25H_2O$ [*stratlingite*].

A third hydrated product, C_4AH_{13} ($4CaO \cdot Al_2O_3 \cdot 13H_2O$), is a metastable phase that appears during the initial stages of hydration. During ageing at ambient temperature C_4AH_{13} spontaneously decomposes to the more stable solid phases C_3AH_6 (hydrogarnet) and portlandite [69]. Rojas and Cabrera [64] indicated the existence of C_4AH_{13} as a stable phase also in the absence of calcium hydroxide under the same curing conditions. These results were obtained in MK-lime pastes with different MK/CH and water/MK+CH [water-to-binder (w/b)] ratios. Murat [63] noticed that the highest compressive strength in lime pastes with the addition of metakaolin is attained when the MK/CH ratio is 1 and the w/b ratio is less than 0.75. He also observed that the presence of sand in mortars implies the use of higher amounts of water in order to reach an optimum consistence and that this modifies the theoretical w/b ratio. Moreover, the amount of calcium hydroxide available to metakaolin is lower than that expected because a slow carbonation of CH takes place in mortars cured at room temperature. Carbonation acts as a competitive reaction against the formation of hydrated phases [63,70,71] since the latter is more rapid at higher temperatures [64,72]. The prevalence of one of these two reactions, carbonation or hydration, influences the mechanical strength of mortar [73]. Wild et al. [74] observed that in ordinary Portland cement (OPC) mortars the enhancement of strength over short and long periods is due to three combined factors: the acceleration of OPC hydration, the filler effect and the pozzolanic activity of metakaolin. Many studies [74-81] have been undertaken to find the optimum amount of metakaolin required

to improve the physical properties of mortar. To this end, the effect that different contents of MK have on hydration rate, pore structure, mechanical strength, water absorption and sulfate resistance have been investigated. According to these tests, the best performances are obtained by adding 10-20 wt% of MK to OPC mortars.

Apart from its beneficial structural and mechanical properties, metakaolin is also appreciated for its "chromatic transparency" [82], which is a crucial aspect of restoration.

1.2.6 The use of admixtures

The use of admixtures is an ancient practice in the field of construction, as already indicated by Vitruvius in *De Archirectura libri decem*. Evidence exists for the addition to lime mortars of organic substances, especially proteinacious ones such as blood, hair, straw, milk, eggs etc. [83] and sugar-based gums and animal glues etc. [7,84,85] to improve their workability, waterproofing, mechanical resistance and durability. Unfortunately, records of the dosages no longer exist and neither are their effects on ancient mortars fully understood.

Nowadays admixtures are essential components of building materials and masons greatly appreciate their use [24]. Nevertheless, their composition, function and characteristics have substantially changed over time since they have had to adapt not only to modern construction techniques but also to the new requirements demanded of industrial mortars.

The effects produced by some industrial additives on the properties of lime mortars were almost unknown until the last decade because research into these materials was limited to cement mortars and concrete [86]. Only lately have researchers been investigating the advantages and disadvantages of the use of admixtures in lime mortars [87-93]. Different additives can be used depending upon the property of the mortar that needs to be improved. Generally these substances are distinguished according to the moment in the mortar's life at which they must act: when fresh during mixing and application, during drying and hardening, or in its hardened state.

- **Admixtures to reduce shrinkage: plasticisers and water-retaining, water-reducing agents and air-entraining agents.**

Plastic shrinkage is closely related to the water-retention capacity of lime and fines, which in turn depends upon the specific surface area and degree of agglomeration of the particles, among other factors (*cf.* Section 1.2.3). Avoiding or reducing particle agglomeration results in an increase in specific surface area and consequently to an improvement in mortar viscosity [29]. Particle dispersion also leads to a reduction in the amount of kneading water necessary to achieve optimum consistence and workability. It is known that plasticisers and water-retaining agents prevent particle agglomeration by attaching themselves to the surface of

the particles. This causes repulsion among the particles and leads to an improvement in the rheological properties of the mortar [89]. The dispersing properties of a plasticiser depend especially upon the molecular weight and anionic groups of the polymer [94]. It has been demonstrated that long-chain polymers, with a high molecular weight, such as polycarboxylates, have a greater dispersing effect [95].

Other admixtures relatively new to lime mortars are the so-called "super absorbent polymers" (SAP), which act as water-retaining agents [96] and reduce shrinkage [97]. These admixtures may, however, worsen the mortar's workability with the consequence that a plasticiser is also required [88].

The effects on mortars of organic polysaccharides such as starch, pectin, alginates and cellulose derivatives have been subject to considerable scrutiny since they have shown themselves to behave as good plasticisers, dispersing agents, and water-retaining agents. For example, starch confers better hydric and mechanical properties and higher durability on lime mortars when it is added in a proportion of 0.5% of the total mass [92]. Moreover, Nopal juice and mucilage (from *Opuntia ficus-indica*) improve considerably the hardened performances of lime mortars due to their dispersing effect [98,99]. This substance is added to the kneading water of repair lime mortars in different areas of Mexico and in the southern United States [98,100].

Other additives that reduce shrinkage are air-entraining agents. Their effect relies on the introduction of small air bubbles ($10<ø<500$ μm) into the mortar matrix during mixing. Besides reducing mortar density these bubbles also reduce any subsequent water penetration into mortar, thus improving its resistance to freeze-thaw processes.

- ## Admixtures to improve durability

Lack of durability in a lime mortar is mainly related to its capillary porosity and interconnections among pores, which favour, on the one hand, the entry of water, salts and contaminants and, on the other, the dissolution of Ca, which goes on to react with SO_2 and NO_x, thus producing soluble salts.

There exist different types of admixtures that help to reduce the harmful effects of these weathering mechanisms in lime mortars, among which are:

- the addition of barium hydroxide to increase durability towards acid rain and sulphate attack [101];
- the use of linseed oil (in quantities up to 1%) to improve resistance towards salt crystallization processes and freeze-thaw cycles by acting as a water repellent [102];
- the inclusion of synthetic or natural fibres to improve compactness and deformability and reduce porosity, besides conferring thermal and acoustic insulating properties [103-105].

Similar properties are achieved with the addition of perlite, a very light, porous, fire-resistant material that derives from a fast heating of obsidian to temperatures between 900 and 1100ºC. Perlite has a very low density

due to air bubbles included inside it, which allow it to expand by as much as 15 to 20 times its original volume. Perlite's characteristics are so peculiar that it is employed in many industrial sectors. Its use as an aggregate, filler and additive to bricks and mortars results in a reduction in the number of shrinkage fissures, with a final improvement in resistance, workability [106] and insulating properties [107].

Diatomaceous earths are also effective in improving the resistance and insulating properties [107] and the durability (especially towards the attack of microorganisms) of mortars [108] and they also confer a certain degree of hydraulicity to the lime [109].

References

[1] Elert K., Rodriguez-Navarro C., Sebastián Pardo E., Hansen E., Cazalla O. Lime mortars for the conservation of historic buildings. Studies in Conservation 47 (2002) 62-75.
[2] Marie-Victoire E., Bromblet P. A new generation of cement based renderings: an alternative to traditional lime based mortars? International Workshop on "Historic Mortars: Characteristics and Tests". RILEM TC-167COM, University of Paisley, Scotland (1999).
[3] Jornet A., Mosca C., Cavallo G., Corredig G. Comparison between traditional, lime based, and industrial, dry mortars. Proceedings of the 2nd Historic Mortars Conference, Prague (2010).
[4] Van Hees R.R.P.J. Repair mortars for historic masonry. From problem to intervention: a decision process. RILEM TC 203-RHM, Prague (2010).
[5] Hughes J.J. The role of mortar in masonry: an introduction to requirements for the design of repair mortars. International Workshop on "Repair mortars for historic masonry". RILEM TC 203-RHM, Prague (2010).
[6] Burnell G.R. Rudimentary Treatise on Limes, Cements, Mortars, Concretes, Mastics, Plastering, Etc. Ed. London G. Weale (1900).
[7] Cowper A.D. Lime and Lime mortars. Donhead Ed. (1927), reprinted by Building Research Establishment Ltd. In 1998.
[8] Groot C., Bartos P., Huges J. Historic mortars: characteristics and test concluding summary and state of the art. International Workshop on Historic Mortars, Paisley (UK) (1999).
[9] Maurenbrecher A.H.P. Mortars for repair of traditional masonry. Practice Periodical on Structural Design and Construction 9 (2) (2004) 62-65.
[10] Cazalla O. Morteros de cal. Aplicación en el Patrimonio Histórico. PhD Thesis, Universidad de Granada, Spain (2002).
[11] Bicer-Sismir B. Testing of repair mortars for historic masonry. RILEM TC 203-RHM, Prague (2010).
[12] Boletín AFAM. Morteros. Guía General. (2003).
[13] Hall C., Hoff WD. Rising damp: capillary rise dynamics in walls. Proc Roy Soc 463 (2007) 1871–84.
[14] Groot C.J.W.P. Performance and repair requirements for renders and plasters. International Workshop on "Repair mortars for historic masonry". RILEM TC 203-RHM, Prague (2010).
[15] Groot C.J.W.P., Gunneweg J. Two views to deal with rain penetration problems in historic fired clay brick masonry. Proceedings of the 2nd Historic Mortars Conference, Prague (2010).
[16] Wood C. Understanding and controlling the movement of moisture through solid stone masonry caused by driving rain. MSc Thesis, University of Oxford, UK (2010).
[17] Veiga M.R. Conservation of historic renders and plasters: from lab to site. Proceedings of the 2nd Historic Mortars Conference, Prague (2010).

[18] Barbero Barrera M.M. Mejora del comportamiento térmico de los morteros de cal aditivados y su empleo en la rehabilitación de inmuebles. PhD Thesis, Universidad Politecnica de Madrid, Spain (2011).
[19] AFAM. Morteros de revestimiento. Madrid (2006).
[20] ANCADE (Asociación Nacional de Cales y Derivados de España). Guía Práctica de la cal y el estuco. Grupo CALCINOR, Ed. de los Oficios, León (1998).
[21] Moropoulou A., Bakolas A., Anagnostopoulou S. Composite Materials in ancient structures. Cem Concr Compos 27 (2005) 295-300.
[22] Callebaut K., Elsen J., Van Balen K., Viaene W. Nineteenth century hydraulic restauration mortars in the Saint Michael's Church (Leuven, Belgium). Natural hydraulic lime or cement? Cem Concr Res 31 (2001) 397-403.
[23] Veniale F., Setti M., Rodriguez-Navarro C., Lodola S., Palestra W., Busetto A. Thaumasite as decay product of cement mortar in brick masonry of a church near Venice. Cem Concr Compos 25 (2003) 1123-1129.
[24] Hendrickx R. The adequate measurement of the workability of masonry mortar. PhD Thesis, Katholieke Universiteit of Leuven, Belgium (2009).
[25] Rattazzi A. Conosci il grassello di calce? $Ca(OH)_2$ + H_2O. Origine, produzione e impiego del grassello di calce in architettura, nell'arte e nel restauro. Ed. Edicom Monfalcone (2007).
[26] Rodríguez-Navarro C., Hansen E., Ginell W. Calcium Hydroxide Crystal Evolution upon Aging of Lime Putty. J Am Ceram Soc 81 (1998) 3032-3034.
[27] Cazalla O., Rodríguez-Navarro C., Sebastián E., Cultrone G., De La Torre M. J. Aging of Lime Putty: Effects on traditional Lime Mortar Carbonation. J Am Ceram Soc 83 (5) (2000) 1070-1076.
[28] Ruiz Agudo E., Rodríguez Navarro C. Microstructure and rheology of lime putty Langmuir 26 (6) (2010) 3868–3877.
[29] Rodríguez-Navarro C., Ruiz Agudo E., Ortega-Huertas M., Hansen E. Nanostructure and irreversible colloidal behaviour of $Ca(OH)_2$: implication in Cultural Heritage Conservation. Langmuir 21 (24) (2005) 10948–10957.
[30] EN 459 (2002). Description Building lime.
[31] Middendorf B., Klein D., Hogewoning S., Schmidt S-O. The new groups of formulated limes (FL) of lime standard EN 459 – Bane or Boon? Proceedings of the 2nd Historic Mortars Conference, Prague (2010).
[32] Moropoulou A., Tsiourva Th. Bisbikou K., Biscontin G., Bakolas A., Zendrit E. Hot lime technology imparting high strength to historic masonry. Constr Build Mater 10 (2) (1996) 151-159.
[33] Malinowski E., Hansen T. Hot lime mortars in conservation – repair and replastering of the facades of Läkö Castle. Proceedings of the 1st Historic Mortars Conference, Lisbon (2008).
[34] Margalha G., Veiga R., Santos Silva A., de Brito J. Traditional methods of mortar preparation: the hot lime mix method. Cem Concr Compos 33 (2011) 796-804.

[35] Hu J. Effects of aggregate on flow properties of mortar. Proceeding of the 2005 Mid-Continent Transportation Research Symposium, Ames, Iowa, August 2005.
[36] Stefanidou M., Papayanni I. The role of aggregates on the structure and properties of lime mortars. Cement and Concr Compos 27 (2005) 914-919.
[37] Venkatarama B.V.R., Gupta A. Influence of sand grading on the characteristics of mortars and soil-cement block masonry. Constr Build Mater 22 (2007) 1614-1623.
[38] Romagnoli M., Rivasi M.R. Optimal size distribution to obtain the densest packing: A different approach. J Eur Ceram Soc 27 (2007) 1883-1887.
[39] Westerholm M., Lagerblad B., Silfwerbrand J., Forssberg E. Influence of fine aggregate characteristics on the rheological properties of mortars. Cem Concr Compos 30 (2008) 274-282.
[40] Banfill P.F.G. Rheological methods for assessing the flow properties of mortar and related materials. Constr Build Mater 8 (1) (1994) 43-50.
[41] Bager D.H., Geiker M.R., Jenses R.M. Rheology of self-compacting mortars. Influence of particle grading. Nordic Concrete Research, Pubblication 25 (2001).
[42] Funk J.E., Dinger D.R. Predictive process control of crowded particulate suspensions. Applied to Ceramic Manifacturing. Kluwer Academic Publishers (1982).
[43] Feret R. Compacité des mortiers hydraulique. Annales des Ponts et Chaussées (1894).
[44] Fuller W.B., Thompson S.E. The laws of proportioning conrete. Proc Am Soc Civil Eng 33 261 (1907).
[45] Dinger D.R. Particle Packing and Pore Size Distributions. (1980) Volume 1, No. 9. (un update 2003) avalaible on www.dingerceramics.com
[46] Furnas C.C. Grading Aggregates, I, Mathematical relations for beds of broken solids of maximum density. Ind & Eng Chemistry 23 (9) (1931) 1052-1058.
[47] Andreasen A., Andersen J. Über die Bezieung zwischen Kornabstufung und Zwischenraum in Produkten aus losen Körnern (mit einigen experimenten). Kolloid-Zeitschrift 50 (1930) 217-228.
[48] Bolomey J. The grading of aggregate and its influence on the characteristics of concrete. Revue des Matériaux de Construction et Travaux Publiques, Edition C. 147 (1947).
[49] UNE-EN 933-1:1998/A1 (2006). Tests for geometrical properties of aggregates. Part 1: Determination of particle size distribution. Sieving method. AENOR, Madrid.
[50] ASTM C-144 (2004). Standard Specification for Aggregate for Masonry Mortars. ASTM International Standards Worldwide, Pennsylvania (USA).
[51] ASTM C-33 (2007). Standard Specification for Concrete Aggregates. ASTM International Standards Worldwide, Pennsylvania (USA).

[52] Von Konow T. Design of non-hydraulic and hydraulic lime mortars appropriate for restoration in the Nordic climate. Proceeding of the 1st Historic Mortars Conference, Lisbon (2008).
[53] Baronio G, Binda L. Study of the pozzolanicity of some bricks and clays. Constr Build Mater 11 (1) (1997) 41–46.
[54] Baronio G, Binda L, Lombardini N. The role of brick pebbles and dust in conglomerates based on hydrated lime and crushed bricks. Constr Build Mater 11 (1) (1997) 34–40.
[55] Papayianni I. The longevity of old mortars. Appl Phys A-Mater 83 (2006) 685–688.
[56] Papayianni I, Stefanidou M. Durability aspects of ancient mortars of the archeological site of Olynthos. J Cult Her 8 (2007) 193–196.
[57] Collepardi M. La lezione dei Romani: durabilità e sostenibilità delle opere architettoniche strutturali. Politecnico di Milano (2003) http://www.forumcalce.it/nel_restauro.html
[58] Frías M., Sánchez de Rojas M.I., Cabrera J. The effect that the pozzolanic reaction of metakaolin has on the heat evolution in metakaolin-cement mortars. Cem Concr Res 30 (2000) 209-216.
[59] Murat M. Hydration reaction and hardening of calcined clays and related materials. II. Influence of mineralogical properties of the raw-kaolinite on the reactivity of metakaolinite. Cem Concr Res 13 (1983) 511-518.
[60] Murat M., Comel C. Hydration reaction and hardening of calcined clays and related materials. III. Influence of the calcination process of kaolinite on mechanical strengths of hardened metakaolinite. Cem Concr Res 13 (1983) 631-637.
[61] Samet B., Mnif T., Chaabouni M. Use of kaolinitic clay as pozzolanic material for cements: Formulation of blended cement. Cem Concr Compos 29 (2007) 741-749.
[62] Frías M., Cabrera J. Influence of MK on the reaction kinetics in MK/lime and MK-blended cement systems at 20ºC. Cem Concr Res 31 (2001) 519-527.
[63] Murat M. Hydration reaction and hardening of calcined clays and related materials. I. Preliminary investigation on metakaolinite. Cem Concr Res 13 (1983) 259-266.
[64] Rojas M.F., Cabrera J. The effect of temperature on the hydration rate and stability of the hydration phases of metakaolin-lime-water systems. Cem Concr Res 32 (2002) 133-138.
[65] Saikia N., Kato S., Kojima T. Thermogravimetric investigation on the chloride binding behaviour of MK-lime paste. Thermochim Acta 444 (2006) 16-25.
[66] De Silva P.S., Glasser F.P. Phase relations in the system CaO-Al_2O_3-SiO_2-H_2O relevant to metakaolin-calcium hydroxide hydration. Cem Concr Res 23 (1993) 627-639.
[67] Ambroise J., Maximilien S., Pera J. Properties of metakaolin blended cements. Adv Cem Based Mater 1 (1994) 161-168.

[68] Moropoulou A., Bakolas A., Aggelakopoulou E. Evaluation of pozzolanic activity of natural and artificial pozzolans by thermal analysis. Thermochim Acta 420 (2004) 135-140.
[69] Matschei T, Lothenbach B, Glasser FP. The role of calcium carbonate in cement hydration. Cem Concr Res 37 (2007) 551–558.
[70] Wild S., Khatib J.M. Portlandite consumption in metakaolin cement pastes and mortars. Cem Concr Res 27 (1997) 137-146.
[71] Cizer O. Competition between carbonation and hydration on the hardening of calcium hydroxide and calcium silicate binders. PhD Thesis, Katholieke Universiteit Leuven, Belgium (2009).
[72] Cabrera J., Rojas M.F. Mechanism of hydration of the metakaolin-lime-water system. Cem Concr Res 31 (2001) 177-182.
[73] Fortes-Revilla C., Martínez-Ramírez S., Blanco-Varela M.T. Modelling of slaked lime-metakaolin mortar engineering characteristics in terms of process variables. Cem Concr Compos 28 (2006) 458-467.
[74] Wild S., Khatib J.M., Jones A. Relative strength, pozzolanic activity and cement hydration in superplasticised metakaolin concrete. Cem Concr Res 26 (1996) 10, 1537-1544.
[75] Khatib J.M., Wild S. Sulphate resistance of metakaolin mortar. Cem Concr Res 28 (1) (1998) 83-92.
[76] Frías M., Cabrera J. Pore size distribution and degree of hydration of metakaolin-cement pastes. Cem Concr Res 30 (2000) 561-569.
[77] Brooks J.J., Johari M.A.M. Effect of metakaolin on creep and shrinkage of concrete. Cem Concr Compos 23 (2001) 495-502.
[78] Courard L., Darimont A., Schouterden M., Ferauche F., Willem X., Degeimbre R. Durability of mortars modified with metakaolin. Cem Concr Res 33 (2003) 1473-1479.
[79] Lee S.T., Moon H.Y., Hooton R.D., Kim J.P. Effect of solution concentrations and replacement levels of metakaolin on the resistance of mortars exposed to magnesium sulfate solutions. Cem Concr Res 35 (2005) 1314-1323.
[80] Al-Akhras N.M. Durability of metakaolin concrete to sulfate attack. Cem Concr Res 36 (2006) 1727-1734.
[81] Parande A.K., Babu B.R., Karthik M.A., Kumaar D.K.K., Palaniswamy N. Study on strength and corrosion performance for steel embedded in metakaolin blended concrete/mortar. Constr Build Mater 22 (2008) 127-134.
[82] Pesce G.L.A., Ricci R. The use of metakaolinite as hydraulic agent of aerial lime plasters and mortars. A case study of Genoa (Italy). From the Proceedings of the HMC08 First Historical Mortars Conference, Lisbon (2008).
[83] RILEM TC 203-RHM: Repair mortars for historic masonry. Mater Struct 42 (2009) 853-865.
[84] Sickels L.B. Organic additives in mortars. Edinburgh Architecture Research 8 (1981) 7-20.
[85] Garate Rojas, E. Las Artes de la Cal. CBRIC-MEC, Madrid (1993).
[86] Edmeades RM, Hewlett PC Cement admixtures. Lea's Chemistry of Cement and Concrete. 5th ed. Arnold (1998).

[87] Ruiz-Agudo E, Rodriguez-Navarro C. Effects of additives on lime putty rheology: applications in the design of mortars for conservation purposes. Proceedings of the 1st Historic Mortars conference, Lisbon (2008).
[88] Paiva H, Esteves LP, Cachim PB, Ferreira VM. Rheology and hardened properties of single-coat render mortars with different types of water retaining agents. Constr Build Mater 23 (2009) 1141-1146.
[89] Seabra MP, Paiva H, Labrincha JA, Ferreira VM. Admixtures effect on fresh state properties of aerial lime based mortars. Constr Build Mater 23 (2009) 1147-1153.
[90] Izaguirre A, Lanas J, Alvarez JI. The use of water-repellent admixtures on the behaviour of aerial lime-based mortars. Cem Concr Res 39 (2009) 1095-1104.
[91] Izaguirre A, Lanas J, Alvarez JI. Aging of lime mortars with admixtures: durability and strength assessment. Cem Concr Res 40 (2010) 1081-1095.
[92] Izaguirre A., Lanas J., Alvarez J.I. Characterization of aerial lime-based mortars modified by the addition of two different water-retaining agents. Cem Concr Compos 33 (2011) 309-318.
[93] Ventolà L., Vendrell M., Giraldez P., Merino L. Traditional organic additives improve lime mortars: new old materials for restoration and building natural stone fabrics. Constr Build Mater 25 (8) (2011) 3313-3318.
[94] Vieira M.C., Klemm D., Einfeldt L., Albrecht G. Dispersing agents for cement based on modified polysaccharides. Cem Concr Res 35 (2005) 883-890.
[95] Winnefeld F., Becker S., Pakusch J., Gotz T. Effects of the molecular architecture of comb-shaped superplasticizers on their performance in cementitious systems. Cem Concr Compos 29 (4) (2007) 251–262.
[96] Yang T., Sun N., Guo W., Zhang J., Pei M., Wang Y. Effect of Super-absorbent Polymer as Admixture on the Mechanical Properties of Mortars. Adv Mater Res 306-307 (2011) 1683-1687.
[97] Kong X., Li Q. Influence of super absorbent polymer on dimension shrinkage and mechanical properties of cement mortar. J Chi Ceram Soc 37 (5) (2009) 855-861.
[98] Cardenas, A., Arguelles, W.M. & Gyocoolea, F.M. On the Possible Role of Opuntia ficus-indica Mucilage in Lime Mortar Performance in the Protection of Historical Buildings. J Professional Assoc for Cactus Development 3 (1998) 64-71.
[99] Hansen E., Baron, S., Kindon, A., Keeney, J. & Schilling, M. Factors to be considered in the evaluation of a traditional lime plaster technology: use of an aqueous extract of Nopal (Opuntia spp., Cataceae). WAAC Annual Meeting (1999).
[100] Heredia Zavoni E.A., Bariola Bernales J.J., Vargas Neumann J., Mehta P.K. Improving the moisture resistance of adobe structures. Mater Struct 21 (1988) 213-221.
[101] Karatasios I., Kilikoglou V., Theoulakis P., Colston B., Watt D. Sulphate resistance of lime-based barium mortars. Cem Concr Compos 30 (2008) 815-821.

[102] Checová E., Papayanni I., Stefanidou M. Properties of lime-based restoration mortars modified by the addition of linseed oil. Proceedings II Historical Mortars Conference, Prague (2010).
[103] Elfordy S., Lucas F., Tancret F., Scudeller Y., Goudet L. Mechanical and thermal properties of lime and hemp concrete (''hempcrete'') manufactured by a projection process. Constr Build Mater 22 (2008) 2116-2123.
[104] Erdogmus E., Armwood C.K., Haider H., Yang Y. Flexural Strength of fiber reinforced lime mortars for historic masonry structures. Proceedings II Historical Mortars Conference, Prague (2010).
[105] Arnaud L., Gourlay E. Experimental study of parameters influencing mechanical properties of hemp concretes. Constr Build Mater 28 (1) (2012) 50-56.
[106] Topçu I. B., Isikdag B. Manufacture of high conductivity resistant clay bricks containing perlite. Build Environ 42 (2007) 3540-3546.
[107] Barbero Barrera M.M. Characteristics and properties of lightweight lime mortars for renders. 1st WTA-International PhD Symposium on "Building materials and building technology to preserve the built Heritage", Leuven, Belgium (2009) 235-251.
[108] Wang J.Y., De Belie N., Verstraete W. J Ind Microbiol Biotechnol. Diatomaceous earth as a protective vehicle for bacteria applied for self-healing concrete. DOI 10.1007/s10295-011-1037-1 (2011).
[109] Kastis D., Kakali G., Tsivilis S., Stamatakis M.G. Properties and hydration of blended cements with calcareous diatomite. Cem Concr Res 36 (2006) 1821-1826.

2. MATERIALS AND METHODS

2.1 Materials used

2.1.1 Mortars components

Both the binders and the additives used in this thesis were industrial manufactured; hence, they were used in the form of dry powders. Aggregates used were natural and crushed.

- *Binders*

Calcitic lime (CL): dry hydrated lime (CL90-S, UNE EN 459-1 [1]) produced by ANCASA (CALCINOR group, Seville, Spain) and supplied by ARGOS Derivados del Cemento, S.L. (Granada, Spain)

Dolomitic lime (DL): dry hydrated lime (DL85-S, UNE EN 459-1 [1]) produced in United States of America and supplied by LHOIST-Recherche et Développement S.A. (Nivelles, Belgium).

White Portland cement (WPC): cement (BL II/A-LL 52.5 R, UNE EN 197-1 [2]) produced by CEMEX commercial (Valencia, Spain) and supplied by ARGOS Derivados del Cemento, S.L. According to the technical specifications of this product, its degree of whiteness (L*) is ≥ 85 [3].

The WPC was used in substitution of 25 wt.% of lime in the elaboration of some of the mortars designed in this thesis.

- *Aggregates*

Siliceous aggregate (SA): it is a natural granular aggregate (UNE EN 13139 [4]) with a granulometry in the range of $0.1 \leq ø \leq 0.5$ mm, proceeding from a quarry in Arcos de la Frontera (SIBELCO, Cadiz, Spain) and supplied by ARGOS Derivados del Cemento, S.L.

Calcareous aggregate (CA): it is a crushed granular aggregate (UNE EN 13139 [4]) with a granulometry in the range of $0.063 \leq ø \leq 1.5$ mm. The granulometry of this aggregate was obtained by the combination of three granulometric fractions of the same calcareous stone, proceeding from a quarry in Granada and supplied by ARGOS Derivados del Cemento, S.L.

The cumulative graph (Fig.1) shows the continuity in size grading of the calcareous aggregate, which approaches the Fuller model more than the other ones, and the discontinuity of the siliceous one, due to the absence of some size fractions in the grading of the latter. This is represented in the size distribution curves as a horizontal line that covers the lacking sizes.

Distribution moduli (n) for the calcareous and siliceous aggregates are shown in Table 1. According to the European standard classification for aggregate grading (UNE EN 933-2 [5]), both SA and CA can be classified as fine aggregates.

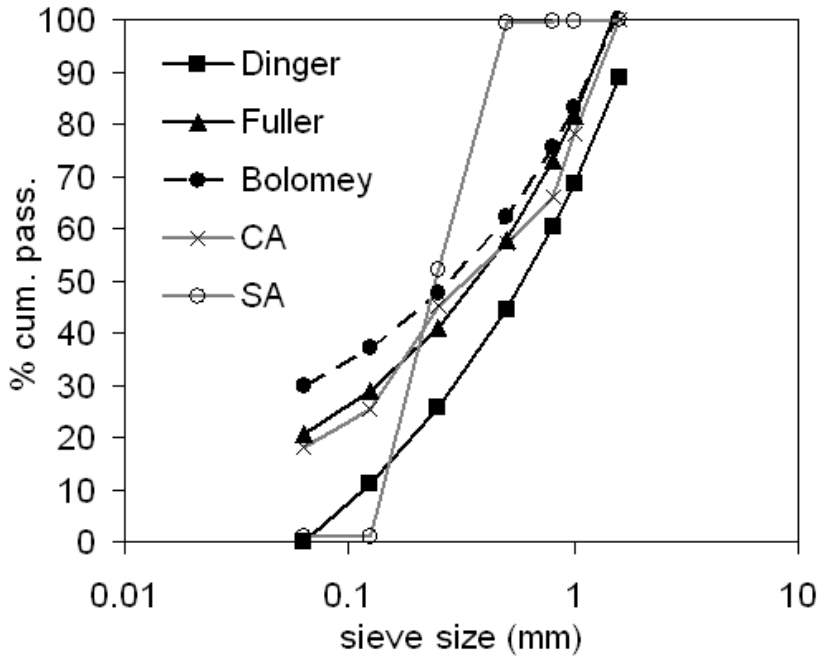

Figure 1 *Cumulative graph representing the cumulative percentage (% cumul. Pass.) of calcareous and siliceous aggregates grains passing from each sieve size (in log mm). Dinger', Fuller' and Bolomey's ideal granulometric curves are also represented in this graph, according to Eqs. 1, 2 and 3 (cf. section 2.2.1).*

Aggregate	n
CA	1.9±0.5
SA	1.5±0.5

Table 1 *Values of distribution modulus (n) for the calcareous (CA) and siliceous (SA) aggregates.*

- ***Additives and admixtures***

Metakaolin (MK): calcined clay (CLASS N POZZOLAN, ASTM C618-08 [6]), produced by Burgess Pigment Company (USA) and supplied by ARGOS Derivados del Cemento, S.L. This pozzolan was used in combination with the calcitic lime for the elaboration of some of the mortars designed in this thesis. Since this component was added in low amounts (10-20 wt.% of lime), MK was considered as an additive.

Perlite (P): Otaperl 0/1-TR, produced by Otavi Iberica Slu and supplied by ARGOS Derivados del Cemento. It is an expanded perlite, added as admixture with the function of lightweight aggregate.

Cellulose derivative (C): Tylose MHS 10012 P6, produced by SE Tylose GmbH&CO.KG (Germany) and supplied by ARGOS Derivados del Cemento. It is a methylhydroxyethylcellulose added as admixture with the function of water-retaining agent.

Polycarboxylate (R): Rheomix GT205 MA, produced by BASF Chemical Company and supplied by ARGOS Derivados del Cemento. It is a polycarboxylate with log side-chains added as admixture with the function of plasticiser.

Specific characteristics of these admixtures are reported in Appendix I, according to their technical sheet.

2.1.2 Mortars elaboration

The elaboration and curing of mortars samples were carried out at the laboratory of ARGOS Derivados del Cemento enterprise, following the UNE EN 1015-2 [7] and UNE EN 1015-11 [8] standards as well as the modifications proposed by Cazalla [9], regarding the curing conditions and time.

- *Mixing*

After weighing and careful mixing the dry components, they were poured into a stainless steel container where the kneading water was previously added. The amount of water was established according to the flow table method (*cf.* Section 2.2.1). The mortar mixing was carried out in an automatic mixer that assured a uniform distribution of all the components particles within the fresh mortar mixture. Mixing lasted 90 seconds at slow velocity, as indicated in the UNE EN 1015-2 [7] standard.

- *Casting*

Normalized stainless steel moulds (UNE EN 1015-2 [7]) with three separate sections of 4×4×16 cm each were used for the mortars casting. The internal surfaces of the moulds were lightly lubricated with a very low viscosity non-resin mineral oil to avoid a too high adhesion of the fresh mortar to the surfaces and thus ease the subsequent removal from the mould (UNE EN 1015-2 [7]). The moulding was carried out pouring the fresh mixture up to the half part of the mould and then compacting the mortar giving 15 hits with a metal bar. After this, the second half part of the mould was filled and 15 more hits were given to compact the mortar in the mould (UNE EN 1015-2 [7]). The exceeding material was eliminated with a ruler inclined at 45º that left the surface flat and without hollows.

- *Curing and removal from the mould*

Mortars were cured at controlled conditions of temperature (20 ± 5 ºC) and relative humidity (60 ± 5 %) until their study. They were removed from the mould after 7 days of curing and not after 5 days, following the modification of the UNE EN 1015-11 [8] standard proposed by Cazalla [9], in order to ensure a sufficient hardening of the mortars.

Mortar name	Binder	Aggregate	B/A	Other binders, additives (wt.% of the lime) and admixtures	Water (%)
CC	CL	CA	1:3 (wt.)	-	31.0
CS	CL	SA	1:3 (wt.)	-	27.0
DC	DL	CA	1:3 (wt.)	-	35.0
DS	DL	SA	1:3 (wt.)	-	34.0
CC1:1 (vol.)	CL	CA	1:1 (vol.)	-	32.3
CC1:2 (vol.)	CL	CA	1:2 (vol.)	-	31.9
CC1:3 (vol.)	CL	CA	1:3 (vol.)	-	20.0
CC1:4 (vol.)	CL	CA	1:4 (vol.)	-	22.7
CC1:2 (wt.)	CL	CA	1:2 (wt.)	-	29.5
CC1:3 (wt.)	CL	CA	1:3 (wt.)	-	31.3
CC1:4 (wt.)	CL	CA	1:4 (wt.)	-	24.0
CC1:6 (wt.)	CL	CA	1:6 (wt.)	-	20.0
CD1:3 (wt.)	CL	CDA*	1:3 (wt.)	-	27.0
CS 1:3 (wt.)	CL	SA	1:3 (wt.)	-	26.5
CPC	CL	CA	1:3 (wt.)	WPC (25)	27.5
CCM	CL	CA	1:3 (wt.)	MK (20)	31.5
CCMP	CL	CA	1:3 (wt.)	MK (20) + P	30.5
CCMPC	CL	CA	1:3 (wt.)	MK (20) + P + C	31.6
CCMPCR	CL	CA	1:3 (wt.)	MK (20) + P + C + R	29.0
CCMPCR3 or M3	CL	CA	1:3 (wt.)	MK (10) + P + C + R	28.0
CCMPCR4 or M4	CL	CA	1:4 (wt.)	MK (10) + P + C + R	26.5
CCMPCR6 or M6	CL	CA	1:6 (wt.)	MK (10) + P + C + R	21.5
CCMPCR9 or M9	CL	CA	1:9 (wt.)	MK (10) + P + C + R	20.0

**CDA is the same calcareous aggregate but with a discontinuous grading.*

Table 2 *Summary of the mortars types elaborated and studied in this thesis.*

2.2 Methodology

2.2.1 Physical characterization of components and mortars

- *Granulometry*

- Lime particle size distribution

The particle size distribution of the limes was determined by means of a GALAI CIS-1 particle size analyzer (CIC, University of Granada), which measures by laser particles in a range of size between 0.5 and 600 μm. For this measurement, the limes powder was dispersed in ethanol and sonicated for 20 s.

- Aggregate grain size distribution

The determination of the granulometric distribution of the aggregates was carried out with a mechanical sieve (ARGOS Derivados del Cemento, S.L., Granada), according to the standard UNE EN 933-2 (1996). The sizes of sieves used were: 2-1.6-1-0.8-0.5-0.25-0.125-0.063. The bigger sieves indicated in the standard were not used, because the aggregates did not present coarse fractions.

The aggregates granulometric curves were created by combining different granulometric fractions, according to three different models: Fuller [10], Bolomey [11] and Dinger [12]. The particle size distribution equations used are the followings:

Fuller: $$CP = 100\sqrt{\frac{d}{D}} \qquad \text{[Eq. 1]}$$

where the cumulative percent (CP, in %) by the sieve with "d" size (in mm), while D is the largest particle size (in mm).

Bolomey: $$CP = f + (100 - f)\sqrt{\frac{d}{D}} \qquad \text{[Eq. 2]}$$

where *f* is an empirical constant related to the workability degree of a mixture of concrete, for a defined consistence of the concrete and morphology of the aggregate. *f* values are reported in Table 3.

Shape of particles aggregate	Concrete consistence		
	Dry	Plastic	Fluid
Rounded	6 - 8	10	12
Angular	8 - 10	12 - 14	14 - 16

Table 3 *f values according to Bolomey's theory.*

The *f* values corresponding to a plastic consistence were chosen in order to get the optimum workability in mortars. So, according to Table 3, *f* was 10 for SA and 12 for CA. However, it is important to remember that

these values, here adopted for lime-based mortars, are referred to concretes.

$$\textit{Dinger:} \qquad \text{CPFT} = 100\,\frac{D^n - D_S{}^n}{D_L{}^n - D_S{}^n} \qquad \text{[Eq. 3]}$$

where CPFT is the Cumulative Percent Finer Than (%), D is the particle diameter (in mm), D_L is the largest particle size (in mm), D_S is the smallest particle size.

The distribution modulus (or fineness modulus) (n) was calculated adding the cumulative retained percentages obtained for each sieve size, divided by 100:

$$n = \frac{\Sigma\ \%\ cumul.ret.}{100} \qquad \text{[Eq. 4]}$$

This value is not an index of the aggregate grading, but it is useful for the preparation of aggregates with a given granulometry. In fact, different values of fineness modulus measured in aggregates with the same origin indicate an alteration of them.

- ***Electrophoretic mobility and ζ-potential***

The electrophoretic mobility (μ_e) and ζ-potential, which was determined with the Smoluchowski model [13], of the aqueous solutions ($\varphi \sim 0.01$; $11.2<pH<11.4$) of portlandite ($Ca(OH)_2$) and brucite particles ($Mg(OH)_2$) were obtained at 25 ºC, using a Malvern Zetasizer 2000 instrument (Department of Applied Physics, University of Granada).

The aqueous solutions were prepared from the saturated solutions of each lime. The value of ionic force of the saturated solutions, equal to 0.052 at pH 12.48 and 0.01988 M, was calculated by means of the PHREEQC software [14]. After stirring, solutions were injected in the equipment and nine measurements were carried out for each solution.

- ***Density***

- Solid density

Solid (or particle) density (ρ, g/cm^3) of limes and aggregates was measured by pycnometer analysis (Department of Civil Engineering, Catholic University of Leuven, Belgium). Measurements were carried out according to the ASTM D 854-92 [15] standard; pycnometers were calibrated and filled with white spirit.

- Apparent density, RLP and RCP values

Two methods were used to measure the dry bulk density (ρ_b, g/cm^3) of limes and aggregates.

In the first one, the powders were poured loosely into a container without any additional compaction. From this measure, the random loose packing (RLP) of the dry particles [16] was determined.

In the second method, the dry bulk density (ρ_b*, g/cm^3) was determined after vibrating them at 0.3 mm of amplitude and 50Hz of frequency during 300 s. Then, the random close packing (RCP), which is the densest packing having random structure, was obtained.

- Packing density of the dry particles

The value of packing density (φ_{dry}) of the dry components was determined as:

$$\varphi_{dry} = \frac{\pi}{\varphi_{dry}} \qquad \text{[Eq. 5]}$$

where ρ_s and ρ_s represent the bulk and the solid densities of the granular component, respectively.

- Packing density of the wet mixtures

The value of packing density was also determined by estimating the solid concentration of the wet mixture of lime and aggregate, according to Wong and Kwan's wet packing method [17]:

$$\varphi = \frac{\frac{M}{V}}{\rho_w u_w + \rho_\alpha R_\alpha + \rho_\beta R_\beta + \rho_s R_s} \qquad \text{[Eq. 6]}$$

where M/V represents the wet bulk density of the paste; α and β are two different cementitious materials; s is the aggregate; ρ_w is the density of the water; ρ_α, ρ_β, and ρs are the solid densities of α, β, and s; u_w is the W/B ratio by volume; and R_α, R_β, and R_s are the volumetric ratios to the granular material.

• *Specific surface area and micropore volume*

The N_2 Adsorption technique was performed to determine the specific surface area (SSA) and micropore volume of limes, values determined with Brunauer-Emmet-Teller (BET) [18] and Barret–Joyner–Halenda (BJH) [19] methods, respectively. These values are fundamental to know, since they indicate the surface of lime particles that is available to the absorption of water molecules (i.e. solvation) and surfactants (present in additives and admixtures) and to the exchange of chemical reagents.

The equipment used was a Micromeritics 3000 Tristar (Department of Mineralogy and Petrology, University of Granada), which worked under continuous adsorption conditions at a temperature of 77 K. Prior to the measurements, two samples per lime were outgassed at 10^{-3} Torr and 110 ºC for 4 hours, by means of a Micromeritics Flowprep.

- ***Rheological analyses***

Three different rotational rheometers were used for the study of lime suspensions.

- Viskomat PC

The viscosity measurements were performed with Viskomat PC equipment (Fig. 2) (Department of Civil Engineering, Catholic University of Leuven, Belgium). A controlled rate (CR) procedure was applied and consisted of two phases:

(i) *pre-shearing* during 120 s at a velocity 120 rpm, which was performed so as to ensure a comparable start point for all materials;

(ii) *step-down phase*, consisting of a gradual decrease in rate from 120 to 10 rpm. Each step of 10 rpm lasted 30 s. This procedure was chosen so as to avoid a misinterpretation of the flow behaviour caused by structural changes occurring between the rest period and the shearing.

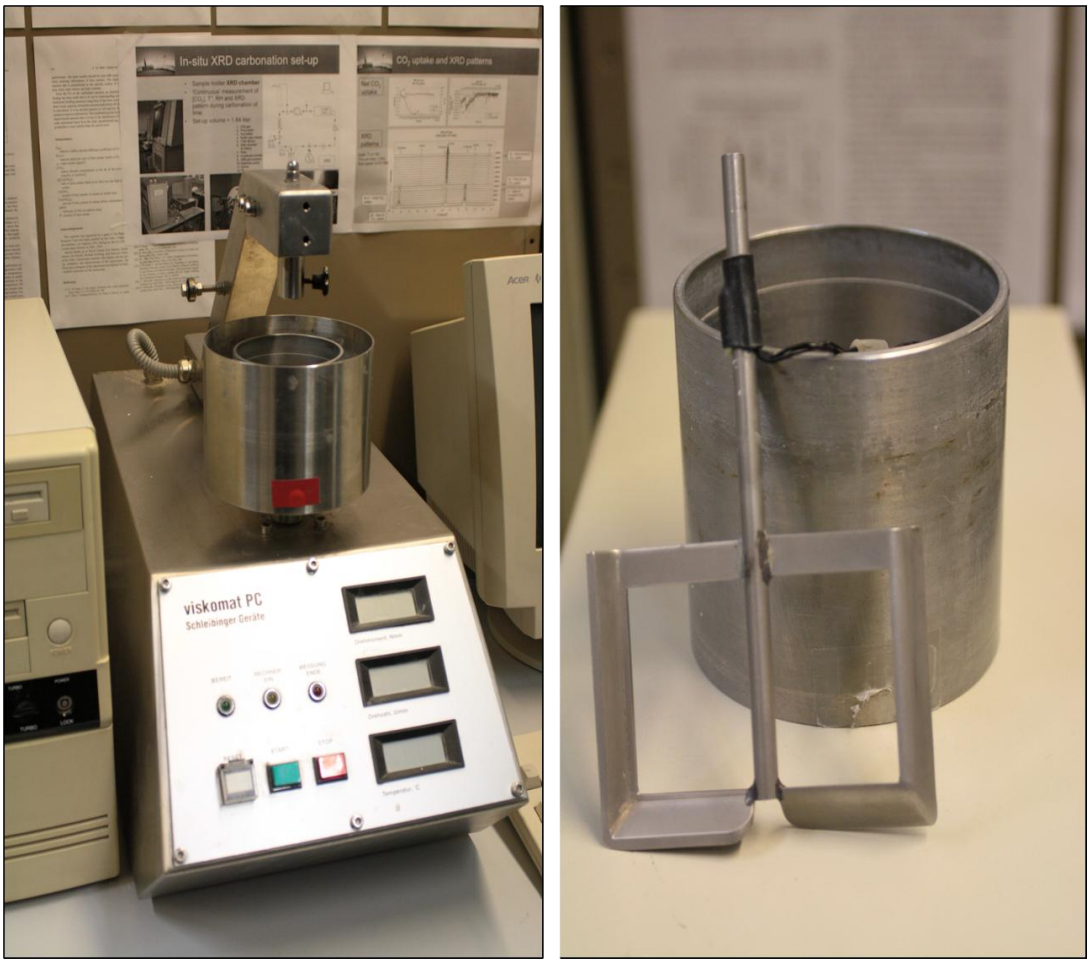

Figure 2 *Photos of the Viskomat PC used (a) and geometry of the paddle (b).*

The suspensions of limes in water were prepared with different solid fractions. Besides in water, viscosity measurements of lime suspensions

were also carried out in glycerine to obtain very dilute suspensions ($0.01<\varphi<0.1$), in which the relative viscosity increase as a function of φ corresponds to the intrinsic viscosity of the suspended material, without any dependence on particle interactions and packing.

- Brookfield LVT Viscosimeter

Since the viscosity of glycerine is strongly dependent on temperature, this was measured at different temperatures by means of a Brookfield LVT Viscometer (Department of Civil Engineering, Catholic University of Leuven, Belgium). Then, the viscosity value for the solvent was adjusted according to the temperature recorded in the suspensions of lime in glycerine at the different rotation speeds. This is shown in Figure 3.

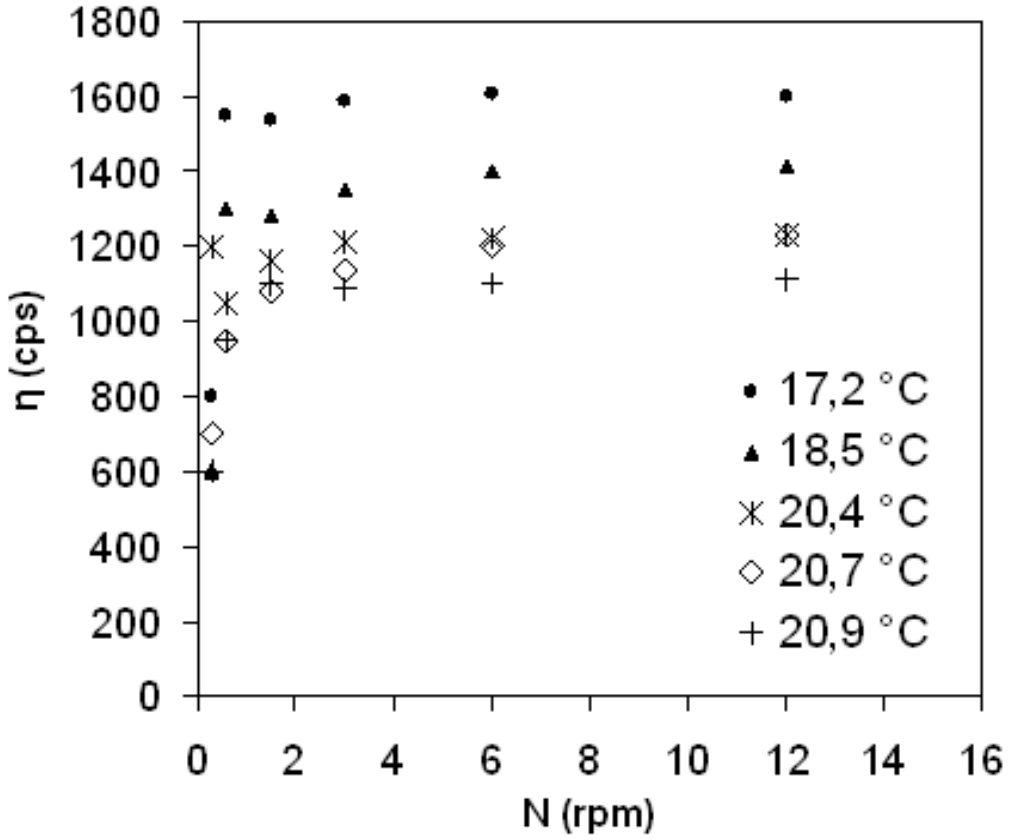

Figure 3 *Viscosity (η, in cps) of glycerine (100%) represented in function of the velocity (N, in rpm,) measured at different temperatures.*

- Brookfield R/S

The same test carried out in the Viskomat PC was performed in a Brookfield R/S rheometer (Department of Mineralogy and Petrology, University of Granada), equipped with a coaxial cylinder geometry and smooth internal surface. This equipment was also used to perform complete loop tests, with increasing and decreasing shear rates, at controlled rate (CR) and controlled stress (CS). In both cases, the profile measurements had three stages:
(i) a logarithmic increase of the shear rate from 0 to 1000 s^{-1} in 225 s;

(ii) a 30 s plateau at the maximum shear rate (1000 s-1);
(iii) a final stage of logarithmic decrease of from 1000 to 0 s^{-1} in 225 s.

A pre-shearing of the suspensions was performed at 250 s^{-1} for 150 s. Temperature was maintained at 25 (±0.5) ºC during measurements using a circulatory water bath.

- Data treatment

The averaged data for torque T (Nmm) and velocity V (rpm) was processed to obtain the values for shear rate (s^{-1}) and viscosity η (Pas), according to the procedure based on the Couette analogy and developed by Bousmina et al. [20] and Aït-Kaidi et al. [21].

The shear rate is calculated as follows:

$$\dot{\gamma} = \frac{\Omega}{\ln\left(\frac{R_e}{R_i}\right)} \qquad \text{[Eq. 7]}$$

where Ω = 2πN is the angular velocity (rad/s); R_e/R_i is the ratio of the outer and inner cylinder radius of the viscosimeter, in this case 1.154 [22]. This is not the real (physical) value, which is considerably smaller, but the calculated value according to Bousmina et al. [20].

The viscosity was obtained as:

$$\eta = \frac{T}{\Omega} \cdot \frac{\left(\frac{R_e}{R_i}\right)-1}{4\pi L R_e^{\,2}} \qquad \text{[Eq. 8]}$$

being L the paddle length.

From the viscosity measurements, six values of apparent viscosity were chosen at six different rotation speeds: 10, 30, 50, 70, 90 and 110 rpm, which correspond to the following shear rates, according to equation 5: 7.31, 21.93, 36.55, 51.18, 65.8 and 80.42 s^{-1}.

By fixing the viscosity value of the solvent, which for water is 0.001 Pas, viscosity data were fitted to the Krieger-Dougherty model [23] (Eq. 9), in which the relative viscosity η_r is equal to:

$$\eta_r = \left(1-\frac{\phi}{\phi_m}\right)^{-[\eta]\phi_m} \qquad \text{[Eq. 9]}$$

where η_r represents the viscosity ratio of the material and the solvent; φ is the solid fraction; φ_m is the maximum solid fraction and [η] is the intrinsic viscosity.

The pair of results maximum solid fraction (φ_m) and intrinsic viscosity ([η]) was obtained for each selected velocity. The average value for φ_m

was fixed and used to recalculate [η] by the linear fitting of the logarithmic transformation of equation 9, keeping a fixed value for the solvent viscosity.

For the suspensions in glycerine, the same experimental routine as for the more concentrated aqueous suspensions was performed. The intrinsic viscosity was obtained as follows:

$$[\eta] = \lim_{\phi \to 0} \frac{\eta - \eta_s}{\phi \eta} \qquad \text{[Eq. 10]}$$

- ***Consistence of fresh mortars mixtures***

The consistence defines the workability of a mortar and it is achieved with the addition of a correct amount of water that varies in function of the mortar granulometry, the amount of fine particles, the presence of additives and the environmental conditions [24]. The most accepted method to determine the consistence of a mortar is the flow table test, indicated in the UNE EN 1015-3 [25] standard and adopted in this thesis. The consistence was determined by measuring the deformation of a mortar fresh sample that is poured inside a conical frustum, on the surface (made of stainless steel and lightly lubricated with very low viscosity non resin mineral oil) of the flow table, and then lifted every second for 15 s.

In the standard UNE EN 1015-6 [26] three types of consistence are distinguished, as expressed in Table 4.

Mortar consistence	Flow
Fluid	> 200
Plastic	140 - 200
Dry	≤ 140

Table 4 *Type of consistence for established ranges of flow (in mm), as established in the UNE EN 1015-6* [26] *standard.*

Since the consistence depends on the amount of water added to the mortar mixture, this property was used to establish the optimum amount of kneading water needed to obtain workable mortars.

- ***Shrinkage of mortars***

The plastic (or drying) shrinkage is the volume reduction that a mortar suffers due to the water evaporation occurring during the drying process. This phenomenon was measured by means of the following methods. In both of them the shrinkage is determined by measuring the mortar dimensional variations over time.

- Shrinkage Measuring Device

A SWG-H-400 shrinkage-measuring device (ARGOS Derivados del Cemento, S.L., Granada) (Fig. 4) was used to measure the initial shrinkage of mortars. This apparatus measures the horizontal dimensional variations of a fresh mortar, by means of two sensors connected to a PC.

The internal surfaces of the apparatus were covered with a polyethylene film to easy the mortar removal after the measurement. The fresh mortar mixture (~ 3 kg) was poured into the apparatus and the sensors were connected to the two extremities. Theses sensors recorded the length of the mortar sample each 30 minutes during 7 days and data were collected simultaneously by a computer. This allowed obtaining a curve of shrinkage over time, the slope of which corresponded to the shrinkage coefficient (C_{shr}, in mm/h). In addition, the shrinkage percentage on the length of the sample measured was determined.

Figure 4 SWG-H-400 shrinkage measuring device.

- Sample length variation

Shrinkage of hardened mortars was determined measuring the dimensional variations (expressed as percentage) of mortars samples, on three perpendicular directions: a, parallel to the compaction plane; b, parallel to the compaction plane along the largest face of the sample; c, perpendicular to the compaction plane. Measurements were carried out on three samples per mortars.

2.2.2 Chemical, mineralogical and petrographical characterization of components and mortars

- ***Chemical study***

- X-ray fluorescence (XRF)

The X-ray fluorescence technique was used to analyze the chemical composition of major and minor elements of the mortars components.

Samples were analyzed by means of a Bruker S4 Pioneer X-ray fluorescence spectrometer (IACT-CSIC, University of Granada) with wavelength dispersion, equipped with a goniometer that analyzes crystals (LIF200/PET/OVO-55) and a Rh X-ray tube (60 kV, 150 mA). Measurements were performed in a vacuum with a rotating sample. Semiquantitative scanning spectra were obtained using Spectraplus software.

Before the analysis, samples were grinded and powders (~ 5g) were dispersed in KBr, deposited in an aluminium cup and then pressed at 10 ton to obtain a pressed pellet (40 mm sample disc).

- Ion cromatography

Ion chromatography analysis was performed by means of a Dionex IC DX500 instrument (School of Geography and the Environment, Oxford, United Kingdom), in order to determine and quantify the concentration of soluble ions (Na^+, NH_4^+, Ca^{2+}, Mg^{2+}, Cl^-, NO_2^-, SO_4^{2-}) in mortars samples.

Prior to the analysis, three samples per mortar were grinded in an agate mortar, then 1 g of powder was dissolved in 68 mL of ultradeionised water and, finally, the solution was sonicated during 60 minutes.

- ***Mineralogical study***

- X-ray diffraction (XRD)

The mineralogical characterization of components and mortars was carried out by powder X-ray diffraction. Samples were grinded in an agate mortar and then characterized by means of two diffractometers.

In the first part of this thesis, samples were analyzed by a Philips PW-1710 diffractometer (disoriented powder method) (Department of Mineralogy and Petrology, University of Granada) equipped with an automatic slit window. Analysis conditions were: radiation CuK_α (λ: 1.5405 Å), 40 kV voltage and 40 mA current intensity. Explored area was between 3º and 60º 2θ and goniometer speed of 0.1º 2θ/s.

Later on, samples were analyzed by a Panalytical X'Pert PRO MPD diffractometer (Department of Mineralogy and Petrology, University of Granada), with automatic loader. Analysis conditions were: radiation CuKα (λ=1.5405 Å), 4 to 70 º2θ explored area, 45 kV voltage, 40 mA current intensity and goniometer speed using a Si-detector X'Celerator of 0.01 º2θ/s.

In both cases, the interpretation and identification of the mineral phases was performed using the X-Powder software package [27].

- Thermogravimetric analysis (TGA)

The thermal treatment of samples allowed identifying and quantifying the mortar phases. Moreover, this showed to be a useful method for the study of the carbonation degree of mortars and for the identification of mineral phases with low-cristallinity (i.e. silicate and aluminate hydrated phases), which were difficult to detect by means of X-ray diffraction.

Thermal measurements were performed with a Shimadzu TGA-50H analyzer (CIC, University of Granada). Approximately 50 mg of sample was heated in an alumina crucible, in a flushed-air atmosphere (100 mL/min), at a heating rate of 5º/min over a range of 25-950 ºC. TGA data treatment was carried out according to the UNE EN ISO 11358 [28] standard.

- Evaluation of the carbonation degree of mortars

In both analyses (XRD and TGA), the decrease in portlandite content was taken as a reference to estimate the carbonation degree index (I_{CD}, in %), according to the equation:

$$I_{CD} = \frac{CH_0 - CH_x}{CH_0} \times 100 \qquad \text{[Eq. 11]}$$

where CH_x is the amount of portlandite at time x and CH_0 is the initial content of portlandite (at time 0). This value was determined at different intervals of time to obtain a curve that shows the evolution of the carbonation process over time.

• Petrographical study

The petrographical characteristics (texture and mineralogy) of mortars were studied by means of optical and electron microscopy. These techniques are qualitative tools that allow identifying the individual components of the mortar samples and, in some cases, the interaction between these constituents. In particular, they were useful for the study of the cohesion between matrix and aggregate grains at the interface transition zone (ITZ) and for the characterization of minerals morphology (crystal habit, shape and size) and particle agglomeration. Microscopic observations were also helpful in the evaluation of mortars shrinkage.

- Polarized optical microscopy (POM)

Microscopic observations were carried out using an Olympus BX-60 microscope equipped with digital microphotography camera (Olympus DP10) (Department of Mineralogy and Petrology, University of Granada). To this end, polished thin sections were prepared with a minimum quantity of water, in order to avoid calcite dissolution in fresh mortars

samples. Observations were performed both under transmitted and reflected (polarized) light.

- Field emission scanning electron microscopy (FESEM)

The observation at micro-scale of the limes, aggregates and mortars was performed by means of a Carl Zeiss Leo-Gemini 1530 microscope (CIC, University of Granada).

The limes were observed both in form of powder and as paste, oven dried for 24 h at 100 ºC and then carbon-coated. The same procedure was adopted for the aggregate grains and the mortars fragments (~ 1 cm) before their observation.

- High-resolution transmission electron microscopy (HRTEM)

The observation at nano-scale of the limes was performed by using a Philips CM20 equipped with an EDAX solid-state ultrathin-window energy dispersive X-ray (EDX) detector that operated at a 200 kV acceleration voltage (CIC, University of Granada). Before the analysis, limes were dispersed in ethanol and were sonicated 15 s. Then, particles were deposited on carbon-coated copper grids and they were observed using a 40 μm objective aperture. A low concentration was used to reduce particles agglomeration. No contrast agent was added to the limes, since a good contrast is obtained with these materials alone.

The identification of mineral phases was possible by performing selected area electron diffraction (SAED), using a 10 μm objective aperture.

- Environmental scanning electron microscopy (ESEM)

Micro-scale crystallization cycles were performed to observe the crystalline phases of a salt at different degree of hydration present in mortars after the salt crystallization durability tests. This study was carried out by using a Philips Quanta 400 microscope (CIC, University of Granada) on mortars fragments of ca. 1 cm, without need of previous drying and sputter coating. Before observation, the microscope chamber was purged at a temperature of 10 ºC and a range of pressures between 0.9 and 5 torr, corresponding at this temperature to about 8% and 40% of relative humidity, respectively.

• *Characterization of the pore system*

- Mercury intrusion porosimetry

This technique was used to determine the open porosity (P_o, %), pore size distribution (PSD) and bulk (ρ_b, g/cm^3) and solid (ρ_s, g/cm^3) density in a range of pore radius comprised between 0.002 and 200 μm. The equipment used was a Micromeritics Autopore III 9410 porosimeter (Department of Mineralogy and Petrology, University of Granada). Mortar fragments of ca. 1 cm^3 were oven-dried for 8 h at 100 ºC before analysis.

- N_2 adsorption

This technique gave the same information as the MIP analysis but in a smaller range of pore radius, comprised between 0.0001 and 0.025 μm (15<d<500 Å). A Micromeritics 3000 Tristar (Department of Mineralogy and Petrology, University of Granada) was used to obtain N_2 sorption isotherms (T = 77 K) under continuous adsorption. Before the measurements, samples were heated to 110 ºC for 4 h and outgassed to 10^{-3} Torr using a Micromeritics Flowprep. Pore size distribution curves were obtained by applying the Barret–Joyner–Halenda (BJH) [19] method.

• *Study of the hydric properties*

The study of the hygric properties of mortars is fundamental for the evaluation of their quality and durability, since water (in the solid, liquid and vapour state) is one of the main factors that drive construction materials to deterioration [29,30].

The influence of the characteristics of mortars pore system on the amount of water absorbed and the kinetics of absorption was carried out by means of different hygric assays. In each one of them, the mass variation of mortars samples was measured over time, due to movement of the water in the pore system.

- *Free water absorption and drying*

Water absorption depends on the characteristics of the pore system of the mortar (pore form, size, distribution and interconnection). Basically, the quantity of water absorbed at the end of the test depends on the total volume of pores and the interconnection among them, whilst the absorption kinetics depends on the porometric distribution. Moreover, absorption is conditioned, in a certain way, by the pressure, temperature and relative humidity [30].

The absorption assay was carried out according to the UNI EN 13755 [31] standard, on three mortars samples of 4×4×4 cm in size. Mortar samples were oven-dried at 100 ºC for 24 h before measurements were taken.

Free water absorption (A_b) (absorption of water at atmospheric pressure) was measured as follows:

$$A_b = \frac{M_L - M_0}{M_0} \times 100 \qquad \text{[Eq. 12]}$$

Where M_L is the mass of the sample saturated with water at atmospheric pressure (until constant mass is reached) and M_0 is the initial mass of the sample.

The absorption coefficient (C_a) was determined as the slope of the first two points in the curve representing the mass variation as a function of the square of time (4 minutes after the beginning of the test) (UNI EN 13755 [31]).

The *water-drying* test was performed according to the NORMAL 29-88 [32] standard, on the same samples at the end of the free water absorption test. Drying was followed by measuring the mass drop of samples, due to the loss of water over time. The drying index (I_d) was measured according to the equation [32]:

$$I_d = \frac{\int_{t_0}^{t_f} f(M_t)dt}{M_s t_f} \qquad \text{[Eq. 13]}$$

Where M_t represents a decreasing water weight content as a function of time, M_s is the saturated mass and t_f is the end time of the test.

- Capillary uptake

The capillary uptake test was performed according to the UNI EN 1925 [33] standard, on three samples of 4×4×16 cm.

Two capillary coefficients (A and B) were determined according to the Beck et al. [34] procedure:

$$A = \frac{\Delta M}{S\sqrt{t}} \qquad \text{[Eq. 14]}$$

and

$$B = \frac{h}{\sqrt{t}} \qquad \text{[Eq. 15]}$$

which correspond to the slop of the two curves representing the weight increase (ΔM, in g) per surface unit (S, in m^2) and the height of the capillary front (h, in mm) versus the square of time (√t, in $min^{-1/2}$).

- Hydraulic conductivity

The hydraulic conductivity (or water permeability) of mortars was determined with the falling head method, by means of the experimental apparatus performed by Domenico and Scwartz [35]. The falling-head permeameter (School of Geography and the Environment, Oxford University, United Kingdom) is configured to suit the measurement of material over a large range of permeabilities from approximately 10^{-6} ms^{-1} (typical of coarse grained sandstones / silty sediments) to 10^{-11} ms^{-1} (fine grained limestone / consolidated clay).

The apparatus (Fig. 5) consisted of ten rigid Perspex tubes as the standpipe with 4 mm internal diameter. The tubes were mounted on a board covered in a graph paper with gridlines marking 1, 5 and 10 mm, to allow head measurement (Fig. 5a and b). The standpipe was terminated in an inverted Y connector of which one arm was used to fill the standpipe with water using a syringe and the other connected to the sample. Each arm had a clamp placed on it in order to control flow in each pipe. The sample was connected to the standpipe using a rubber bung that was pushed into the sleeving of the prepared sample (Fig. 5c and d). To set up

the apparatus the valve on the sample side arm was closed and water was injected using a big syringe through the other arm. Once the water level had reached a sufficient height in the tube, the syringe side valve was closed and water was allowed to flow from the sample side arm to remove air bubbles trapped in the system as this may affect the results. To start a measurement, water was again filled in the tube, syringe valve was closed and sample valve was opened to allow water to flow through the sample. The time required for a given change in head at different intervals was noted manually and used in the Eq. 16 to determine the hydraulic conductivity (K_h, in ms^{-1}) of mortars as follows:

$$K_h = \frac{aL}{At} \ln\left(\frac{h_1}{h_2}\right) \qquad \text{[Eq. 16]}$$

where a is the cross sectional area of the tube (in m^2), L is the length of core (in m), A is the cross sectional area of cores (in m^2), t is the time (in s) taken for head fall from initial head h_1 to final head h_2. This equation is derived from equating flow through the tube with flow through the sample.

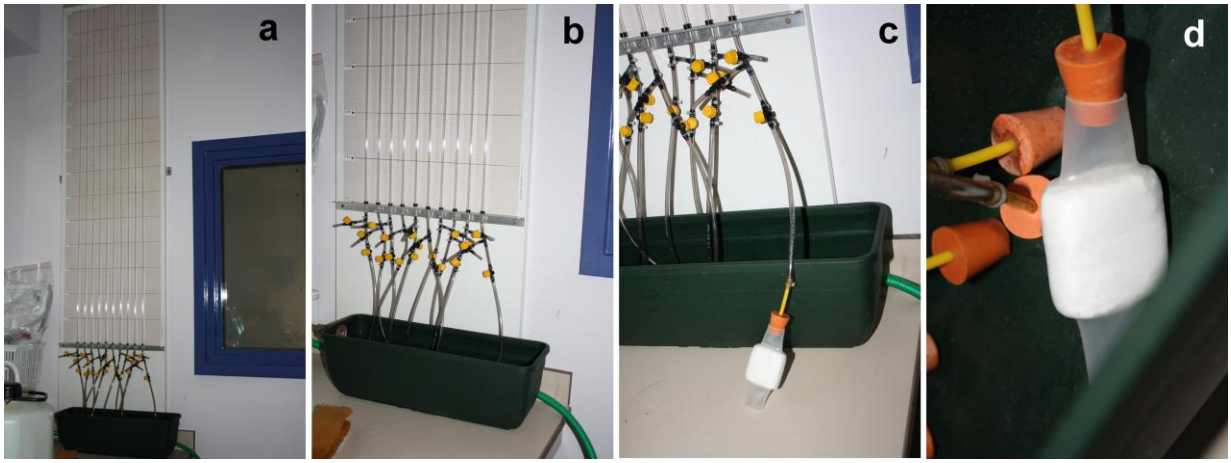

Figure 5 *Falling-head permeameter. (a) and (b): standpipes mounted on a board covered in a graph paper with gridlines; (c) and (d): connection of the sample to the standpipe by means of a rubber bung.*

Previous to the experiment, samples (2×4×4 cm) were polished to reduce as much as possible the roughness in the surface and their edges were rounded off (Fig. 6a). This was necessary for the next preparation step, in which samples were wrapped in a single length PTFE tape (plumber's thread sealing tape) to create at least ten overlapping layers that completely cover the largest surface of the sample (Fig. 6b). To compress the tape-layer into the surface of the mortar and produce a watertight sleeve, samples were then encapsulated with electrician's heat shrinkable sleeving (Fig. 6c). The heat shrinkable sleeving was shrunken with a hot-air gun to its minimum diameter. The water flow during the permeability test would be possible only in one direction, through two

parallel surfaces of the samples, as shown in Fig. 4c and d. Samples were stored underwater for one day and then completely saturated under vacuum before the test.

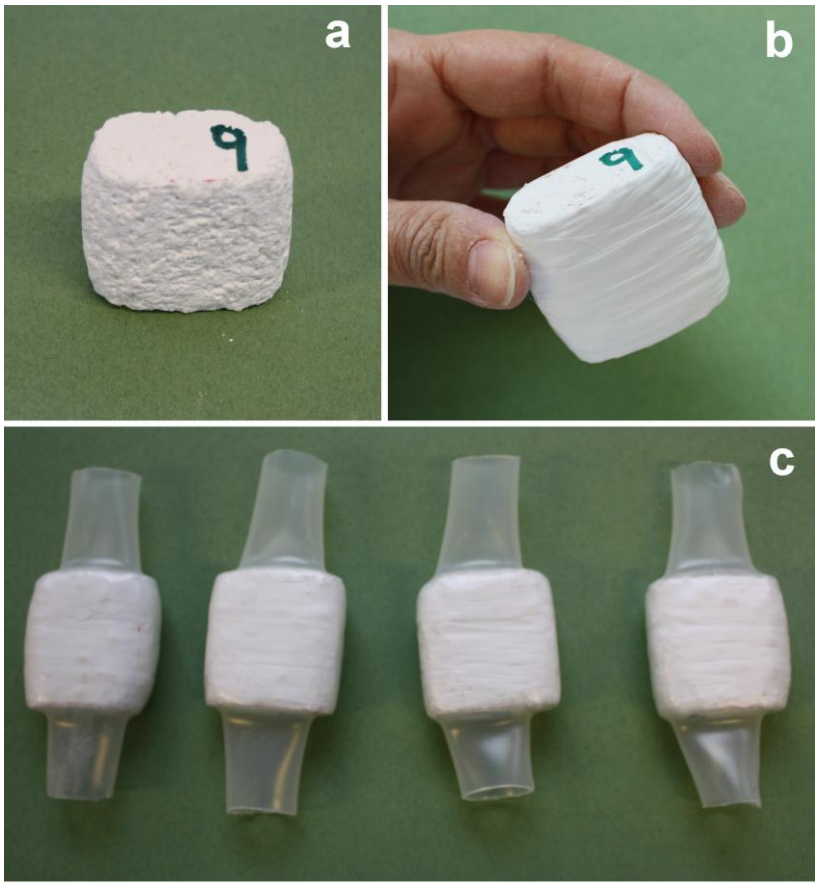

Figure 6 *Sample preparation before the permeability test. (a): polishing and smoothing of the sample; (b): covering of the sample surface with PTFE tape; (c): aspect of the samples after being encapsulated with electrician's heat shrinkable sleeving.*

- Water vapour permeability

Water permeability is the capacity of a material to transmit water, as liquid or vapour, through it. Mortars with high water vapour permeability are preferred because they allow the masonry to breathe and dry out quickly, thus preventing the trapping of water behind the substrate and reducing damage due to freeze-thaw phenomenon. Moreover, it is fundamental that the mortar has a higher vapour transmission rate than the masonry substrate.

The water vapour permeability (K_v) is the quantity of water vapour passing per time unit and surface units through a porous material under isothermal conditions. For the determination of this parameter, three samples per mortar of 1.5×4×4 cm in size were oven-dried at 90 ºC for 24 hours. Afterwards, they were placed in experimental permeameters filled with deionised water, avoiding the contact of water with the sample

surface. Permeameters were then sealed by using dishes of silicon rubber (Fig. 7).

The water vapour permeability assay was performed for 5 days in total, at controlled conditions of temperature (T = 25 ºC). The whole mass (permeameter + sample + water) was recorded every day and a lineal trend curve was obtained from the mass drop over time.

Figure 7 Image of a water vapour permeameter.

The water vapour permeability (K_v, g/m^{2}h) was calculated according to the following equation:

$$K_v = \frac{\frac{\Delta M}{S}}{t} \cdot 0.7378 \cdot e \qquad \text{[Eq. 17]}$$

Where ΔM/S is the mass variation of the permeameter + sample + water per surface unit (surface of the sample exposed to vapour), t is the duration time of the assay, 0.7378 is a correction factor applied to determine the water vapour permeability value at T = 20 ºC, as established in the NORMAL 21/85 [36] and *e* is the sample thickness.

- ***Study of the mechanical properties***

- Flexural and compressive resistances

Flexural and compressive strength (R_f and R_c) were measured by means of an INCOTECNIC-Matest hydraulic press (ARGOS Derivados del Cemento), S.L., Granada). According to the UNE-EN 1015-11 [8] standard, flexural assays were carried out on three samples per mortar (of 4×4×16 cm). The six samples obtained after the flexural rupture were used for the compressive assays.

- Micromechanical model

A micromechanical model was applied to study the changes of the mechanical characteristics of mortars due to the carbonation process. Moreover, it allowed studying the differences in the evolution of the

carbonation process between the exterior and the interior of mortars. To this end, two micro-samples (10×10×10 mm) were obtained from the first 10 mm and from the core of each mortar prism. Then, the micro-samples were tested in an Instron 4411 uniaxial compression press (Department of Earth Science and Environment, University of Alicante), which can achieve a maximum load of 5000 kN and a constant load velocity of 0.1 MPa/s. The stress-strain curve was recorded and strength (in MPa) and Young modulus (in MPa) were calculated for each sample.

- Ultrasonic measurements

The ultrasonic wave propagation technique was used to determine the elastic-dynamic properties of mortars, which are related to their mechanical resistance and degree of compactness. Measurements were performed using a Panametrics HV Pulser/Receiver 5058 PR coupled with a Tektronix TDS 3012B oscilloscope (Department of Mineralogy and Petrology, University of Granada and Department of Earth Science and Environment, University of Alicante), in transmission-reception mode. A couple of non-polarized piezoelectric transducers were used, with a frequency spectrum of 1 MHz. Measurements were carried out on mortar samples of 4×4×16 cm along three perpendicular directions: a, parallel to the compaction plane; b, parallel to the compaction plane along the largest face of the sample; c, perpendicular to the compaction plane. The velocity of propagation of primary (V_p) and secondary (V_s) waves within the mortar samples was determined as the ratio between the specimen length and the transit time of the pulse.

Once calculated the average velocity of V_p and V_s waves along a, b and c directions for three samples of each type of mortar and knowing the bulk density (ρ_b, g/cm^3) of the mortar at each time, the Poisson coefficient (v), and the rigidity (G), Young (E) and volume (or compressive) moduli (K) of the mortars were calculated using the following equations:

$$v = \frac{\left(\frac{V_p}{V_s}\right)^2 - 2}{2\left(\frac{V_p}{V_s}\right)^2 - 1} \qquad \text{[Eq. 18]}$$

$$G = \rho_b V_s^{\,2} \qquad \text{[Eq. 19]}$$

$$E = 2G(1+\nu) \qquad \text{[Eq. 20]}$$

$$K = \frac{E}{3(1-2\nu)} \qquad \text{[Eq. 21]}$$

2.2.3 Study of the durability of mortars

- *Accelerated ageing tests*

To study the durability of mortars, they were subjected to different accelerated weathering tests that simulated changes of temperature and relative humidity, solar radiation, rain, salt fog and salt capillary absorption. Four different tests were performed: 1) weathering cycles with T, light and RH variations (WS); 2) weathering cycles and rain simulation (WS+R); 3) weathering cycles and salt resistance by capillary absorption (WS+SS); and 4) weathering cycles and salt resistance by surface deposition (salt fog) (WS+SD).

All the tests were carried out in a Sanyo-FE 300H/MP/R20 environmental cabinet (internal dimensions of 675W 630D 650H mm) (School of Geography and the Environment, Oxford University, United Kingdom), which can operate at temperature range of -20 to +100°C and can be programmed with different conditions of temperature, relative humidity and light.

Previous to the weathering, samples of 2×4×4 cm were oven-dried and then placed on a sand layer (ca. 4 cm thick) in a tray, following the experimental procedure as in Goudie and Parker [37] and Goudie et al. [38]. The smaller surface (2×4 cm) was put in contact with sand and the larger surface (4×4 cm) perpendicular to it (Fig. 8). In this way, samples reproduced the real situation of a render (1-3 cm thick) on a wall.

Figure 8 *Durability study. (a): mortars samples placed in a tray over a sand layer; (b) and (c): interior of the environmental cabinet, where the samples were analysed.*

Each climatic cycle lasted 12 hours and consisted of 4 steps, of 3 hours duration each step, with a cooling and warming rate of 25 ºC/hour.

Rain was simulated by spraying both the sand (water level of 2 mm) and the mortar surface with around 25 mL of tap water, which was applied every 4 cycles just before the step at the lowest temperature. The water absorbed by the samples (by capillary rise from the sand and by absorption from the wetted surface) froze when temperature decreased below 0 ºC and dried when temperature increased up to 40 ºC, with the consequence that freeze-thaw cycles were also simulated in this test.

The experimental design proposed by Goudie et al. [38] was used, with some modifications, to evaluate the damage caused by the capillary uptake of a saline (sodium sulphate) ground water within the mortar. In

this test, samples were placed in a tray on sand 4 cm thick and sodium sulphate was dispersed in the sand (1:10 salt to sand ratio by weight). Tap water (water level of 1 mm) was applied over the tray for around 60 s, using a spray every 4 cycles before the step at the highest temperature.

Finally, to analyse the damage caused by the deposition of a salt fog on the mortar surface, a sodium sulphate solution (14% w/w) was sprayed on the surface of the mortar samples, every two cycles before the step at the highest temperature.

During the weathering tests, samples were weighed and photos taken every day in order to record any morphological change in mortars.

Temperature and relative humidity trends were also checked with a data logger (ibutton® Hygrolog which records temperature and RH) to ensure that the programmed cycle was reproduced accurately (Fig. 9).

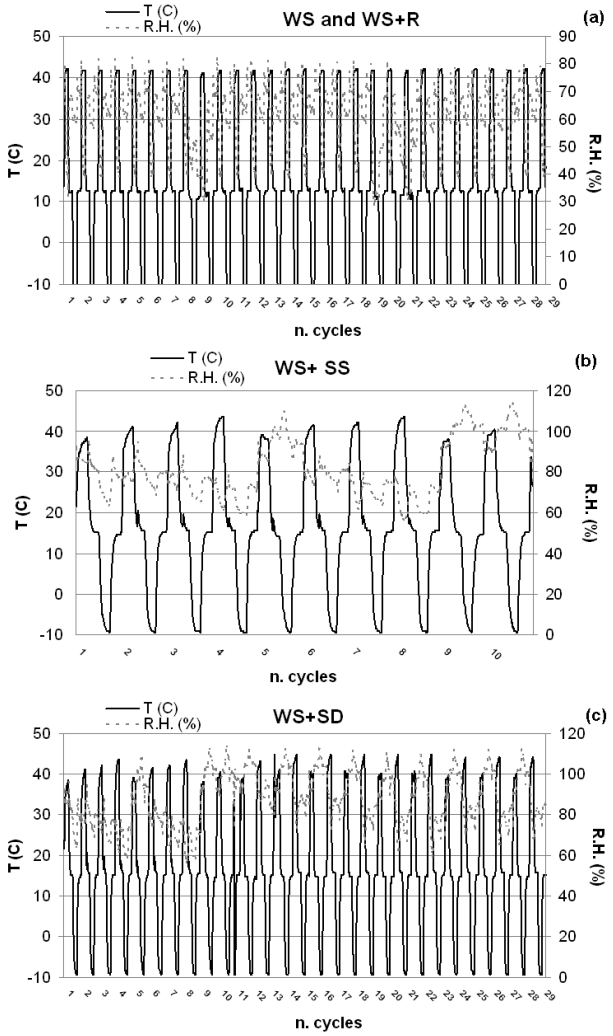

Figure 9 *Temperature (T, in °C) and relative humidity (RH, in %) variations during the cycles performed in the weathering tests: WS, normal weathering; WS+R, weathering study and rain simulation; WS+SS, weathering study and salt resistance by capillary absorption; WS+SD, weathering study and salt resistance by surface deposition.*

References

[1] UNE EN 459-1 (2002). Description Building lime - Part 1: Definitions, specifications and conformity criteria. AENOR, Madrid.
[2] UNE EN 197-1 (2000). Cement - Part 1: Composition, specifications and conformity criteria for common cements. AENOR, Madrid.
[3] UNE EN 80305 (2001). White cements. AENOR, Madrid.
[4] UNE-EN 13139 (2003). Aggregates for mortars. AENOR, Madrid.
[5] UNE EN 933-2 (1996). Tests for geometrical properties of aggregates - Part 2: Determination of particle size distribution - Test sieves, nominal size of apertures. AENOR, Madrid.
[6] ASTM C618-08 (2008). Standard Specification for Coal Fly Ash and Raw or Calcined Natural Pozzolan for Use in Concrete. Annual Book of ASTM Standard, 4.02. ASTM International Standards Worldwide, Pennsylvania (USA).
[7] UNE EN 1015-2 (1999). Methods of test for mortar for masonry - Part 2: Bulk sampling of mortars and preparation of test mortars. AENOR, Madrid.
[8] UNE EN 1015-11 (1999). Methods of test for mortar for masonry. Part 11: Determination of flexural and compressive strength of hardened mortar. AENOR, Madrid.
[9] Cazalla O (2002). Morteros de cal. Aplicación en el Patrimonio Histórico. Ph.D. Thesis. Universidad de Granada.
[10] Fuller W.B., Thompson S.E. The laws of proportioning concrete. Proc. Am. Soc. Civil Engr. 33 (1907), 261.
[11] Bolomey J. The grading of aggregate and its influence on the characteristics of concrete. Revue des Matériaux de Construction et Travaux Publiques, pp. 147–149, 1947.
[12] Dinger D.R. Particle Packing and Pore Size Distributions. (1980) Volume 1, No. 9. (un update 2003) available on www.dingerceramics.com.
[13] Von Smoluchowski M. Bull. Int. Acad. Sci. (1903), 184.
[14] Parkhurst D.L., Appelo C.A.J. Users Guide to PHREEQC (version 2)-A Computer Program for Speciation, Batch Reaction, One-Dimensional Transport, and Inverse Geo-chemical Calculations. U.S. Geological Survey Water-Resources Investigation Report 99-4259 (1999), 312.
[15] ASTM D854-92 (1993). Standard test method for specific gravity of soils. ASTM International Standards Worldwide, Pennsylvania (USA).
[16] Shapiro A.P., Probstein R.F. Random packings of spheres and fluidity limits of monodisperse and bidisperse suspensions. Phys. Rev. Lett. 68 (9) (1992), 1422-1425.
[17] Wong H.H.C., Kwan A.K.H. Packing density of cementitious materials: part 1-measurement using a wet packing method. Mater. Struct. 41 (4) (2008), 689-701.
[18] Brunauer S., Emmett P.H., Teller J. Adsorption of gases in multimolecular layers. J. Am. Chem. Soc., 60 (1938), 309.
[19] Barret E.P., Joyner L-J., Halenda P. The determination of pore volume and area distributions in porous substances. I. Computations from nitrogen isotherms. J. Am. Chem. Soc., 73 (1951), 373-380.

[20] Bousmina M., Aït-Kaidi A., Faisant J.B.: "Determination of shear rate and viscosity from batch mixer data", J. Rheol., 43(2) (1999), 415-433.
[21] Aït-Kaidi A., Marchal P., Choplin L., Chrissemant A. S., Bousmina M.: "Quantitative analysis of mixer-type rheometers using the Couette analogy", Can. J. Chem. Eng., 80 (2002), 1166-1174.
[22] Hendrickx R.: The adequate measurement of the workability of masonry mortar, PhD Thesis, Catholic University of Leuven (2009).
[23] Krieger I. M., Dougherty T. G.: A mechanism for non-Newtonian flow in suspensions of rigid spheres, Trans. Soc. Rheol., 3 (1959), 137-152.
[24] Boletín AFAM (2003). Morteros. Guía General.
[25] UNE EN 1015-3 (1999). Methods of test for mortar for masonry. Determination of consistence of fresh mortar (by flow table). AENOR, Madrid.
[26] UNE EN 1015-6 (1999). Methods of test for mortar for masonry. Determination of bulk density of fresh mortar. AENOR, Madrid.
[27] Martín Ramos J.D. XPowder. A software package for powder X-ray diffraction analysis. Lgl. Dep. GR 1001/04 (2004).
[28] UNE EN ISO 11358 (1997). Thermogravimetry (TG) of polymers - General principles. AENOR, Madrid.
[29] Esbert R.M., Montoto M., Ordaz J. La piedra como material de construcción: durabilidad, deterioro y conservación. Materiales de Construcción, 41 (1997) 221, 61-71.
[30] De La Torre M.J. Caracterización de las propiedades hídricas de los materiales lapídeos. Cuadernos Técnicos. Metodología de diagnóstico y evaluación de tratamientos para la conservación de los edificios históricos. Villegas R., Sebastian E., eds, (2003) 104-111.
[31] UNI EN 13755 (2008). Natural stone test methods — Determination of water absorption at atmospheric pressure. CNR-ICR, Rome.
[32] NORMAL 29/88 (1988). Measurement of the drying index. CNR-ICR, Rome.
[33] UNI EN 1925 (2000). Natural stone test methods — Determination of water absorption by capillarity. CNR-ICR, Rome.
[34] Beck K., Al-Mukhatar M., Rozenbaum O., Rautureau M. Characterization, water transfer properties and deterioration in tuffeau: building material in the Loire valley, France. Build Environ 38 (2003), 1151-1162.
[35] Domenico P.A., F.W. Schwartz. Physical and Chemical Hydrogeology, John Wiley & Sons, New York, (1990), 824 p.
[36] NORMAL 21/85 (1985). Permeability to water vapour. CNR-ICR, Rome.
[37] Goudie A.S., Parker A.G. Experimental simulation of rapid rock block disintegration by sodium chloride in a foggy coastal desert. J. Arid Environ. (1998) 40, 347-55.
[38] Goudie A.S., Wright E., Viles H.A. The role of salt (sodium nitrate) and fog in weathering: a laboratory simulation of conditions in the northern Atacama Desert, Chile. Catena (2002) 48, 255-66.

3. RESULTS AND DISCUSSION

PART I

Limes and aggregates: a study of their influence on mortar hardening properties and an initial assessment of the most suitable proportions.

Objectives

The first part of this thesis tackles important variables that needed to be considered prior to the design of mortars. I especially refer to the selection of the most suitable types of lime and aggregate to be used as the main components of the designed mortars.

Chapter I.1 deals with the micro-structural and rheological properties of the two industrial limes (calcitic and dolomitic) considered in this thesis, with the aim of understanding their influence in the development of the plasticity and workability of the fresh mortar mixtures.

The following chapters focus on the comparison between the mineralogical, textural and physical-mechanical properties of mortars prepared with different binders (*chapter I.2*) and aggregates (*chapters I.2, I.3, I.4* and *I.5*).

A special attention is given to the evolution of mortars properties due to carbonation (*chapters I.3, I.4* and *I.5*). The main aim of these studies is to investigate whether and how aggregates of different mineralogy, grading and texture influence the outcome of this process.

In particular, *chapters I.4* and *I.5* claim to point out the effectiveness of non-destructive and low-destructive techniques as tools for the textural characterization of mortars.

In these two chapters, the selection of the optimal binder-to-aggregate proportions is also discussed, although this topic will be tackled practically throughout the thesis.

Chapter I.1

Differences in the rheological properties of calcitic and dolomitic lime slurries: influence of particle characteristics and practical implications in lime-based mortar manufacturing.

Arizzi A., Hendrickx R., Cultrone G., Van Balen K.
Materiales de Construcción (2012)
DOI 10.3989/mc.2011.00311

Abstract

The study of the rheological properties of lime suspensions is a useful means to evaluate the workability of lime mortars. In this work, we studied the flow behaviour of two industrial hydrated limes, one of calcitic and the other of dolomitic composition, by means of two types of rheometer with different geometry and setup mode. The obtained results were interpreted taking into account the differences in microstructure and surface properties of the suspended particles. Calcitic lime dry particles are formed by angular and polydisperse clusters and, once dispersed in water, they behave like thixotropic materials. On the other hand, the dolomitic lime is formed by nanoparticles and small round cluster and it shows a pronounced plastic behaviour in suspension. This fundamental difference between the two materials explains the traditional preference for dolomitic lime mortars for plastering and rendering applications.

1. Introduction

The preparation of a mortar paste with high plasticity is essential for obtaining good performance of the mortars in both the fresh and hardened states, and this is why mortar workability and the factors affecting it are now being widely investigated. Several studies have pointed out that a workable mortar paste is achieved by optimally combining the effects of packing density [1], water/binder ratio, particle shape and size distribution [2-4], air content [5,6], presence and type of admixtures [6,7] and filler addition [8].

In addition to these factors, the workability of a mortar mixture depends greatly on the effect of the lime particles on the viscosity in suspension. For equal compositions the viscosity was demonstrated to be higher when lime putty is used instead of dry hydrated lime [9]. The latter is obtained in powder by adding a stoichiometric amount of water vapour to the quicklime (CaO), whereas lime putties are slaked with water in excess and left submerged in water for some time. It is also stated in literature that DL has better rheological properties than CL for certain applications (for renders, for example) [10]. More specifically, the first is claimed to behave more "plastic".

This paper concentrates on the difference of plasticity between calcitic and dolomitc lime by means of a rheological study of the micro- and nano-structural characteristics of their particles, as well as their properties in suspension. Differences found in the flow behaviour of the two limes were linked to their microstructure and surface properties. The determination of the surface charge of the particles (defined by the ζ-potential) was fundamental for corroborating the interpretation of the colloidal forces (repulsion or attraction) established between particles in water [11], which has an important influence on their state of aggregation.

To this objective, lime slurries were prepared with different lime concentrations, considering the plasticity that is typically required for practical purposes.

Particle packing density is a key parameter in the rheology of CL and DL. The approach in this article follows the terminology of Shapiro and Probstein [12], which correlates the fluidity limit with the random loose packing fraction (RLP) of the solid particles and which defines the random close packing (RCP) as the densest packing with random structure. The RLP and RCP values of the two limes will be compared with the maximum solid fraction (φ_m) that will be obtained by means of the rheological measurements.

2. Materials and methods

Two dry powder hydrated limes were studied: one of calcitic composition (CL) CL90-S, produced by ANCASA (Seville, Spain) and one dolomitic (DL) DL85-S, produced in the USA and supplied by LHOIST

enterprise (Nivelles, Belgium). The mineralogy of the limes is indicated in the abbreviations, as set out in the European standard [13].

An extensive characterisation of the limes was carried out before making the rheological measurements. Specific surface area (SSA) and micropore volume (determined with BET [14] and BJH [15] methods, respectively) were measured by using the N_2 Adsorption technique, by means of an equipment Micromeritics 3000 Tristar, which workes under continuous adsorption conditions at a temperature of 77 K. Prior to the measurements, two samples per lime were outgassed at 10^{-3} Torr and 110 ºC for 4 hours, by means of a Micromeritics Flowprep.

Particle size distribution (PSD) was determined by using a GALAI CIS-1 particle size analyzer. For this measurement, the lime samples were dispersed in ethanol and were sonicated for 20 s.

Particle shape and microstructure were observed using a field emission scanning electron microscope (FESEM, Carl Zeiss, Leo-Gemini 1530). Two samples of each lime with a thickness of about 1 cm^3 were oven dried for 24 h at 100 ºC and then carbon-coated before their observation.

Observations were also performed with more detail by means of a high-resolution transmission electron microscopy (HRTEM), by using Philips CM20 equipment that operates at a 200 kV acceleration voltage, in order to calculate the aspect ratio (r_p, Eq. I.1.1) of the micro-sized lime particles, according to the equation:

$$r_p = \frac{d}{l} \qquad [I.1.1]$$

In Eq. I.1.1, d is the particle length measured along [100] and l is the thickness measured along [001]. The r_p value was calculated on a total of 100 particles For the HRTEM analysis, limes were dispersed in ethanol and were sonicated 15 s. Then, particles were deposited on carbon-coated copper grids and they were observed using a 40 μm objective aperture whilst selected area electron diffraction (SAED) was performed using a 10 μm objective aperture. A low concentration was used to reduce particles agglomeration. No contrast agent was added to the limes, since a good contrast is obtained with these materials alone.

Solid (or particle) density (ρ, g/cm^3) of the limes was measured by pycnometer analysis. Measurements were carried out according to the ASTM, D 854-92 standard [16]; pycnometers were calibrated and filled with white spirit.

Two methods were used to measure the dry bulk density (ρ_b, g/cm^3) of the limes. In the first one, the limes were poured loosely into a container without any additional compaction and the RLP value was obtained [12]. In the second one, the dry bulk density (ρ_b^*, g/cm^3) was determined after vibrating them at 0.3 mm of amplitude and 50Hz of frequency during 300 s. In this case, the calculated value corresponds to the RCP [12].

The electrophoretic mobility (μ_e) and ζ-potential (determined with the Smoluchowski model [17]) of the aqueous solutions ($\varphi \sim 0.01$;

11.2<pH<11.4) of portlandite ($Ca(OH)_2$) and brucite particles ($Mg(OH)_2$) were obtained at 25 ºC, using a Malvern Zetasizer 2000 instrument.

The aqueous solutions were prepared from the saturated solutions of each lime. The value of ionic force of the saturated solutions, equal to 0.052 at pH 12.48 and 0.01988 M, was calculated by means of the PHREEQC software [18]. After stirring, solutions were injected in the equipment and nine measurements were carried out for each solution.

The RLP and RCP of the two limes were compared with the maximum solid fraction (φ_m) obtained by means of the rheological measurements, in order to evaluate eventual differences due to the lime state.

For the rheological measurements, five CL suspensions and four DL suspensions were prepared with different solid fractions (Tab. I.1.1).

CL suspensions				*DL suspensions*			
Name	*W/B ratio*	ρ_{wb}	φ	Name	*W/B ratio*	ρ_{wb}	φ
CL1	1.1	1.41	0.28	**DL1**	2.0	1.27	0.18
CL2	1.2	1.39	0.26	**DL2**	2.2	1.26	0.17
CL3	1.3	1.36	0.24	**DL3**	2.5	1.26	0.15
CL4	1.4	1.33	0.23	**DL4**	3.0	1.24	0.13
CL5	1.5	1.31	0.22	**-**	-	-	-

Table I.1.1 *Values of W/B ratio (by mass), wet bulk density (ρ_{wb}, g/cm^3) and solid fraction (φ) for calcitic (CL) and dolomitic (DL) lime slurries.*

Due to the differences in plasticity of the two lime suspensions, different ranges of solid fractions were considered for CL and DL, as the main objective of this study was to determine the visual plasticity of workable pastes. For the determination of the plasticity of the pastes we did not use any numerical criterion, because to fulfil the objectives of this work, one of the established requirements was to respect the conditions of preparation and mixing of mortars paste applied in-situ (i.e. during building works).

Three different rotational rheometers were used for the study of lime suspensions. The viscosity measurements were performed with Viskomat PC equipment. In this case, a controlled rate (CR) procedure was applied and consisted of a first phase of pre-shearing (120 s at 120 rpm) followed by a gradual decrease in rate from 120 to 10 rpm. Each step of 10 rpm lasted 30 s. The pre-shearing was performed so as to ensure that we had a comparable start point for all the materials, while the step-down procedure was chosen so as to avoid a misinterpretation of the flow behaviour caused by structural changes that occur during the time between the rest period and the shearing. The rate range we chose was considered the most appropriate for analysing the viscosity of the suspensions, since in everyday practical uses of mortars, such as spreading over a surface, the real shear rate applied to the lime pastes is within this range. The averaged data for torque T (Nmm) and velocity V (rpm) was processed to obtain the values for shear rate $\dot{\gamma}$ (s^{-1}) and

viscosity η (Pas), according to the procedure based on the Couette analogy and developed by Bousmina et al. [19] and Aït-Kaidi et al. [20].

The shear rate is calculated as follows:

$$\dot{\gamma} = \frac{\Omega}{\ln\left(\frac{R_e}{R_i}\right)} \qquad \text{[I.1.2]}$$

where $\Omega = 2\pi N$ is the angular velocity (rad/s); R_e/R_i is the ratio of the outer and inner cylinder radius of the viscosimeter, in our case 1.154 [5]. This is not the real (physical) value, which is considerably smaller, but the calculated value according to Bousmina et al. [19]. The obtained parameters allow calculating the following viscosity η:

$$\eta = \frac{T}{\Omega} \cdot \frac{\left(\frac{R_e}{R_i}\right) - 1}{4\pi L R_e^{\,2}} \qquad \text{[I.1.3]}$$

being L the paddle length.

From the viscosity measurements, six values of apparent viscosity were chosen at six different rotation speeds: 10, 30, 50, 70, 90 and 110 rpm, which correspond to the following shear rates, according to equation 2: 7.31, 21.93, 36.55, 51.18, 65.8 and 80.42 s^{-1}. By fixing the viscosity value of the solvent, which for water is 0.001 Pas, viscosity data were fitted to the Krieger-Dougherty model [21] (Eq. I.1.4), in which the relative viscosity η_r is equal to:

$$\eta_r = \left(1 - \frac{\phi}{\phi_m}\right)^{-[\eta]\phi_m} \qquad \text{[I.1.4]}$$

where η_r represents the viscosity ratio of the material and the solvent; φ is the solid fraction,; φ_m is the maximum solid fraction and [η] is the intrinsic viscosity.

The pair of results maximum solid fraction (φ_m) and intrinsic viscosity ([η]) was obtained for each selected velocity. The average value for φ_m was fixed and used to recalculate [η] by the linear fitting of the logarithmic transformation of equation I.1.4, keeping a fixed value for the solvent viscosity.

Besides in water, viscosity measurements of lime suspensions were also carried out in glycerine to obtain very dilute suspensions ($0.01<\varphi<0.1$), in which the relative viscosity increase as a function of φ corresponds to the intrinsic viscosity of the suspended material, without any dependence on particle interactions and packing. Also the viscosity measurements of the lime suspensions in glycerine were performed in the Viskomat PC, following the same procedure as the lime suspensions in

water. The interest in comparing the values of viscosity and maximum solid fraction obtained in diluted (in glycerine) and concentrated (aqueous) suspensions stays in the possibility of evaluating the weight that particles interaction factors has in real suspensions (at higher concentration).

For the suspensions in glycerine, we followed the same experimental routine as for the more concentrated aqueous suspensions. The intrinsic viscosity was obtained as follows:

$$[\eta] = \lim_{\phi \to 0} \frac{\eta - \eta_s}{\phi \eta} \qquad [I.1.5]$$

Since the viscosity of glycerine is strongly dependent on temperature, this was measured at different temperatures by means of a Brookfield LVT Viscometer.

Finally, a Brookfield R/S rheometer equipped with a coaxial cylinder geometry and smooth internal surface was also used to perform the same test carried out in the Viskomat as well as complete loop tests, with increasing and decreasing shear rates, at controlled rate (CR) and controlled stress (CS). In both cases, the profile measurements had three stages: (i) a logarithmic increase of the shear rate from 0 to 1000 s^{-1} in 225 s; (ii) a 30s plateau at the maximum shear rate (1000 s^{-1}); and (iii) a final stage of logarithmic decrease of $\dot{\gamma}$ from 1000 to 0 s^{-1} in 225 s. A pre-shearing of the suspensions was performed at 250 s^{-1} for 150 s. Temperature was maintained at 25 (±0.5) ºC during measurements using a circulatory water bath.

Whilst all the rheological parameters has been obtained by means of Viskomat measurements, the use of a coaxial cylinder rheometer allowed us to study the flow behaviour (thixotropic or anti-thixotropic) of lime suspensions in a wider range of shear rates with the aim to verify the differences existing in the rheological properties of the two limes.

3. Results and discussion

3.1 Characterisation of limes

Dry hydrated calcitic lime (CL) particles exhibit a great tendency to agglomeration, phenomenon driven by capillary forces that overcome electrostatic repulsion during drying [9]. Aggregates are polydisperse and angular-shaped, both at nano- (Fig. I.1.1a) and micro-scale (Fig. I.1.2a-d). They are predominantly formed by portlandite nanocrystals and, occasionally, by sub-microsized particles of between 400 nm and 1 μm (Fig. I.1.2c). Clusters of nanoparticles are predominantly randomly oriented (Fig. I.1.1a), although a few alignments were found (Fig. I.1.1c and I.1.2d). Individual nanocrystals with a hexagonal habit were also observed, such as the plate-like $Ca(OH)_2$ nanocrystal shown in Fig. I.1.1b. The majority of aggregates are 4-6 μm in size, which corresponds to the main peak found in the PSD curve of calcitic lime (Fig. I.1.3).

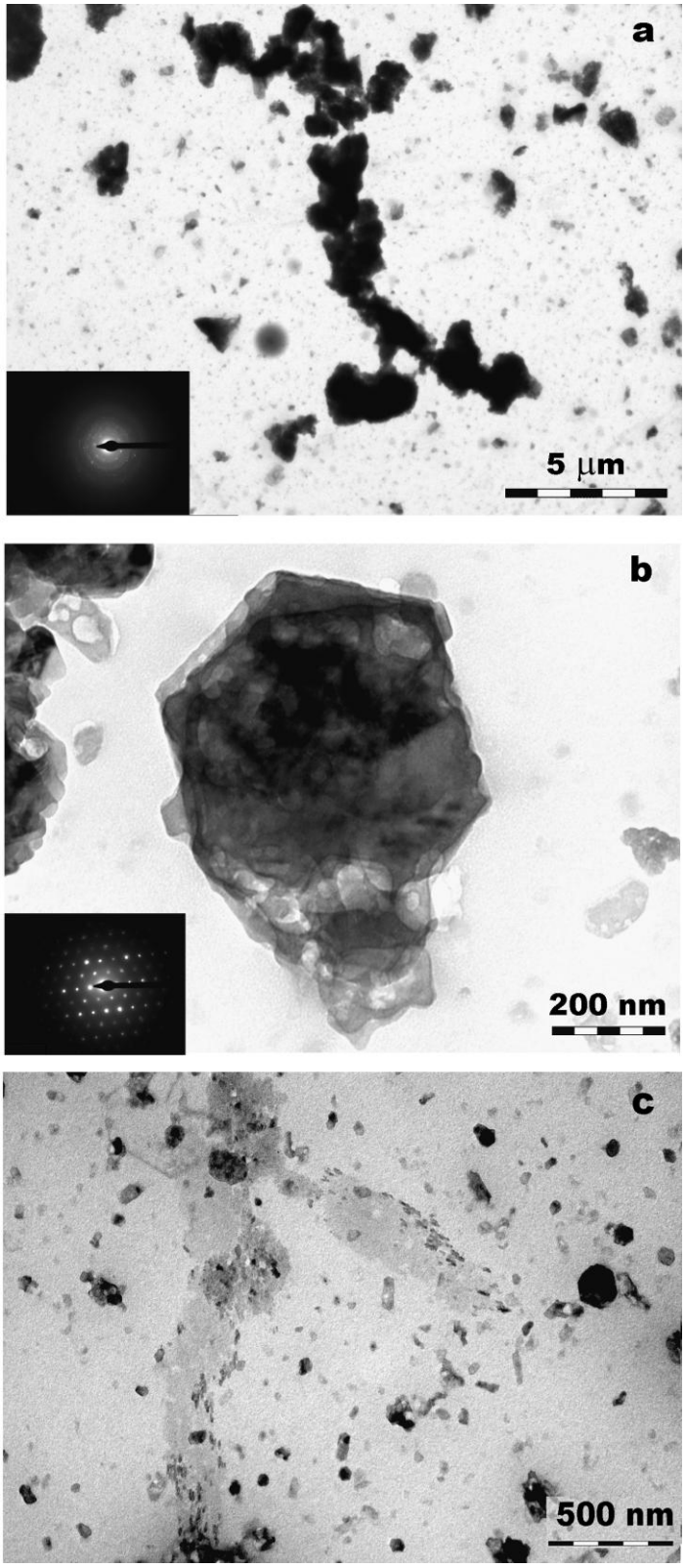

Figure I.1.1 *HRTEM images of the calcitic lime CL. (a) Micro-sized aggregates formed by randomly oriented $Ca(OH)_2$ nanoparticles, as shown by the diffraction rings in the SAED pattern (inset). (b) Plate-like $Ca(OH)_2$ nanocrystal; the basal plane (0001) is normal to the image plane, as shown by the SAED pattern (inset). (c) Individual nanoparticles and small aligned aggregates.*

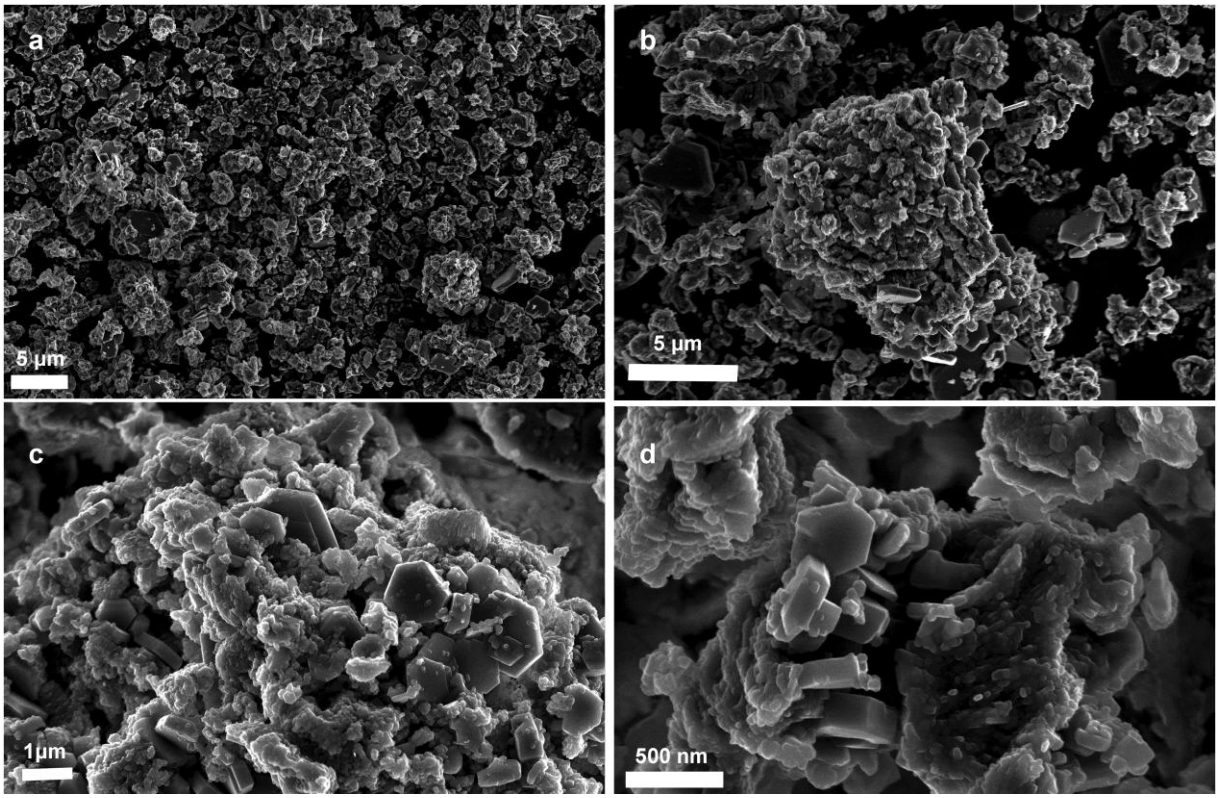

Figure I.1.2 FESEM images of the calcitic lime CL. (a) and (b) Aggregates of sub-microsized particles of different sizes. (c) and (d) Aggregates of individual sub-microsized prism-shaped $Ca(OH)_2$ crystals and oriented aggregates of colloidal particles.

Dolomitic lime (DL) by contrast is predominantly characterised by nanoparticles, while the sub-micro- and micro-prismatic crystals observed in CL are absent. In fact, FESEM observations dismiss the presence of individual particles of over 500 nm. Dolomitic lime particles give rise to monodisperse and round aggregates, which are mainly between 1 and 2 µm in size (Fig. I.1.4a-c).

According to the PSD curve (Fig. I.1.3), DL is also characterised by large clusters of over 10 µm. HRTEM observations show that dolomitic lime is characterized by hexagonal platelets of portlandite and brucite, which are different in length and thickness (Fig. I.1.5a-c). Microanalyses performed at a nanoscale by means of TEM indicate that plate-like crystals with an average length of 124 nm (d) and a thickness of 17 nm (l) are brucite crystals (Fig. I.1.5a). For these particles, the aspect ratio (r_p) (calculated with Eq. I.1.1) is 7.4. Another type of platelet that was bigger both in length and thickness (d=163 nm, l=63 nm) corresponded to portlandite crystals (Fig. I.1.5a and I.1.5c), with an average r_p equal to 2.6. In TEM images (Fig. I.1.5), brucite and portlandite platelets are easy to distinguish, because the former are clearer and more elongated than the latter. The clusters of DL particles have no orientation, although we did observe some brucite platelets that appeared to be aligned perpendicularly to the [001] direction (Fig. I.1.5b).

For calcitic lime particles, r_p was found to be equal to 2.5, which is very similar to the aspect ratio found for portlandite crystals in dolomitic lime. However, this value is much lower than that found by Ruiz Agudo and Rodríguez Navarro [22] for plate-like portlandite crystals in lime putty (r_p=7.5). This discrepancy is due to the thickness of the plate-like crystals, which is higher in dry hydrated calcitic lime (CL) ($\bar{l}$ =34.8 nm) than in calcitic lime putty ($\bar{l}$ =11.5 nm) [22], while the crystal length is almost the same ($\bar{d}$ is 87 nm and 85 nm in CL and lime putty [22], respectively).

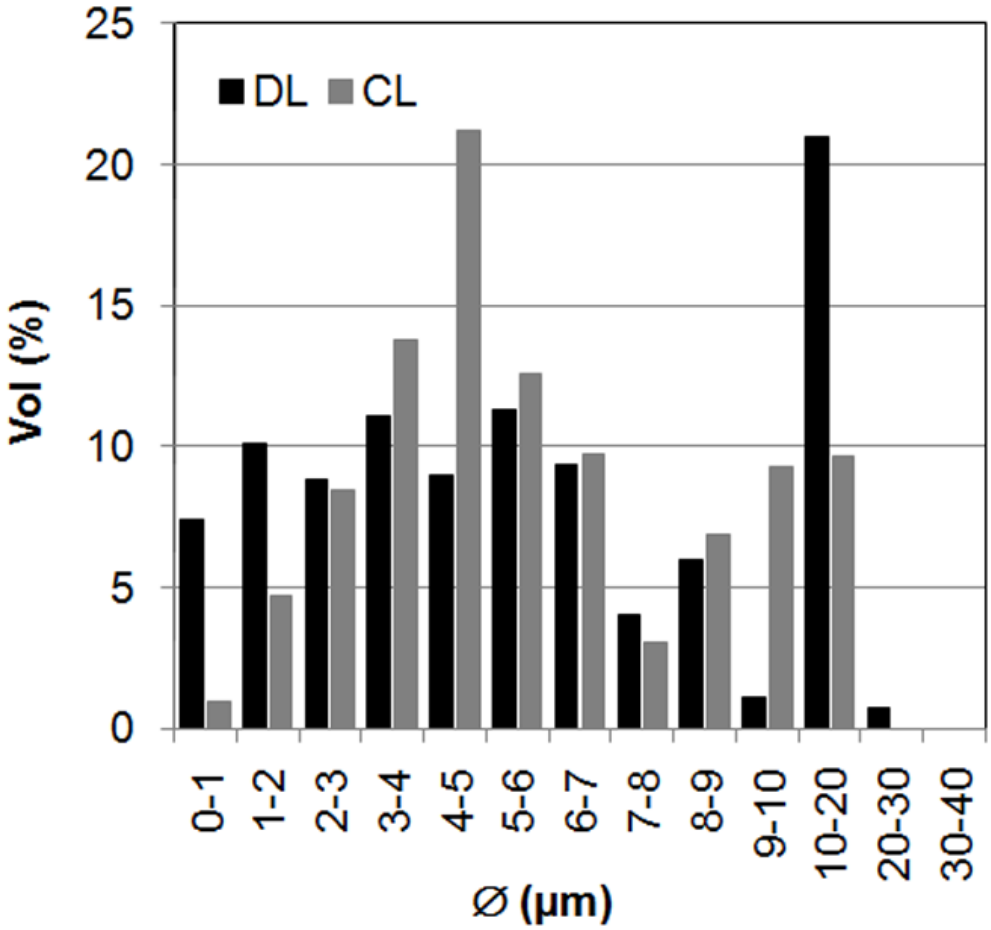

Figure I.1.3 *Particle size distribution of the calcitic (CL) and dolomitic (DL) limes. The volume (in %) of particles is represented on the basis of the particle diameter (in µm).*

The electrophoretic mobility (μ_e) and ζ-potential values found for the two limes are significant for the estimation of the kinetic stability of the lime dispersions in water (Tab. I.1.2). The higher ζ-potential in DL corresponds to a higher surface charge density, which is logical, given that the volume of the Ca atom (29,9 cm^3/mol) is twice that of the Mg atom (Mg=14,0 cm^3/mol). This may be why DL dispersions, characterised by smaller particles (according to the higher value of SSA, Tab. I.1.2), are more stable than those of CL, knowing that relative kinetic stability depends on particle size (the smaller, the more stable) [23].

The ζ-potential value in CL particles is slightly lower than 34 mV, which is the value indicated by Giorgi et al. [24] for portlandite. This is probably due to the wider PSD of portlandite particles in the dry hydrated calcitic lime with respect to the calcium hydroxide synthesized by these authors. In fact, the increase of particle size would lead to a decrease in kinetic stability [23], and therefore of the ζ-potential.

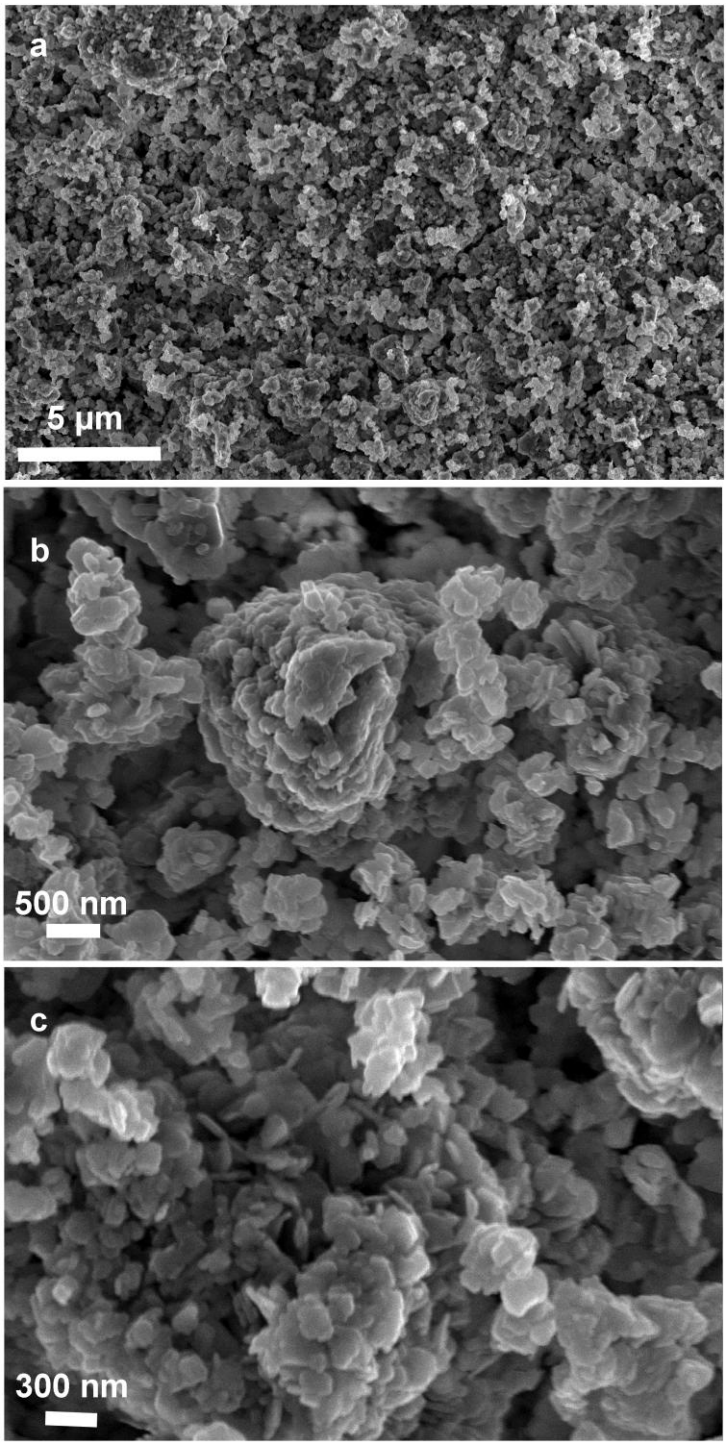

Figure I.1.4 FESEM images of the dolomitic lime DL. (a) and (b) Aggregates of particles. (c) Nanosized particles.

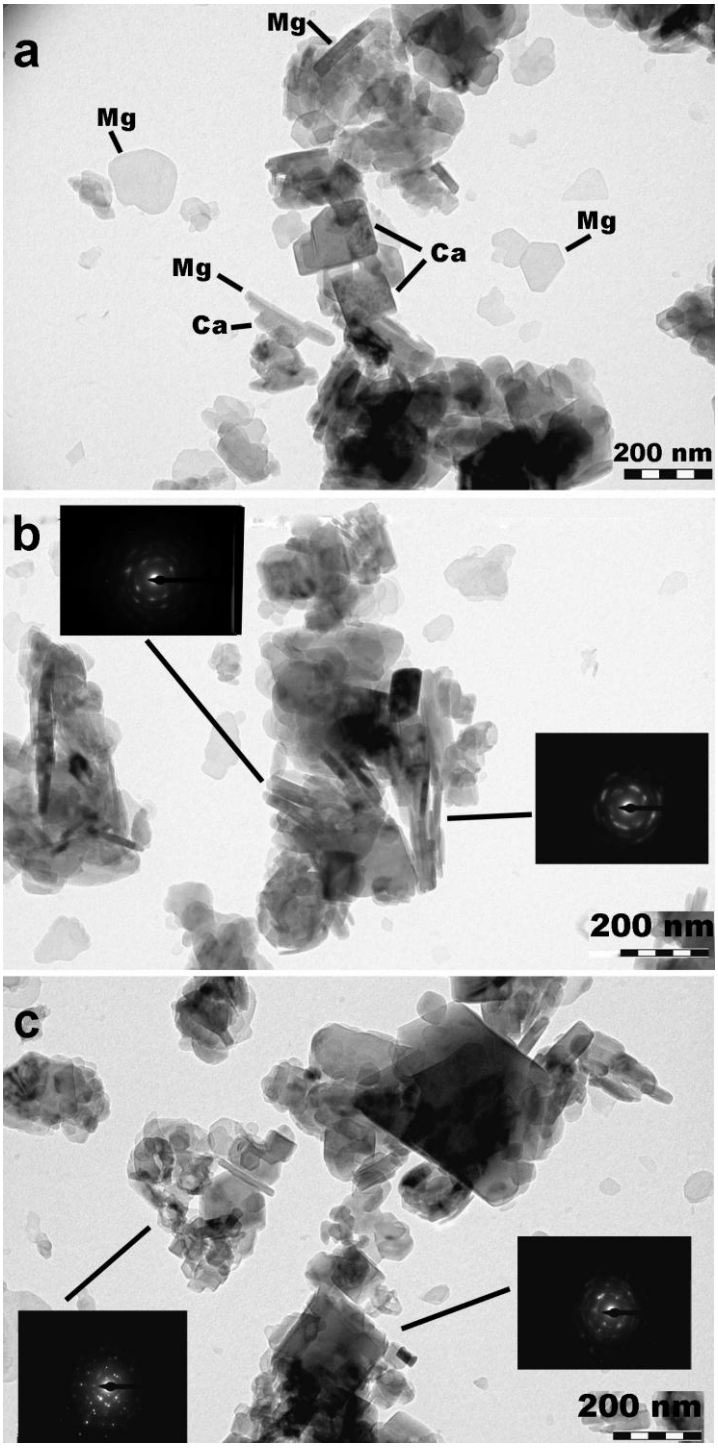

Figure I.1.5 *HRTEM images of the dolomitic lime DL. (a) Clusters formed by portlandite ($Ca(OH)_2$) and brucite ($Mg(OH)_2$) crystals, according to the microanalysis performed on the particles indicated by the dark lines. (b) Two clusters of apparently oriented brucite platelets. (c) Clusters of polydisperse portlandite crystals and brucite platelets. The white points in the SAED pattern (inset in b and c) indicate that there are various crystals with the same habitus, although they are not exactly oriented in the aggregates.*

Dry lime powder		
	CL	DL
SSA	13.8	23.1
μVol.	0.0569	0.0898
ρ	2.42	2.38
ρ_b	0.496	0.416
ρ_b^*	0.611	0.496
RLP	0.205	0.175
RCP	0.253	0.208
Dispersions in water		
	CL	DL
μ_e	2.31±0.25	2.81±0.35
ζ-pot.	29.43±3.23	34.33±4.83

Table I.1.2 *Particle properties of the dry powders of calcitic (CL) and dolomitic (DL) limes and of the dispersions of CL and DL in water: specific surface (SSA, m^2/g); micropores volume (μVol., $cm^3 \cdot g$); solid (or particle) density (ρ, cm^3/g); bulk density determined without compaction (ρ_b, cm^3/g); bulk density determined with compaction (ρ_b^*, cm^3/g); Random Loose Packing (RLP, m^3/m^3); Random Close Packing (RCP, m^3/m^3); electrophoretic mobility (μ_e, $m^2 \cdot V^{-1} \cdot s^{-1}$); electrokinetic potential (ζ-pot., mV).*

The isotherm curves are typically S-shaped (Fig. I.1.6a). The low-pressure portion is concave to the pressure axis, that of higher pressure is convex to the pressure axis and the intermediate region is more or less linear with respect to pressure [14]. These curve shapes correspond to Type II, which indicates a monolayer-multilayer adsorption typical of non-porous adsorbents [25]. Moreover, the hysteresis loop, both for the CL and the DL isotherm, is of type H_3 (inset in Fig. I.1.6a), which is typical of aggregates of plate-like particles [9]. Dolomitic lime presents a higher volume of pores with a diameter comprised between 20 and 500 Å (Tab. I.1.2 and Fig. I.1.6b). This is consistent with the higher SSA value found for DL (Tab. I.1.2), which has to be attributed to the lower size of its particles and aggregates.

It is interesting to notice that lime suspensions always show higher values of solid fractions than the maximum packing estimated for dry lime powders, both vibrated and unvibrated (RCP and RLP values, respectively; Tabs. I.1.1 and I.1.2). This underestimation of the packing density in dry powders is due to the tendency to agglomerate of dry particles of less than 100 μm [26], which gives rise to the polydisperse agglomerates described above. However, during the preparation of the lime suspensions in a polar medium such as water [27], aggregates are dispersed because of the electrostatic forces between the charges present on the surface of portlandite crystals [22, 27-28].

Although the suspensions of DL prepared for the rheological measurements have lower solid fractions ($0.13<\varphi<0.18$) than the CL suspensions ($0.22<\varphi<0.28$), their viscosity (or plasticity), estimated manually, is considerably higher than that of CL pastes. The higher

surface charge of DL (*cf.* ζ-potential in Tab. I.1.2) may also cause higher water adsorption capacity of this lime. Besides, water molecules may be immobilized between ions and not available in the suspensions, thus increasing the apparent solid volume fraction and, consequently, the viscosity of the suspension.

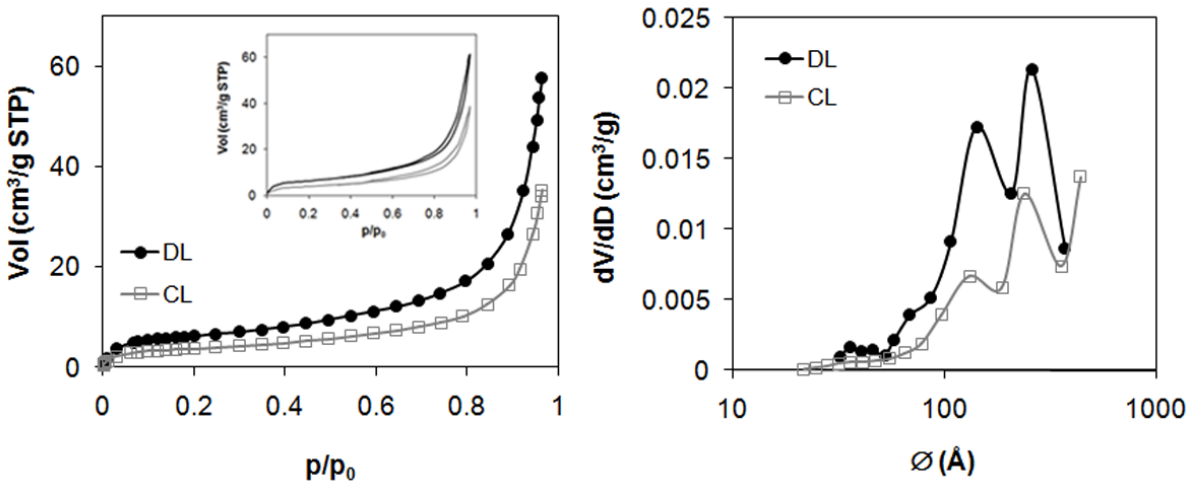

Figure I.1.6 *N_2 sorption analysis of the calcitic (CL) and dolomitic (DL) limes: (a) adsorption isotherms, in which the relative pressure (p/p_0, where p_0 is the saturation pressure of the pure adsorptive at the temperature of the measurement) is plotted against the adsorbed volume (in cm^3/g STP), determined at standard conditions of temperature and pressure. The inset in (a) shows the adsorption-desorption isotherms with a H_3 hysteresis loop. (b) BJH pore size distribution curves, in which the pore diameter (in Å) is plotted against the incremental volume (in cm^3/g).*

3.2 Viskomat rheometry

Viscosity and flow curves for CL and DL suspensions are plotted in Figs. I.1.7. The higher viscosity of DL with respect to CL for comparable solid fractions is due to the higher number of particle-particle collisions and the higher charge density of Mg ions, which attract more water molecules that lead to a higher apparent solid fraction. Moreover, the interactions between electric double layers, which are bigger in DL particles, increase the viscosity and the bulk stress.

The viscosity curves (Figs. I.1.7a and c) show a decrease in apparent viscosity as the shear rate increases. Both DL and CL show a Bingham-like behaviour, characterised by a high yield stress, which increases with increasing solid fraction (Tab. I.1.3). The plastic viscosity decreases for CL but remains approximately constant for the DL.

This shear-thinning behaviour observed in CL suspensions (Fig. I.1.7a), typical of non-Newtonian suspensions [11], is attributed to disagglomeration and orientation of lime particles which, in conditions of high pH and low ionic force, form a disordered "house-of-cards" structure, described by other authors to explain the arrangement of suspensions at rest of angular and polydisperse hexagonal plate-like particles [28] and, more specifically, of calcitic lime particles [22]. At increasing shear rate

this structure is destroyed because hydrodynamic forces overcome electrostatic interactions between opposite charges present in the basal planes (positive-charged) and in the side-planes (negative-charged) of individual plate-like particles [22]. As the shearing continues, platelets may align spontaneously with the direction of the flow [29].

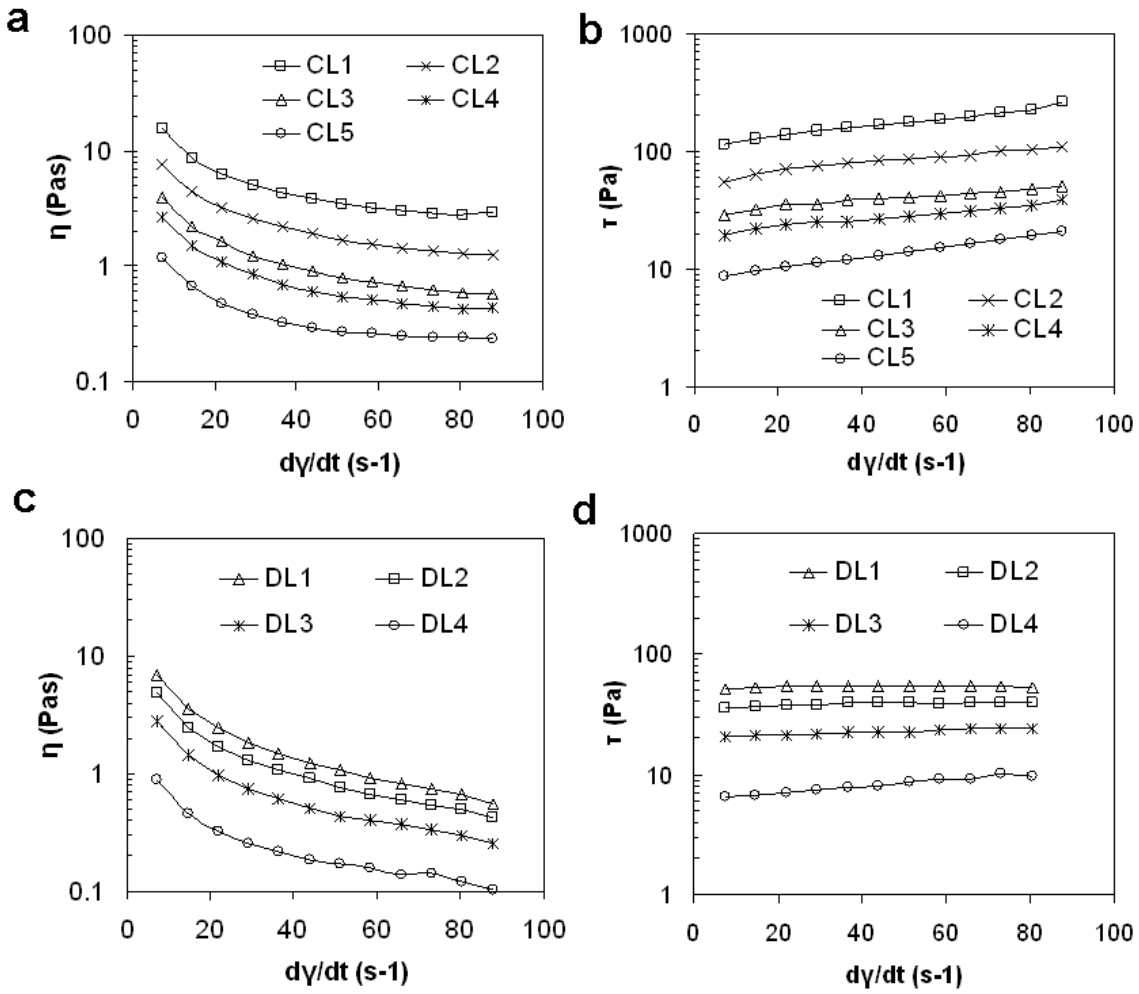

Figure I.1.7 Semi-logarithmic curves obtained for calcitic (CL) and dolomitic (DL) lime slurries, by means of the Viskomat: viscosity curves for CL (a) and DL (c) slurries, in which shear rate (dγ/dt, s-1) is plotted against apparent viscosity (η, Pas); flow curves for CL (b) and DL (d) slurries, in which shear rate (dγ/dt, s-1) is plotted against shear stress (τ, Pa).

	Calcitic lime suspensions					*Dolomitic lime suspensions*			
	CL1	CL2	CL3	CL4	CL5	DL1	DL2	DL3	DL4
φ	0.28	0.26	0.24	0.23	0.22	0.18	0.17	0.15	0.13
η_{pl}	1.43	0.61	0.23	0.21	0.15	0.07	0.06	0.05	0.05
τ	106.11	55.44	28.89	18.14	7.03	51.26	35.71	20.12	6.07

Table I.1.3 Analysis of the Bingham parameters of calcitic (CL) and dolomitic (DL) lime suspensions in water: solid fraction (φ); plastic (Bingham) viscosity (η_{pl}, in Pas); yield stress (Bingham) (τ, in Pa).

The thixotropic nature of the CL slurries was verified by performing constant rate experiments where suspensions were subjected to constant speeds rotation of 120, 110, 30, 20 and 10 rpm, each for 10 min. At 120 rpm, the torque decreases sharply during the first 3 minutes until it reaches a constant level. In this case, the spontaneous alignment of platelets with the flow direction leads to a lower resistance to the flow. At 110 rpm, the torque is quite constant, so we can assume that no changes happen in the microstructure at this shear rate. Finally, at 30, 20 and 10 rpm, the torque increases because hydrodynamic forces are again overcome by colloidal forces and particles tend to recover their initial structure of "house of cards".

The flow curves for DL slurries (Fig. I.1.7d) are quite flat, which means that there is almost no change in shear stress at increasing shear rate. The high decrease in viscosity and the narrow shear stress range obtained for DL suspensions (Fig. I.1.7c and I.1.7d) may be related with the shear localisation effect. Given the colloidal character of DL particles, we may assume a flocculation of these particles during shearing which creates regions at different concentration and shear rate, resulting in an "apparent slip" of the suspended particles (or "shear localisation effect"). These heterogeneous zones are formed inside the suspension, likewise other authors studied [22, 30], given that the geometry of mixer-type rheometers like the Viskomat considerably reduces the slip at the wall of the container ("wall slip").

According to Barnes [31], the slipping effect depends on particle size, state of dispersion and concentration of the suspension and it can be assumed in suspensions of nanometric particles, as in the case of DL. At high shear rates, hydrodynamic forces decrease the resistance of particles to flow. On the other hand, flocculation is enhanced at these conditions because the collision frequency increases [29] and this results in higher stresses. The final result of these opposing effects is manifested in the flow curves of DL (Fig. I.1.7d), in which a constant shear stress is registered. Whilst in CL the achievement of a constant viscosity value is due to a equilibrium between particle dispersion (which increases η) and particle orientation (which decreases η), in DL this equilibrium is more difficult to achieve, due to difficulty in dispersing the flocks.

3.3 Coaxial cylinders rheometry

The same measurement conditions used in the Viskomat were applied in the Brookfield rheometer, in order to study the influence of instrument geometry on the flow behaviour of the suspensions. The loop experiments were done over a high shear rate range and without reaching steady states. Viscosity and flow curves of DL and CL were found to show similar trends to those obtained with the Viskomat.

Interesting results were obtained when lime suspensions were subjected to a wider speed range in CR mode (described in section 2). The hysteresis curves, shown in Fig. I.1.8, indicate that the flow changes with time but in opposite flow way for the two limes. In fact, in CL we obtained

a hysteresis curve typical of thixotropic suspensions, for which viscosity decreases over time. In the downward part of the curve, as the shear rate decreases, the shear stress obtained is lower than the value registered in the upward section of the curve. This curve confirms the assumptions discussed above on the microstructure of CL suspensions under shearing. On the other hand, DL behaves anti-thixotropically, because the shear stress increases in the downward part of the curve. This result is an experimental evidence of the flocculation occurring under shearing in a suspension of dolomitic lime particles, which have a very small size and a high surface charge. In fact, anti-thixotropic (or rheopectic) behaviour is frequently associated with gelification processes [28], which involve the development of a new structure, such as flocculation (i.e. formation of agglomerates of colloidal particles).

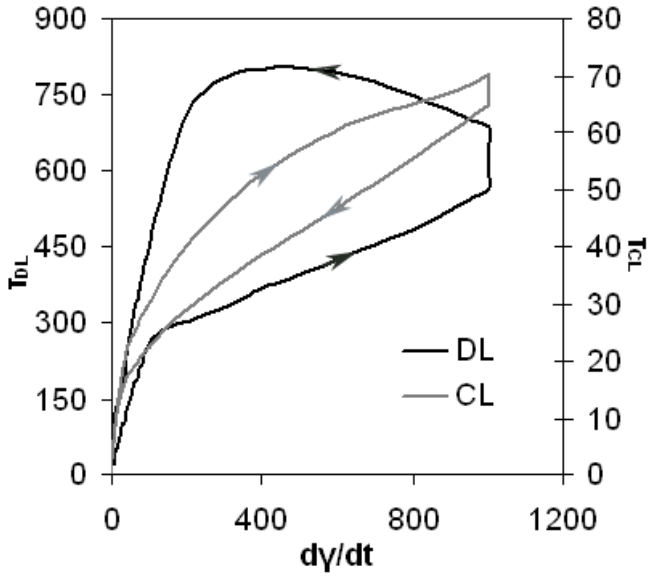

Figure I.1.8 Flow behaviour of the calcitic CL (φ=0.23) and the dolomitic DL (φ=0.19) lime suspensions, studied by means of a Brookfiled rheometer with coaxial cylinders geometry, in CR mode and in a wide range of shear rates. Flow curves, in which shear rate (dγ/dt, s^{-1}) is plotted against shear stress (τ, Pa). Arrows show the up and down branch of the hysteresis curves, indicating the thixotropic and anti-thixotropic behaviour of calcitic and dolomitic lime, respectively.

3.4 Intrinsic viscosity and maximum packing fraction

Apparent viscosity values obtained from measurements in the Viskomat were plotted to the solid fraction of the suspensions. As expected, the viscosity tends to infinity at the value for the maximum solid fraction. For CL slurries, the values of maximum solid fraction (φ_m) and intrinsic viscosity ([η]) obtained were not the same at different velocities (Tab. I.1.4). The increase in the maximum solid fraction with increasing shear rate has been attributed to the ability of particles to pack more densely when subjected to higher shear rates [32]. In fact, particles tend to disagglomerate with shearing, so that a closer packing is possible.

Likewise, the decrease in the intrinsic viscosity at the higher shear rates may be related to changes in the degree of agglomeration of the suspended particles and also to the Brownian motion contributions [29].

CL Slurries						
N	10	30	50	70	90	110
[η]	19.75	18.58	17.97	17.71	17.66	17.42
φ_m	0.36	0.38	0.39	0.40	0.41	0.41

Table I.1.4 *Values of intrinsic viscosity ([η]) and maximum solid fraction (φ_m) found for calcitic lime (CL) slurries at different rotation speeds (N, rpm).*

The average value of φ_m obtained for CL (0.39) is twice the RLP value found for the dry CL (0.20, Tab. I.1.2). Once more, this is an effect of the agglomeration of CL particles in the dry state, which gives a lower maximum packing value. This result supports Wong and Kwan's statement about the inaccuracy of the dry method for the determination of maximum packing [6].

In our case the φ_m obtained for calcitic lime was lower than the expected, given the theoretical values of maximum packing for monodisperse ($\varphi_m \approx 0.52$-0.74) and polydisperse particles ($\varphi_m \approx 0.87$). The discrepancy between the values we obtained and the theoretical ones is due to the fact that the double layer of lime particles has not been considered in the calculations. In reality, the presence of surface charges on particles produces a higher particle diameter (effective diameter) and lower volume fraction (effective volume fraction).

The intrinsic viscosity average value found for calcitic lime (18.1) approach the value obtained by Hendrickx [5] for calcitic hydrated lime (19.1).

For DL suspensions, we did not obtain a good fitting of the Krieger-Dougherty model at any shear rate. On the other hand, it was possible to fit the viscosity values of particles dispersed at very low concentrations in glycerine (Eq. I.1.5), which yields a value of [η] equal to 16.82 for DL, which is higher than what would be expected from the high solid fraction data of the concentrated aqueous suspensions. Considering the reliability of the direct method in glycerine this different result indicates the existence of a non-homogeneous flow in suspensions at high concentrations, because of the presence of a zone with lower solid fraction and viscosity. The [η] value found for DL in the diluted regime (in glycerine) is slightly lower than the obtained for CL ([η] = 17.60) at the same conditions. This can be explained by the fact that whilst diluted suspensions of DL in glycerine are formed by individual colloidal particles, suspensions of CL are presumably formed by particle agglomerates which cannot disperse in a medium with a small dipole moment like glycerine. Logically, round-shaped nanoparticles give rise to a lower value of intrinsic viscosity than clusters of particles, which are larger.

The value of φ_m for DL is expected to be lower than the value found for CL with the Krieger-Dougherty model. As we know that the double layer of DL particles is bigger than that of CL particles, we can state that the effective volume of DL particles is bigger and this inevitably results in a lower packing density.

4. Conclusions

The differences in flow behaviour between calcitic and dolomitic lime hydrate slurries were investigated in the light of the properties of the particles. CL particles occur in micro- and nano-scale polydisperse and angular aggregates and clusters are randomly oriented. On the other hand, DL is characterised by nanoparticles in more monodisperse and round aggregates. It has higher SSA and ζ -potential than CL and more pores in the nano-range. Four important rheological differences were discussed and linked to micro-structural aspects of the materials. Firstly the viscosity of DL slurries is higher than of CL slurries when both are made with the same solid fraction. This is due to the higher electrical potential of DL, which leads to higher apparent solid fraction and also to electroviscous effects. Secondly CL slurries present a pseudo-plastic behaviour whereas DL approaches perfect plastic materials, having a more horizontal flow curve. For CL the plastic viscosity shows a similar dependence. A third difference is in the solid fraction dependence of viscosity. For CL slurries a clear Krieger-Dougherty relation was found, whilst for the DL slurries the rheological parameters were not obtained by fitting this model. Notwithstanding, a direct measurement (in diluted suspensions) of the intrinsic viscosity indicates a slightly lower value than for CL, due to differences of particles shape, size and aggregation state.

Finally rate-controlled loop experiments revealed that CL follows the expected trend for thixotropic materials whilst DL shows an anti-thixotropic behaviour. Both phenomena are related to shear-driven breakdown and build-up of the particles in suspension.

This study fulfils the main proposed objectives regarding the practical aspects of the use of two limes for mortars manufacturing, given that the rheological parameters have been determined in a range of concentrations and shear stresses similar to those adopted in mortars manufacturing processes. Besides, these findings confirm and quantify the more qualitative practical knowledge about the plasticity of plasters and renders made with DL. From a practical point of view, the dolomitic lime presents the most suitable behaviour for the application of mortars, because it results in a constant resistance of the mortar at any spreading rate. This is the reason of the traditional preference for dolomitic lime mortars for plastering and rendering applications.

However further investigations are necessary in order to gain deeper insight in the mechanisms taking place in limes suspension. Future work should concentrate on particle observation and flow field visualisation during shear (by Nuclear Magnetic Resonance, for example) in order to clarify the observed phenomena.

Acknowledgements:

This study was financially supported by Research Group RNM179 of the Junta de Andalucía and by Research Project MAT2008-06799-C03-03. We are grateful to Jan Mewis and Carlos Rodríguez Navarro for their useful suggestions and to Nigel Walkington for his assistance in translating the original text.

References

[1] Ferraris C. F., De Larrard F.: "Testing and Modeling of Fresh Concrete Rheology", *NISTIR-6094*, Gaithersburg, Maryland (1998).
[2] Bager D. H., Geiker M. R., Jensen R. M.: "Rheology of self-compacting mortars. Influence of particle grading", *Nord. Concr. Res.*, Vol. 26 (2001), pp. 1-16.
[3] Fletcher, Hill: "Making the connection - particle size, size distribution and rheology", http://www.chemie.de/articles/e/61207/
[4] Westerholm M., Lagerblad B., Silfwerbrand J., Forssberg E.: "Influence of fine aggregate characteristics on the rheological properties of mortars", *Cem. Concr. Compos.*, Vol. 30, n° 4 (2008), pp. 274-282.
[5] Hendrickx R.: "The adequate measurement of the workability of masonry mortar", PhD Thesis, Catholic University of Leuven (2009).
[6] Wong H. H. C., Kwan A. K. H.: "Packing density of cementitious materials: part I – measurement using a wet packing method", *Mater. Struct.*, Vol. 41, n° 4 (2007), pp. 773-784.
[7] Golaszewski J., Szwabowski J.: "Influence of superplasticizers on rheological behaviour of fresh cement mortars", *Cem. Concr. Res.*, Vol. 34, n° 2 (2004), pp. 235-248.
[8] Yahia A., Tanimura M., Shimoyama Y.: "Rheological properties of highly flowable mortar containing limestone filler-effect of powder content and W/C ratio", *Cem. Concr. Res.*, Vol. 35, n° 3 (2005), pp. 532-539.
[9] Rodriguez Navarro C., Ruiz Agudo E., Ortega Huertas M., Hansen E.: "Nanostructure and irreversible colloidal behavior of $Ca(OH)_2$: implications in cultural heritage conservation", *Langmuir*, Vol. 21, n° 24 (2005), pp. 10948-10957.
[10] Thomson M. L.: "Plasticity, water retention, soundness and sand carrying capacity: what a mortar needs", Bartos P., Groot C., Hughes J. J. (Eds.), International RILEM workshop on historic mortars: characterisation and tests, RILEM, Pasley, Scotland (2000), pp. 163-172.
[11] Barnes H. A., Hutton J. F., Walters K.: *Introduction to Rheology*, p 201, Ed. K. Walters, Elsevier, Amsterdam, 1st edn. (1989).
[12] Shapiro A. P., Probstein R. F.: "Random packings of spheres and fluidity limits of monodisperse and bidisperse suspensions", *Phys. Rev. Lett.*, Vol. 68, n° 9 (1992), pp. 1422-1425.
[13] UNE-EN 459-1:2001. "Building lime – Part 1: Definitions, specifications and conformity criteria", Madrid (2002).
[14] Brunauer S., Emmet P. H., Teller J.: "Adsorption of gases in multimolecular layers", *J. Am. Chem. Soc.*, Vol. 60 (1938), pp. 309-319.

[15] Barret E. P., Joyner L. J., Halenda P.: "The determination of pore volume and area distributions in porous substances. I. Computations from nitrogen isotherms", *J. Am. Chem. Soc.*, Vol. 73 (1951), pp. 373-380.
[16] ASTM D 854-92. Test Method for Specific Gravity of Soils (1993).
[17] Von Smoluchowski M. *Bull. Int. Acad. Sci.* (1903), p. 184.
[18] Parkhurst D.L., Appelo C.A.J. Users Guide to PHREEQC (version 2)-A Computer Program for Speciation, Batch Reaction, One-Dimensional Transport, and Inverse Geo- chemical Calculations. U.S. Geological Survey Water-Resources Investigation Report 99-4259, (1999) p. 312
[19] Bousmina M., Aït-Kaidi A., Faisant J.B.: "Determination of shear rate and viscosity from batch mixer data", *J. Rheol.*, Vol. 43, n° 2 (1999), pp. 415-433.
[20] Aït-Kaidi A., Marchal P., Choplin L., Chrissemant A. S., Bousmina M.: "Quantitative analysis of mixer-type rheometers using the Couette analogy", *Can. J. Chem. Eng.*, Vol. 80 (2002), pp. 1166-1174.
[21] Krieger I. M., Dougherty T. G.: "A mechanism for non-Newtonian flow in suspensions of rigid spheres", *Trans. Soc. Rheol.*, Vol. 3 (1959), pp. 137-152.
[22] Ruiz Agudo E., Rodríguez Navarro C.: "Microstructure and rheology of lime putty", *Langmuir*, Vol. 26, n° 6 (2010), pp. 3868–3877.
[23] Ambrosi M., Dei L., Giorgi R., Neto C., Baglioni P.: "Colloidal Particles of $Ca(OH)_2$: Properties and Applications to Restoration of Frescoes", *Langmuir*, Vol. 17, n° 14 (2001), pp. 4251-4255.
[24] Giorgi R., Dei L., Ceccato M., Schettino C., Baglioni P.: "Nanotechnologies for Conservation of Cultural Heritage: Paper and Canvas Deacidification", *Langmuir*, Vol. 18, n° 21 (2002), pp. 8198-8203.
[25] Sing K. S. W., Everett D. H., Haul R. A. W., Moscou L., Pierotti R. A., Rouquérol J., Siemeniewska T.: "Reporting physisorption data for gas/solid systems", *Pure & Appl. Chem.*, Vol. 57, n° 4 (1985), pp. 603-619.
[26] Yu A. B., Bridgwater J., Burbidge A.: "On the modelling of the packing of fine particles", *Powder Technol.*, Vol. 92, n° 3 (1997), pp. 185-194.
[27] Ren J., Lu S., Shen J., Hu B., Dispersion characteristics of fine particles in water, ethanol and kerosene. Chin. Sci. Bull., Vol. 45 n° 15 (2000), pp. 1376-1380.
[28] Moreno Botella R.: *Reología de suspensiones cerámicas*. CSIC, ISBN 84-00-08322-9 (2005).
[29] Wierenga A. M., Philipse A. P.: "Low-shear viscosity of isotropic dispersions of (Brownian) rods and fibres; a review of theory and experiments", *Colloids Surf.*, Vol. 137 (1998), pp. 355-372.
[30] Møller P. C. F., Mewis J., Bonn D.: "Yield stress and thixotropy: on the difficulty of measuring yield stress in practice", *Soft Matter*, Vol. 2, n° 4 (2006), pp. 274-283.
[31] Barnes H. A.: "A review of the slip (wall depletion) of polymer solutions, emulsions and particle suspensions in viscometers: its cause, character and cure", *J. Non-Newtonian Fluid Mech.*, Vol. 56, n° 3 (1995), pp. 221-251.

[32] Struble L., Sun G. K.: "Viscosity of Portland cement paste as a function of concentration", *Adv. Cem. Based Mater.*, Vol. 2 (1995), pp. 62-69.

Chapter I.2

The difference in behaviour between calcitic and dolomitic lime mortars set under dry conditions: the relationship between textural and physical-mechanical properties

Arizzi A., Cultrone G.
Submitted to *Cement and Concrete Research*
(accepted)

Abstract

Differences in the texture, mineralogy, hygric and mechanical properties of mortars prepared with dry hydrated limes of calcitic and dolomitic composition are investigated in this work. Special attention is given to the influence of the lime microstructure and the mortars curing condition. The effect of using two different aggregates (natural and crushed of calcitic and siliceous composition) is also examined. Results showed that the use of dolomitic lime is not recommendable if mortars are applied in dry areas since, under these conditions, a great shrinkage occurs and no strength improvement is induced. Moreover, dolomitic mortars presented a pore network that negatively affects the water transfer properties. On the contrary, calcitic mortars present higher carbonation degree and better physical-mechanical properties. Finally, the use of a calcareous aggregate is preferred because it produces better cohesion in the mortar.

1. Introduction

At the present time, when designing repair mortars, nobody questions the recommended preference for aerial or hydraulic limes [1-3] with respect to Portland cement, knowing the deleterious effects that this binder has provoked in ancient building [4,5].

If an aerial binder is selected, often the question is which lime, whether calcitic or dolomitic, has to be preferred for elaborating repair mortars.

In the past, this choice depended mostly on the availability of the geological source (namely the proximity to stone quarries to be exploited for obtaining the raw material), as demonstrated recently by Diekamp et al. [6] who identified dolomite in more than 250 samples of renders and plasters collected in buildings from Northern (Austria) and Southern Tyrol (Italy).

However, the choice can be controversial if it is grounded on the properties that each lime confers to the mortar. One of the reasons is that the quality of a lime depends on different factors, burning [7] and slaking [7,8] are some of them, which are in part overcome by the adoption of standardised limes [9], in which the amounts of portlandite ($Ca(OH)_2$), brucite ($Mg(OH)_2$) and calcite ($CaCO_3$) are strictly controlled. However, although standardization guarantees the production of limes with the same compositional quality, potential differences in their microstructure may still exist depending on the manufacturing process of the lime (industrial or traditional). This can be influential on the out coming of the carbonation process [10] and, therefore, on the final quality of the mortar, together with other factors, such as curing conditions [11] and aggregate type [12,13].

Conflicting results about the characteristics of the dolomitic limes in suspension are published in literature. Arizzi et al. [14] stated that dolomitic dry hydrated limes show a much more pronounced plasticity than the calcitic ones, therefore the dolomitic lime requires higher amount of water to attain the same consistence as calcitic lime suspensions. On the contrary, Chever et al. [15] found that the dolomitic lime possesses a lower water demand than the calcitic one although, finally, it leads to a greater shrinkage.

Further uncertainty exists regarding the hardened performances of dolomitic lime mortars. Some studies agree that dolimitic lime mortars are good for masonry mortars [6,15] because of their expected durability. On the other hand, Cultrone et al. [16] strictly warned not to use dolomitic lime for the elaboration of repair mortars exposed to urban environment, since the sulphation of this binder leads to the formation of highly soluble and deleterious hydrated magnesium sulphates, such as epsomite and hexahydrite, and the total amount of sulphates developed is higher compared to calcitic limes.

With respect to the physical-mechanical properties of dolomitic lime mortars, previous studies agree that they show higher mechanical strengths and lower porosity and capillary suction than the corresponding

calcitic mortars [13,15,17]. Dheilly et al. [17] attributed the higher strength of dolomitic lime mortars to the formation, under high moist conditions (RH = 98%), of a network of fine plate-like particles of hydromagnesite ($Mg_5(CO3)_4(OH)_2{\cdot}4H_2O$) that improve the cohesion between binder and aggregate grains. Similarly, other authors observed that the Mg-lime binders perform superiorly in areas subject to presence of moisture [18]. This can be explained with a feeble hydraulic character that the dolomitic lime seems to posses [19].

Since the formation of magnesite and hydromagnesite is kinetically hindered below 52ºC [20], this strength enhancement is not expected to occur under dry conditions. Lanas et al.'s study [13] on dolomitic lime mortars set under atmospheric conditions (T = 20±5 ºC and RH = 60±10 %) reports that the strength enhancement is due to the formation of portlandite and calcite after a dedolomitization process, which occurs when dolomite is present in the mortar.

In this work, dry hydrated dolomitic and calcitic limes are used, with the consequence that the microtextural characteristics of the lime can be consistently different than those of a lime slaked manually from a light calcined calcite or dolomite (as in Lanas et al.'s study [13]). The microstructure and flow behaviour of the limes used have been studied previously [14] and this allowed us to find a relation between the rheological properties of calcitic and dolomitic limes, and the quality of the fresh and hardening mortars prepared with them.

In this work we compared the mineralogical, textural, hygric and mechanical properties of calcitic and dolomitic lime mortars, in order to find out which lime (whether calcitic or dolomitic) is the most appropriate for the elaboration of repair rendering mortars to be applied in dry or low-moist zones. Especially, we claim to know if mortars prepared with a dry hydrated dolomitic lime still show good physical-mechanical properties under a dry environment and to investigate the cause of an eventual improvement.

In this sense, it is important to remember that when a mortar is applied as coating of wall or building facades, mechanical strength is not a crucial property as it may be in masonry mortars, whilst water capillary absorption, porosity and shrinkage are characteristics that need to be strictly controlled.

The influence of the characteristics and mineralogy of the aggregate is also investigated.

2. Materials and methods

2.1. Limes and aggregates

The calcitic lime (CL) chosen is a CL90-S [9], produced by ANCASA (Seville, Spain) whilst the dolomitic lime (DL) is a DL85-S [9], produced in the USA and supplied by LHOIST enterprise (Nivelles, Belgium).

Two aggregates of calcareous (CA, 0.063<ø<1.5 mm) and siliceous (SA, 0.1<ø<0.5 mm) composition were used. Following the European

standard classification for aggregate grading [21], CA and SA can be classified as fine aggregates.

2.1.1 Characterization of the limes

The mineralogical phases of the limes were determined by X-ray diffraction (XRD), using a Philips PW-1710 (disoriented powder method). Analysis conditions were: radiation CuK_α (λ=1.5405 Å), 3 to 60 º2θ explored area, 40 kV voltage, 40 mA current intensity and goniometer speed of 0.1 º2θ/s. The interpretation and quantification of the mineral phases were performed by using the X-Powder software package [22].

Specific surface area (SSA) and micropore volume (determined with BET [23] and BJH [24] methods, respectively) were measured by using the N2 Adsorption technique, by means of an equipment Micromeritics 3000 Tristar that works under continuous adsorption conditions at a temperature of 77 K. Prior to the measurements, two samples per lime were outgassed at 10^{-3} Torr and 110 ºC for 4 hours, by means of a Micromeritics Flowprep.

Solid density (ρ, g/cm^3) of the limes was measured by pycnometer analysis. Measurements were carried out according to the ASTM D 854-92 standard [25]; pycnometers were calibrated and filled with white spirit.

The bulk density of the limes was measured without (ρ_b, g/cm^3) and with (ρ_b^*, g/cm^3) compaction. In the first case, the limes were poured loosely into a container without any additional compaction. In the second one, the bulk density was determined after vibrating them at 0.3 mm of amplitude and 50 Hz of frequency during 300 s.

2.2 Mortars preparation and curing

Four types of mortars were prepared with a binder-to-aggregate ratio of 1:3 by weight. Their names and composition are shown in Table I.2.1. The water amount (Tab. I.2.1) was determined in order to obtain mortars with a plastic consistence. The flow was calculated as the average of the spread diameter (in mm) measured on three fresh samples during the flowability assay [26] and it was equal to 150±5 mm. After the preparation [27], mortars were cured for 7 days in normalized steel moulds (4×4×16 cm) at RH = 60±5% y T = 20±5 °C and, after desmoulded, cured for further 21 days in the same laboratory (modification of the standard UNE-EN 1015-2 [27] proposed by Cazalla [28]). Mortars samples were cured at RH = 60±5% y T = 20±5 °C for the whole period of the study.

Mortar name	CC	CS	DC	DS
Lime	CL	CL	DL	DL
Aggregate	CA	SA	CA	SA
W (%)	31	27	35	34

Table I.2.1 *Composition, names and water amount (W, expressed in % on the total mass) of the four mortars studied, with a binder-to-aggregate ratio of 1:3 by weight. CL: calcitic lime; DL: dolomitic lime; CA: calcareous aggregate; SA: siliceous aggregate.*

2.3 Mortars characterization

In order to follow mineralogical, textural and physical mortars changes due to the carbonation process, mortar samples were analyzed after 28 days and 2 months since their elaboration.

2.3.1 Carbonation degree

The mineralogical phases of mortars were determined by means of thermogravimetric analyses (TGA), by using a Shimadzu TGA-50H equipment. Approximately 50 mg of sample was heated in an alumina crucible, in a flushed-air atmosphere (100 mL/min), at a heating rate of 5º/min and 25-950 ºC interval. TGA data treatment was carried out according to the standard UNE-EN ISO 11358 [29]. Mortars phases were determined by measuring the weight loss corresponding to the stoichiometric reactions of brucite (300<T<400 ºC) and portlandite (450<T<550 ºC) dehydroxylation and calcite thermal decomposition (700<T<900 ºC). The decrease in portlandite and brucite content was taken as a reference to estimate the carbonation degree index (I_{CD}, in %) at the same time intervals indicated above, according to the equation:

$$I_{CD} = \frac{(P_0 + B_0) - (P_x + B_x)}{(P_0 + B_0)} \times 100 \qquad [I.2.1]$$

where P_x and B_x are the amounts of portlandite and brucite at the time x and P_0 and B_0 are the initial content of portlandite and brucite (at the time 0).

2.3.2 Textural study

The observation of internal and external zones of the mortars microstructure (morphology, cohesion, porosity) was carried out by means of optical (OM) and field emission scanning electron microscopy (FESEM). In the first case, thin sections were observed by using an Olympus BX-60 microscope equipped with digital microphotography camera (Olympus DP10). In the second case, mortars fragments previously dried and carbon coated were analyzed by using a Carl Zeiss, Leo-Gemini 1530 microscope. The application of FESEM was also useful for the observation of the aggregate morphology at micro-scale whilst the use of OM on hardening mortars allowed observing the cohesion of mortars samples.

Both external (1 cm from the surface to the core) and internal (core) zones of the mortars samples were periodically analyzed.

2.3.3 Pore system

The pore system was evaluated by means of mercury intrusion porosimetry (MIP). Open porosity (P_o, %) and pore size distribution (PSD, in a range of 0.002<r<200 μm) were determined using a Micrometics Autopore III 9410 porosimeter with a maximum injection pressure of 414 MPa. Three measurements were performed on mortar fragments of ca. 1

cm^3 collected in the internal and external zones, which were oven-dried for 24 h at 60 ºC before the analysis.

2.3.4 Hydric properties

The water capillary imbibition test was performed to study mortars hygric properties after two months of carbonation. Three samples (4×4×16 cm) per mortar were oven-dried at 100 ºC during 24 h before the measures. Two imbibition coefficients (A and B) were determined from the mass uptake per surface unit and the height during the time, according to Beck et al. [30] procedure.

2.3.5 Mechanical properties

Flexural and compressive strength were measured by means of a hydraulic press INCOTECNIC-Matest. According to the UNE-EN 1015-11 [31] standard, flexural assays were carried out on three samples per mortar (of 4×4×16 cm). The six samples obtained after the flexural rupture were used for the compressive assays.

3. Results and discussion

3.1 Mineralogy of limes

The main mineral phases detected by means of XRD (Fig. I.2.1) are portlandite and brucite (the latter only in DL). The X-ray pattern of the limes also shows the presence of a small quantity of calcite (around 5%), which reveals that a little carbonation occurred during limes storage and use. Even if it is preferable to use non-carbonated limes, the amount of calcite found is very low and it cannot affect importantly the limes reactivity.

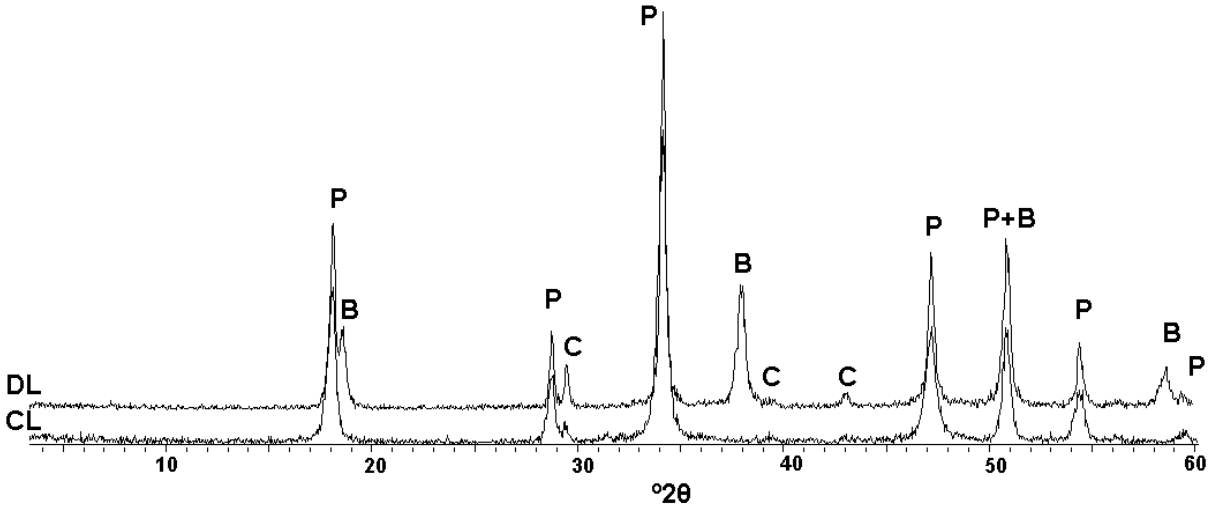

Figure I.2.1 X-ray diffraction patterns of the calcitic (CL) and dolomitic (DL) limes: P, portlandite; B, brucite; C, calcite.

3.2 Behaviour of mortars in the fresh state

In agreement with a previous study [14], the dolomitic lime conferred a higher plasticity to the mortar pastes and required a bigger amount of water compared to CL (Tab. I.2.1). This is due to the higher values of specific surface area (SSA) and micropore volume (μ-Vol) of DL (Tab. I.2.2) and depend on the differences in the microstructure of the dry limes, which give rise to opposite behaviours when the limes are in suspension [14]. SSA and μ-Vol are the parameters that influence the water content rather than the lime composition. In fact, the finer the lime, the higher the water demand. In a similar way, Chever et al. [15] reported that calcitic mortar pastes show a higher water demand than the dolomitic ones to achieve a specific flow (175±10 mm), since the calcitic lime they studied had a greater fineness than the dolomitic one. In our opinion, differences in the microstructure of limes with the same composition can be caused by variations in the manufacturing process that produced them. Notwithstanding, knowing the morphology of $Mg(OH)_2$ and $Ca(OH)_2$ particles (brucite particles are thinner and larger than portlandite ones [14]), we would expect always a greater fineness in the dry hydrated lime of dolomitic composition.

	CL	DL
SSA	13.8	23.1
μ-Vol	0.0569	0.0898
ρ	2.42	2.38
ρ_b	0.496	0.416
ρ_b^*	0.611	0.496

Table I.2.2 *Particle properties of the dry powders of calcitic (CL) and dolomitic (DL) limes: specific surface (SSA, m^2/g); micropores volume (μ-Vol, $cm^3 \cdot g$); solid density (ρ, cm^3/g); bulk density determined without (ρ_b, cm^3/g) and with (ρ_b^*, cm^3/g) compaction.*

Differences in the amount of kneading water were also observed depending on the type of aggregate used: mortars elaborated with the calcareous aggregate required more water than those prepared with the siliceous one (Tab. I.2.1). This is because CA is a crushed aggregate, formed by angular and porous grains, whilst SA is characterized by rounded, harder and smoother grains that absorb less water.

3.3. Characteristics of mortars in the hardening state

3.3.1 Carbonation degree of mortars

According to TGA curves (Fig. I.2.2), the amount of portlandite (P) decreased in time, always faster in the exterior than in the interior of mortars. On the other hand, the amount of brucite (B) remained almost unvaried for the all duration of the study, being only a 1% less in the

internal zones of the samples at every time interval. This is because in dolomitic lime mortars (DC and DS) only a part of the lime, corresponding to portlandite ($Ca(OH)_2$), is involved in the carbonation process, whilst the rest of the binder, composed of brucite ($Mg(OH)_2$), does not undergo to any transformation at these curing conditions, as also observed by other authors [13]. This is why the carbonation degree index is lower in dolomitic lime mortars at the end of this study (Tab. I.2.3).

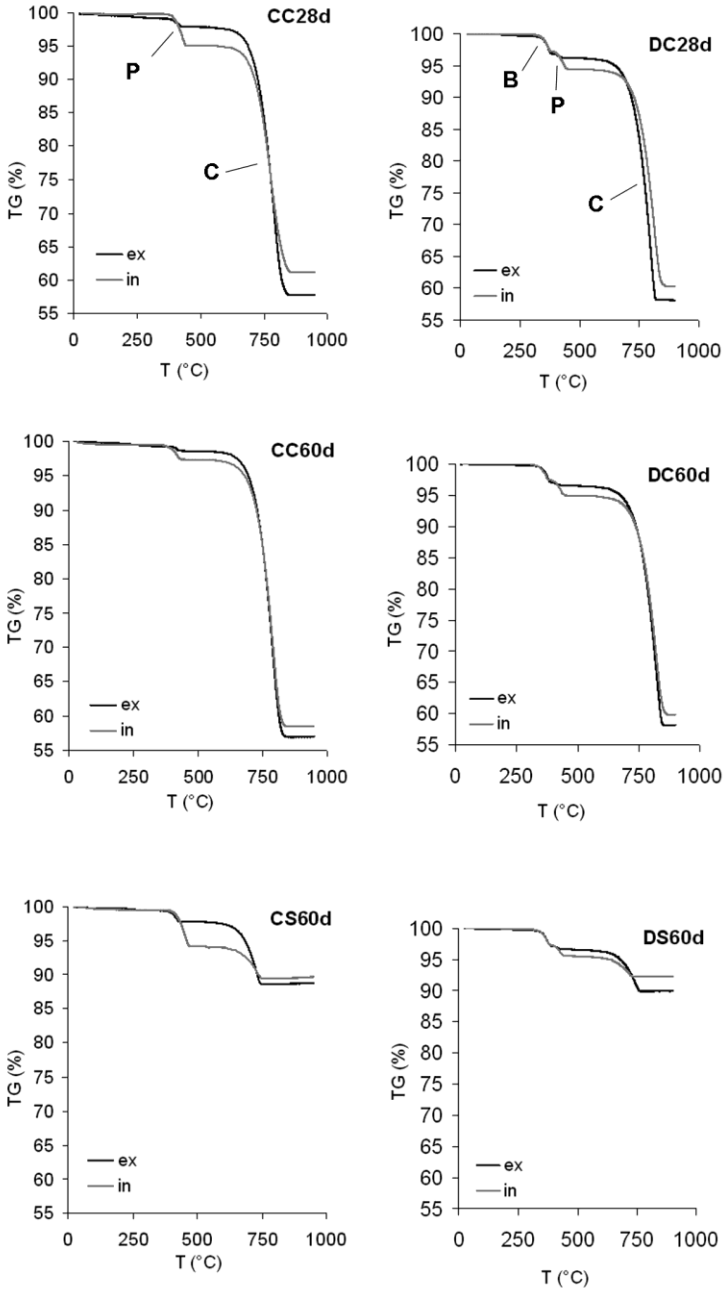

Figure I.2.2 Most representative TGA curves of the four types of mortars after 28 and 60 days of carbonation. CC: calcitic lime+calcareous aggregate; CS: calcitic lime+siliceous aggregate; DC: dolomitic lime+calcareous aggregate; DS: dolomitic lime+siliceous aggregate; P: portlandite; B: brucite; C: calcite.

In mortars with siliceous aggregate (CS and DS) the weight loss recorded is much lower since quartz does not undergo to any transformation in the range of temperature analysed during thermogravimetric analyses (*cf.* Section 2.3.1).

Mortar name	I_{CD} (%)	
	Ex	In
CC	74.3	53.8
CS	73.0	16.8
DC	50.6	20.8
DS	51.9	32.1

Table I.2.3 *Carbonation degree index (I_{CD}, in %) of the external (Ex) and internal (In) zones of the four mortars at the end of the study (2 months of carbonation). CC: calcitic lime+calcareous aggregate; CS: calcitic lime+siliceous aggregate; DC: dolomitic lime+calcareous aggregate; DS: dolomitic lime+siliceous aggregate.*

3.3.2 Mortars texture and morphology

FESEM images show the loss of some siliceous grains from the surface of CS and DS samples (Fig. I.2.3a and b). The rounded and smooth surface of the siliceous aggregate does not allow a strong attachment of the matrix particles (formed by the binder and the newly-formed calcite) to the surface of the aggregate grains (Fig. I.2.3c), thus causing desegregation in some cases. A better cohesion is observed in CC and DC mortars, because of the rough and more porous surface of the calcareous aggregate (Fig. I.2.3d and e).

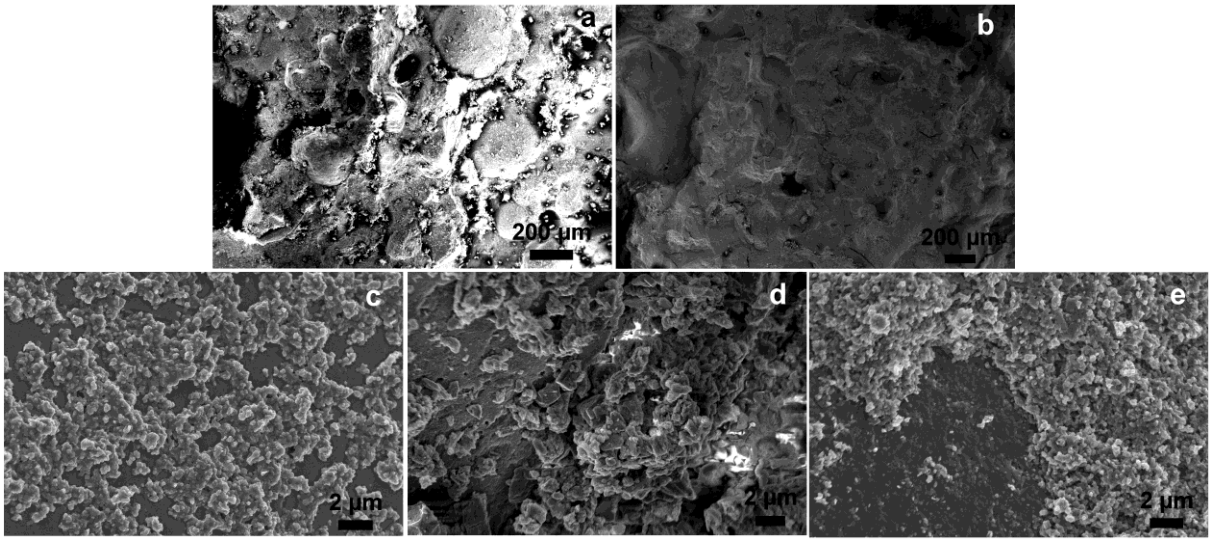

Figure I.2.3 *FESEM images of calcitic (a and d) and dolomitic (b, c and e) lime mortars: loss of some siliceous grain from the matrix of CS (a) and DS (b); cohesion between the matrix and the siliceous (c) and calcareous (d and e) grains.*

The particles of calcite formed after carbonation of portlandite have different morphology in calcitic and dolomitic lime mortars (Fig. I.2.4a and

b). Distinguishing them in the matrix was possible only in limited zones of the samples observed, where they appear more compact than the matrix (Fig. I.2.4c and d).

The calcitic lime is composed by agglomerates of nano- and, occasionally, micro-crystals (around 1 μm in size) of portlandite with hexagonal habit (plate-like particles) (Fig. I.2.4e). On the other hand, the dolomitic lime is predominantly characterized by nanoparticles that present certain homogeneity in size (not bigger than 500 nm) (Fig. I.2.4f), confirming the previous study by Arizzi et al. [14]. FESEM observations of the mortars samples also revealed that the morphology of the new particles of calcite precipitated after carbonation is conditioned by that of the original particles of portlandite. In fact, in dolomitic mortars, the calcite particles are smaller and their shape is homogeneous (Fig. I.2.4b). In calcitic lime mortars, by contrast, the calcite particles present different morphology and sizes (Fig. I.2.4a), as well as the portlandite particles from which they originate (Fig. I.2.4e).

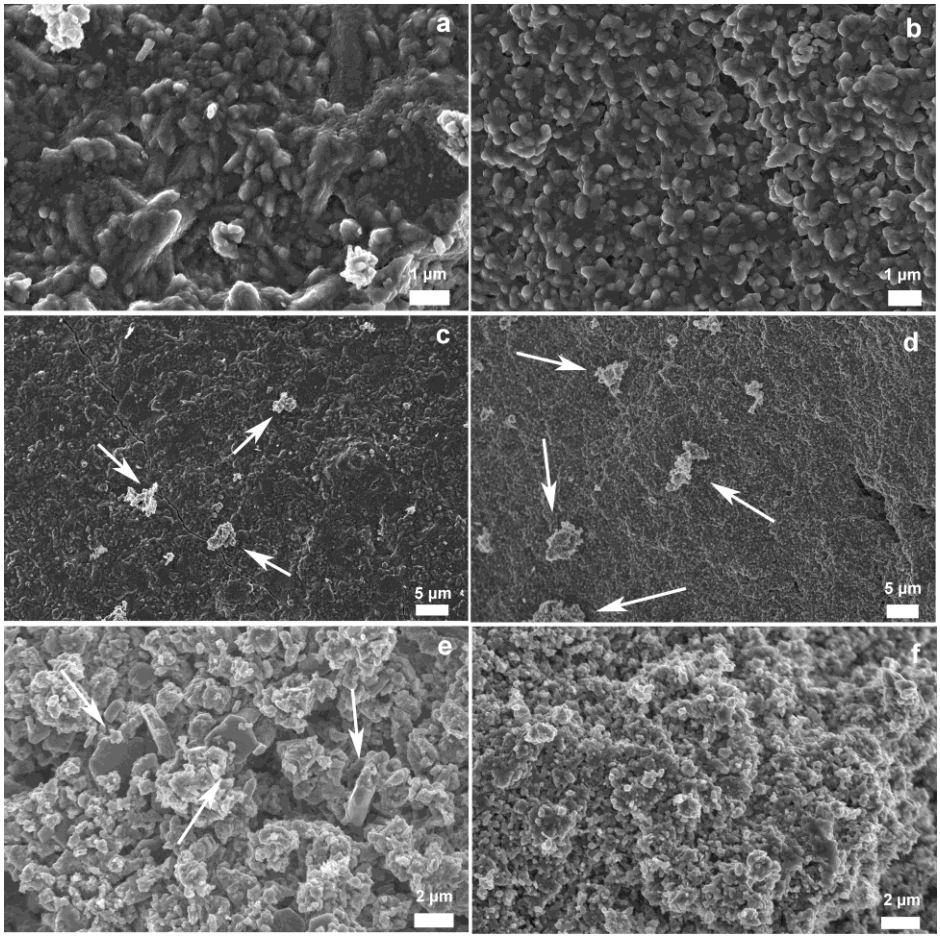

Figure I.2.4 *FESEM images of calcitic (a, c and e) and dolomitic (b, d and f) lime mortars: newly-formed calcite in calcitic (a and c) and dolomitic (b and d) lime mortars; the clearer agglomerates indicated by the arrows (in c and d) are formed by the binder particles. Calcitic (e) and dolomitic (f) lime in mortars; the arrows (in e) indicate the hexagonal plate-like sub-micro particles of portlandite, whose size is around 2 μm, which are present in calcitic lime mortars.*

By means of optical microscopy little dark spots (between 5 and 40 μm in size) were observed in some localised areas of the dolomitic mortars (Fig. I.2.5). These spots were defined by Diekamp et al. [32] as "brownish patches" or "magnesium enriched areas" of size comprised between 20 and 300 μm (larger than the ones observed here), because of the higher concentration of Mg in these zones.

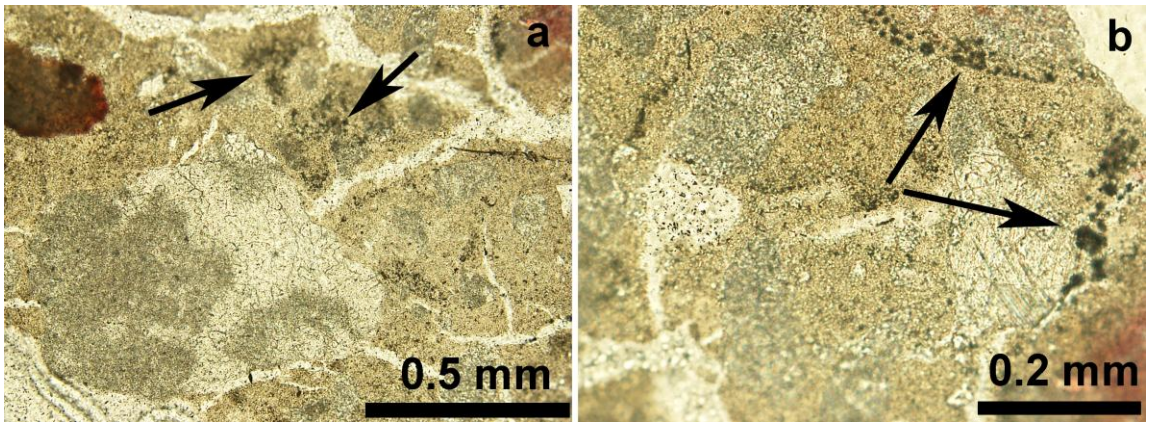

Figure I.2.5 *OM images of the black spots in dolomitic lime mortars.*

A proof of the preferential localisation of Mg is the sporadic identification of hydromagnesite particles, by means of FESEM (Fig. I.2.6), in pores of around 10 μm in size, which probably correspond to some zones with high Mg content recognised by optical microscopy. In 28-days old samples, hydromagnesite is characterized by nanometric plate-like particles (up to 1 μm in size) (Fig. I.2.6a) as those formed under moist conditions described by Dheilly et al. [17]. In 60-days old samples, the hydromagnesite particles appear more elongated (Fig. I.2.6b), being more similar to the phases observed by Diekamp et al. [32] in old dolomitic mortars samples. This indicates a growth of the hydromagnesite particles over time.

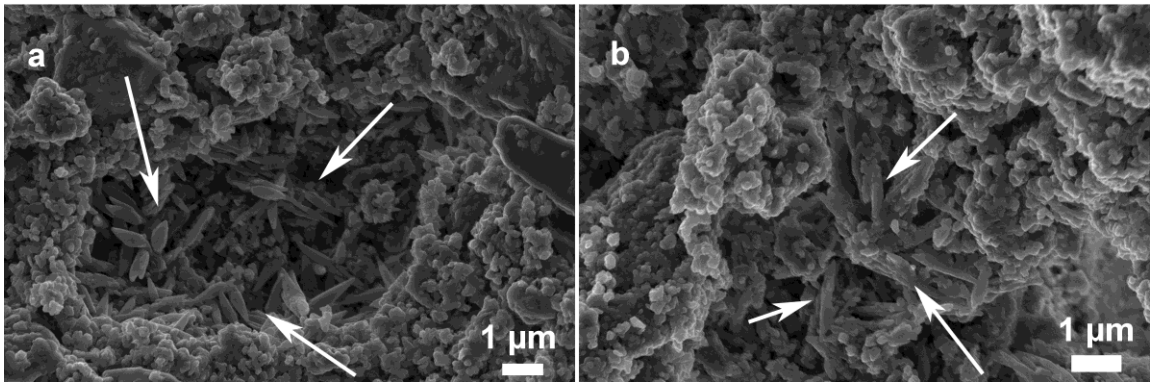

Figure I.2.6 *FESEM image of the internal samples of dolomitic lime mortar after 28 (a) and 60 (b) days of curing. Arrows indicate some nanometric plate-like (up to 1 μm in size) (a) and more elongated (b) particles of hydromagnesite.*

If nesquehonite formation is favoured at atmospheric conditions this is not the case of hydromagnesite (T = 20 ºC, according to Lanas et al. [13]), unless it has grown under disequilibrium conditions [32]. The

identification of hydromagnesite is an unexpected finding since until now it was found only in old mortars or in young samples cured under moist conditions. However, its amount is very low in the mortar because it was not detected by TG analyses at any time during the study. Interestingly, hydromagnesite has been detected in the core of the mortar, which is a zone characterized by a much slower drying than the exterior. Then, we can assume that the formation of hydromagnesite, although very scarce, has been favoured by the combined presence of a higher humidity together with the high concentration of magnesium in this zone.

The transformation of a small content of $Mg(OH)_2$ into hydromagnesite would explain the little variations in its amount found by means of TGA (*cf.* Section 3.3.1).

3.3.3 Pore system of the mortars

Calcitic and dolomitic lime mortars present very different pore size distribution curves (Fig. I.2.7). On the one hand, the PSD of CC and CS is characterized by a main peak comprised between 0.1 and 1 μm (Fig. I.2.7a and b), which is typical of calcitic lime pastes and mortars [28,33,34].

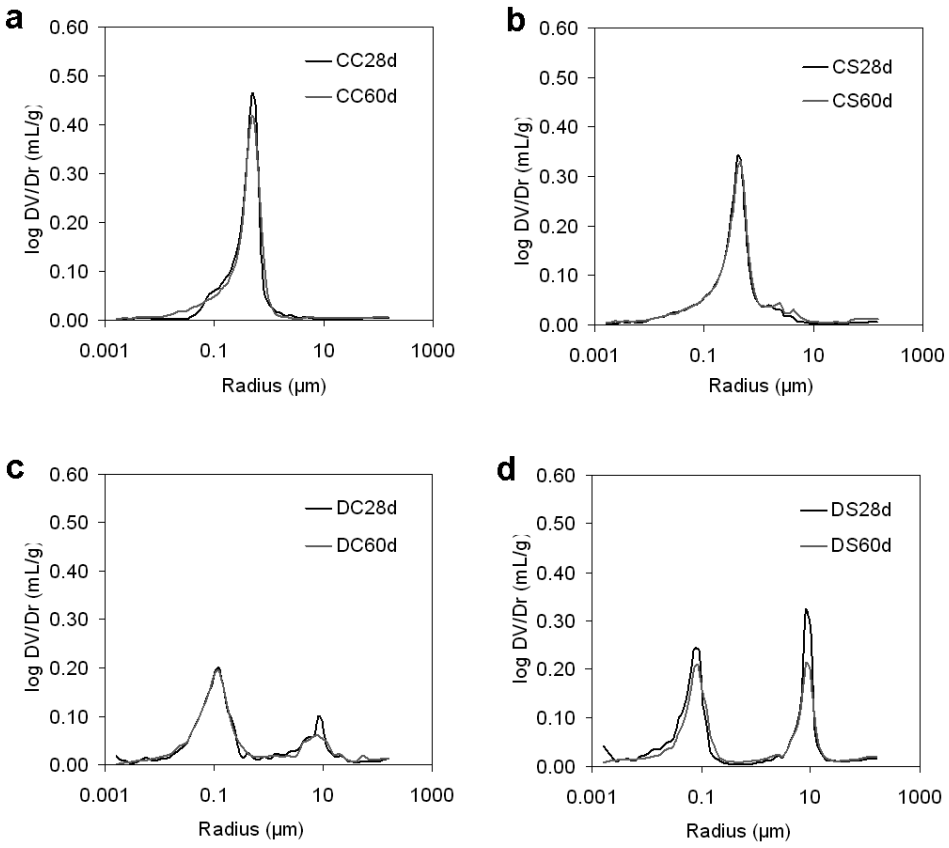

Figure I.2.7 Pore size distribution curves of the calcitic (CC and CS) (a and b) and dolomitic (DC and DS) (c and d) lime mortars with calcareous (CC and DC) (a and c) and siliceous (CS and DS) (b and d) aggregate after 28 (28d) and 60 (60d) days from their elaboration.

On the other hand, DC and DS present two main families of pores with different volumes: one of them includes pores with radius equal to 0.01-

0.5 μm, the other peak correspond to pores whose radius is comprised between 2 and 25 μm (Fig. I.2.7c and d). Bimodal curves in the dolomitic lime mortars were also observed by other authors [16,28] who calcined the dolomite and slaked the lime manually for the preparation of the dolomitic lime mortars. The similarities found in the pore size distribution curves between our dry hydrated limes and other limes differently produced may suggest that the lime manufacturing processes do not affect very much the pore size distribution of the mortar. The composition of the lime, in turn, influences strongly the mortar pore system.

Another factor to take into account is the effect of the aggregate on the volume of the bigger pores of the mortars. In calcitic lime mortars, the siliceous aggregate gives rise to the formation of a small family of pores in the range of 1<r<10 μm (Fig. I.2.7b). In the dolomitic ones, the presence of the same aggregate produces an increase of the pores of radius comprised between 2 and 25 μm (DS, Fig. I.2.7d). This porosity has to be related to the poor cohesion between the matrix and the aggregate grains found in mortars with siliceous aggregate (*cf.* Section 3.3.2).

During carbonation, the volume of the main pores decreases slowly in the four mortars types (Fig. I.2.7), because the lime is progressively transformed into calcite. Nevertheless, the open porosity values found after 60 days are in some cases higher (in CC and CS, Tab. I.2.4) or remain almost unvaried (DC and DS, Tab. I.2.4). This can be due to the formation of small calcite particles that fill the pores left by the portlandite and brucite particles but, at the same time, create new smaller pores (r~0.01 μm) that are especially visible in CC mortar (Fig. I.2.7a), since the carbonation process in dolomitic mortars is slower.

Mortar name	P_o (%)	
	28d	60d
CC	32.5±2.74	35.0±1.10
CS	32.8±3.34	34.3±3.39
DC	34.4±1.56	34.2±0.64
DS	36.4±1.17	37.5±2.01

Table I.2.4 *Open porosity (P_o, in %) values and standard deviation of the four mortars types after 28 (28d) and 60 (60d) days from their elaboration.*

3.3.4 Hydric behaviour

- Water capillary imbibition

Figure I.2.8 shows the different behaviour of mortars during the water capillary uptake. We have to mention that mortars samples were not totally carbonated when the capillary test was performed, therefore potential reactions between water and the binders might have occurred, thus influencing the results. Between the calcitic lime mortars, CC absorbs the biggest amount of water, due to its higher porosity (Tab. I.2.4), but the weight saturation is reached almost at the same time than in CS (Fig. I.2.8a). The same occurs with the visual saturation of CC and CS samples,

which is attained when the capillary front achieves the top of the samples (Fig. I.2.8b). At the end of the capillary test, in calcitic mortars samples all connected pores are filled and both mass and visual saturations are achieved because the majority of the pores are in the same range of size (0.1<r<1 μm, Fig. I.2.7a and b).

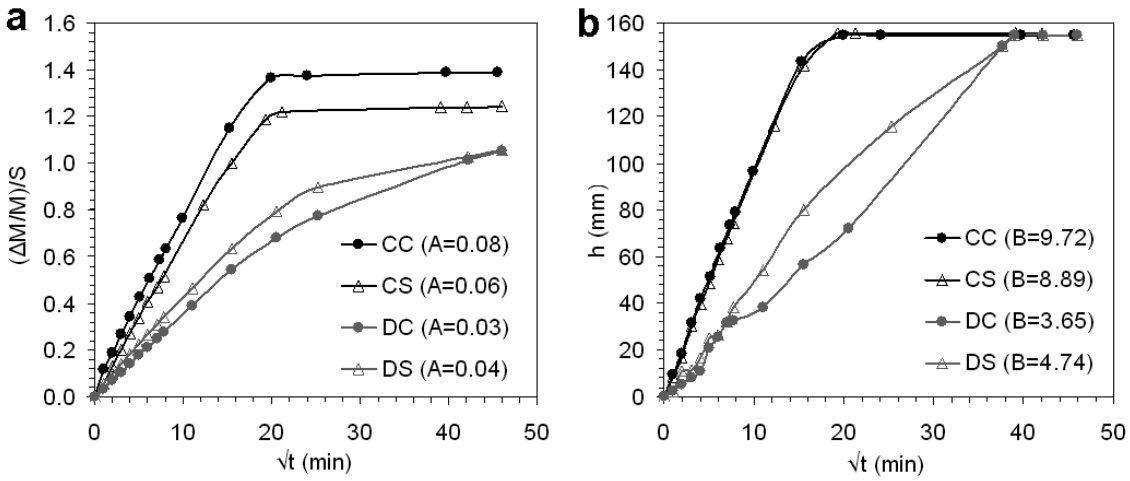

Figure I.2.8 Capillarity curves of calcitic and dolomitic lime mortars after 60 days of carbonation, representing the weight increase (ΔM, in g) per surface unit (S, in m^2) and the height of the capillary front (h, in mm) versus the square of time (√t, in $min^{-1/2}$). The imbibition coefficients (A, in $g/cm^2\ min^{1/2}$ and B, in $cm/min^{1/2}$), which correspond to the slop of the two curves, are indicated in each graphic.

On the other hand, in dolomitic mortars (DC and DS), the water absorbed during time is much lower than in calcitic ones. Moreover, the curve representing the mass taking over time (Fig. I.2.8a) is not linear but it is formed by two sections with different slops, due to the fact that the pore system of these mortars is characterized by two main families of pores with small (0.01<r<0.5 μm) and big (2<r<25 μm) radius [30] (Fig. I.2.7c and d). In this kind of pore network, water is absorbed faster by the biggest pores, through which it reaches the top of the sample (as shown in Fig. I.2.8b). However, sample continues absorbing water even after the visual saturation because the smallest pores, in which the capillary pressure is higher (according to Laplace's equation), absorb water from the biggest ones [35-37]. This causes a time lag between the visual and the real saturation of the sample [30] (Fig. I.2.8). The test was ended after the total saturation of the calcitic lime mortars; it is evident that DC and DS mortars have still not reached a constant weight and further increase is expected considering their higher porosity (Tab. I.2.4) and the characteristics of their pore system (Fig. I.2.7c and 7d).

- Shrinkage and water-retention capacity

Dolomitic lime mortars experimented a much bigger shrinkage compared to the calcitic ones, as observed by means of optical and electron microscopy (Fig. I.2.9). The plastic shrinkage, namely the mortar volume reduction due to water evaporation, depends on the amount of

water in excess present in the mixture but, above all, it is related to the water-retention capacity of the lime. Generally, a lime with a higher specific surface area gives rise to a mixture with higher viscosity and better water-retention capacity [38]. The dolomitic lime presents these characteristics (*cf.* SSA value in Tab. I.2.1) and, in fact, the DC and DS fresh mixtures showed a higher viscosity and needed a bigger amount of water with respect to CC and CS (Tab. I.2.2). Then, we wondered why DC and DS are characterized by such big shrinkage. Since the shrinkage is a consequence of the water evaporation, it is sensible to relate the drying behaviour of the dolomitic mortars to the water transport properties and, as a consequence, to the pore system of these mortars. According to Scherer [39], the shrinkage due to drying of a solid porous body is the result of internal stresses produced by capillary forces and the probability of cracking is related to the strength of the pore network, among other factors. In a heterogeneous pore system, the largest pores empty first and the capillary pressure compresses the smaller pores, causing great tensions that finally crack the network. This is what occurred in the dolomitic mortars, which are characterized by both large and small pores (*cf.* Section 3.3.3). As consequence of the formation of shrinkage fissures, an increase in the volume of the largest pores is likely to have occurred, especially in the DS mortars (Fig. I.2.7d).

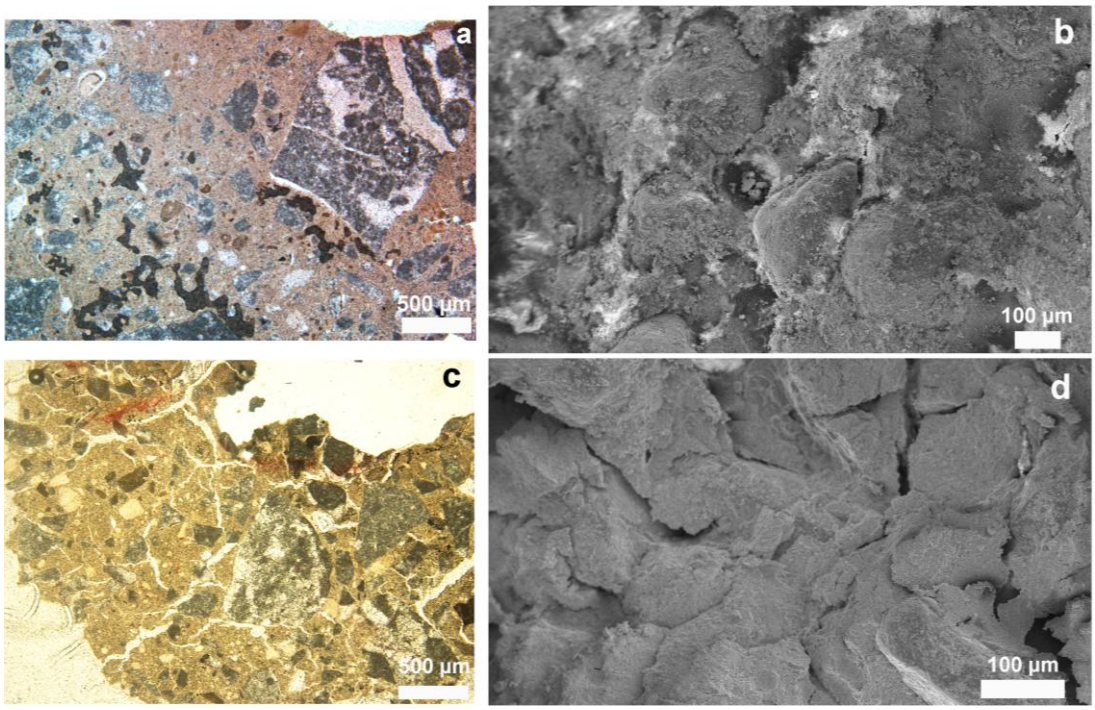

Figure I.2.9 *OM (a and c) and FESEM (b and d) images of the shrinkage fissures observed in calcitic (a and b) and dolomitic (c and d) limes mortars.*

3.3.5 Mechanical behaviour

After 28 days of curing, mortars achieve quite low mechanical strengths (Tab. I.2.5) because mortars are in the early stage of carbonation and resistances are not extensively developed yet. Contrary to that studied by other authors, dolomitic lime mortars are characterized

by very low mechanical strengths, especially DS. In fact, when the siliceous aggregate was used, extremely weak dolomitic mortars samples were obtained, to such a degree that their strength could not be measured by the mechanical press.

Mortar name	R_f	R_c
CC	1.43±0.16	1.03±0.03
CS	1.35±0.16	0.05±0.00
DC	1.15±0.16	0.90±0.19
DS	-	-

Table I.2.5 *Flexural (R_f, in MPa) and compressive (R_c, in MPa) strengths and standard deviation of the four mortars types after 28 days since their elaboration.*

Our results disagree with Dheilly et al.'s study [17] on the mechanical resistances of dolomitic lime mortars after 28 days of curing. However the curing conditions in this study were not the same (we exposed mortars to a dry environment instead to a moist one) and this seems to be a crucial factor on the development of strengths. Moreover, the fragility shown by the dolomitic lime mortars was expected since they have been subjected to internal stresses, due to shrinkage, that obviously affected the mechanical performances.

In addition to this, it is important to point out that the formation of hydromagnesite in some small areas of the dolomitic mortars samples (*cf.* Section 3.3.2) did not yield any strength improvement, as expected due to the low amount of this phase.

4. Conclusions

This work claims to clarify the uncertainty that arises due to different and, sometimes, conflicting results published in literature about the performances of dolomitic lime mortars; uncertainty that makes controversial the choice of the correct lime for the elaboration of repair mortars.

Two are the interesting aspects of this research: 1) the calcitic and dolomitic limes used were standardised limes industrially manufactured in the state of dry powder (i.e. dry hydrated limes); 2) the mortars were cured under dry conditions. By comparing our results with those published in literature up to know, we have understood that the manufacturing process of the dolomitic lime (i.e. manually or industrially calcined and slaked) and the curing conditions (dry or moist) are the main causes of the variability of the mortars properties. The first factor affects the microstructure of the lime, then the water demand and the viscosity of the fresh mortar mixture; the second one influences the formation of different mineralogic phases, then the development of strength. As respect this last point, we have observed that the brucite amount remains almost unvaried during carbonation, unless it turns into small amounts of hydromagnesite.

We found that the formation of hydromagnesite is possible at ambient conditions if a low humidity is present, but its presence does not increase the mechanical resistances of the dolomitic mortar. A great strength improvement can be expected only in dolomitic mortars exposed to moisture areas.

The heterogeneous pore network of the dolomitic lime mortars, characterized by micropores connected to large pores, has demonstrated to be crucial in the capillary imbibition behaviour and the drying cinetic, which caused a great shrinkage and produced low mechanical strengths. These microstructural characteristics and the fragility of the dolomitic mortars studied here indicate that they might be more susceptible to weathering than the calcitic mortars.

The textural characterisation of calcitic and dolomitic lime mortars showed that the calcite particles formed during carbonation are similar in morphology (shape and size) to the original particles of portlandite from which they originate. In this sense, the dolomitic lime generates a more uniform texture.

Finally, differences due to the aggregate type are especially visible in the textural properties of the mortars, more specifically in the degree of cohesion between the surface of the grains and the matrix. About this, calcareous aggregates, which present an angular, rough and porous surface, perform better than siliceous aggregates, with a smoother and rounded surface.

The main conclusion that can be drawn from this study is that the use of a calcitic dry hydrated lime should be preferred to a dolomitic one for the elaboration of repair mortars to be applied in dry zones. In practice, however, it is possible to reduce the shrinkage of dolomitic mortars by wetting the surface during rendering and by keeping the render moist during the initial setting. Moreover, we rely on the better performances that the dolomitic lime generally confers to mortars when cured in moist areas.

Acknowledgements:

This study was financially supported by Research Group RNM179 of the Junta de Andalucía and by Research Project P09-RNM-4905. We thank the revision of an anonymous referee.

References

[1] A.D. Cowper, Lime and lime mortars. Donhead Ed. (1927), reprinted by building Research Establishment Ltd. In 1998.

[2] C. Groot, P. Bartos, J. Hughes, Historic mortars: characteristics and test concluding summary and state of the art. International Workshop on Historic mortars, Paisley, UK (1999) 443-454.

[3] A.H.P. Maurenbrecher, Mortars for repair of traditional masonry. Practice Periodical on Structural Design and Construction 9 (2) (2004) 62-65.

[4] K. Callebaut, J. Elsen, K. Van Balen, W. Viaene, Nineteenth century hydraulic restauration mortars in the Saint Michael's Church (Leuven, Belgium). Natural hydraulic lime or cement? Cem. Concr. Res. 31 (2001) 397-403.
[5] F. Veniale, M. Setti, C. Rodriguez-Navarro, S. Lodola, W. Palestra, A. Busetto Thaumasite as decay product of cement mortar in brick masonry of a church near Venice. Cem. Concr. Compos. 25 (2003) 1123-1129.
[6] A. Diekamp, J. Konzett, W. Wertl, R. Tessadri, P.W. Mirwald, Dolomitic lime mortar – a commonly used material for medieval buildings in western Austria and northen Italy. Proceedings of the 11th International Congress on deterioration and conservation of stone, Torun, Polland (2008) 597-604.
[7] C. Atzeni, L. Massidda, U. Sanna, Magnesian lime. Experimental contribution to interpreting historical data. Sci. Tech. Cult. Herit. 5 (2) (1995) 29-36.
[8] G.F. Dornap, The slaking of lime – Effect on quality of calcium hydroxide. English translation. Zement Kalkund Gips, nº 1/77 (1977) 34-39.
[9] UNE-EN 459-1. Cales para la construcción. Parte I: definiciones, especificaciones y criterios de conformidad para los cementos comunes. AENOR, Madrid (2000).
[10] O. Cazalla, C. Rodríguez-Navarro, E. Sebastián, G. Cultrone, M.J. De La Torre, Aging of lime putty: effects on traditional lime mortar carbonation. J. Am. Ceram. Soc. 83 (5) (2000) 1070-1076.
[11] K. Van Balen, Carbonation reaction of lime, kinetics at ambient temperature, Cem. Concr. Res. 35 (2005) 647-657.
[12] S. Pavía, B. Toomey, Influence of the aggregate quality on the physical properties of natural feebly-hydraulic lime mortars. Mater. Struct. 41 (2008) 559-569.
[13] J. Lanas, J.L. Perez Bernal, M.A. Bello, J.I. Alvarez, Mechanical properties of masonry repair dolomitic lime-based mortars. Cem. Concr. Res. 36 (2006) 951-960.
[14] A. Arizzi, R. Hendrickx, G. Cultrone, K. Van Balen, Differences in the rheological properties of calcitic and dolomitic lime slurries: influence of particle characteristics and practical implications in lime-based mortar manufacturing. Mater. Construc. 60 (2011) DOI: 10.3989/mc.2011.00311.
[15] L. Chever, S. Pavía, R. Howard, Physical properties of magnesian lime mortars. Mater. Struct. 43 (2010) 283-296.
[16] G. Cultrone, A. Arizzi, E. Sebastián, C. Rodriguez-Navarro, Sulfation of calcitic and dolomitic lime mortars in the presence of diesel particulate matter. Environ. Geol. 56 (2008) 741-752.
[17] R.M. Dheilly, A. Bouguerra, B. Beaudoin, J. Tudo, M. Queneudec, Hydromagnesite development in magnesian lime mortars. Mater. Sci. Eng. A268 (1999) 127-131.
[18] S. Pavía, B. Fitzgerald, R. Howard, Evaluation of properties of magnesian lime mortar. WIT Transactions on The Built Environment. C.A. Brebbia and A. Torpiano eds. WIT Press 83 (2005) 375-384.

[19] L.J. Vicat (1837) Mortars and cements. Donhead, Shaftesbury, 2003.
[20] J. Lanas, J.I. Alvarez, Dolomitic limes: evolution of the slaking process under different conditions. Thermochimica Acta 423 (2004) 1-12.
[21] UNE EN 933-2. Ensayos para determinar las propiedades geométricas de los áridos. Parte 2: Determinación de la granulometría de las partículas. Tamices de ensayo, tamaño nominal de las aberturas. AENOR, Madrid (1999).
[22] J.D. Martín Ramos, XPowder. A software package for powder X-ray diffraction analysis, Lgl. Dep. GR 1001/04 (2004).
[23] S. Brunauer, P.H. Emmet, J. Teller Adsorption of gases in multimolecular layers. J. Am. Chem. Soc. 60 (1938), 309-319.
[24] E.P. Barret, L.J. Joyner, P. Halenda The determination of pore volume and area distributions in porous substances. I. Computations from nitrogen isotherms. J. Am. Chem. Soc. 73 (1951) 373-380.
[25] ASTM D 854-92. Test Method for Specific Gravity of Soils (1993).
[26] UNE EN 1015-3. Métodos de ensayo de los morteros para albañilería. Parte 3: Determinación de la consistencia del mortero fresco (por la mesa de sacudidas). AENOR, Madrid (1998).
[27] UNE EN 1015-2. Métodos de ensayo de los morteros para albañilería. Parte 2: Toma de muestra total de morteros y preparación de los morteros para ensayo. AENOR, Madrid (1999).
[28] O. Cazalla Morteros de cal. Aplicación en el patrimonio histórico. PhD Thesis, University of Granada (2002).
[29] UNE-EN ISO 11358. Plásticos. Termogravimetría (TG) de polimeros. Principios generales. AENOR, Madrid (1997).
[30] K. Beck, M. Al-Mukhatar, O. Rozenbaum, M. Rautureau, Characterization, water transfert properties and deterioration in tuffeau: building material in the Loire valley-France, Build. Environ. 38 (2003) 1151-1162.
[31] UNE-EN 1015-11. Metodos de ensayo de los morteros para albañileria. Parte 11: Determinación de la resistencia a flexión y a compresión del mortero endurecido. AENOR, Madrid (2000).
[32] A. Diekamp, J. Konzett, P.W. Mirwald, Magnesian lime mortars - Identification of magnesium-phases in medieval mortars and plasters with imaging techniques. 12th Euroseminar on Microscopy Applied to Building Materials, Dortmund, Germany (2009).
[33] M. Arandigoyen, J.L. Pérez Bernal, M.A. Bello López, J.I. Alvarez, Lime-pastes with different kneading water: Pore structure and capillary porosity, Appl. Surf. Sci. 252 (2005) 1449-1459.
[34] R.M. Lawrence, T.J. Mays, S. Rigby, P. Walker, D. D'Ayala, Effects of carbonation on the pore structure of non-hydraulic lime mortars, Cem. Concr. Res. 37 (2007) 1059-1069.
[35] Benavente D., Lock P., García del Cura M.A., Ordóñez S. Predicting the capillary imbibition of porous rocks from microstructure. Transport Porous Med. 49 (2002) 59-76.
[36] Mamillan M. Connaissances actuelles des problemes de remontées d'eau par capillarite dans les murs. The conservation of stone II. Cent per la Conservazione delle Sculture all'aperto. Bologna (1981) 59–72.

[37] Hall C., Hoff W.D. Water transport in brick, stone and concrete. Ed. Taylor and Francis, London and New York (2002).
[38] Boletín AFAM. Morteros. Guia General (2003).
[39] G.W. Scherer Theory of drying. J. Am. Ceram. Soc. 73 (1) (1990) 3-14.

Chapter I.3

Microstructural changes and the evolution of the physical-mechanical properties of aerial lime-based mortars due to carbonation. The influence of aggregate mineralogy and morphology

Arizzi A., Cultrone G.

Submitted to *Quarterly Journal of Engineering Geology and Hydrogeology*

Abstract

The aim of this study was to investigate the influence of the aggregate mineralogy and morphology on the microstructure and macroscopic properties of aerial lime-based mortars. We also sought to understand the role of the aggregate in the outcome of the carbonation process. To do that, mortars set with two aggregates (calcareous and siliceous) were cured for two years under standard conditions and studied at different time intervals by means of textural and mineralogical analyses and hydric and physical-mechanical assays. Results show that differences in the initial properties of the mortar depend on the morphology of the aggregate and that the aggregate affects the evolution of mortar properties. We also found that the calcareous aggregate induced higher carbonation and better textural and physical-mechanical properties than the siliceous aggregate, mostly due to the compositional and textural differences between the two aggregates.

1. Introduction

In the case of mortars in which aerial lime is the only binder, hardening occurs due to the carbonation process, during which portlandite is transformed into the less soluble calcite, so causing an increase in weight and in volume of 35% and 11.8%, respectively.

Although the reaction is presented in Eq. I.3.1 as a single step,

$Ca(OH)_2 + CO_2 \rightarrow CaCO_3 + H_2O$ [I.3.1]

it actually involves 3 main stages:

1) Diffusion of CO_2 within the material;
2) Dissolution of CO_2 and $Ca(OH)_2$ in the pore water;
3) Precipitation of $CaCO_3$.

The factors that control these different stages are: CO_2 permeability, relative humidity and temperature [1-4].

In general, the carbonation process causes an increase in compactness and strength, and a change in the pore system of the mortar [5-6]. But in most cases, these changes take a long time because the formation of calcite at the expense of portlandite decreases the porosity and reduces the permeability of the material to CO_2, so slowing the process down. The diffusion of CO_2, governed by Fick's and Knudsen's laws, depends strongly on the pore size and the tortuosity of the mortar [3] and is generally higher (and the carbonation enhanced) at the interface between the surface of the grains and the matrix (ITZ, Interfacial Transition Zone) than in the matrix itself [7]. An increase in porosity in this area was observed by Lawrence et al. [5], who attributed it to the formation of amorphous and semi-amorphous calcium carbonate aggregates at the border of the grains.

The characteristics of the lime particles (shape, size and aggregation) influence the speed of carbonation and the performance of the final product [9-12].

Moreover, the presence of non-carbonated areas in an apparently carbonated mortar is due to the heat released (74 kJ/mol) during the carbonation reaction, which is sufficient to evaporate the water produced by the reaction and sometimes also the free and capillary water in the paste [4].

It is evident that all the factors that affect the microstructure of the mortar influence the outcome of this process. For this reason, during the preparation of mortars the components and their proportions must be selected carefully to ensure the best textural properties. In the non-carbonated mortar, the total porosity and the pore size distribution (PSD) depend to a large extent on the binder-to-aggregate (B/A) and water-to-binder (W/B) ratios, the binder composition, the presence of additives and also the shape and grading of the aggregate [13]. In general, aggregates with an angular shape, rough surface (crushed aggregates) and large surface area need more water than round aggregates with a smoother surface (natural aggregates) [14]. In addition, aggregates with continuous grading produce a well-packed system in which voids between grains of

the same size are filled by smaller grains, thus reducing the porosity [15-17]. Water content varies depending on the properties of the fine aggregate (ø<4 mm, [18]) (particle shape, surface area, porosity, roughness and roundness).

Previous research has shown that the use of different aggregates produces mortars with different microstructures [19]. Moreover, as the carbonation process is strongly influenced by the microstructure, the velocity of transformation of portlandite into calcite is likely to vary depending on the aggregate used. Secondly, aggregates with the right shape and grading improve the textural and mechanical properties of the mortar. Finally, aggregate mineralogy is another factor to consider especially with regard to mortar durability. Siliceous aggregates composed exclusively of quartz are inert from a chemical point of view (i.e. resistant to sulphate attack), the main reason why they are so commonly used in mortars. By contrast, a calcareous aggregate is weaker than quartz and more easily damaged by salt crystallization and contamination products, especially if dolomite is present.

The indirect role of aggregate in the carbonation process is then evident because:

1) the shape and grading of the aggregate influence the microstructure of the mortar paste (i.e. the porous system), while its mineralogical composition mostly influences the mechanical properties and the durability of the hardened mortar;

2) the speed and the degree of carbonation depend on the pore characteristics of the paste;

3) the formation of calcite leads to changes in the pore system of the mortar.

The objective of this work is therefore to study the influence of aggregate in the microstructural changes of mortars made with two aggregates of different morphology and composition and evaluate the physical and mechanical properties of the mortars for two years, so as to find out which is the most suitable aggregate to use in the design of aerial lime-based mortars. An aerial lime and a fixed B/A ratio were used for the preparation of mortars, so that differences in the amount of water would be due only to the absorption characteristics of the aggregate used.

2. Materials and methods

2.1. Components of mortars

2.1.1 Binder

The binder used in the preparation of the mortars is a dry hydrated lime (CL90-S, [20]) supplied by ANCASA (Seville, Spain).

2.1.2 Aggregates

Two mortars were prepared, one using a natural siliceous aggregate (SA) and the other using a crushed calcitic aggregate (CA) [21]. Their granulometric curves were created by combining different granulometric

fractions according to three different models: Dinger [22], Bolomey [23] and Fuller [24]. The grading of the calcitic aggregate approaches the Fuller model very well, whilst for the siliceous aggregate (SA) it was more difficult to achieve a continuous grading in the fine particle range, because quartz is harder (H = 7) than calcite (H =4). According to the European standard classification for aggregate grading [18], both SA and CA can be classified as fine aggregates.

2.1.3 Characterization of binder and aggregates

The chemical composition (major and minor elements) of the components of the mortars was studied using a Bruker S4 Pioneer X-ray fluorescence spectrometer (XRF), with wavelength dispersion equipped with a goniometer that analyses crystals (LIF200/PET/OVO-55) and a Rh X-ray tube (60 kV, 150 mA). Semiquantitative scanning spectra were obtained using Spectraplus software. Mortar powders (ca. 5g) were dispersed in KBr, deposited in an aluminium cup and then pressed at 10 ton to obtain a pressed pellet (40 mm sample disc). Measurements were performed in a vacuum with a rotating sample.

The mineralogical phases of binder and aggregates were determined by X-ray diffraction (XRD) and thermogravimetric analysis (TGA). In the first case, we used a Panalytical X'Pert PRO MPD, with automatic loader. Analysis conditions were: radiation CuK_{α} (λ=1.5405 Å), 4 to 70 º2θ explored area, 45 kV voltage, 40 mA current intensity and goniometer speed using a Si-detector X'Celerator of 0.01 º2θ/s. The interpretation and quantification of the mineral phases was performed using the X-Powder software package [25]. Thermal measurements were made with a Shimadzu TGA-50H analyzer. Approximately 50 mg of sample was heated in an alumina crucible, in a flushed-air atmosphere (100 mL/min), at a heating rate of 5º/min over a range of 25-950 ºC. TGA data treatment was carried out according to the UNE-EN ISO 11358 standard [26].

2.2 Mortars preparation

Two types of mortar were prepared with a calcitic dry hydrated lime (CL) and a binder/aggregate ratio of 1:3 by weight: CC (CL+CA) and CS (CL+SA).

The amount of water, established in order to obtain mortars with a plastic consistency, was 31% and 27% of total mass, for CC and CS mortars, respectively. The flow was calculated as the average of the spread diameter (in mm) measured on three fresh samples during the flowability assay [27], in the range of 150-200 mm. After preparation [28], the mortars were cured for 7 days in standard steel moulds (4×4×16 cm) at RH = 60±5% and T = 20±5 °C and, after removal from the moulds, were cured for a further 21 days in the same laboratory (modification of the UNE-EN 1015-11 standard [28] proposed by Cazalla [29]). Mortar samples were cured at RH = 60±5% and T = 20±5 °C throughout the study.

2.3. Mortars characterization

In order to monitor the mineralogical, textural and physical changes in the mortars due to the carbonation process, we analysed the mortar samples after 7, 15 and 28 days, 2 and 6 months and 1 and 2 years.

2.3.1 Study of the carbonation degree of the mortars

The mineralogical phases of the mortars were determined by XRD and TGA using the same analytical devices described in section 2.1.3. Mortar phases were determined by measuring the weight loss resulting from the stoichiometric reactions of portlandite dehydroxylation (450<T<550 ºC) and calcite thermal decomposition (700<T<900 ºC). In both analyses (XRD and TGA), the decrease in portlandite content was taken as a reference to estimate the carbonation degree index (ICD, in %) at the same time intervals indicated above, according to the equation:

$$I_{CD} = \frac{CH_0 - CH_x}{CH_0} \times 100 \qquad [I.3.2]$$

where CH_x is the amount of portlandite at time x and CH_0 is the initial content of portlandite (at time 0).

Both inner (core) and outer (1 cm^3 from the surface to the core) parts of the mortars samples were analysed periodically.

2.3.2 Textural characterization of mortars

We observed the inner and outer areas of the microstructure of the mortars (morphology, cohesion, porosity) using optical (OM) and field emission scanning electron microscopy (FESEM). In the first case, we observed thin sections using an Olympus BX-60 microscope equipped with digital microphotography camera (Olympus DP10). In the second case, we used a Carl Zeiss Leo-Gemini 1530 microscope to analyse previously dried, carbon-coated mortar fragments. FESEM was also useful for observing aggregate morphology at a micro-scale whilst the use of OM on hardening mortars allowed us to assess the cohesion in the area between the aggregate grains and the matrix.

2.3.3 Pore system of mortars

The pore system was evaluated using two complementary techniques: mercury intrusion porosimetry (MIP) and N_2 adsorption. Open porosity (P_o, %) and pore size distribution (PSD, in a range of 0.002<r<200 μm) were determined using a Micromeritics Autopore III 9410 porosimeter. Mortar fragments of ca. 1 cm^3 collected in the internal and external areas were oven-dried for 8 h at 100 ºC before analysis. A Micromeritics 3000 Tristar was used to obtain N2 sorption isotherms (T = 77 K) under continuous adsorption. Before the measurements, samples were heated to 110 ºC for 4 h and outgassed to 10^{-3} Torr using a Micromeritics Flowprep. Specific Surface Area (SSA) was determined according to the BET method [30].

The BJH method [31] was applied to determine PSD and pore volume (in a range of 15<d<500 Å).

2.3.4 Hydric properties

Free water absorption, drying and capillary uptake tests were performed to study the hydric properties of the mortars. Hydric tests were not performed until the mortars had been cured for 28 days, because "younger" mortars are less compact and therefore may dissolve in water. Mortar samples were oven-dried at 100 ºC for 24 h before measurements were taken. The absorption and drying kinetics were evaluated on three samples (4×4×4 cm) per type by measuring the changes in the mass of mortar samples over time, due to the movement of the water in the pore system. The absorption coefficient (C_a) was determined as the slope of the first two points in the curve representing the weight increase as a function of the square of time (4 minutes after the beginning of the test) [32]. The drying index (I_d) was measured according to the NORMAL 29-88 standard [33]. The capillary uptkae was performed on three samples of 4×4×16 cm. Two imbibition coefficients (A and B) were determined from the mass uptake per surface unit and the height over time, according to the Beck et al. [34] procedure.

2.3.5 Physical-mechanical properties

Flexural and compressive strength of mortars were measured using an INCOTECNIC-Matest hydraulic press, according to the UNE-EN 1015-11 [28] standard.

The ultrasonic wave propagation technique was also used to determine the elastic-dynamic properties of mortars, which are related to their mechanical resistance and degree of compactness. Measurements were performed using a Panametrics HV Pulser/Receiver 5058 PR coupled with a Tektronix TDS 3012B oscilloscope, in transmission-reception mode. A couple of non-polarized piezoelectric transducers were used, with a frequency spectrum of 1 MHz. Measurements were carried out on three mortar samples of 4×4×16 cm along three perpendicular directions: a, parallel to the compaction plane; b, parallel to the compaction plane along the largest face of the sample; c, perpendicular to the compaction plane. The velocity of propagation of primary (V_p) and secondary (V_s) waves within the mortar samples was determined as the ratio between the specimen length and the transit time of the pulse.

Once we had calculated the average velocity of V_p and V_s waves along a, b and c directions for three samples of each type of mortar and knowing the bulk density (ρ_b, g/cm^3) of the mortar at each time, the elastic moduli (Poisson coefficient, v; rigidity modulus, G; Young modulus, E; volume (or compressive) modulus, K) of the mortars were calculated using the following equations:

$$v = \frac{\left(\frac{V_p}{V_s}\right)^2 - 2}{2\left(\frac{V_p}{V_s}\right)^2 - 1} \quad [I.3.3]$$

$$G = \rho_b V_s^2 \quad [I.3.4]$$

$$E = 2G(1+\nu) \quad [I.3.5]$$

$$K = \frac{E}{3(1-2\nu)} \quad [I.3.6]$$

3. Results and discussion

3.1 Characteristics of the aggregates

Calcitic aggregate (CA) is composed of grains with irregular edges (Fig. I.3.1a), covered by micrometric particles of calcite that make the surface of the aggregate rough and porous (Fig. I.3.1b). The siliceous aggregate (SA) however is composed of rounded grains of quartz with a smooth surface and few discontinuities (Fig. I.3.1b and d).

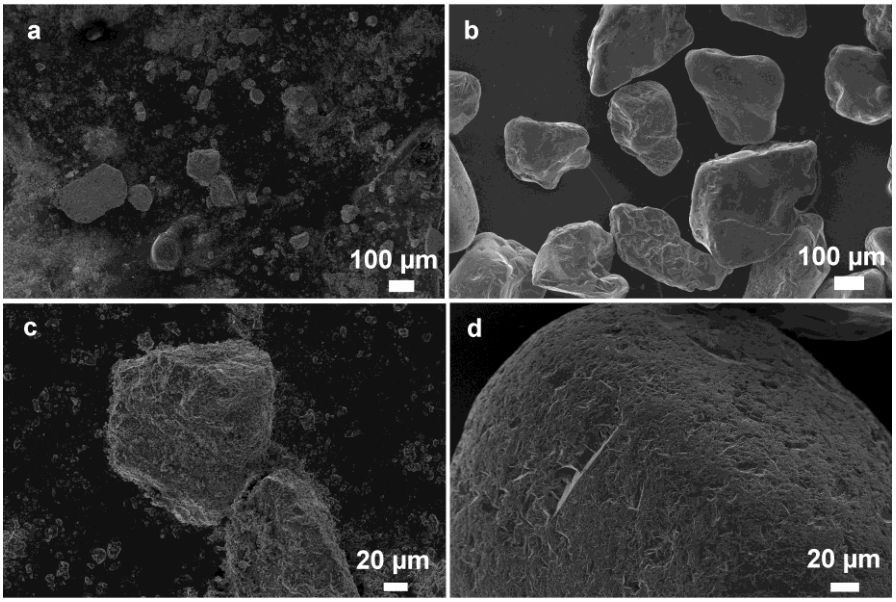

Figure I.3.1 *FESEM images of the smallest fraction of the grading of calcitic (a and c) and siliceous (b and d) aggregates at different magnifications.*

Using optical microscopy, we also observed that the calcareous grains were quite heterogeneous in shape, especially the grains of around 0.5 mm in size that appear more oblate than spherical (Fig. I.3.2a and b). The siliceous aggregate, on the other hand, is characterised only by rounded grains (Fig. I.3.2 c and d). In the first week of curing, the calcitic aggregate mortars had higher porosity in the ITZ (Fig. I.3.2).

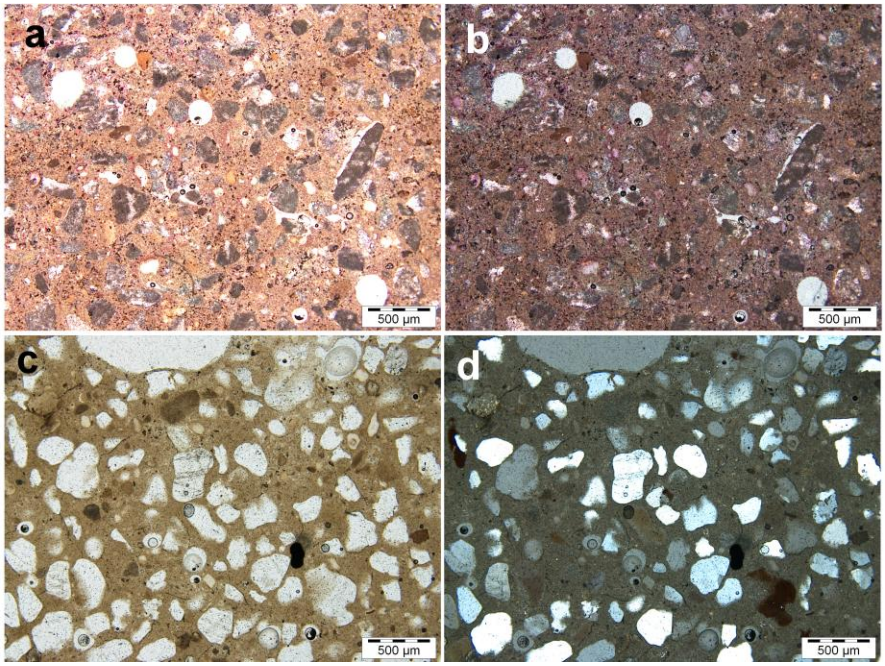

Figure I.3.2 *OM images with plane (a and c) and crossed (b and d) polars of CC (with calcitic aggregate) (a and b) and CS (with siliceous aggregate) (c and d) mortars.*

Table I.3.1 shows the chemical and mineralogical composition of the lime and aggregates used, characterized by the absence of impurities.

Chemical composition (XRF)			
(Oxides %)	CL	SA	CA
SiO_2	0.35	95.11	0.16
CaO	78.01	0.35	59.59
SO_3	1.39	0.05	0.03
MgO	0.70	0.25	0.87
Fe_2O_3	0.10	0.21	0.04
Al_2O_3	0.18	0.55	0.06
K_2O	0.05	0.26	0.01
P_2O_5	0.04	0.10	0.01
Mineralogical composition (XRD)			
Mineral phases (%)	CL	SA	CA
CC	3.8	-	100
CH	96.2	-	-
Qtz	-	100	-
Mineralogical composition (TGA)			
Mineral phases (%)	CL	SA	CA
CC	8.9	*	99.5
CH	87.1	*	-
Qtz	-	*	-

Table I.3.1 *Chemical (X-ray fluorescence analysis, XRF) and mineralogical (X-ray diffraction analysis, XRD) composition of calcitic lime (CL), calcareous (CA) and siliceous (SA) aggregates. CC = calcite; CH = portlandite; Qtz = quartz. *Thermogravimetric analysis (TGA) was not*

performed on SA because quartz only undergoes structural transformation (quartz α→quartz β) within the established temperature, with no weight loss.

The specific surface area (SSA, Tab. I.3.2) as determined by N_2 adsorption was found to be much higher in CA (0.6555 m^2/g) than SA (0.0493 m^2/g), which explains why more water is required in the preparation of CC mortars (4% more) than CS. Generally, under the same composition and proportion conditions, differences in the amount of kneading water depend on the absorptiveness of the aggregate, which is in turn related to its particle shape [35]. Hence, the high difference in the SSA values of the two aggregates is due to both the micrometric particles observed on the surface of the CA grains (by FESEM) and the oblate and angular shape of these grains.

Mortar name	Time	P_o	SSA	Pore volume
CC	7D	39.9(1.30)	4.04	0.011
	15D	35.2(1.68)	4.13	0.013
	28D	32.5(2.74)	3.56	0.023
	2M	35.0(1.10)	3.35	0.021
	6M	41.0(2.06)	3.27	0.005
	1Y	39.0(3.09)	2.32	0.008
	2Y	38.6(0.06)	2.25	0.007
CS	7D	36.8(2.18)	2.91	0.010
	15D	37.8(1.58)	2.32	0.008
	28D	32.8(3.34)	3.10	0.027
	2M	34.3(3.39)	3.62	0.029
	6M	37.4(0.25)	3.69	0.010
	1Y	35.7(0.22)	2.37	0.008
	2Y	35.3(0.73)	2.13	0.006

Table I.3.2 *Open porosity (P_o, in %) and standard deviation in square brackets obtained by mercury injection porosimetry (MIP), specific surface area (SSA, in m^2/g) and pore volume (cm^3/g) obtained by N_2 adsorption, of lime mortars made with calcitic (CC) and siliceous aggregates (CS) after 7 (7D), 15 (15D) and 28 (28D) days, 2 (2M) and 6 (6M) months, 1 (1Y) and 2 (2Y) years.*

3.2 Carbonation degree of the mortars

The quantification of the mineral phases was carried out from the initial amounts of calcite, portlandite and quartz in mortars determined by XRD and TGA. As we knew that 96.2% of the lime (CL) is portlandite (Tab. I.3.1) and the binder represents 25% of the total mass, we calculated an initial amount of portlandite of 24.05%. Both XRD and TGA techniques show that portlandite content decreases over time, a process that occurs more quickly on the exterior of the mortars than on the inside, because carbonation progresses from the surface to the core [29,36].

The fall in the portlandite content of the mortars over time is an indicator of the carbonation degree, which is expressed here as I_{CD} (in %). This parameter was calculated according to Eq. I.3.2 and represented as a

function of time (Fig. I.3.3). The slopes of the curves provide interesting information about the carbonation rate inside and on the surface of the two types of mortar.

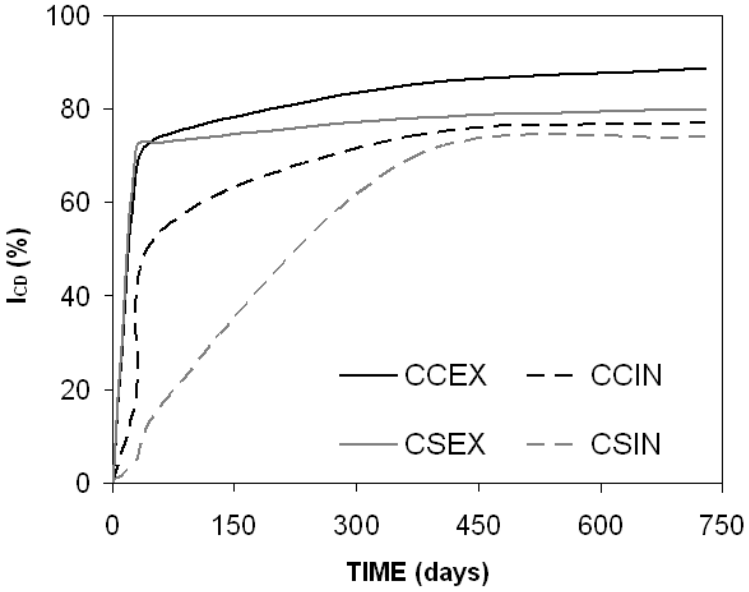

Figure I.3.3 *Evolution of the carbonation process: carbonation degree index (I_{CD}, in %) represented as a function of the time (in days) for the outer (-EX) and inner (-IN) areas of CC (with calcitic aggregate) and CS (with siliceous aggregate) mortars after 28 days (28D), 2 (2M) and 6 (6M) months, 1 (1Y) and 2 (2Y) years. I_{CD} was calculated from the amount of portlandite obtained at each time interval by means of thermogravimetric analysis.*

The outer part of the mortars carbonates very fast within the first two months of curing (at 28 days for CS and at 2 months for CC), when the carbonation degree is almost 75% in both mortars. From this point onwards the I_{CD} increases much more slowly (about 1% a month) and after two years reaches 89% in the outer part of CC as compared to 80% for CS. The carbonation reaction is enhanced in the CC mortar due to both the compositional continuity of the mortar system [29] and the grain morphology. In fact, calcite precipitates more easily in the nucleation sites of aggregates whose grains have an angular shape and a rough surface, such as calcitic aggregates [13]. The curve for the surface of the mortars shows a slight final slope that suggests that carbonation is still ongoing in this area after two years of curing.

The trend of the curves showing the carbonation of internal samples indicates that carbonation is much lower inside the mortar than on the surface, due to the fact that it is difficult for CO_2 to diffuse from a carbonated network (i.e. the surface), which is less porous, to the non-carbonated part (i.e. the core) of the mortar [3]. Moreover, carbonation is much faster in CC internal samples during the first months of curing. This indicates that the CC mortar has a more open, more permeable pore network than the CS at the beginning of the process, as the values for open porosity also show (Tab. I.3.2). After two years of carbonation, the

degree of carbonation inside the mortars is 77% in CC mortars and 74% in CS mortars.

3.3 Textural characteristics of mortars

Carbonation led to a fall in porosity and an improvement in the cohesion of the mortars, as observed by FESEM over 2 years (Fig. I.3.4). Interestingly, CC mortars, which were characterized by the worst textural properties over the first month, showed a bigger increase in compactness after the first year (Fig. I.3.4c and e) and an improved cohesion between the matrix and the grain surface. The higher degree of carbonation recorded in CC mortars at this time is responsible for this improvement. By contrast, we observed poor cohesion between the newly formed calcite and the surface of the siliceous grains in CS mortars even after 2 years of carbonation. In fact, in CS mortars the aggregate grains were easily visible at different magnification (Fig. I.3.4f), whilst in CC mortars it was almost impossible to recognise the calcareous grains, as their surface was completely covered by the newly-formed calcite (Fig. I.3.4e).

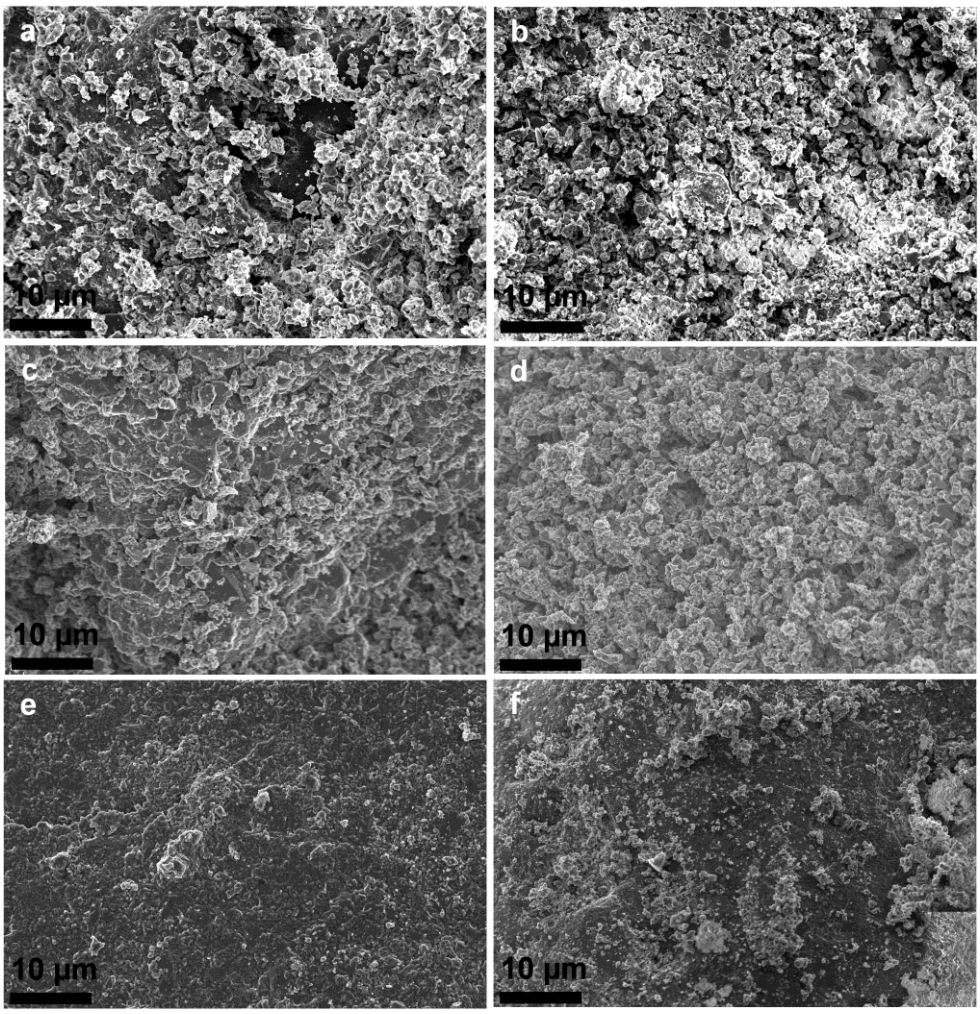

Figure I.3.4 *FESEM images of CC (with calcitic aggregate) (a, c and e) and CS (with siliceous aggregate) (b, d and f) mortars after 28 days (a and b), 1 (c and d) and 2 (e and f) years.*

3.4 Pore system of mortars

Pore size distributions obtained by means of the MIP and N_2 adsorption techniques are shown in the same graphs (Figs. I.3.5 and I.3.6).

CC and CS mortars are mainly composed of pores with a radius of between 0.1 and 1 μm, which is a structural peak typical of lime pastes, whose height depends on the amount of water initially added when making the mortars and then evaporated [5,37].

The porosity of CC mortars decreases during the first month (Tab. I.3.2), the period in which the carbonation process is fastest (Fig. I.3.3), leading to a 12% increase in volume caused by the transformation of portlandite into calcite. The clearest result of the carbonation process in mortars is the rapid disappearance of the family of largest pores (r>1μm) (Fig. I.3.5) that are filled by both microcrystalline and amorphous calcite [4]. This is because a phase is more likely to precipitate inside the larger pores, where the energy required for their growth is lower than in the smaller pores [38]. Interestingly, an increase in the porosity percentage is recorded from 1 to 6 months after the experiment began (Tab. I.3.2) and this is due to an increase in the volume of pores in the 0.01 - 0.15 μm size range (Fig. I.3.5) This phenomenon was also observed by Lawrence et al. [5] and is due to the formation of agglomerates of small calcite particles at the interface between aggregate grains and matrix. On the other hand, Arandigoyen et al. [39] found that in lime and blended pastes the volume of pores with a radius of between 0.01 and 0.03 μm falls sharply during carbonation. This apparent discrepancy demonstrates the important influence of the aggregate on the microstructure of the mortar.

The volume of the smaller pores continues increasing until it reaches a stable value after 1 year.

No clear relation was found between carbonation time and the changes in the main family of pores (0.1<r<1 μm). During the first month, when most of the microstructural changes caused by the carbonation process took place, the main peak on the x-axis shifted slightly towards greater radii (from 0.41 to 0.48 μm) and the volume of pores within this range increased. During the following five months, the volume of these pores increased but their size did not. After 1 year the main peak has the same shape (size and volume) observed after the first two weeks of carbonation. These small changes in the size of the main pores must be due to the heterogeneity of mortar samples and not to the carbonation process.

CS mortars show a smaller volume of pores between 0.1 and 1 μm (Fig. I.3.6), due to the fact that less kneading water is used in the preparation of this mortar (*cf.* Section 2.2). CS mortars are characterized by the presence of large pores (1<r<10 μm) that are likely to exist at the ITZ, where poor cohesion was found (*cf.* Section 3.3). In CC mortars, the presence of large pores at the ITZ was observed only after 7 days of curing (*cf.* Section 3.1), as the pore size distribution curve at this time also confirms (Fig. I.3.5). PSD curves obtained for CC at other time intervals do not show the presence of large pores and this indicates, once more, that these pores are filled by newly-formed calcite.

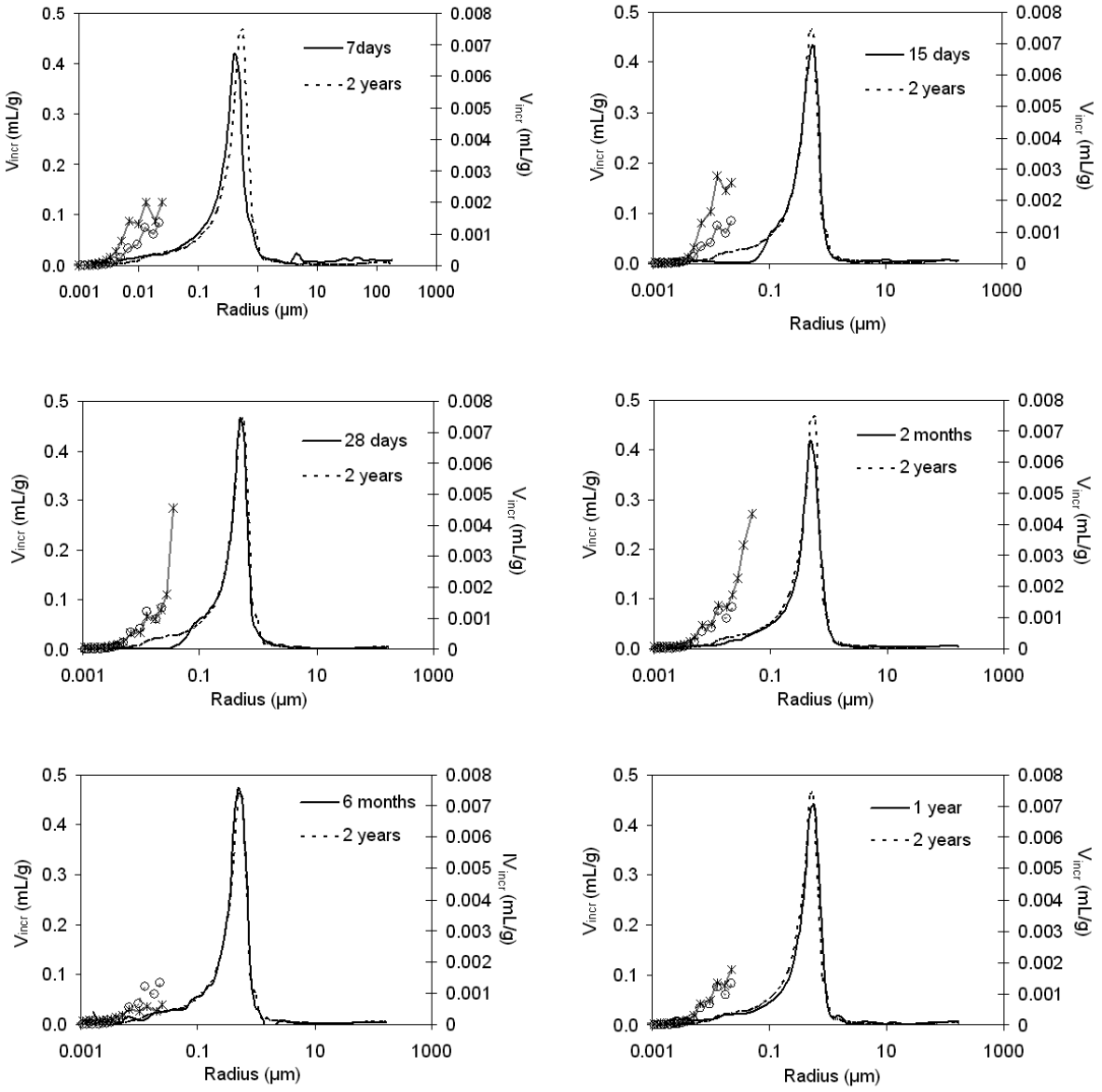

Figure I.3.5 *Pore size distribution curves of CC mortars (with calcitic aggregate) determined after 7, 15 and 28 days, 2 and 6 months, 1 and 2 years of carbonation. The grey curves refer to the secondary y-axis, which is the incremental volume (cm^3/g) of nanopores determined with the BJH method. In these curves, the circles indicate the 2 year-old mortars and the asterisks refer to the samples studied at the different time intervals.*

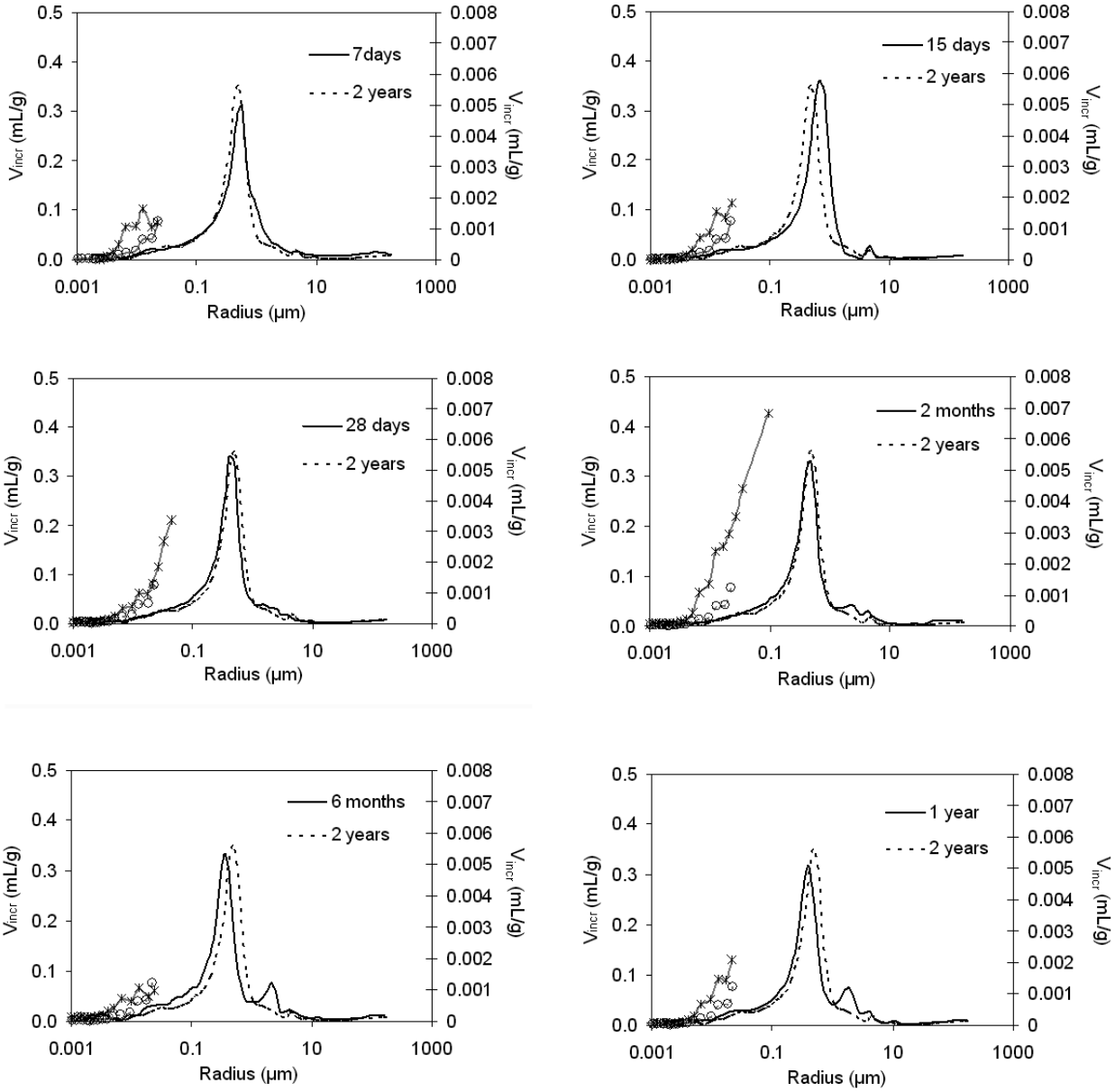

Figure I.3.6 *Pore size distribution curves of CS mortars (with siliceous aggregate) determined after 7, 15 and 28 days, 2 and 6 months, 1 and 2 years of carbonation. The grey curves refer to the secondary y-axis, which is the incremental volume (cm^3/g) of nanopores determined with the BJH method. In these curves, the circles indicate the 2 year-old mortars and the asterisks refer to the samples studied at the different time intervals.*

This also occurs in CS mortars but after one year of carbonation and to a lesser extent than in CC mortars. The porosity values of CS mortars are quite constant in the first month of carbonation and only a bit higher after 1 year.

In Table I.3.2, SSA values are obtained from N_2 adsorption measurements, because this technique is more precise than MIP especially in the smallest pores (when "ink-bottle" pores are analysed, the smallest pores are overestimated and the biggest ones are underestimated). In both mortars the specific surface area decreases from one year of carbonation onwards and almost no differences were found in the SSA values of CC and CS. However, the SSA value of the CC mortar is higher in samples after 28 days of curing due to the fact that the calcitic aggregate has a higher initial specific surface area (*cf.* Section 3.1). In the same way, the volume of nanopores obtained by N_2 adsorption increases until 28 days in CC and two months in CS mortars, after which it decreases again.

3.5 Hydric properties

CC mortars absorb a higher quantity of water than CS mortars but this quantity decreases for both mortars as carbonation progresses (*cf.* C_a values, Tab. I.3.3). In samples with 28 days of curing, CC and CS appear to be saturated after around 10 hours of the free water absorption test (Figs. I.3.7a and b). Nonetheless, mortar samples continue absorbing water very slowly over the next three days. This part of the curve, more pronounced in CC mortars, reflects the differences in the volume of pores of mortars already detected by MIP. In particular, the decrease in the absorption rate indicates the presence of small pores, as research has shown that the absorption rate slows down when water encounters smaller pores [40].

Mortar name	Time (days)	C_a	I_d	A	B
CC	28D	12.67	0.68	0.21	3.25
	2M	-	-	0.08	9.72
	6M	8.03	0.88	0.08	7.47
	1Y	11.92	0.80	0.09	9.50
	2Y	-	-	0.07	9.14
CS	28D	11.00	0.77	0.06	8.45
	2M	-	-	0.06	8.89
	6M	10.87	0.88	0.07	7.20
	1Y	11.09	0.80	0.07	9.63
	2Y	-	-	0.07	7.43

Table I.3.3 *Absorption coefficient (C_a, in g/min$^{1/2}$), drying index (I_d) and imbibition coefficients (A, in g/cm^2 min$^{1/2}$ and B, in cm/min$^{1/2}$) of CC and CS mortars after 28 days (28D), 2 (2M) and 6 (6M) months, 1 (1Y) and 2 (2Y) years. – Absorption and desorption tests were not performed at 2 months and 2 years of carbonation.*

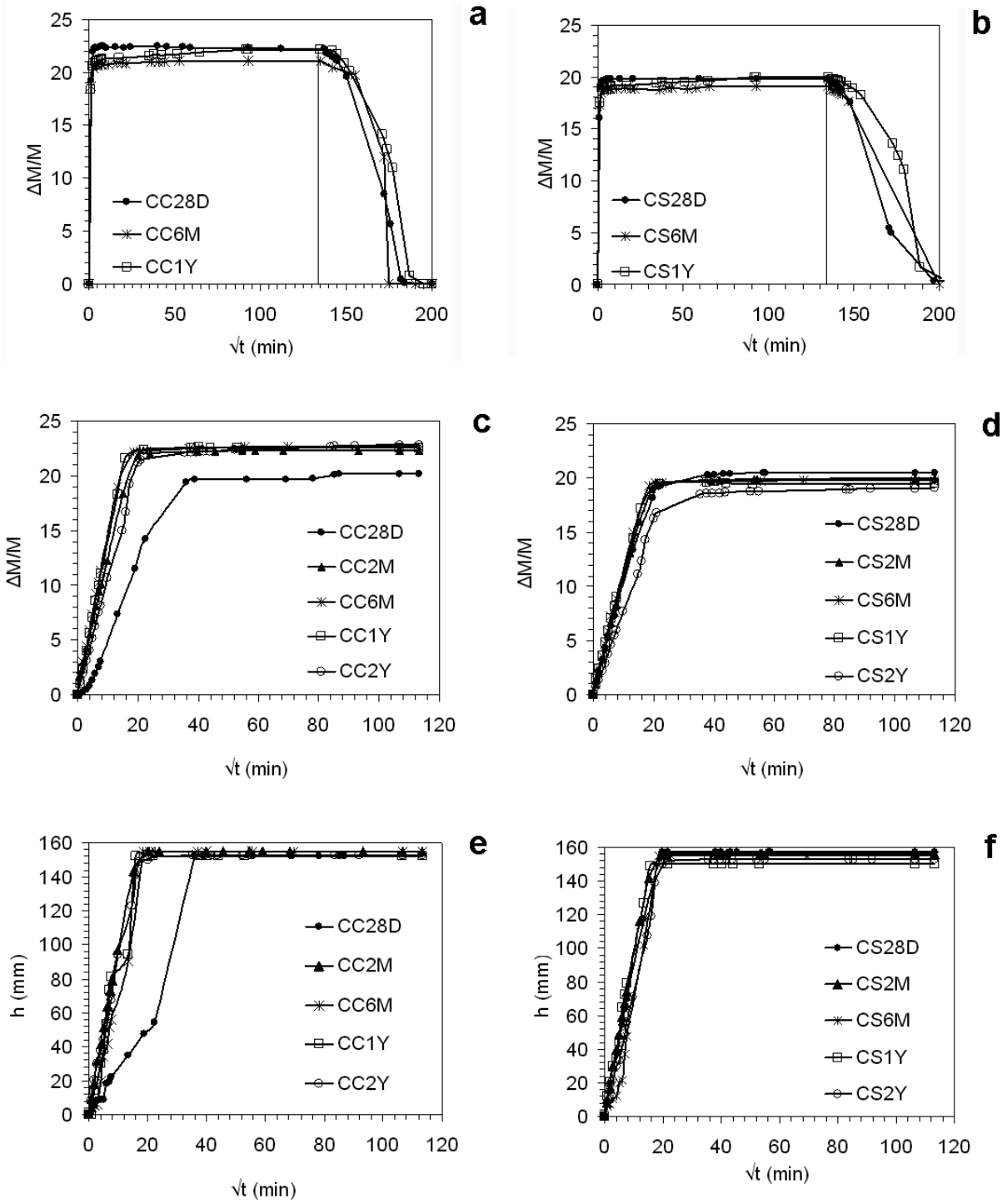

Figure I.3.7 *Free water absorption and drying curves of CC (with calcitic aggregate) (a) and CS (with siliceous aggregate) (b) mortars after 28 days (-28D), 6 months (-6M) and 1 year (-1Y) of carbonation; the solid line indicates the beginning of the free water drying of mortars samples. Capillarity curves of CC (with calcitic aggregate) (c and e) and CS (with siliceous aggregate) (d and f) mortars after 28 days (-28D), 2 (-2M), 6 (-6M) months and 1 (-1Y) and 2 (-2Y) years of carbonation. Time (√t, in $min^{-1/2}$) is plotted versus the weight increase (ΔM/M, in %) (c and d) and the water uptake level (h, in mm) (e and f).*

As regards drying, more than one slope is observed in the curves of CC and CS samples, especially in samples with six months and one year of carbonation that dry more slowly than samples that have been cured for shorter periods (Figs. I.3.7a and b), as indicated in the I_D values for mortar samples (Tab. I.3.3). This results in a worsening of the hydric properties of both mortars, because slower drying means that water is retained longer in the mortar pore system, thus affecting their durability. Once again, the pore system is responsible for the different drying speeds, as larger pores are the first to empty, whilst smaller pores remain full of liquid [41].

Another consideration that must be drawn from these curves regards the absorption and drying ability of mortars during carbonation. A high absorption of water is obtained in samples carbonated for 28 days, as a consequence of the higher porosity and shrinkage fissures of samples at this age, as was also found by Martys and Ferraris in mortars and concrete [40]. The decrease of the water absorbed in samples with six months' curing seems in contrast with the increase in open porosity observed by MIP from two to six months of carbonation (Tab. I.3.2). However, if we observe the PSD curves for both mortars (Figs. I.3.5 and I.3.6) we can see that in this period the volume of pores with a radius of between 0.01 and 0.15 μm decreased, which indicates that these pores do influence water absorption in mortars. Finally, after one year of carbonation, water absorption was similar to that obtained at 28 days in both mortars.

The capillarity test also shows that the amount of water absorbed by CC mortars is higher than in CS mortars (Figs. I.3.7c and d). Water imbibition is slower in CC samples with 28 days of carbonation, as indicated by the higher A value (Tab. I.3.3). A partial dissolution of portlandite in water is likely to occur in fresh samples and this slows down the water rise. In 2 and 6 month-old CC samples, water capillary uptake is faster than in less cured samples (28 days) (Fig. I.3.7c). These observations are confirmed by the values for imbibition coefficients A and B, presented in Table I.3.3. The opposite trend was observed for CS mortars (Fig. I.3.7d).

The capillary front reaches the top of the samples after 6 hours in CC and after 8 hours in CS, as shown in Figures I.3.7e and f. Nonetheless, this visual saturation does not coincide exactly with real saturation, which occurs three hours later as the mass uptake curves show (Fig. I.3.7c and d). This small time lag between visual and real saturation of the sample indicates that although the water has already reached the top of the sample (as shown in Figs. I.3.7e and f), it continues filling the pores at a lower velocity because of the presence of different pore ranges. When all connected pores are filled the sample stops absorbing water and mass saturation is achieved. However, the pore network of both types of mortar can be considered quite homogeneous (the majority of pores are between 0.1 and 1 μm, *cf.* Section 3.3) because the capillary ascent and mass taking represented as a function of the square root of time are linear in the majority of the samples [34] and the time-lag between visual and real

saturation is not as big as in other heterogeneous materials (such as tuff) that are characterised by a higher volume of large pores.

It is important to bear in mind that the interpretation of hydric tests in mortars is often complicated by the fact that portlandite can dissolve during water absorption, especially during the first months of mortar life. Clear evidence of this can be seen in Figure I.3.8, in which part of a 28-day-old mortar sample dissolved when water was forced into it. Interestingly, the non-dissolved zone is located at the border of the sample and is 4 mm deep. This coincides with the advancing carbonation margin (from the surface to the core) [29,36]. In the same way, during water capillary imbibition in CS samples, two different zones were clearly distinguished on the top surface, one saturated and the other still dry. The wet zone formed a contour at the edges of the surface, which resembled the carbonation border. In CC samples, saturation was reached in a more uniform way and no clear border was perceived. The presence of carbonated and non-carbonated zones in mortars produces a heterogeneity that directly affects the hydric properties of the mortars.

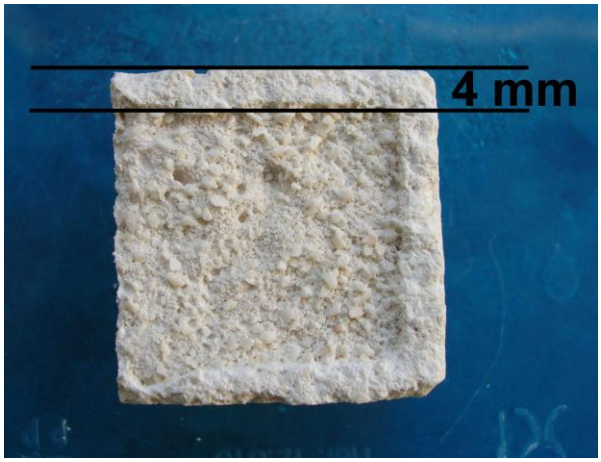

Figure I.3.8 *Appearance of the mortar samples when water is forced into the mortar. The dissolved part marks a clear edge of about 4 mm that highlights a carbonation border.*

3.6 Mechanical properties

Our mechanical assays demonstrated that mortars prepared with calcitic aggregate (CC) show higher compactness and cohesion between matrix and aggregate grains, compared to CS mortars (Fig. I.3.9a). This behaviour coincides with that observed by Lanas and Alvarez-Galindo [13] for mortars prepared with calcareous and siliceous aggregate. CS mortars are more fragile and show a high tendency to pulverize during and after rupture, especially when they are submitted to mechanical assays when only one month old.

Mortar strength increases during the carbonation process, especially during the first 6 months, after which resistance values remain quite constant.

The way in which mortars broke during compressive assays is shown schematically in Fig. I.3.9b. In mortars, the first visible effect of the compressive strength applied along the direction perpendicular to the

compactation plane is the detachment of superficial layers. It is well known that the carbonation process causes mortars to develop high mechanical resistance (due to the increase in compactness and the decrease in porosity). Nevertheless, we think that this higher strength does not develop at the same time throughout the whole material. A lower degree of cohesion must exist between the carbonated and the non-carbonated zone of the sample, due to the fact that fractures mostly develop at this interface. This heterogeneity is bigger at the beginning of the process, when the type of rupture shown in Figure I.3.9b occurs (outer layers break off), and is expected to decrease, due to the progress of carbonation through the core of the samples.

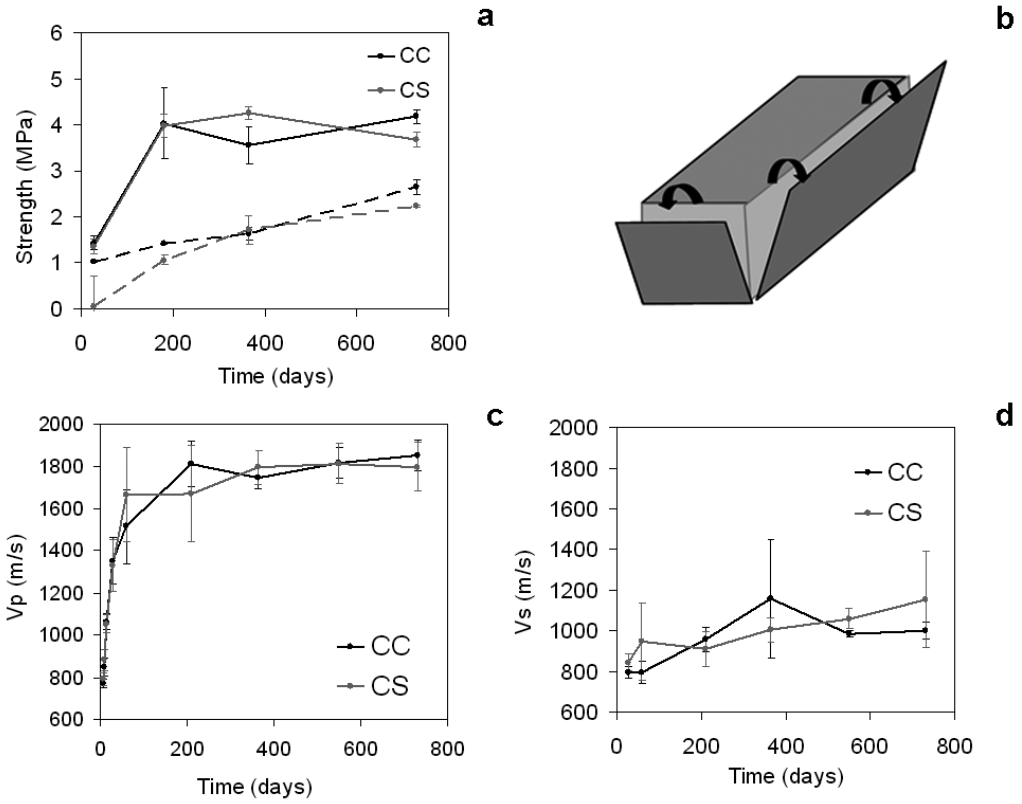

Figure I.3.9 *(a) Mechanical strengths (in MPa) of CC (with calcitic aggregate) and CS (with siliceous aggregate) mortars determined within 2 years. Solid and dotted lines refer to compressive and tensile strength, respectively; (b) rupture in sheets of a mortar sample after the compressive assay; velocity of p waves (V_p, in m/s) (c) and s waves (V_s, in m/s) (d) in CC (with calcitic aggregate) and CS (with siliceous aggregate) mortars. Error bars represent the standard deviation of the values at each time interval.*

The application of ultrasounds was useful for corroborating the results obtained with the mechanical assays. Ultrasounds propagate more rapidly in CC mortars and the increase in velocity is higher in these mortars than in CS, especially after 6 months (Fig. I.3.9b and c). A close correspondence was found between P waves' propagation velocity and the carbonation degree of mortars. This similarity is clear in the curves in Figures I.3.3 and I.3.9c, in which we can see a common initial steep slope

during the first month, followed by a slight and almost constant slope until 2 years of carbonation. This common trend indicates that the carbonation process induces microstructural changes that have a direct effect on the macroscopic properties of mortars. In addition, the most carbonated mortars at the end of the study are also the strongest and the most compact, which is the case of CC mortars. This tight correlation with the degree of carbonation of the mortars was not found for the V_s values, although this parameter also increases over time (Fig. I.3.9c). However, the study of V_s value has been dismissed by other authors [42-43] because secondary waves (S) proved to be useless for the characterisation of stone materials.

As shown in Table I.3.4, the elastic moduli values for the mortars increase over time and this coincides with the improvement in the cohesion and compactness of mortars. In general, CS mortars are characterised by slightly higher elastic moduli values, although this is more likely due to the different composition of the aggregate than to the microstructure of the mortars. The exception in this general trend is the Poisson coefficient value, which decreases after one year of carbonation. These variations are probably due to the bulk density values (obtained by MIP) used for calculating these moduli (*cf.* Section 2.3.5), which may be affected by the high heterogeneity of mortar samples.

4. Conclusions

In this work we have investigated in detail the influence of the aggregate in the carbonation process of aerial lime mortars. A dry hydrated lime and two aggregate types (calcitic and siliceous) were used to prepare sample mortars. The study of the textural characteristics of the aggregates and their relationship with the carbonation of lime help us to understand the physical-mechanical properties of mortars and their evolution over time.

The carbonation degree index, which combines and contrasts the results provided by X-ray diffraction and thermogravimetric analyses, has been shown to be an accurate method for studying the evolution of the carbonation process on the surface and in the core of mortars. Results showed that the transformation of portlandite into calcite occurs mainly in the first two months after preparation of the mortars, after which the transformation rate falls sharply. Mortars with a calcitic aggregate are more carbonated than those with a siliceous aggregate, both on the outer part and in the core of the samples. This is due to the active role of the calcareous aggregate in the transformation of portlandite into calcite because of its composition and irregular morphology. After two years, 3% to 6% of non-carbonated binder was found in all the samples, confirming how slow the carbonation process is in aerial lime mortars.

The specific surface area values indicate that the water required during the preparation of the mortars also varies depending on the aggregate used; the calcitic aggregate requires more water than the siliceous one. This results in a higher open porosity of the mortars made with calcitic

aggregate due, above all, to the shrinkage fissures observed in these mortars at the beginning of their life. Interestingly, in mortars with a calcareous aggregate the cohesion at the interface between the binder and the aggregate is greatly improved during carbonation and this is reflected in the pore size distribution of mortars. In fact, three main families of pores have been observed: the largest family contains pores of between 0.1 and 1 μm and is larger in mortars made with calcitic aggregate because they require more water; a second peak of pores with a radius of more than 1 μm was only obtained in calcitic aggregate mortars after 7 days, whilst it was present in siliceous aggregate mortars throughout the study; a third peak of smaller pores (ranging between 0.01 and 0.15 μm) is produced due to the formation of calcite and its height increases especially in the first months, when carbonation is faster. This phenomenon is particularly evident in mortars made with calcitic aggregate because of the growth of new micrometric calcite crystals on the surface of the calcite grains.

This heterogeneous pore network is reflected in the hydric properties of the mortars. The higher absorption observed in mortars made with calcitic aggregate suggests that the pores with a radius of between 0.1 and 1 μm have the greatest influence on capillary uptake, as there is a higher volume of these pores in this type of mortar.

Furthermore, the volume of pores with a radius of between 0.01 and 0.15 μm influences the amount of water absorbed during the free water absorption test.

Pores larger than 1 μm have less influence on total water uptake but they play an important role in the capillary absorption rate. In this sense, mortars with siliceous aggregate absorb water more slowly than those with calcitic aggregate, since the former have more large pores.

Finally, we found that portlandite partially dissolves in water during hydric assays, especially in fresh samples (i.e. low-carbonated samples), and this slows down water absorption and rise.

The greater compactness of mortars with calcitic aggregate produces higher mechanical resistance in these mortars, and a higher propagation velocity of ultrasounds within the material. A close correlation has been found between the carbonation degree index at each time and the evolution of the propagation velocity of primary waves in all mortars. This shows that ultrasounds are a useful tool for characterizing the physical properties of mortars.

The results obtained from this research indicate that the aggregate strongly affects the mortar microstructure and the evolution of its textural and physical properties. We have also found that it is better to use a calcareous aggregate when making aerial lime mortars than a siliceous one, because the former promotes higher carbonation and better textural and physical-mechanical properties.

Acknowledgements:

This study was funded by the Research Group RNM179 of the Junta de Andalucía and by Research Project MAT2008-06799-C03. We are grateful to ARGOS DERIVADOS DEL CEMENTO S.L. (Granada) for providing the raw materials used in this study.

References

[1] Van Balen, K. 2005. Carbonation reaction of lime, kinetics at ambient temperature. Cement and Concrete Research, 35, 647-657.
[2] Sánchez-Moral, S., García-Guinea, J., Luque, L., Gonzalez-Martín, R. & López-Arce, P. 2004. Carbonation kinetics in roman-like lime mortars. Materiales de Construcción, 275 (54), 23-37.
[3] Houst, Y. F. & Wittmann, F. H. Influence of porosity and water content on the diffusivity of CO2 and O2 through hydrated cement paste. 1994. Cement and Concrete Research, 24 (6), 1165-1176.
[4] Moorehead, D. R. 1986. Cementation by the carbonation of hydrated lime. Cement and Concrete Research, 16, 700-708.
[5] Lawrence, R. M., Mays, T. J., Rigby, S., Walker, P. & D'Ayala, D. Effects of carbonation on the pore structure of non-hydraulic lime mortars. 2007. Cement and Concrete Research, 37, 1059-1069.
[6] Ngala, V. T. & Page, C.L. 1997. Effects of carbonation on pore structure and diffusional properties of hydrated cement pastes. Cement and Concrete Research, 27 (7), 995-1007.
[7] B. Bourdette, E. Ringot, J.P. Ollivier, Modelling of the transition zone porosity, Cem. Concr. Res. 25 (4) (1995) 741-751.
[8] C. Rodríguez-Navarro, E. Hansen, W. Ginell, Calcium hydroxide crystal evolution upon aging of lime putty, J. Am. Ceram. Soc. 81 (1998) 3032-3034.
[9] O. Cazalla, C. Rodriguez-Navarro, E. Sebastian, G. Cultrone, Aging of lime putty: effects on traditional lime mortar carbonation, J. Am. Ceram. Soc. 83 (5) (2000) 1070-1076.
[10] C. Rodríguez-Navarro, O. Cazalla, K. Elert, E. Sebastian, Liesegang pattern development in carbonating traditional lime mortars, Proc. R. Soc. London 458 (2002) 2261-2273.
[11] C. Rodríguez-Navarro, E. Ruiz Agudo, M. Ortega Huertas, E. Hansen, Nanostructure and irreversible colloidal behaviour of Ca(OH)2: implications in cultural heritage conservation, Langmuir 21 (2005) 10948-10957.
[12] E. Ruiz Agudo, C. Rodríguez-Navarro, Microstructure and rheology of lime putty, Langmuir 26 (6) (2010) 3868–3877.
[13] J. Lanas, J. Alvarez-Galindo, Masonry repair lime-based mortars: factors affecting the mechanical behaviour, Cem. Concr. Res. 33 (11) (2003) 1867-1876.
[14] M. Westerholm, B. Lagerblad, J. Silfwerbrand, E. Forssberg, Influence of fine aggregate characteristics on the rheological properties of mortars, Cem. Concr. Compos. 30 (2008) 274-282.

[15] A.K.H. Kwan, W.W.S. Fung, Packing density measurement and modelling of fine aggregate and mortar, Cem. Concr. Compos. 31 (2009) 349-357.
[16] W.W.S. Fung, A.K.H. Kwan, H.H.C. Wong, Wet packing of crushed rock fine aggregate, Mater. Struct. 42 (5) (2008) 631-643.
[17] M. Romagnoli, M.R. Rivasi, Optimal size distribution to obtain the densest packing: A different approach, J. Eur. Ceram. Soc. 27 (2007) 1883-1887.
[18] UNE EN 933-2. Ensayos para determinar las propiedades geométricas de los áridos. Parte 2: Determinación de la granulometría de las partículas. Tamices de ensayo, tamaño nominal de las aberturas. AENOR, Madrid (1999).
[19] Venkatarama B.V.R., Gupta A. Influence of sand grading on the characteristics of mortars and soil-cement block masonry. Construction and Building Materials 22 (2007) 1614-1623.
[20] UNE-EN 459-1. Cales para la construcción. Parte 1: Definiciones, especificaciones y criterios de conformidad. AENOR, Madrid (2002).
[21] UNE EN 13139. Áridos para morteros. AENOR, Madrid (2003).
[22] D.R. Dinger, Particle Packing and Pore Size Distributions, 1 (9) (1980) (an update 2003) available on www.dingerceramics.com.
[23] J. Bolomey, Revue Matèr. Constr. Trav. Publ., Edition C, 147 (1947).
[24] W.B. Fuller, S.E. Thompson, The laws of proportioning concrete, Proc. Am. Soc. Civil Engr. 33 (1907) 261.
[25] J.D. Martín Ramos, XPowder. A software package for powder X-ray diffraction analysis, Lgl. Dep. GR 1001/04 (2004).
[26] UNE-EN ISO 11358. Plásticos. Termogravimetría (TG) de polimeros. Principios generales. AENOR, Madrid (1997).
[27] UNE EN 1015-3. Métodos de ensayo de los morteros para albañilería. Parte 3: Determinación de la consistencia del mortero fresco (por la mesa de sacudidas). AENOR, Madrid (1998).
[28] UNE-EN 1015-11. Metodos de ensayo de los morteros para albañileria. Parte 11: Determinación de la resistencia a flexión y a compresión del mortero endurecido. AENOR, Madrid (2000).
[29] O. Cazalla, Morteros de cal. Aplicación en el Patrimonio Histórico, Ph.D. Thesis, Universidad de Granada (2002).
[30] E.P. Barret, L-J. Joyner, P. Halenda, The determination of pore volume and area distributions in porous substances. I. Computations from nitrogen isotherms, J. Am. Chem. Soc. 73 (1951) 373-380.
[31] S. Brunauer, P.H. Emmett, J. Teller, Adsorption of gases in multimolecular layers, J. Am. Chem. Soc. 60 (1938) 309.
[32] UNI-EN 13755. Metodi di prova per pietre naturali. Determinazione dell'assorbimento d'acqua a pressione atmosférica. CNR-ICR, Rome (2008).
[33] NORMAL 29-88. Misura dell'indice di asciugamento (drying index). CNR-ICR, Rome (1988).
[34] K. Beck, M. Al-Mukhatar, O. Rozenbaum, M. Rautureau, Characterization, water transfer properties and deterioration in tuffeau:

building material in the Loire valley-France, Build. Environ. 38 (2003) 1151-1162.
[35] J.P. Gonçalves, L.M. Tavares, R.D. Toledo Filho, E.M.R. Fairbairn, E.R., Cunha. Comparison of natural and manufactured fine aggregates in cement mortars, Cem. Concr. Res. 37 (2007) 924-932.
[36] R.M.H. Lawrence, T.J. Mays, P. Walker, D. D'Ayala, Determination of carbonation profiles in non-hydraulic lime mortars using thermogravimetric analysis, Thermochim. Acta 444 (2006) 179-189.
[37] M. Arandigoyen, J.L. Pérez Bernal, M.A. Bello López, J.I. Alvarez, Lime-pastes with different kneading water: Pore structure and capillary porosity, Appl. Surf. Sci. 252 (2005) 1449-1459.
[38] C. Rodríguez-Navarro, E. Doehne, Salt weathering: influence of evaporation rate, supersaturation and crystallization pattern, Earth Surf. Processes Landforms 24 (3) (1999) 191-209.
[39] M. Arandigoyen, B. Bicer-Sismir, J.I. Alvarez, D.A. Lange, Variation of microstructure with carbonation in lime and blended pastes. Appl. Surf. Sci. 252 (2006) 7562-7571.
[40] N.S. Martys, C. Ferraris Capillary transport in mortars and concrete, Cem. Concr. Res. 27 (5) (1997) 747-760.
[41] G.W. Scherer, Theory of drying, J. Am. Ceram. Soc. 73 (1) (1990) 3-14.
[42] D. Benavente, J. Martínez-Martínez, P. Jáuregui, M.A. Rodríguez, M.A. García del Cura, Assessment of the strength of building rocks using signal processing procedures, Constr. Build. Mater. 20 (2006) 562-568.
[43] J. Martínez-Martínez, Influencia de la alteración sobre las propiedades mecánicas de calizas, dolomías y mármoles. Evaluación mediante estimadores no destructivos (ultrasonidos), PhD Thesis, University of Alicante (2008).

Chapter I.4

Ultrasonic wave propagation through lime mortars: an alternative and non-destructive tool for textural characterization

Arizzi A., Martínez-Martínez J., Cultrone G.
Submitted to *Materials and Structures*
(under review)

Abstract

The detailed textural characterization of lime mortars can be a difficult task when samples collection is restricted (i.e. in historic buildings). In these situations, non-destructive techniques, such as ultrasonic tests, represent a powerful alternative, due to their wide possibilities. In this paper the response of the wave propagation velocity (v_p) and spatial attenuation (α_s) in mortars with different binder-to-aggregate proportions, kneading water content, aggregate mineralogy and grading, and carbonation degree was analysed. Results show that the main textural parameters controlling v_p and α_s are mortar porosity and carbonation degree. The former is related to the amount of kneading water added during mortar preparation, whilst the latter depends on the age of lime mortar. Two empirical equations have been obtained in order to assess the porosity and carbonation degree of mortars from ultrasonic measurements, establishing the first step for characterizing the texture of lime mortars in future, by means of non-destructive procedures. These results have been corroborated by means of optical and electronic microscopy, X-ray diffraction and mercury intrusion porosimetry analyses.

1. Introduction

The non-destructive evaluation of mortars is a major issue for estimating the quality, durability and characteristics of pieces in which samples cannot be collected. For example, the study of mortars employed in architectural heritage requires the use of techniques as low invasive as possible. Among all non-destructive testing methods available, the ultrasonic waves is, probably, the most used tool due to the possibility of determining the elastic properties (such as Young Modulus), and also of characterizing micro-structural properties of materials (porosity, grain size or micro-cracks). On the other hand, the correct interpretation of ultrasonic signals is difficult because these micro-structural aspects have different effects on wave propagation, i.e. on velocity and/or attenuation [1]. Consequently, knowing the influence of a specific factor (for example: porosity) on wave velocity or attenuation is very difficult and requires a deep study by means of both empirical and numerical approximations, and only when this influence is completely understood it will be possible to assess mortar characteristics from ultrasonic data with enough exactitude.

The most crucial parameter affecting mortar quality (in terms of its durability) is the water dosage [2], because it is directly related to the pore system characteristics (quantity, size and connectivity of pores), and, as a consequence, it determines the water accessibility as well as the mortar resistance against salt crystallization processes [3]. Several works have been carried out to assess the porosity and the strength of mortars and concretes by means of the use of ultrasounds [4-9]. However, the effects of porosity on ultrasounds are disguised by other wave disruptions caused by aggregates, for example. In fact, the ultrasonic signal obtained after its propagation through the mortar is the result of the initial signal modified by the scattering and the delay caused by pores and sand. Moreover, mortars with different aggregate content, mineralogy and grading can be elaborated, and they will have different ultrasonic response.

In the case of mortars and concretes, ultrasonic test may be also useful to study the changes in mechanical properties and microstructure caused by hardening. Generally, carbonation and hydration processes produce an increase in mechanical strength and compactness that determine a proportional increase in the velocity of propagation of longitudinal waves, as well as to a decrease in the anisotropy of the sample [7]. However, the great majority of these studies are focused on cement mortars and concrete, whilst a lack of information exists about the factors that influence the propagation of ultrasonic waves within lime-based mortars. In fact, the latter are characterized by a hardening process (i.e. carbonation) that is much slower in time with respect to the hydration reactions that occur in cement mortars and concrete. Initially, a lime-based mortar is composed of aggregates surrounded by a matrix, in which the main mineralogical phase is portlandite ($Ca(OH)_2$), although small quantities of calcite ($CaCO_3$) can be present as a result of a previous slight

carbonation of the lime. The carbonation of a lime-mortar takes place when CO_2 dissolves in the condensed water and reacts with dissolved portlandite. This reaction results in the precipitation of calcium carbonate, due to the rapid supersaturation with respect to $CaCO_3$ in the solution existing in the mortar pores [10-13]. As it has been commented above, the carbonation process is much slower in time than the hydration of cement components, and in fact, portlandite has been detected in Roman mortars after more than 2000 years after their elaboration. The hardening products (calcite in lime-based mortars, aluminates and silicates hydrated phases in cement and concrete) do not produce the same mineralogical ad microstructural changes in the mortars matrix, with the consequence that the ultrasonic response within lime mortars cannot be correctly interpreted only on the basis of the previous studies on cement mortars and concrete.

The aim of this study is to clarify the influence of mineralogy, grading and dosage of the aggregate on the propagation velocity and the spatial attenuation of P waves within lime-based mortars. To this purpose, four binder-to-sand ratios and two aggregates with different composition (siliceous and calcareous) and grading (continuous and discontinuous) were used for the preparation of six types of lime mortars. Differences in mortar microstructure and mineralogy are considered to understand the differences in the values of propagation velocity and attenuation of P waves. Moreover, the evolution of elastic properties during the carbonation process of lime-based mortars was considered as an important point to study. In order to evaluate this evolution, textural and mineralogical characterization of each mortar type were carried out as well as ultrasonic measurements of every sample, at 7, 10, 15, 60 and 730 days since mortar elaboration.

2. Materials and methods

2.1. Mortars components and preparation

A calcitic dry hydrated lime (CL90S, [14]) was used for the preparation of six types of mortars, with different proportion, as shown in Table I.4.1. Three types of aggregate were used: a calcareous one with both continuous (CA, 0.063<ø<1.5 mm) and discontinuous (CDA, 0.1<ø<0.8 mm) grading, and a siliceous one, with a discontinuous grading (SA, 0.1<ø<0.5 mm). CA was used to prepare mortars with increasing aggregate volume, corresponding to the following binder-to-aggregate ratios by weight (B/A): 1:2, 1:3, 1:4 and 1:6 (mortars named CC1:2, CC1:3, CC1:4 and CC1:6 in Table I.4.1). Mortars with CDA and SA were prepared with a unique B/A ratio, equal to 1:3 (mortars named CD and CS, Tab. I.4.1). The amount of water (i.e. kneading water) was established in order to obtain mortars with plastic consistence, which corresponded to a flow comprised between 145 and 150 mm [15].

After the mixing, mortars were left during 7 days in normalized steel moulds (4×4×16 cm) at RH = 60±5% and T = 20±5°C and after removal

from the mould, they were cut in prisms of 4×4×5 cm. In total, 54 mortar samples were tested in this study (9 of each mortar type) and they were kept at the same temperature and relative humidity during carbonation.

Mortar name	Aggregate	B/A	B	A	W/TOT
CC1:2	CA	1:0.65	60.4	39.6	29.5
CC1:3	CA	1:1	50.4	49.6	31.3
CC1:4	CA	1:1.3	43.3	56.7	24.0
CC1:6	CA	1:2	33.2	66.8	20.0
CD1:3	CDA	1:1	50.4	49.6	27.0
CS1:3	SA	1:1	50.6	49.4	26.5

Table I.4.1 Proportions used during the preparation of the six types of mortar: B/A, binder-to-aggregate ratio by volume; W/TOT, water amount expressed in % of the total mass; B, proportion of the binder expressed in % by volume; A, proportion of the aggregate expressed in % by volume. Legend: CC = mortar with calcitic lime and calcareous aggregate with continuous grading; CD = mortar with calcitic lime and calcareous aggregate with discontinuous grading; CS = mortar with calcitic lime and siliceous aggregate with discontinuous grading; CA = calcareous aggregate with continuous grading; CDA = calcareous aggregate with discontinuous grading; SA = siliceous aggregate with discontinuous grading; 1:2, 1:3, 1:4, 1:6 of mortars name indicate the B/A proportions by weight.

2.2. Textural and mineralogical characterization

2.2.1 Optical and electronic microscopy (OM and FESEM)

The observation of mortars texture and microstructure (morphology, cohesion, porosity) was carried out on thin sections by means of a polarized microscope (OM) (Olympus BX-60) equipped with digital microphotography camera (Olympus DP10). Mortars fragments, previously dried, were carbon-coated and analysed by using a Leo-Gemini 1530 field emission scanning electron microscopy (FESEM).

2.2.2 Mercury intrusion porosimetry (MIP)

Open porosity (P_o, %) and pore size distribution (PSD, in a range of $0.002<r<200$ μm) were determined by means of a Micrometics Autopore III 9410 porosimeter. Three measurements per mortar type were performed on samples with 15, 60 and 730 days (2 years) of carbonation. Mortar fragments of ca. 2 cm^3 were oven-dried for 24 h at 60 ºC before the analysis.

2.2.3 X-ray diffraction (XRD)

The identification and quantification of the mineralogical phases of mortars was carried out by means of a Panalytical X'Pert PRO MPD, with automatic loader. Analysis conditions were: radiation CuK_α (λ=1.5405 Å), 4 to 70 º2θ explored area, 45 kV voltage, 40 mA current intensity and goniometer speed using Si-detector X'Celerator of 0.01 º2θ/s. The

interpretation and quantification of the mineral phases was performed by using the X-Powder software package [16]. The decrease in portlandite content was taken as reference to estimate the carbonation degree of mortars (I_{CD}, %).

The analysis was performed at different intervals of time: 7, 10, 15 and 60 days and 2 years of carbonation.

2.3. Mortars components and preparation

A Panametrics HV Pulser/Receiver 5058 PR coupled with a Tektronix TDS 3012B oscilloscope was used to perform the ultrasonic tests in transmission-reception mode. A couple of non-polarized piezoelectric transducers was employed, with a frequency spectrum of 1 MHz. Ultrasonic measurements were carried out on six prisms (40×40×50 mm) of each mortar samples along three perpendicular directions, perpendicular and parallel to the compaction plane, and they were performed at the following intervals of time: 7, 10, 15, 60 and 730 (2 years) days of carbonation. From the ultrasonic measurements we obtained propagation velocity (v_p) and spatial attenuation (α_s) values. The former parameter (v_p) was determined as the ratio between the specimen length and the transit time of the pulse. The latter (α_s) quantifies the energy lost during the wave propagation through the material [17]. This quantification was carried out by comparing the amplitude of the signal emitted by the transmitter sensor and the amplitude of the signal received by the receptor. Moreover, spatial attenuation was normalised according to the distance between transmitter and receptor. The α_s value (in dB/cm) was calculated as:

$$\alpha_s = \frac{20\log\left\lfloor \frac{A_e}{A_{mx}} \right\rfloor}{L} \qquad \text{[I.4.1]}$$

where A_e is the maximum amplitude emitted by the transmitter sensor, A_{mx} is the maximum amplitude (in absolute values) registered by the receptor sensor, and L is the length of the sample.

3. Results and discussion

3.1 Texture and porosity of the mortars samples

A mortar system is characterized by the presence of aggregate grains surrounded by a matrix in continuous transformation. In fact, since the first hours of curing at standard conditions water evaporation takes place. This first step of mortar life, named drying process, affects importantly the matrix texture, because it produces a big porosity in the mortar, as observed in CC1:2, CC1:4 and CC1:6 (Fig. I.4.1) in the form of occasional shrinkage fissures and rounded pores that are more or less big depending on the amount of water [13].

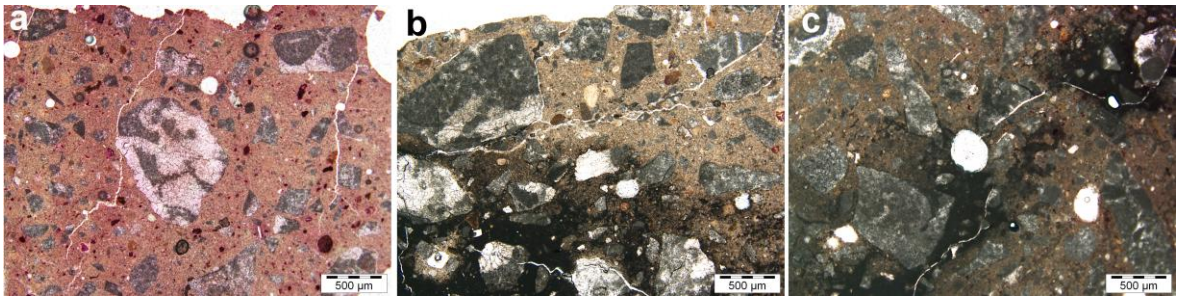

Figure I.4.1 *Optical images taken at the same magnification with plane polars. Large pores and shrinkage fissures in CC1:2 (a), CC1:4 (b) and CC1:6 (c).*

The values of open porosity measured by MIP after 15 days since mortars elaboration are comprised between 30 and 40% (Tab. I.4.2) and are lower in mortars with decreasing content of lime. The differences among these values can be linked to the amount of kneading water used in each mix, as also found by Arandigoyen et al. [13] for lime pastes. In fact, CC1:3, which was prepared with the biggest amount of water (Tab. I.4.1), shows the highest value of open porosity among all the mortars (Tab. I.4.2), while CC1:6 mortar presents the lowest porosity (Tab. I.4.2), because of the least amount of water used for its preparation, followed by CC1:4.

Mortar name	Time	P_o
CC1:2	15	41.0
	60	40.8
	730	35.7
CC1:3	15	35.2
	60	35.0
	730	35.7
CC1:4	15	34.5
	60	34.3
	730	31.1
CC1:6	15	30.0
	60	32.1
	730	27.9
CD1:3	15	34.5
	60	36.0
	730	32.7
CS1:3	15	37.8
	60	34.2
	730	35.1

Table I.4.2 *Average values of open porosity (P_o, in %) determined by MIP of mortars after 15 and 60 days and 2 years (730) from their elaboration. Standard deviation of open porosity values ranges between 0.05 and 3.50.*

When we consider mortars prepared with the same binder-to-aggregate ratio (1:3), CD1:3 shows the lowest porosity, followed by CS1:3 and CC1:3 (Tab. I.4.2). Notice how in the case of CS mortar there is no relationship between the amount of water (Tab. I.4.1) and the porosity, as in CC and CD. The reason of this discrepancy stays in the different morphology of the siliceous aggregate, which is not porous (Fig. I.4.2a) and, consequently, it does not absorb a part of the added water, as it occurs with the calcareous aggregate that presents pores and many fissures (Fig. I.4.2b). After mixing, this water remains free in the CS mortar paste and it is likely to evaporate faster than in the other mortars during drying, thus producing a porosity bigger than the expected (Tab. I.4.2).

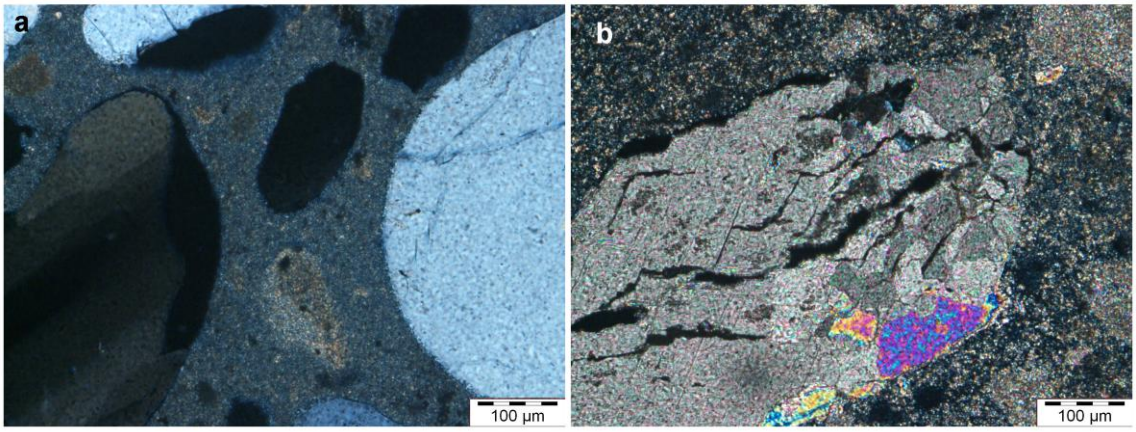

Figure I.4.2 *Optical images taken at the same magnification with crossed polars. Morphology of the aggregates: (a) grain of siliceous aggregate, with rounded and smooth surface, in which no internal porosity appears; (b) grain of calcareous sand with irregular edges and rough surface, which presents a big internal porosity and some fissures parallel to the exfoliation planes of calcite.*

After 2 years of carbonation, the values of porosity (Tab. I.4.2) decreases in all mortars, of around 2-5%, whilst it remains almost unvaried in CC1:3 mortar. The porosity decreases due to the growth of new-formed calcite that has a bigger volume than portlandite and fills the pores of the matrix [10].

Pore size distribution (PSD) curves give important information about the micro- and nanopores that are not easily visible by means of optical microscopy. The main peak obtained in the PSD curves of mortars corresponds to radius of pores comprised between 0.1 and 1 µm (Figs. I.4.3). This is a structural peak typical of lime pastes and it can appear more or less shifted in the x axis, depending on the amount of water added during mixing [13].

The same pores size distribution is maintained after two years of carbonation although there is a decrease in the amount of pores with radii comprised between 0.1 and 1 µm (Fig. I.4.3). Since MIP analysis only detects interconnected pores, the volume reduction of pores of the same

size indicates that the interconnection among these pores decreases. This occurs due to calcite crystallization during the carbonation process [18].

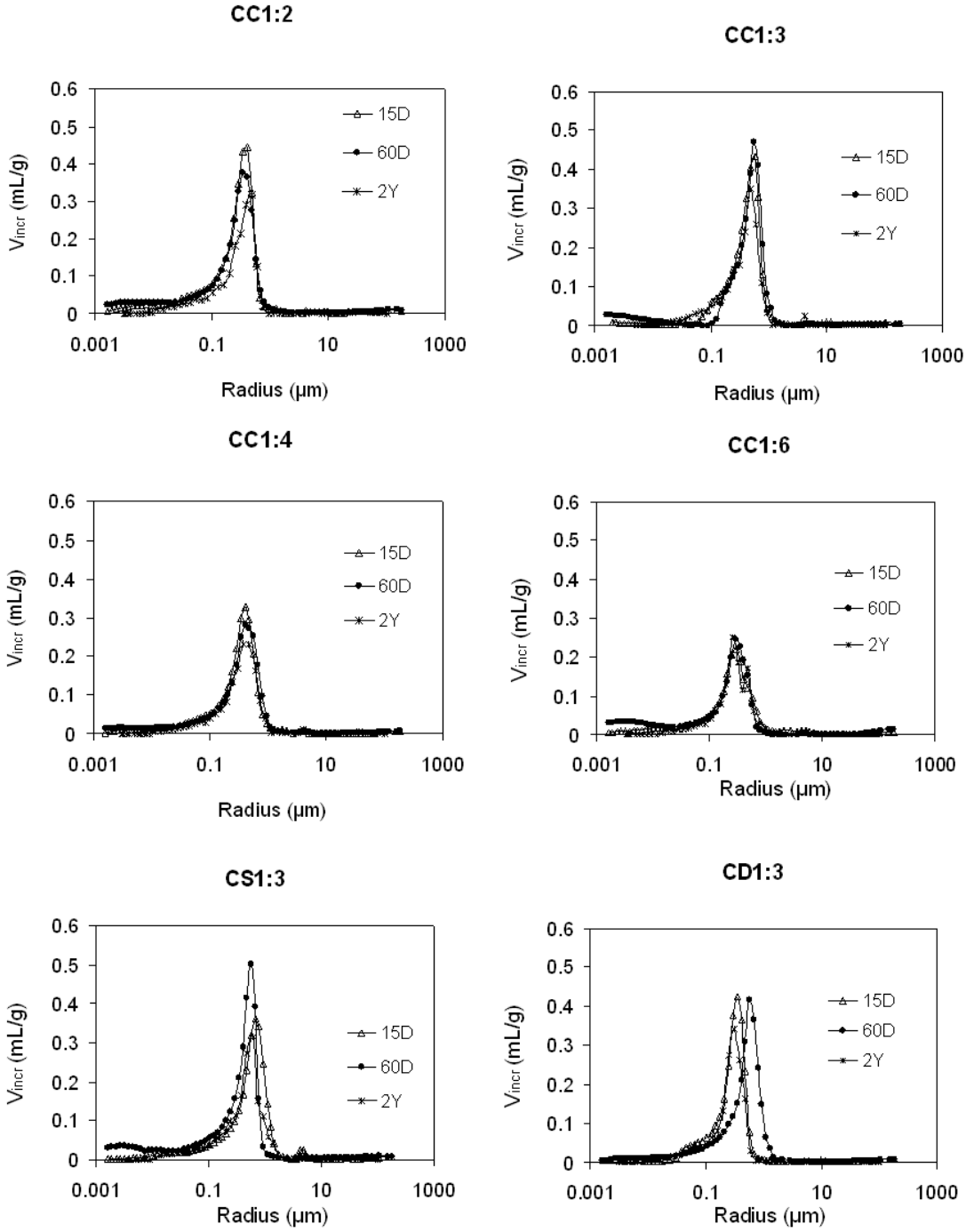

Figure I.4.3 Pores size distribution curves of CC1:2, CC1:3, CC1:4, CC1:6, CD1:3 and CS1:3 (f) mortar samples after 7 days (7D) and 2 years (2Y) since their elaboration.

Apart from porosity, the micro-characteristics of mortars are defined by the form of the mineral phases present in the matrix, namely if they appear in agglomerates or in single particles, as well as their shape and size.

Mortars matrix is mainly characterized by agglomerates of particles, which consist in portlandite crystals and agglomerate, as well as in new

formed calcite crystals (Fig. I.4.4) that occasionally surround the aggregate grains (Figs. I.4.4b and f).

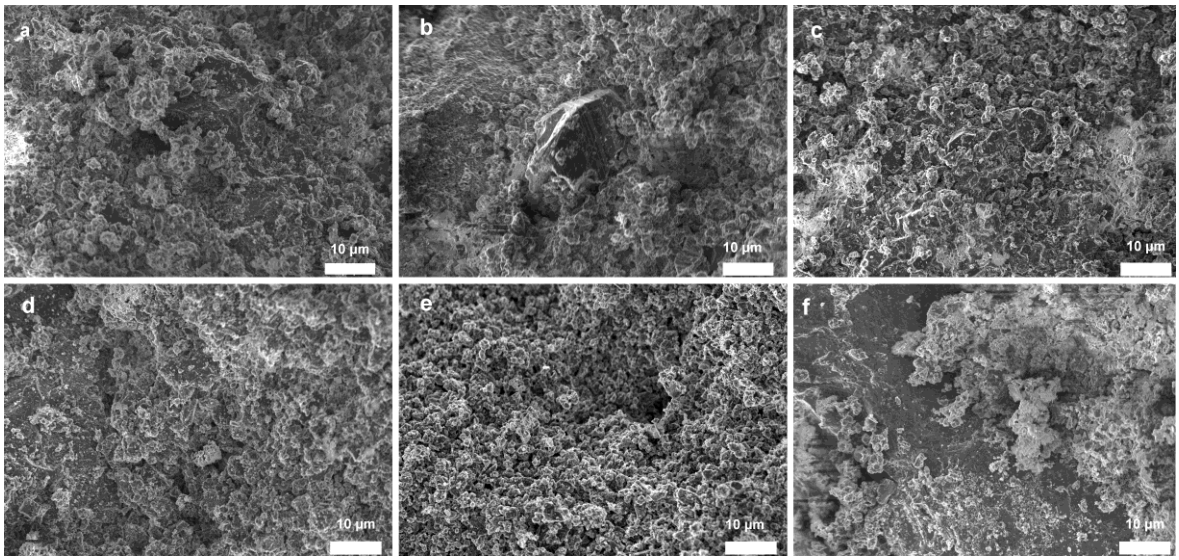

Figure I.4.4 *FESEM images of the mortars after 15 days of carbonation: CC1:2 (a), CC1:3 (b), CC1:4 (c), CC1:6 (d), CD1:3 (e), CS1:3 (f).*

This calcite has precipitated under semi-crystalline or amorphous particles that have maintained the aspect (in form and size) of the original component of the mortars matrix. In fact, there is a similarity between these particles and both the polydisperse aggregates of microsized particles (about 1 µm in size) of the calcitic lime (Fig. I.4.5a), and the finest fraction of the calcareous aggregate (Fig. I.4.5b).

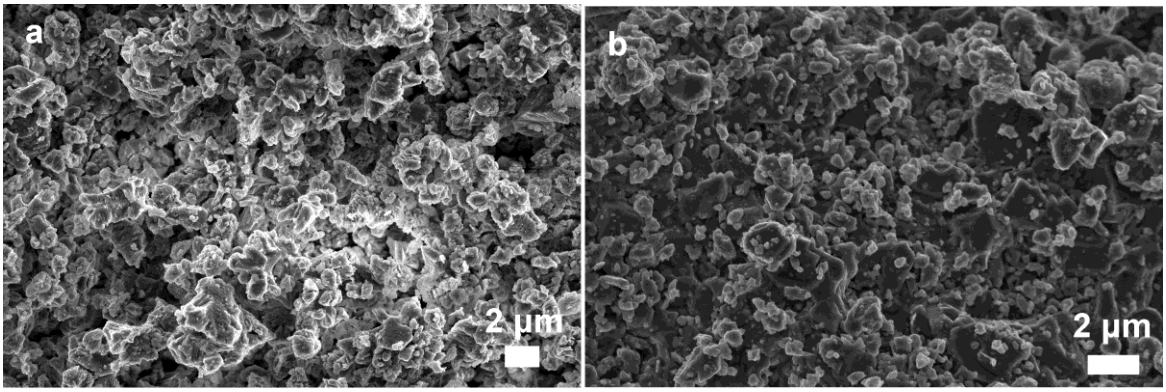

Figure I.4.5 *FESEM images of the calcitic dry hydrated lime (CL) (a) and of the fine fraction of the aggregate (b).*

The precipitation of calcite is especially favoured in nucleation sites of the aggregate when it is characterized by grains with angular shape and rough surface [19], such as the case of the calcareous aggregate. This increases the cohesion in the zone between mortar grains and matrix (interfacial transition zone, ITZ). The optical and electronic observations performed on mortars with aggregates of different mineralogy (CC and CS) agree with this finding. In fact, a worse cohesion was observed in the ITZ of CS1:3 (Fig. I.4.4f), compared to the other mortars prepared with calcareous aggregate (CC and CD). The grains of the siliceous aggregate

have rounded shape and smoothed surface (Fig. I.4.2a) that do not favour the joining with new-formed phases and create a zone of disconnection between sand and matrix. In addition to the grain morphology, the heterogeneous textural properties of CS mortars are provided also by the different mineralogy and hardness of the mineral phases present in the matrix and in the grain (calcite/portlandite and quartz, respectively). On the contrary, in mortars prepared with calcareous aggregate there is a compositional continuity that may enhance the transformation of portlandite into calcite. Therefore, CA morphology favours the nucleation and growth of the new crystals or amorphous agglomerates of calcite, which often recover the surface of the grains (Figs. I.4.4a, c-e).

3.2 Carbonation degree of the mortars samples

Carbonation of aerial lime mortars is a slow process that involves three main steps: 1) CO_2 diffusion within the mortars; 2) $Ca(OH)_2$ and CO_2 dissolution in the pore water; 3) precipitation of $CaCO_3$ [10]. The carbonation degree depends both on curing conditions (RH and T are two controlling factors, [10, 20-21]) and on the microcharacteristics of the mortar system (i.e. porosity). Here, curing conditions were the same for all mortars (*cf.* Section 2.1.), so that any variation in the carbonation degree has to be attributed to the intrinsic properties of mortars.

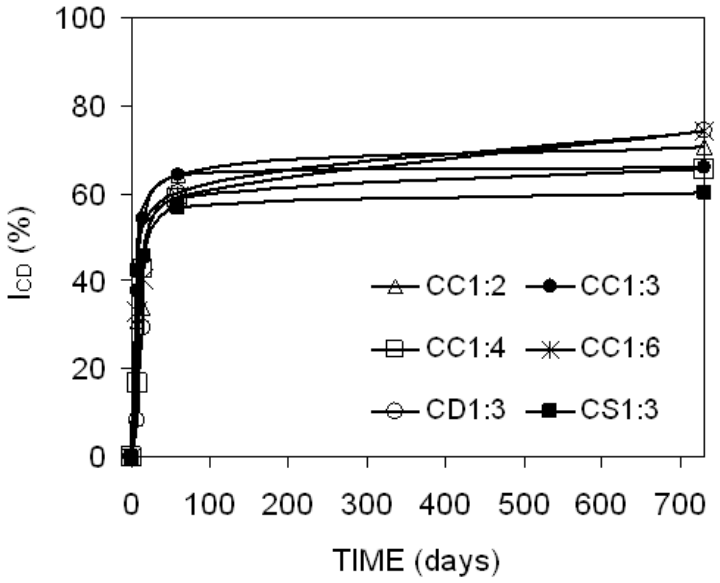

Figure I.4.6 *Carbonation curves of the six mortars. I_{CD} (%) is the carbonation degree index, estimated considering the decrease in portlandite content, which was determined by means of X-ray diffraction quantitative analysis.*

The carbonation curves (Fig. I.4.6) present three slopes: a rapid increase of the carbonation degree index (I_{CD}) during the first month, when about half of the portlandite has turned into calcite; a slower increase of I_{CD} in the second month (60-65%) and a final section in which I_{CD} undergoes to a very slight increase (I_{CD} after 2 years is around 70%). The final values of carbonation degree suggest that among the studied

mortars, those prepared with calcareous aggregate (CC and CD mortars) are the most carbonated whilst CS1:3 is the least carbonated at all time intervals. This result can be linked with the compositional and morphological discontinuities that are present in CS and do not favour carbonation, according to our previous considerations (*cf.* Section 3.2.). Among CC mortars, CC1:6 is the most carbonated one followed by CC1:2, whilst CC1:3 and CC1:4 present the lowest carbonation degree of their group. CD1:3 mortar, which was one of the least carbonated at the beginning of the process, achieves after 2 years the same I_{CD} value than CC1:6.

3.3 Ultrasonic response

3.3.1 Influence of components dosages on ultrasounds

Table I.4.3 shows both the v_p and α_s values measured in mortar samples with different components dosage.

	Time	Mortar name					
	(days)	CC1:2	CC1:3	CC1:4	CC1:6	CD1:3	CS1:3
V_p	15	1255±53	1064±40	1307±57	1492±70	1317±67	1052±43
	28	1512±52	1295±38	1641±54	1795±63	1611±65	1320±43
	60	1693±78	1379±38	1729±44	1873±75	1719±35	1406±32
	730	1898±58	1452±29	1885±60	2090±97	1875±30	1553±35
α_s	15	1.23±0.16	1.43±0.14	1.31±0.16	1.26±0.17	1.13±0.15	1.33±0.09
	28	1.10±0.15	1.32±0.12	1.25±0.17	1.16±0.14	1.00±0.16	1.25±0.05
	60	1.09±0.09	1.19±0.11	1.22±0.23	1.08±0.13	0.97±0.96	1.23±0.10
	730	0.99±0.05	1.17±0.10	1.19±0.07	1.05±0.10	0.99±0.26	1.27±0.10

Table I.4.3 *Average and standard deviation values of v_p (in m/s) and α_s (in dB/mm) measured in the different mortar types studied at 7 days of carbonation.*

Lime mortar can be considered ideally as a two-phase media constituted by an aggregate and a porous matrix. The ultrasonic wave propagation is different in both phases, and the final registered v_p value depends on the particular wave velocity of matrix and aggregate, as well as on the relative volume content of each component in the sample. Differences in both matrix and aggregate velocities (v_p^m and v_p^a, respectively) are due basically to differences in the pore content and, in some cases, in mineralogy, considering constant other parameters such as crystal and pore size.

The final v_p value is proportional to the sum of v_p^m and v_p^a, which correspond to the propagation velocities within the matrix and the aggregate, respectively. According to this, v_p can be expressed as:

$$v_p = v_p^m \cdot \chi^m + v_p^a \cdot \chi^a \qquad [I.4.2]$$

where, χ^m and χ^a are the relative volumes of sample matrix and aggregate, respectively.

According to previous studies [2], the wave velocity increases when calcareous aggregate is added to the lime paste. This increase is higher in mortars with higher sand content. The obtained data in the present work (Tab. I.4.3) seems to corroborate the general trend shown in bibliography. v_p is higher when the aggregate content in the mortar increases, varying from 1255 m/s to 1492 m/s between CC1:2 and CC1:6, respectively (at 15 days since mortar elaboration). However, CC1:3 is an exception in this general trend, since this mortar has a higher aggregate content than CC1:2 but a lower ultrasonic velocity. This finding suggests that the sand content in lime mortars is not the most important factor controlling ultrasonic propagation, as it will be discussed below.

It has been possible to determine measuring it directly on a stone sample of the quarry from which the calcareous aggregate is obtained. This stone is a micritic limestone with very low porosity (<2%). The value of v_p measured in this stone was 6120 m/s.

Taking into account the propagation velocity value obtained for the aggregate (v_p^a), the ultrasonic velocities measured in the mortar samples (Tab. I.4.3) and the relative volumes of matrix and aggregate (χ^m and χ^a) established during the preparation of mortars (Tab. I.4.1), it is possible to know the specific velocity at which the ultrasonic wave propagated through the lime matrix (replacing data in equation I.4.2). For instance, v_p of mortar CC1:2 is 1255 m/s after 15 days since mortar elaboration. Knowing that χ^m and χ^a are 60.4% and 39.6%, respectively, and v_p^a is 6120 m/s, it is possible to calculate de propagation velocity value for the matrix in this mortar. In this case, v_p^m would be -1935 m/s. If these calculations are repeated in every mortar at each age, it will be possible to observe that negative values are always obtained for the propagation velocity of ultrasound through the matrix mortar. These negative values indicate that equation I.4.2 is not valid for the study of mortars, since the propagation velocity of ultrasonic waves cannot be negative. It becomes evident the fact that the aggregate content has a very low influence on the wave propagation through these materials, as it will be discussed in the next subsection.

3.3.2 Acoustic impedances and wave reflection

The low significance of aggregate content on v_p is related to the strong differences between both matrix and aggregate acoustic impedance. This parameter (acoustic impedance, Z) represents the opposition to the flow of sonic wave through a material, and it is dependent on the density of the material in which wave propagates through. Numerically, acoustic impedance is quantified by:

$$Z = \rho \cdot c \qquad [I.4.3]$$

where Z is the characteristic acoustic impedance, ρ is the density of the medium, and c is the ultrasonic wave velocity. When an ultrasonic wave crosses an interface between two media with different acoustic impedance, the wave divides in two components: a transmitted and a reflected wave. The amount of reflected and transmitted wave depends on the impedance of each one of the media, and it is quantified by the reflection coefficient, R:

$$R = \frac{Z_2 - Z_1}{Z_2 + Z_1} = \frac{\rho_2 V_2 - \rho_1 V_1}{\rho_2 V_2 + \rho_1 V_1} \qquad [I.4.4]$$

where Z, ρ and V are the impedance, bulk density and ultrasonic wave velocity of the first and second medium (subscripts 1 and 2, respectively).

The R value varies between -1 and 1. When R<0, the impedance (the ease of wave propagation) of the medium 1 is much higher than Z_2, and consequently, the reflection process is more important than transmission. R = -1 means that the ultrasonic wave is completely reflected and no fraction of the incident wave will be propagated to the second medium. When R >0 a higher wave fraction will be transmitted and a small part will return as reflected wave. R =1 means the complete transmission of the ultrasonic wave.

By analysing the aggregate surroundings in mortars from an acoustic point of view, the aggregate surface constitutes an interface which separates two media with different impedance. The aggregates have an average bulk density of 2.66 g/cm^3 and an average v_p of 6200 m/s, but it is not possible to know exactly the density and the propagation velocity values of the mortar matrix. In order to obtain a critical value of impedance, matrix is considered as an ideal homogeneous material without porosity (unreal conditions). Under these conditions, matrix density is 2.24 g/cm^3 (corresponding to the portlandite density) and is 6750 km/s (propagation velocity through an ideal portlandite crystal). Considering these values, the acoustic impedances of both aggregates and the ideal matrix are 19.77 and 15.12 MPa·s/m, and the reflection coefficient for a wave travelling from the aggregate to the matrix results of -0.13. It means that around the 56.5% of the incident wave is reflected and the transmitted wave is strongly attenuated. This value is a critical (optimum) approximation considering the most favourable conditions for the wave propagation (ideal homogeneous matrix without porosity). However, if more real characteristics are supposed for mortar matrix, such as a matrix bulk density of 1.57 g/cm^3 (considering a matrix porosity of 30%) and a propagation velocity of 2000 m/s (closer to the total mortar v_p), a reflection coefficient of -0.68 is obtained. It means that when ultrasonic waves go from the aggregate to the matrix, 84% of the incident wave is reflected and only a small component of the initial wave is propagated into the matrix.

Taking into account any of both situations (ideal or real matrix characteristics), it is clear that the ultrasonic wave is strongly attenuated and delayed when it travels from aggregates to matrix, and consequently,

the final received signal at the end of the mortar sample corresponds mainly to the wave propagated through the matrix.

At the beginning of Section 3.4.1, a direct relationship between mortar aggregate content and v_p was found. This can seem a contradiction after our previous discussion, in which it is demonstrated that the aggregate has not a significant influence on v_p. Effectively, the connection between mortar dosage and v_p is not due to the aggregate content, but to the initial quantity of water added to the mortar mixture in order to obtain an optimum workability (kneading water). The lower the binder content in the mortar, the lower the kneading water (Tab. I.4.1). Mortars with low kneading water result in samples with less porous matrix, and consequently, they present better characteristics to the wave propagation.

Aggelis and Philippidis [2] observed that the water content has a small impact on pulse velocity concluding that cement paste samples with low w/c specimens exhibit slightly higher pulse velocities. The trend is the same than that observed in this study, but the influence of water content on v_p is much higher in our case. This difference in the importance of the effects of the kneading water on v_p is due to the fact that in cement mortars, the majority of the water is consumed in the hydration process of cement components and the water in excess evaporates producing porosity. On the other hand, hydration processes do not take place in lime mortars and the whole water content evaporates producing a more porous matrix and, consequently, a more important wave delay.

When the relationship between mortar aggregate content and v_p was studied at the beginning of Section 3.4.1, CC1:3 was an exception since this mortar had a higher aggregate content than CC1:2 but a lower ultrasonic velocity. Now it is possible to understand the apparently anomalous behaviour of CC1:3, attending to the amount of kneading water employed in each case. Table I.4.1 shows that CC1:3 is the mortar with the highest content of kneading water (higher than CC1:2 and CC1:4), and consequently, it has the most porous matrix and the worst characteristics to ultrasonic propagation.

3.3.3 Influence of aggregate content and kneading water on spatial attenuation

Values of spatial attenuation are very similar in all mortar types (Tab. I.4.3). However, a small α_s decrease is observed when the aggregate content of mortars increases. This trend is valid for all samples except for CC1:3 in which it was measured a higher wave attenuation than in CC1:2, although CC1:3 has a bigger aggregate content. As discussed above, differences between mortars are not mainly due to aggregate content, but to the water content. Since CC1:3 is the mortar with the highest water content, and consequently with the most porous matrix, it is predictable that it will be the mortar with the highest wave attenuation values.

Ultrasonic waves can be attenuated by several causes, such as absorption in each of the individual phases, visco-inertial losses due to density discrepancies of the constituent materials, thermal dissipation losses, and scattering [22]. Several works demonstrate that scattering is

the most important causes involving wave attenuation in mortars [2-3,23]. Those studies also demonstrate that the aggregate content has a direct relationship with the wave attenuation due to this phenomenon (the higher the aggregate content, the higher the wave attenuation), and a higher w/c (higher porosity) logically gives place to higher values of the attenuation parameter. In the mortars studied in this paper, the effect of one type of inclusions (pores or aggregate) on wave scattering is offset by the effect of the other one, given that CC1:6 is the mortar with the highest aggregate content, the lowest water content, and consequently, the lowest matrix porosity, whilst the samples with the lowest aggregate content (CC1:2 and CC1:3) are mortars with high w/c ratio. The result is that the water content has a slightly bigger influence on the total wave scattering than the aggregate content in mortars with similar α_s.

3.3.4 Influence of aggregate mineralogy and grading on ultrasounds

In order to evaluate the influence of aggregate mineralogy and grading on v_p and α_s three different mortars have been studied (CC1:3, CD1:3 and CS1:3) which have the same dosage (Tab. I.4.1), but different grading (CC1:3 and CD1:3) or aggregate mineralogy (CD1:3 and CS1:3) (*cf.* Section 2.1 for mortars characteristics). Table I.4.3 shows the measured v_p and α_s in these mortars. Aggelis and Philippidis [2] assert that the grains size is very important in wave attenuation. In their study, mortars prepared with coarse sand exhibit much greater attenuation than mortar with fine sand. This result is coherent with the data shown in this paper, where CC1:3 has the highest aggregate sizes and the highest α_s value (1.63 dB/mm). However, CC1:3 has also a higher water content than CD1:3 (i.e. a higher porosity) and consequently it is not possible to distinguish the weight of the effect of both variables on α_s.

With respect to the influence of grading on wave velocity, no evidences have been found about the dependence of v_p and aggregate size. Previous studies [1] do not show any relationship between both variables, and no apparent connection seems to exist between them according to the results obtained in this paper. The v_p increase observed in data (from 772 to 1093 m/s in CC1:3 and CD1:3, respectively) is related to the lower water content of CD1:3, which causes a lower porosity in the matrix.

Another important aspect is the influence of aggregate mineralogy on both v_p and α_s. In this case, CD1:3 and CS1:3 are composed by aggregates with the same grading (discontinuous) and the same dosage, but different mineralogy (calcareous and siliceous, respectively). Differences in both ultrasonic parameters are observed, showing that the siliceous mortar presents the lowest wave velocity and the highest spatial attenuation. Although quartz has a lower ultrasonic P-wave velocity than calcite (6060 m/s and 6650 m/s, respectively, after Schön [1]), which could cause a slower propagation of the wave through the mortar with siliceous aggregate, differences on aggregate mineralogy can not explain significant variations on v_p and α_s due to the fact that ultrasonic wave is strongly attenuated after its propagation through aggregates (*cf.* Section

3.4.1). Consequently, the causes of ultrasonic variations between siliceous and calcitic mortars have to be related to matrix characteristics.

The quantity of initial water added to the mixture is almost the same in both mortars (27 and 26.5 % in CD1:3 and CS1:3, respectively), so the matrix porosity can be considered practically the same, and therefore, it can not explain the differences in ultrasonic behaviour.

However, there is a strong difference in the pores located at the interfacial zone (ITZ, the zone between the matrix and the surface of grains) of the two mortars. As explained in Section 3.1, mortars prepared with calcareous aggregates have a textural continuity between matrix and sand grains, whilst mortars with siliceous aggregate show some porosity developed at the matrix-aggregate contact. These differences in the ITZ can explain the variations observed in the ultrasonic parameters since a higher nucleation of calcite in the matrix surrounding the aggregate grains offers a slightly more continuous interface between aggregate and matrix, thus favouring the ultrasonic propagation and decreasing the proportion of reflected wave. This certain continuity between aggregate and matrix is exclusive of lime mortars with calcite aggregates, whilst the low cohesion at the ITZ found in CS1:3 contributes to increase the wave reflection, getting more difficult the propagation of ultrasonic pulses. This relationship between low-cohesion in the ITZ and increase of the ultrasonic attenuation was also observed by Chekroun et al. [23].

3.3.5 Influence of carbonation degree on ultrasounds

Figure I.4.7 shows the time evolution of both v_p and α_s during the carbonation process. In these graphs it is possible to observe the mechanical improvement of mortars due to the textural and mineralogical changes led by carbonation. All mortars suffer an increase of v_p and a decrease of α_s and they show parallel trends: a rapid v_p increase and α_s decrease during the first 60 days and a quasi no variation of v_p and α_s (respectively) from 60 days to 2 years.

As explained above, two main changes are produced in mortar during the carbonation process: on the one hand, the mineralogical transformation of portlandite into calcite and, on the other hand, the matrix porosity reduction. The first change is responsible for the rapid changes in the ultrasonic response in the first 60 days. It has been found that carbonation degree increases rapidly in the first moments of the mortar life, reaching about the 70% of the total carbonation in only two months.

The transformation of portlandite into calcite leads to important elastic considerations. It is known that the velocity of the ultrasonic wave propagation through minerals depends directly on two elastic constants: C_{11} and C_{44}; this relation is mathematically expressed after equation I.4.5 and I.4.6:

$$v_p = \sqrt{\frac{C_{11}}{\rho}} \qquad [1.4.5]$$

$$v_s = \sqrt{\frac{C_{44}}{\rho}} \qquad [1.4.6]$$

C_{11} in portlandite and calcite is 102 GPa and 144 GPa, respectively (after data published in Speziale et al. [24] for portlandite and Schön [1], for calcite), while C_{44} is 12 GPa and 33.5 GPa. Taking into account that $\rho_{portlandite}$ = 2.24 g/cc and $\rho_{calcite}$ = 2.71 g/cc, the P-wave velocity in a pure crystal of portlandite and calcite will be 6750 m/s and 7290 m/s, respectively. Therefore, the acceleration of P-waves during the first weeks can be completely explained by the carbonation degree of the sample. Moreover, the porosity reduction also contributes to improve the ultrasonic propagation through mortar.

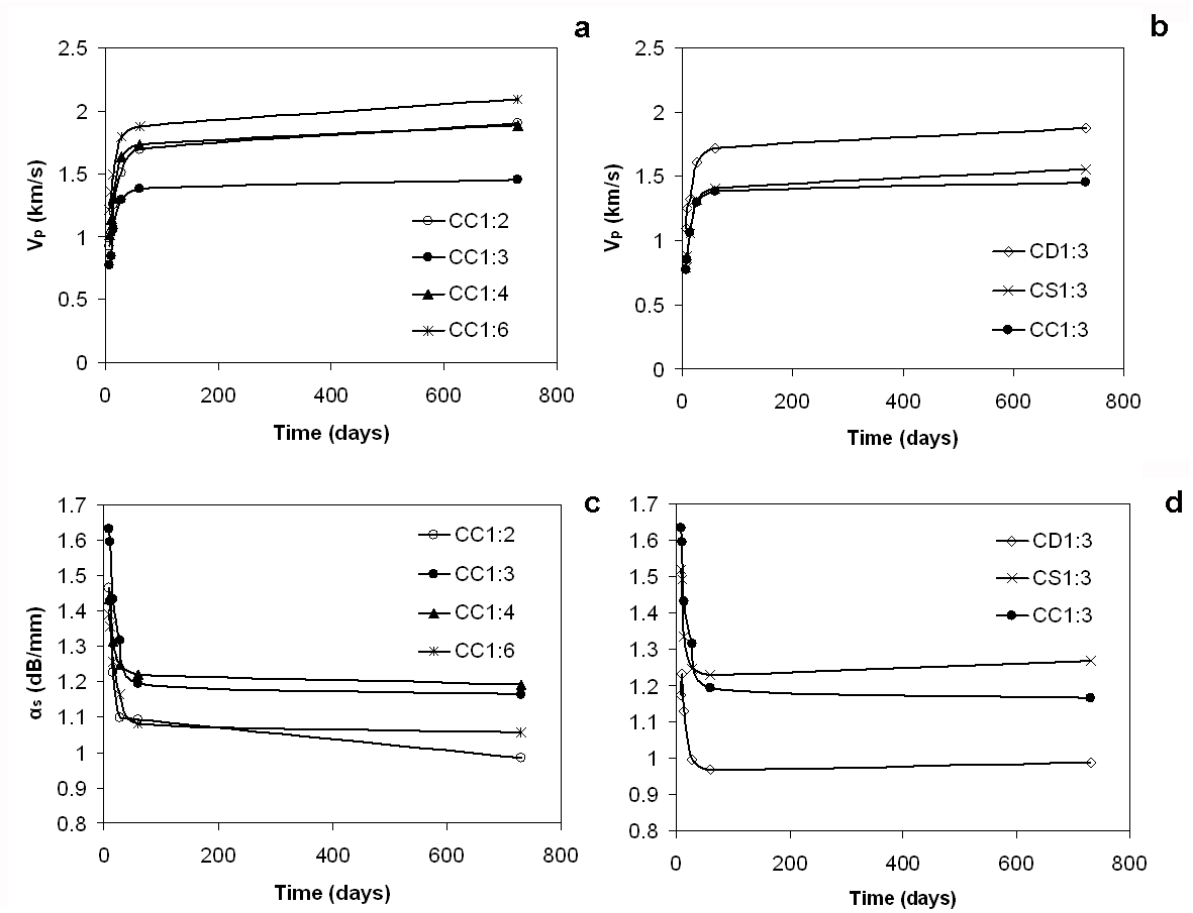

Figure I.4.7 Propagation velocity (V_p) and spatial attenuation (α_s) of ultrasonic waves during the carbonation process.

3.3.6 Quantitative approach to textural influence on ultrasonic propagation

According to previous discussions, ultrasonic wave propagation on lime mortars is mainly influenced by two textural parameters: the porosity of the matrix and the carbonation degree, remaining independent of other aspects such as aggregate mineralogy or grading.

Figure I.4.8 shows the average values of v_p and α_s of each mortar type according to their porosity and their age since preparation (15 days, 60 days or 2 years). Moreover, three additional points are added in the v_p-P_o graph. These points have been calculated from theoretical considerations and correspond to three ideal mortars without porosity (P_o=0%). Propagation velocity at these ideal materials was calculated from the specific velocity of each constituent mineral (6750 m/s and 7290 m/s for porlandite and calcite, respectively) knowing their abundance at different ages after the X-ray diffraction data.

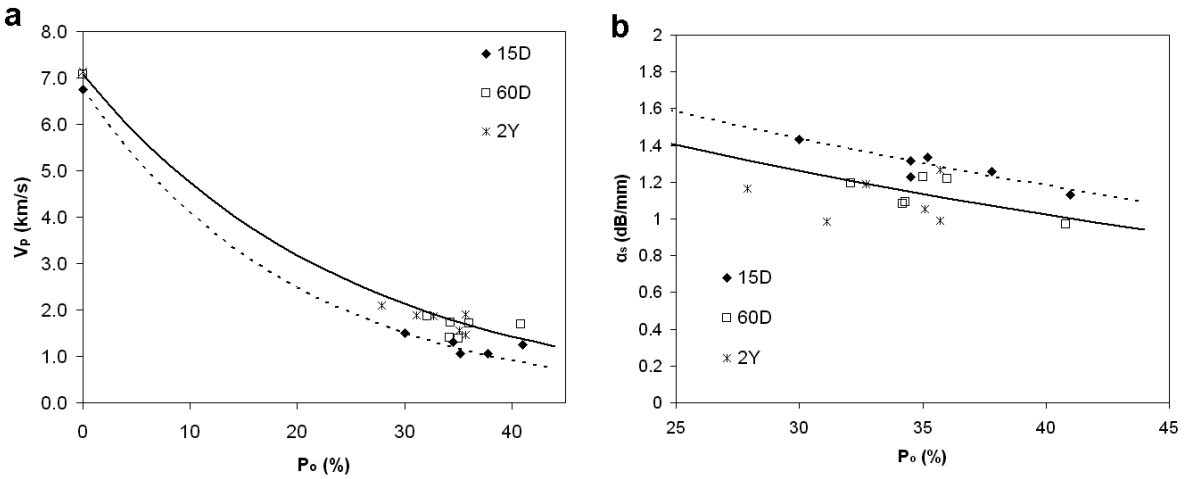

Figure I.4.8 Relationship between porosity, carbonation degree and ultrasonic response, where the open porosity (P_o) is represented as function of the velocity of propagation (v_p) (a) and the spatial attenuation (α_s) (b) of ultrasonic waves. Solid and dot lines represent the exponential (a) and lineal (b) fitting of high and low-carbonated mortars, respectively. Legend: 15D = 15 days; 60D = 60 days; 2Y = 2 years of carbonation.

It has been possible to obtain two line fitting from each graph, finding a numerical relationship between the ultrasonic parameters and both porosity and carbonation degree. Dot lines show the relationship between ultrasonic parameters and porosity for low-carbonated mortars (measures carried out 15 days after mortar preparation). Solid line shows the relationship for high-carbonated mortars. In the case of v_p, measures at 60 days and 2 years fall on the same line, showing a unique trend. In the case of α_s, solid line is fitted only for data at 60 days because values at 2 years appear scattered and no correlation can be established.

We obtained the following empirical equation for v_p, as function of mortar porosity and carbonation degree:

$$v_p = v^m \cdot e^{\frac{-x}{100}(5-\frac{I_{CD}}{100})} \qquad [1.4.7]$$

where x is the porosity (in %) and I_{CD} is the carbonation degree index. v^m is the theoretical velocity obtained from the mineralogical composition of mortar (calculated by X-ray diffraction) and the characteristic ultrasonic

velocity of each constituent mineral. This value (v^m) was obtained by using a second empirical equation:

$$v^m = v_p^p \cdot \chi^p + v_p^c \cdot \chi^c \qquad [1.4.8]$$

where, χ^p and χ^c, v^p and v^c are the relative volumes and specific ultrasonic velocity (respectively) of portlandite and calcite (*p* and *c*, respectively).

A third empirical equation was obtained for α_s, as function of mortar porosity and carbonation degree:

$$\alpha_s = (2.58 - 0.32 I_{CD}) \cdot e^{x\left(\frac{-1.95-0.231 I_{CD}}{100}\right)} \qquad [1.4.9]$$

where x is the porosity (in %) and I_{CD} is the carbonation degree index.

Although these equations are supported by numerous data, it will be necessary to develop a higher amount of tests and measurements in the future in order to confirm the trends and equations obtained in this paper.

4. Conclusions

The aim of this study was to investigate the influence of the textural characteristics of different aerial lime-based mortars on the propagation velocity and the spatial attenuation of P waves. Six types of mortars were studied and divided in two main groups: the first one composed by four mortars of the same composition and different binder-to-aggregate ratios, and the second one constituted by three mortars prepared with the same binder-to sand ratio but different aggregate characteristics. In this second group, two aggregates with different composition (siliceous and calcareous) and grading (continuous and discontinuous) were used for the preparation of mortars. The mineralogical and textural properties of mortars have been studied for two years in order to interpret the ultrasonic response at every interval of time.

Ultrasounds have proved to be a sensitive tool for determining textural characteristics of lime-mortars. Several textural aspects were considered initially as controller factors of the wave propagation through mortars: porosity, binder-to-sand ratio, aggregate mineralogy and grading and carbonation degree of mortars. Finally, only two parameters result to be the most significant for ultrasonic propagation: matrix porosity and carbonation degree.

Textural parameters related to the aggregate (mineralogy, grading and aggregate content) result little influential on wave propagation velocity (v_p) and spatial attenuation (α_s). This fact is due to the strong differences in acoustic impedance between both mortar matrix and aggregates. Aggregates are obtained from a very low-porous limestone (porosity lower than 2%) and considerably high bulk density (around 2.66 g/cm^3). As a result, the propagation velocity of waves through aggregates is high (6200 m/s), and, consequently, its acoustic impedance is high too (around

19.77 Mpa·s/m). On the contrary, mortar matrix has high porosity (~30%), low bulk density and presumably low ultrasonic propagation velocity. The matrix acoustic impedance is estimated at 4 MPa·s/m. This difference between acoustic impedances causes a strong reflectance of the ultrasonic wave when it is propagated from aggregate to matrix (the reflected wave component is estimated at ~80% of the incident wave). Accordingly, the registered wave at the end of the mortar sample corresponds mainly to the front wave propagated through the mortar matrix, and therefore the waveform is a result of the matrix characteristics.

In accordance with previous reasoning, v_p and α_s are a reflection of the porosity and mineralogy of the mortar matrix. The first one is related to the amount of kneading water added during mortar preparation, whilst the second one is dependent on the age of lime mortar. The whole water content evaporates producing pores in the mortar matrix, and, consequently, causing wave delay and scattering. The most porous mortars present the lowest v_p and the highest α_s values. The carbonation process, for its part, causes a mineralogical transformation of the matrix as well as a slight porosity reduction (both factors favour the wave propagation). A high-carbonated matrix (characterized by a high content of calcite) has better elastic characteristics than low-carbonated matrix (with a predominant content of portlandite), and hence, the wave propagation is more favoured in the first one.

Finally, all these results have been integrated in numerical equations that allow assessing the textural characteristics of lime mortars from v_p and α_s measurements.

This study constitutes a useful approximation for the evaluation of lime mortars texture by means of non-destructive tests, which is in many cases a crucial point, such as in the field of Cultural Heritage.

Acknowledgements:

This study was financially supported by Research Group RNM179 of the Junta de Andalucía and by the Research Project MAT2008-06799-C03.

References

[1] Schön JH. Physical properties of rocks: fundamentals and principles of petrophysics. Handbook of geophysical exploration. Section I, Seismic Exploration Vol. 18. Pergamon, New York; 1996.

[2] Aggelis DG, Philippidis TP. Ultrasonic wave dispersion and attenuation in fresh mortar. NDT&E Int 2004; 37:617-31.

[3] Lafhaj Z, Goueygou M. Experimental study on sound and damaged mortar: Variation of ultrasonic parameters with porosity. Constr Build Mater 2009; 23:953-8.

[4] Mishra SR, Kumar S, Park A, Rho J, Losby J, Hoffmeister BK. Ultrasonic characterization of the curing process of PCC fly ash-cement composites. Mater Charact 2003; 50:317-23.

[5] Goueygou M, Lafhaj Z, Soltani F. Assessment of porosity of mortar using ultrasonic Rayleigh waves. NDT&E Int 2009; 42:353-60.
[6] Voigt T, Sun Z, Shah S. Comparison of ultrasonic wave reflection method and maturity method in evaluating early-age compressive strength of mortar. Cem Concr Compos 2006; 28:307-16.
[7] Cazalla O, Sebastián E, Cultrone G, Nechar M, Bagur MG. Three-way ANOVA interaction analysis and ultrasonic testing to evaluate air lime mortars used in cultural heritage conservation projects. Cem Concr Res 1999; 29:1749-52.
[8] Molero M, Segura I, Hernández MG, Izquierdo MAG, Anaya JJ. Characterization of mortar samples using ultrasonic scattering attenuation. Physics Procedia 2010; 3(1):839-45.
[9] Molero M, Segura I, Hernández MG, Izquierdo MAG, Anaya JJ. Ultrasonic wave propagation in cementitious materials: a multiphase approach of a self-consistent multiple scattering model. Ultrasonics 2011; 51(1):71-84.
[10] Moorehead DR. Cementation by the carbonation of hydrated lime. Cem Concr Res 1986; 16:700-8.
[11] Rodriguez-Navarro C, Cazalla O, Elert K, Sebastian E. Liesegang pattern development in carbonating traditional lime mortars. Proc R Soc London 2002; 458:2261-73.
[12] Cazalla O, Rodriguez-Navarro C, Sebastian E, Cultrone G. Aging of lime putty: effects on traditional lime mortar carbonation. J Am Ceram Soc 2000; 83(5):1070-6.
[13] Arandigoyen M, Pérez Bernal JL, Bello López MA, Alvarez JI. Lime-pastes with different kneading water: pore structure and capillary porosity. Appl Surf Sci 2005; 252 :1449-59.
[14] UNE-EN 459-1. Cales para la construcción. Parte 1: Definiciones, especificaciones y criterios de conformidad. AENOR, Madrid; 2002.
[15] UNE-EN 1015-3. Métodos de ensayo de los morteros para albañilería. Parte 3: Determinación de la consistencia del mortero fresco (por la mesa de sacudidas). AENOR, Madrid; 1998.
[16] Martín Ramos JD. XPowder. A software package for powder X-ray diffraction analysis. Lgl. Dep. GR 1001/04; 2004.
[17] Martínez-Martínez J, Benavente D, García-del-Cura MA. Spatial attenuation: The most sensitive ultrasonic parameter for detecting petrographic features and decay processes in carbonate rocks. Eng Geol 2011; 119:84–95.
[18] Cultrone G, Sebastián E, Ortega Huertas M. Forced and natural carbonation of lime-based mortars with and without additives: mineralogical and textural changes. Cem Concr Res 2005; 35:2278-89.
[19] Lanas J, Alvarez-Galindo J. Masonry repair lime-based mortars: factors affecting the mechanical behaviour. Cem Concr Res 2003; 33(11):1867-76.
[20] Van Balen K. Carbonation reaction of lime, kinetics at ambient temperature. Cem Concr Res 2005; 35:647-57.

[21] Houst YF, Wittmann FH. Influence of porosity and water content on the diffusivity of CO2 and O2 through hydrated cement paste. Cem Concr Res 1994; 24(6):1165-76.
[22] Barton N. Rock quality, seismic velocity, attenuation and anisotropy. Balkema Ed., London; 2007.
[23] Chekroun M, Le Marrec L, Abraham O, Durand O, Villain G. Analysis of coherent surface wave dispersion and attenuation for non-destructive testing of concrete. Ultrasonics 2009; 49:743-51.
[24] Speziale S, Reichmann HJ, Schilling FR, Wenk HR, Monteiro PJM. Determination of the elastic constants of portlandite by Brillouin spectroscopy. Cem Concr Res 2008; 38:1148-53.

Chapter I.5

Mechanical evolution of lime mortars during the carbonation process

Arizzi A., Martínez-Martínez J., Cultrone G., Benavente D.
Key Engineering Materials, 465 (2011) 483-486.

Abstract

Lime mortar is one of the most ancient and durable building materials. It is characterized by a slow carbonation during which $Ca(OH)_2$ reacts with CO_2 present in air and forms calcite, giving rise to a stronger and more compact material. This process takes place from the surface to the interior of the material and it is strongly affected by the reaction conditions. The aim of this study is to quantify the increase in strength and elasticity of different lime mortars according to their carbonation degree. For that, six types of mortars were elaborated, with different lime/aggregate proportions and aggregate mineralogy and grading. Mineralogical and textural studies were carried out to follow the carbonation process. Each mortar was tested in a uniaxial compression press after 15, 28, 60 days from the elaboration. In order to differentiate the mechanical behaviour of the external and internal parts of the mortars, two micro-samples (10×10×10 mm) were obtained from the first 10 mm and from the core of each prism. Results show that an increase in strength and especially in the elastic modulus is associated to the carbonation process, but it is different depending on the composition and compactness of the mortars.

1. Introduction

The mechanical resistance of lime mortars is strictly related with their carbonation degree, which represents the quantity of portlandite ($Ca(OH)_2$) transformed into calcite ($CaCO_3$). This transformation ($Ca(OH)_2 + CO_2 \rightarrow CaCO_3$) depends on CO_2 permeability, temperature and humidity, as well as on the textural characteristics of the mortar [1-3]. In turns, the microstructure of mortars strongly depends on the elaboration and curing conditions, so that a correct choice of components and mixing proportions is essential to ensure good final performances. The aim of this work was to link the microstructure of six different types of mortars with their mechanical properties during early carbonation ages (7, 15 and 60 days). For that, micro-compressive essays were performed on micro-samples of each mortar and their behaviour was related to the textural properties studied at the same time intervals.

2. Materials and methods

Six types of mortars were prepared with a calcitic dry hydrated lime (CL90-S, UNE-EN 459-1) whose components and mixing proportions are shown in Table I.5.1. Two types of aggregates were used, a calcitic one with continuous (CA, $0.063<\varphi<1.5$ mm) and dicontinuous grading (CDA, $0.1<\varphi<0.8$ mm), and a siliceous one, with a discontinuous grading (SA, $0.1<\varphi<0.5$ mm). After their preparation, mortars were left during 7 days in normalized steel moulds (4×4×12 cm) at HR = 60±5% y T = 20±5°C and after desmoulding, they were cutted in prisms of 4×4×5 cm. Two micro-samples (10×10×10 mm) were obtained from the first 10 mm and from the core of each mortar prism. The observation of the mortars microstructure (morphology, cohesion, porosity) was carried out by means of *optical microscopy (OM)* (Olympus BX-60) equipped with digital microphotography camera (Olympus DP10). *X-ray diffraction* analyses *(XRD)* were performed in order to identify and quantify the mineralogical phases, by means of a Philips PW-1710 diffractometer. The interpretation of diffractograms was carried out using "X-Powder" software package [4]. Open porosity (P_o, %) and pore size distribution (PSD) were determined using a Micrometics Autopore III 9410 porosimeter (*MIP analysis*).

In order to study the mechanical characteristics of each type of mortar and their evolution during the carbonation process, the whole micro-samples (above described) were tested in an *uniaxial compression press*. This press (Instron 4411) can achieve a maximum load of 5000 kN and a constant load velocity of 0.1 MPa/s was selected for this test. The stress-strain curve was recorded and strength and Young modulus were calculated for each sample.

Mortar name	Time [days]	Aggregate	B/S	W/T [%]	P_{tot} [%]	Strength [MPa]		Young modulus [MPa]	
						Ext.	Int.	Ext.	Int.
CC1:2	7	CA	1/2	29.5	38.22	-	-	-	-
	15				40.96	1.12	0.83	199.32	182.77
	28				-	1.53	1.08	514.29	269.75
	60				40.84	1.67	0.89	815.01	-
CC1:3	7	CA	1/3	31.3	39.87	-	-	-	-
	15				35.18	0.82	1.01	32.45	251.46
	28				-	0.97	0.98	330.41	218.09
	60				35.03	1.13	0.85	501.23	192.91
CC1:4	7	CA	1/4	24.0	33.64	-	-	-	-
	15				34.50	1.16	1.035	173.91	179.98
	28				-	1.04	1.05	239.66	127.93
	60				34.30	1.56	0.94	623.71	147.59
CC1:6	7	CA	1/6	20.0	29.51	-	-	-	-
	15				30.04	0.93	1.10	296.43	154.86
	28				-	1.15	0.91	378.38	112.07
	60				32.12	1.34	1.11	568.82	178.52
CD1:3	7	CDA	1/3	26.5	35.41	-	-	-	´-
	15				34.50	1.12	1.41	343.14	778.85
	28				-	1.33	1.18	680.98	310.32
	60				36.03	1.60	-	803.80	-
CS1:3	7	SA	1/3	27.0	36.77	-	-	-	-
	15				37.82	0.62	0.68	96.67	99.05
	28				-	0.99	0.93	108.49	105.10
	60				34.25	1.05	0.95	373.36	192.10

Table I.5.1 *Sketch of the six types of mortars studied in this work. Several information is showed from each one: aggregate used (CA: calcite aggregate with continuous grading; SA: siliceous aggregate with discontinuous grading; CDA: calcite aggregate with discontinuous grading); binder/sand ratio (B/S, by weight); the amount of water employed in the mass (W/T, expressed in % of the total mass); open porosity (P_o) at 7, 15 and 60 days after mortar preparation; mechanical properties (strength and elastic modulus) of micro-samples obtained from the inner and external part of prisms (Internal and External, respectively).*

3. Results and discussion

The main difference between the textures of each mortar is based on the porosity percentage (Tab. I.5.1) and predominant pore types. Porosity appears in different forms: 1) as shrinkage fissures (present in the matrix and in the interfacial zone (ITZ: surface between the matrix and the grains); 2) as rounded and big pores typical of water evaporation; 3) as interparticle porosity, especially along the exfoliation planes of calcite.

Mortars with the same binder/sand (B/S) ratio (CC1:3, CS1:3 and CD1:3) present similar total porosity value (Tab. I.5.1). However, an important difference between these three mortar types was observed in CS1:3. These three varieties present a good cohesion in the matrix. However, the ITZ in the mortar prepared with siliceous aggregates (CS1:3) shows frequently a dishomogeneous contact (shrinkage fissuration processes).

The highest value of P_o was found in CC1:2, because of the high shrinkage caused by the big amount of lime. By means of OM, shrinkage fissures and big pores (Fig. I.5.1) were observed in CC1:2 and CC1:3, although in lower quantity and smaller size in the latter.

In CS1:3, CC1:2, and partially in CC1:4, rounded and big pores (r>100μm) are observed, due to a rapid water evaporation. CC1:6 mortars present the lowest porosity, because of the lowest B/S ratio and the least amount of water added for their preparation.

The carbonation curves (Fig.I.5.2) show that mortars prepared using calcitic aggregate with continuous grading are the most carbonated ones. Carbonation degree of mortars was estimated considering the decrease in portlandite content, determined by means of X-ray diffraction quantitative analysis. CC1:3 is the most carbonated mortar almost at every time intervals, while its analogous containing siliceous aggregate (CS1:3) presents at the end of the study the least quantity of portlandite transformed into calcite.

In table I.5.1 it is possible to observe the mechanical properties (strength and elastic modulus) of each mortar type, as well as its evolution during the carbonation process. Some interesting results are obtained from these data. External micro-samples (from the first 10 mm of the prism) have always higher strength and Young modulus values at 60 days than at 15 days. Moreover, the values at 60 days obtained in the external micro-samples are always higher than those measured on the internal ones. This is due to the fact that the carbonation process takes place from the surface to the interior of the mortar prisms. Consequently, the external micro-samples will contain progressively more calcite in their matrix from 7 to 60 days. The micro-samples obtained in the prism core, however, contain similar calcite content in every step (there is not strength increase).

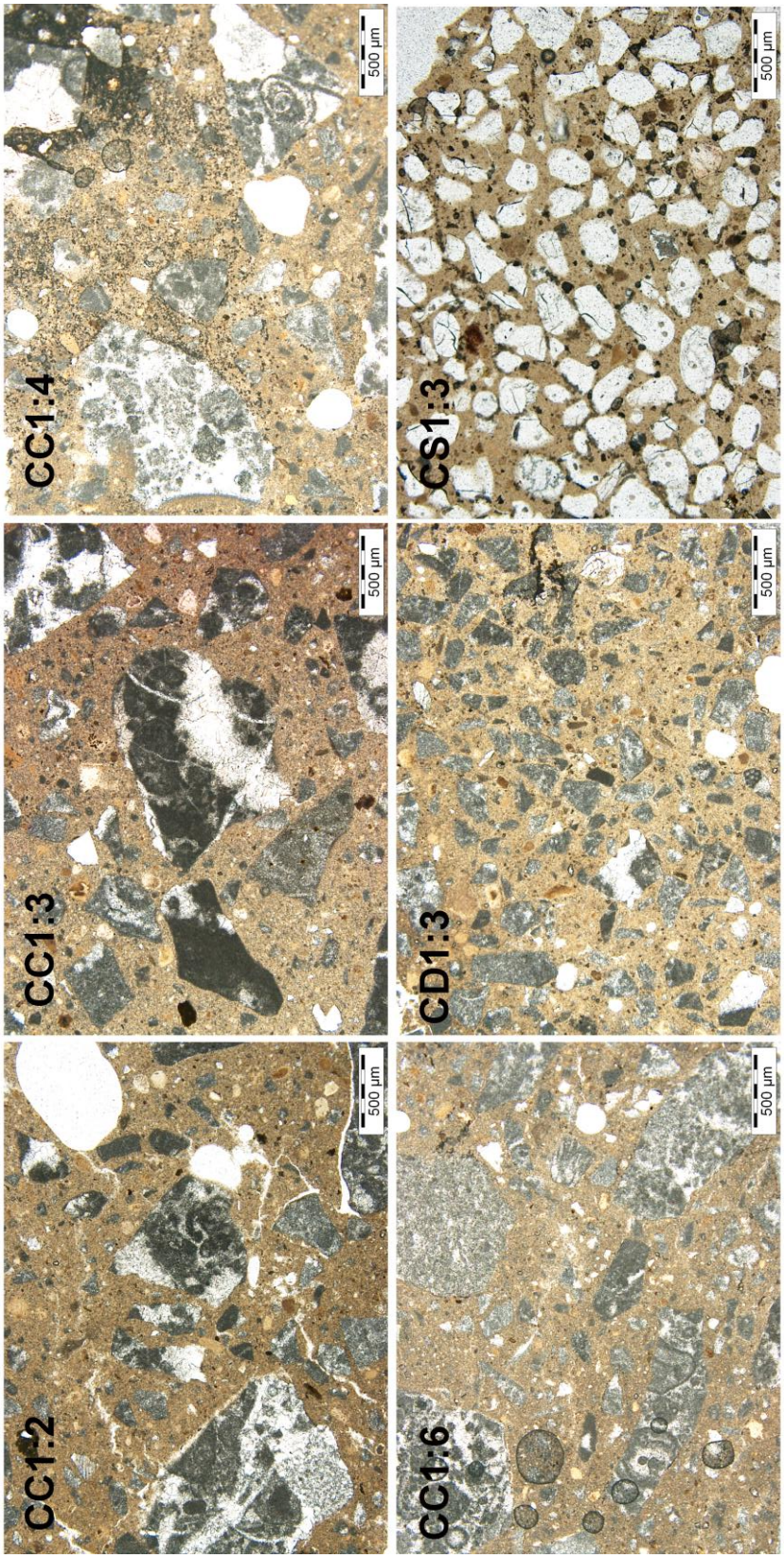

Figure I.5.1 *OM images of all the mortars at 7 days since the elaboration. Images were taken at same magnification with plane polarized Nicols.*

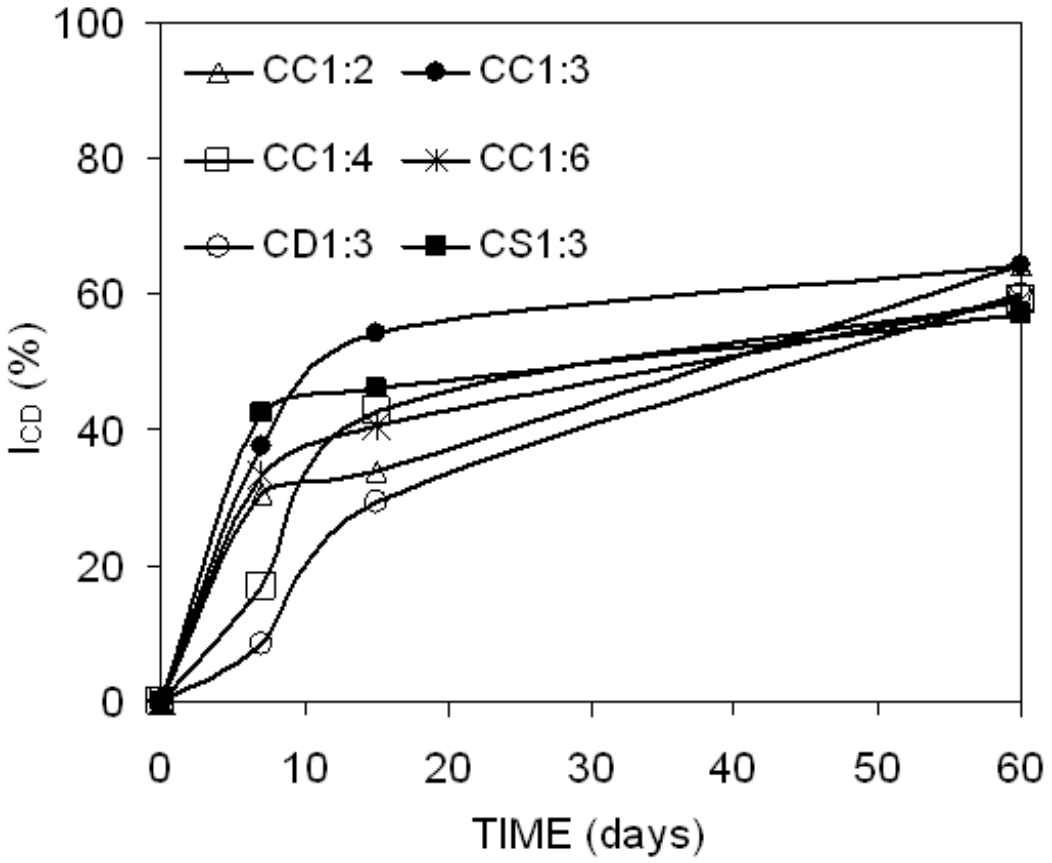

Figure I.5.2 Representation of the carbonation trend in mortar types. I_{CD} (%) *represents the carbonation degree, estimated considering the decrease in portlandite content, determined by means of X-ray diffraction quantitative analysis.*

In addition to the carbonation process, changes in the porous system of the mortar are caused by water evaporation. In general, mortars present a very open structure and high porosity values (between 30 and 40%). These textures involve a very low strength (lower than 2% in every case). Porosity changes during the curing process do not involve significant variations in the mechanical properties of mortars with calcite aggregate. However, mortar CS1:3 (with siliceous aggregate) present both the lowest strength and elastic modulus. This mortar presents shrinkage fissures in the grain-matrix contact surface, making easy the fissure nucleation and its propagation. Moreover, the lowest carbonation degree at 60 days corresponds to this mortar.

Finally, strength and Young modulus of CC1:2, CC1:3, CC1:4 and CC1:6 are defined between the same limits during the whole process. However, CD1:3 presents values of strenght and Young modulus a bit higher with respect to the compositionally similar mortars. Although the only difference between CD1:3 and CC1:3 stays in the grading of the aggregate, the higher value of strength can not be attributed to this factor, because continuous grading always produces more resistant

mortars. The strenght of CC1:3 is lower because the porosity of this mortar is much higher than that of CD1:3. On the other hand, the lowest value of porosity, obtained in CC1:6, does not correspond to the highest resistance. In this case the reason stays in the low amount of lime of this mortar, which produces less compact and resistant matrix.

4. Conclusions

This study confirms that the carbonation process affects positively the mechanical properties of mortars, by producing an increase of strength of these materials, always higher in the external zone that is the most carbonated one. It has been found that the use of calcareous aggregates give place to more carbonated and resistant calcite lime mortars.

Among the six types of mortars studied in this work, CC1:3 showed the highest carbonation degree and one of the highest values of resistance and elastic modulus.

On the other hand, we found that the use of a siliceous aggregate gives place to weaker mortars, in spite of the higher hardness of quartz compared to calcite. The reason of that stays in the insufficient cohesion between the grains of quartz and the matrix.

Acknowledgments

This study was financially supported by Research Group RNM 179 of the Junta de Andalucía and by Reseacrh Project MAT 2008-06799-C03-03.

References

[1] K. Van Balen. Cem. Concr. Res. 35 (2005), p. 647-657.
[2] Y.F. Houst, F.H. Wittmann. Cem. Concr. Res. 24, 6 (1994), p. 1165-1176.
[3] D.R. Moorehead. Cem. Concr. Res. 16 (1986), p. 700-708.
[4] J.D. Martín Ramos. Lgl. Dep. GR 1001/04 (2004).

Concluding Remarks

A deep knowledge of the microstructure of limes, the textural characteristics of aggregates, the mineralogical, textural and physical-mechanical properties of mortars has been achieved in this part of the thesis.

In particular, it has been found that the dry hydrated dolomitic lime confers a more pronounced plasticity to the lime paste than the corresponding calcitic one. This difference in the behaviour between the two limes in suspension is strictly related to their micro- and nanostructure. This study suggests that more workable lime mortars are obtained with the dolomitic lime (*chapter I.1*). Thereby, it is reasonable to think that the dolomitic lime mortars might show also greater performances during hardening to the calcitic ones.

However, the study of the properties of calcitic and dolomitic lime mortars during hardening shows contrasting results regarding the preference of the lime (*chapter I.2*). In fact, even if the dolomitic lime mortars actually show higher workability in the fresh state, they do not maintain the predominance on the calcitic lime mortars during hardening. Moreover, the characteristics of the pore system and the fragility of the dolomitic mortars studied indicate a higher susceptibility to weathering compared to the calcitic lime mortars. The main reason of these contrasts may rise from the curing conditions to which mortars are exposed. Here, dry conditions (T=20 ºC; RH = 60%) have been considered, since the prime objective of this thesis is to design rendering mortars that can be applied in dry or low-moist zones. In accordance with this objective, the calcitic lime is maintained to the detriment of the dolomitic one. Otherwise, the use of dolomitic lime mortars in high-moist zones should not been dismissed.

The researches focused on monitoring the carbonation process have been carried out for a total of two years since mortars elaboration (*chapters I.3* and *I.4*). In agreement with the majority of the studies on carbonation, it has been confirmed that the transformation of portlandite into calcite is a very slow process in aerial lime-based mortars. Our results have shown that carbonation occurs mainly in the first two months of mortars life, after which it continues at a much lower rate.

Three related parameters have been successfully used to qualify and quantify carbonation over time: the carbonation degree index (I_{CD}) (*chapters I.3* and *I.4*) and the propagation velocity (V_p) and spatial attenuation (α_s) of ultrasonic waves through mortars (*chapter I.4*). In particular, a direct correlation has been observed between I_{CD} and V_p values, since the latter reflects changes of the mineralogy in mortars (*chapter I.4*).

Interestingly, another factor that influences both ultrasonic and mechanical parameters is the mortars pore system that, in turn, is mainly

influenced by the initial water dosage (*chapter I.4* and *I.5*). This finding establishes the first step for the textural characterization of mortars by means of non- and low-destructive techniques, such as ultrasounds and mini-compression tests.

Absolutely concordant results have been obtained from different studies (*chapters I.2*, *I.3*, *I.4* and *I.5*) as regards to the selection of a calcareous or a siliceous aggregate. From here onwards, the preference is given to the calcareous one, which gives place to higher carbonation degree, better cohesion at the matrix-grain interface and bigger compactness and resistances, because of the similarity in composition and texture between the mortar components when a calcareous aggregate is used.

Given that no direct relationships has been found between the aggregate content and the parameters studied in this part of the thesis, the selection of the optimal binder-to-aggregate proportions will be still tackled in the following chapters.

PART II

Standardized and non-standardized methods: a study of their adaptability to aerial lime-based mortars.

Objectives

Considering the influence that the initial water dosage has shown to exercise on the performances of mortars during hardening, and the uncertainty that still exists about the optimal binder-to-aggregate ratios, further researches needed to be carried out in order to assess an adequate method for the preparation of mortars with the minimal porosity and the most suitable aggregate proportions.

The second part of the thesis claims to highlight the importance of choosing the correct ratios during the preparation of any type of mortars. With this objective, *chapter II.1* makes a little digression on some of the most used methods of determining the consistence and packing density of granular mixtures, aspects that are strictly related to the water dosage.

Chapter II.1 also stresses the fact that standardized methods originally developed for cement mortars are often unsuitable for lime mortars. From this, the need of adopting new and non-standardized methods that might adapt better to this kind of materials.

Chapter II.1

A comparison of different methods of determining the packing density of fresh granular mixtures: the failure of their application to aerial lime-based mortars

Arizzi A., Cultrone G.
Submitted to *Cement and Concrete Composites*
(under review)

Abstract

Packing density is considered one of the most influential factors on the performances of fresh mortar and concrete. Standardized methods exist for both direct and indirect determination, but in most cases they do not give a realistic estimation of the voids content. In this work, the recently developed "wet packing method" has been used to assess the optimum water-to-binder ratio at which the packing density is achieved in lime mortars with different binder-to-aggregate proportions. To support the validity of this method, data have been compared with those obtained by measuring the bulk density of the dry granular components, with and without vibration applied, and the consistence of the pastes by means of the flowability test. Then, to verify the reliability of the "wet packing method", i.e. to test out if mortars prepared with this method have good properties once hardened, their mineralogical, textural and mechanical properties have been studied after two and six months of carbonation. Results showed that although the wet packing method seems to be more realistic than the majority of standards used for the determination of the voids content and the achievement of the optimum workability in granular mixtures, it is still not the most adequate for the elaboration of aerial lime mortars with good performances in the fresh and hardened state.

1. Introduction

The packing density (φ) of a mixture, which represents the solid volume in a unit total volume [1], is influenced by the random arrangement of the particles and, in turn, depends on particle shape and size distribution. The dependence on the latter parameter is evident in the case of a broad particle size distribution, in which the smaller particles fill up the voids between the coarser ones, thus increasing the value of maximum packing. The influence of particle shape is widely recognized by several studies [2-4], which demonstrate that different values of packing are obtained when spheres, ellipsoids or oblate ellipsoids are used.

In a mortar where a high density is achieved, all components (i.e. binder plus aggregate) are densely packed, and the number of voids between them is reduced compared to less densely packed mixtures. This minimal porosity is saturated by a minimum water dosage. The excess water (i.e. amount of water theoretically free in the mixture) allows the mobility of particles, thus influencing the flow of the mixture. On the other hand, if the water in excess is too high, the shrinkage during drying will be too great and the strength of the hardened mortar will decrease significantly. To design good mortars and concretes, it is fundamental to determine the water-to-binder ratio (W/B) at which the optimum workability is achieved by estimating the maximum packing density of these mixtures. Several theories and models have been created to identify the most suitable aggregate packing for concrete [1, 5-7]. The reduction of voids with consequent improvement of the workability of a mixture can be achieved also adding plasticisers (or superplasticisers) to the mixture that induce a high degree of particles dispersion [8-9].

The value of packing density (φ_{dry}) of individual components has been estimated in the past by measuring the bulk density of the dry materials (i.e. lime, cement, aggregates). This value is determined as:

$$\varphi_{dry} = \frac{\rho_b}{\rho_s} \qquad \text{[II.1.1]}$$

where ρ_b and ρ_s represent the bulk and the solid densities of the granular component, respectively. The voids index (u) of the dry component is:

$$u = \frac{\pi}{\varphi_{dry}} \qquad \text{[II.1.2]}$$

in which π is the porosity, calculated as: $1-\varphi_{dry}$. The dry method not only depends very much on the state of compaction, but also tends to overestimate the void content and underestimate the packing density of fine particles [10].

In the case of a mixture with a cementitious material and an aggregate, indirect and standardized methods exist for the determination of the void content in terms of the amount of water needed to form a paste with a certain consistency (i.e. flow tests, penetration depth of a

plunger). These methods assume there is a minimum amount of water for the formation of a paste in which the void content is also minimized, and the water volume can be considered as the porosity of the dry packing [1]. However, some problems are correlated with the water content needed to saturate the voids and the air content of the paste, therefore, the methods mentioned above for determining packing density of finer particles are neither precise nor realistic. To counter these inconveniences, Wong and Kwan [10] proposed another method to determine the maximum packing by estimating the solid concentration of the wet mixture instead of the packing density of the dry one. The solid concentration obviously depends on the amount of water added, and, for this reason, it does not coincide with the packing density. According to these authors [10], a minimum amount of water produces a mixture with a maximum solid concentration, which corresponds to the packing density. The wet packing method was demonstrated to be valid not only for cementitious materials, but also for fine aggregates and mixtures of both [10-12]. According to this method, the solid concentration (φ) of a mortar is determined as:

$$\varphi = \frac{\frac{M}{V}}{\rho_w u_w + \rho_\alpha R_\alpha + \rho_\beta R_\beta + \rho_s R_s} \qquad \text{[II.1.3]}$$

where M/V represents the wet bulk density of the paste; α and β are two different cementitious materials; s is the aggregate; ρ_w is the density of the water; ρ_α, ρ_β, and ρs are the solid densities of α, β, and s; u_w is the W/B ratio by volume; and R_α, R_β, and R_s are the volumetric ratios to the granular material. In mortars where only a binder is present, ρ_β and R_β values in the equation II.1.3 are equal to zero. By applying this equation to the suspensions prepared with different dosages of water, a maximum value of φ is obtained, which corresponds to the packing density of the mixture [13].

The voids content, indicating the porosity (ε) of the wet mixture, is calculated as:

$$\varepsilon = \frac{u}{1+u} \qquad \text{[II.1.4]}$$

where u is the void ratio, estimated by means of the following formula:

$$\varphi = 1-\varepsilon = \frac{1}{1+u} \qquad \text{[II.1.5]}$$

A minimum value of voids ratio is obtained by plotting u against u_w, and it corresponds to the basic water ratio (u_{wmin}) [10], which is the water content necessary to fill up the voids.

The objective of this work is to establish the optimum W/B ratio at which the packing density is achieved in mortars of calcitic lime and calcareous aggregate mixed with different binder-to-aggregate ratios, in order to obtain fresh mixtures with good workability, without the use of any plasticizers. Since other authors [11-12] have already adopted the

wet packing method as a successful way to fix the packing density of granular mixtures, its validity is proved in this work and compared with other methods, such as the determination of the bulk density of the dry granular components and the consistence of the fresh mixtures by means of the flow test. The reliability of this method is then verified by studying the mineralogical, textural and mechanical properties of the mortars, once hardened.

2. Materials and methods

Components used in this study were a calcareous aggregate (CA), with a continuous grading between 0.063 and 1.5 mm in size, and a calcitic lime (CL), which is a standardized CL90-S [14].

Packing density of single components (φ_{dry}) was measured by means of the dry method (Eq. II.1.1). Pycnometer analysis was performed to measure the solid (or particle) density (ρ_s, gr/cm^3) of lime and aggregate. Measurements have been carried out following the ASTM D854-92 standard [15]; pycnometers have been calibrated and filled with white spirit. Dry bulk density (ρ_b, gr/cm^3) of components was determined by simple pouring, with and without vibration applied. The vibration was led at an amplitude of 0.3 mm during 300 s; the value of dry bulk density obtained after vibrating was indicated as ρ_b^* (gr/cm^3).

Regarding the determination of mortars packing density, four types of mortars were differentiated according to their binder-to-aggregate ratio by volume (B/A): CC1:1, CC1:2, CC1:3, and CC1:4. Six mixtures of each mortar were prepared, maintaining the fixed B/A ratio and changing the water content. Solid concentration and the void ratio of every mixture were calculated by applying Eqs. II.1.3, II.1.4, and II.1.5. Values of minimum (or basic) water content, corresponding to the maximum solid concentration and to the minimum void ratio, were used for the preparation of mortars whose flow was determined with the flow test [16].

After their preparation, mortars were left for 7 days in normalized steel moulds (4×4×16 cm) at T = 20±5°C and HR = 60±5% and after desmoulding, they were maintained under the same conditions for six months in total.

After two months, X-ray diffraction analyses (XRD) were performed in order to identify and quantify portlandite and calcite, by means of a Panalytical X'Pert PRO MPD, with automatic loader; analysis conditions were: radiation CuKα (λ=1.5405 Å), 4 to 70 º2θ explored area, 45 kV voltage, 40 mA current intensity and goniometer speed using a Si-detector X'Celerator of 0.01 2θ/s. At the same time, the carbonation degree index (I_{CD}, in %) of mortars was estimated by measuring the decrease in the portlandite content, according to the equation:

$$I_{CD} = \frac{CH_0 - CH_x}{CH_0} \times 100 \qquad \text{[II.1.6]}$$

where CH_x is the amount of portlandite at time x and CH_0 is the initial content of portlandite (at time 0). The interpretation of diffractograms was carried out using "X-Powder" software package [17].

At the same interval of time, open porosity (P_o, %) and pore size distribution (PSD) were determined using a Micrometics Autopore III 9410 porosimeter (MIP analysis) with a maximum injection pressure of 414 MPa. Three measurements were performed on mortar fragments of ca. 2 cm^3, which were oven-dried for 24 h at 60 ºC before the analysis.

Values of carbonation degree and porosity were obtained both in internal and external samples of mortars (1 cm from the core to the surface).

Six months of carbonation were considered the most adequate period of time for measuring the mechanical resistance developed by mortars. Flexural and compressive strength were measured by means of a hydraulic press INCOTECNIC-Matest. According to the UNE-EN 1015-11 [18] standard, flexural assays were carried out on three samples per mortar (of 4×4×16 cm). The six samples obtained after the flexural rupture were used for the compressive assays.

3. Results and discussion

3.1 Packing density of the dry materials and their suspensions

As shown in Table II.1.1, values of packing density obtained for the dry materials change depending on their preparation procedure (with and without compaction). In fact, when the powder is simply poured into the container without any forces applied to it, the quantity of voids (indicated in Table II.1.1 as porosity, π) is bigger because particles cannot arrange in a more dense system. Vibration causes a reduction of porosity with a consequent increase of packing, which is much bigger in the case of CA, characterized by a continuous grading in which the smaller particles can easily move and set between the coarser ones.

Sample	ρ_s	ρ_b	ρ^*_b	φ_{dry}	φ_{dry}*	π	π*	u	u*
CL	2.421	0.496	0.611	0.205	0.253	0.795	0.747	3.877	2.959
CA	2.550	1.514	1.831	0.594	0.719	0.406	0.281	0.682	0.390

Table II.1.1 *Values of solid density (ρ_s, in g/cm^3), bulk density (ρ_b, in g/cm^3), packing density (φ_{dry}), porosity (π) and voids ratio (u) of the dry granular components CL (calcitic lime) and CA (calcareous aggregate). * is referred to the values obtained when vibration was applied.*

Another factor causes an error in the estimation of the packing density of dry fine powders: the calcitic lime is formed by micro- and nanoparticles that agglomerate due to the interparticle forces acting on them [19]. When water is added, repulsion forces between charged portlandite crystals cause the agglomerates to disperse [20], and particles rearrange into a denser system, achieving a higher packing density in

suspension. As shown in Table II.2.2, φ_{max} of CL suspensions is about three times higher than the value of packing density found in the dry powder. In the case of the calcareous aggregate, a similar increase of packing density was registered, although the value was only 1.5 times higher than that measured for the dry aggregate. This is because in CA only 19% of the total aggregate is formed by particles smaller than 100 μm in size, which disagglomerate in water.

Mortar name	$u_{w\ min}$	φ_{max}	Water (%)	Flow (mm)
CL	1.95	0.77	-	-
CA	0.84	0.98	-	-
CC1:1	0.81	0.59	32.30	172
CC1:2	0.81	0.62	31.94	>180
CC1:3	0.49	0.74	20.00	143
CC1:4	0.58	0.73	22.68	>180

Table II.1.2 *Values of basic water ratio (u_{wmin}) and maximum solid concentration (φ_{max}) of the suspensions of lime (CL), aggregate (CA) and the mortar mixtures, determined by means of the wet packing method. Values of water content on the total granular material (in %) and flow (in mm) were determined only in the case of the fresh mortar mixtures.*

3.2 Packing density and water content of the mortars mixtures

Of the four mortar mixtures, CC1:3 had the best packing (Tab. II.1.2); the basic water content (u_{wmin}) corresponding to this packing was also optimal since a good workability (flow) was achieved with this mixture. In the other mortars, the water content used for the preparation of mixtures (corresponding to the maximum solid concentration) was too high and gave place to quite fluid pastes. However, in all the cases the value of flow is within the range established for a plastic mortar (140-200 mm of flow) [21]. In particular, according to the consistence appreciated during the manual mixing, it is possible to fix the limit of plasticity of lime mortars to a maximum of 170 mm of flow. However, ones must consider that the flow test is not a precise method for the determination of the optimal amount of water, because of the different functionality of lime mortars (i.e. render, structural mortars, etc.) and the low adaptability of standards, which are defined for cement mortars [16,21].

It has been observed that the value of φ_{max} generally increases with the increasing of aggregate volume, except in the case of the highest proportion of aggregate. The basic amount of water, represented by the value u_{wmin}, does not present the same linear trend, because there is a sharp decrease in this value from the 1:2 to the 1:3 B/A ratio. This can be explained by considering the decrease in the amount of lime. In CC1:2, the packing is a bit higher than in CC1:1, but the minimum void ratio (u_{min}) is almost the same (Fig. II.1.1), as is the basic amount of water (u_{wmin}), which is only slightly reduced. The most influential difference is

the amount of lime present in the two mortars, considering that CC1:2 contains half the lime amount than CC1:1. This means that water is not entirely absorbed by the lime but is free in the mixture, producing a much more liquid mortar.

On the other hand, we obtained for CC1:4 a packing density a bit lower than that of CC1:3, which produced a mixture with high flow (due to its higher water content). In CC1:4 mortar, the high packing density is produced quite exclusively by the continuous grading of the aggregate, because the lime content is very low and insufficient to fill the voids. The flow is, however, a bit lower with respect to that of CC1:2 because of reduced quantity of water.

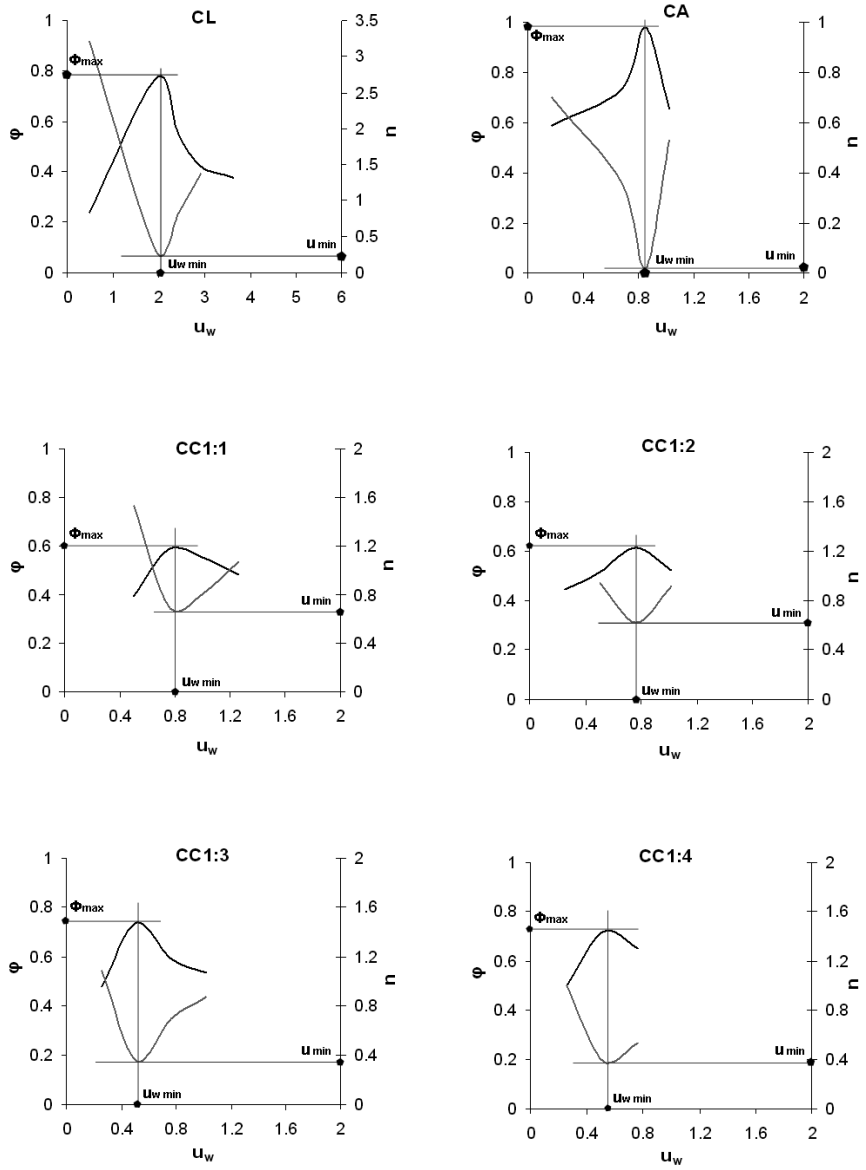

Figure II.1.1 *Curves representing the water ratio (u_w) versus the solid concentration (φ) (black lines) and the void ratio (u) (gray lines) for the calcitic lime (CL), the calcitic aggregate (CA) and the four mortar mixtures. Maximum solid concentration ($φ_{max}$), basic water content (u_{wmin}) and minimum voids ratio (u_{min}) are indicated in each graphic with a •.*

3.3 Physical-mechanical study of mortar types once hardened

The water content determined by the WPM and used for the preparation of CC1:2 and CC1:4 was too high and gave place to too fluid mixes that were not possible to mould. Therefore, only CC1:1 and CC1:3 mortars were studied once hardened, because they showed the best packing, the minimum amount of kneading water and the best workability of the fresh paste compared to the other binder-to aggregate proportions.

The lowest amount of water used for the preparation of CC1:3 (Tab. II.1.2) resulted in a very low porosity (about 25%, Tab. II.1.3), which is similar to that of cement-lime mortars [22]. By contrast, CC1:1 showed a porosity value (about 35%, Tab. II.1.3) that is typical of lime mortars (ranging between 30 and 40%, [23]).

Open porosity (P_o)		
Mortar sample	Ex	In
CC1:1	36.2±0.17	26.3±0.16
CC1:3	35.8±1.76	25.3±0.29
Carbonation degree index (I_{CD})		
Mortar sample	Ex	In
CC1:1	70.5	68.2
CC1:3	97.1	68.0
Mechanical strengths		
Mortar sample	R_f	R_c
CC1:1	0.07±0.01	1.31±0.08
CC1:3	0.07±0.01	1.65±0.18

Table II.1.3 *Values of open porosity (P_o, in %) and carbonation degree index (I_{CD}, in %) determined on the external (Ex) and internal (In) samples of CC1:1 and CC1:3 mortars; and flexural (R_f) and compressive (R_c) strengths (in MPa) of CC1:1 and CC1:3 mortars determined after six months of hardening.*

The pores size distribution (Fig. II.1.2) is the same in both mortar mixtures because they have the same composition, but the volume of the main pores (0.1<r<1 μm) in CC1:1 is twice that of CC1:3. This reflects that CC1:1 has bigger lime content with respect to CC1:3 [24-25]. The smaller pores (r = 0.03 μm) have similar volume in both mortars, although a bit higher in CC1:1.

A tight similarity was found in the pore size distribution of the internal and external parts of mortars, apart some small differences in the position and height of the peaks (i.e. in the radius and volume of the main pores). In fact, in both CC1:1 (Fig. II.1.2a) and CC1:3 (Fig. II.1.2b) the main peak (0.1<r<1 μm) obtained in the PSD of the internal samples is centered at radius slightly smaller than the obtained in the external ones. Moreover, a smaller porosity has been obtained in the same range in the internal samples of CC1:3 (Fig. II.1.2b). Regarding the second peak

(centered at 0.03 μm), its volume is a bit higher in the internal sample of CC1:1 mortar but the position of this peak is the same in all samples.

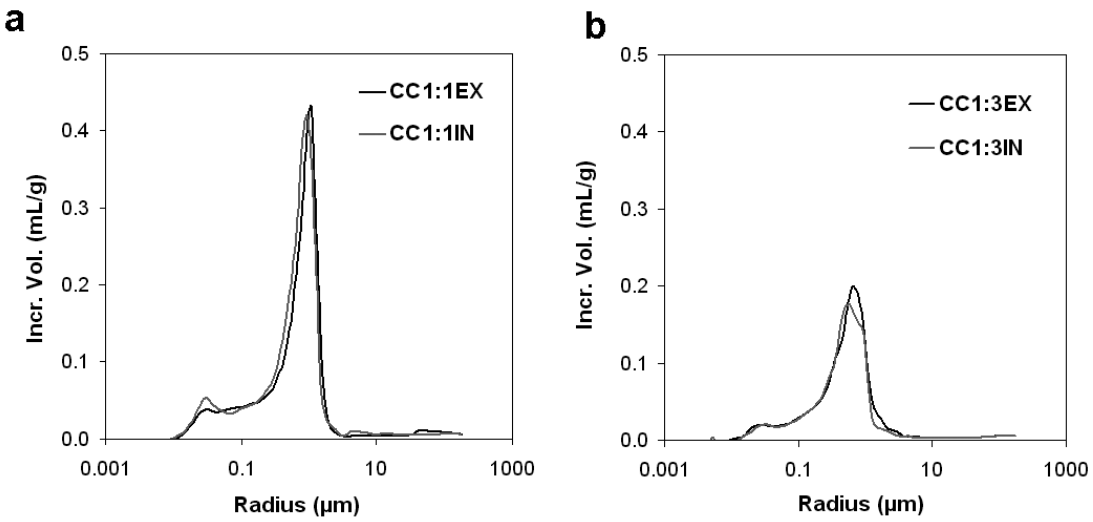

Figure II.1.2 *Pore size distribution curves of the external (EX) and internal (IN) parts of CC1:1 (a) and CC1:3 (b) mortars after six months of curing.*

These small differences found in the porosity of mortars samples must be related with the differences in their carbonation degree. The carbonation degree index (I_{CD}, Tab. II.1.3) is about 70% in CC1:1, both in the upper and the internal zone, whilst it is much higher in the surface of CC1:3. The high I_{CD} value of CC1:3 is contrasted by a much lower carbonation degree measured in the interior of this mortar. This maybe due in part to the lower interconnection among pores in the interior of CC1:3 (as indicated by the smaller volume of pores in the internal sample, Fig. II.1.2b), which makes harder the diffusion of CO_2 in this zone. This fact is certainly not positive, since it may produce physical discontinuities in the material. Moreover, if in CC1:1 a further carbonation can be expected due to the more open system of this mortar, the same cannot be done in the case of CC1:3, if we consider the low porosity registered in this mortar after only two months of hardening.

By means of the mechanical study, we obtained the same value of flexural strength (R_f, Tab. II.1.3) for both mortars, whilst CC1:3 showed a slightly higher value of compressive strength than CC1:1 (R_c, Tab. II.1.3). In theory, much higher R_c and R_f should be expected for CC1:3, given that one of the interests of elaborating mortars with a high packing density is the improvement of mechanical strengths. As commented above, these low resistance values can be a consequence of the different degree of carbonation between the internal and external zone of this mortar.

4. Conclusions

The determination of the packing density of the dry granular materials used for the production of mortars (calcitic lime and calcareous aggregate) was proven to be strongly dependent on the procedure used for the

preparation, being always higher in the vibrated powders compared with the non-vibrated ones. The measurement of solid concentration in fresh pastes by means of the wet packing method has found to be more realistic with respect to the dry method, but also with respect to the flow test, which is imprecise, especially when lime mortars are studied. Notwithstanding, not all the mixtures prepared by adopting the wet packing method have shown a good workability, since half of the mortar mixes studied resulted too liquid to be moulded. Among the four types of mortars, the best values of packing density and basic water ratio were found in the mixture with the 1:3 binder-to-aggregate ratio (CC1:3). This proportion gave place to the most packed mixture, in which the quantity of voids and the amount of water necessary for their saturation were minimal. These important characteristics produced a mortar with optimal workability. However, the properties of this mortar once hardened have found to be slightly contradictory. In fact, CC1:3 mortar presented a much lower porosity than the majority of lime mortars elaborated without any additive. Although the porosity reduction is generally considered a positive aspect for mortar durability, here it has demonstrated to be a negative factor in relation with the outcome of the carbonation process and the development of mechanical strengths.

This research demonstrates that the application to lime mortars of standards and methods originally created for cement mixtures results quite unsatisfactory and controversial. We think that the difference in the rheological properties between aerial lime and cement are one of the main responsible for the low adaptability of these methods to lime based mortars. This fact leads us to expect also different results from the application of these methods to calcitic and dolomitic lime mortars, since the rheological behaviour of these limes in suspension are known to be very different [20]. Further studies are certainly needed in order to customise new methods and standards specific for aerial lime mixtures.

Acknowledgements:

This study was financially supported by Research Group RNM 179 of the Junta de Andalucía and by Research Project MAT 2008-06799-C03-03. We are grateful to ARGOS DERIVADOS DEL CEMENTO S.L. (Granada, Spain) for providing the raw materials used in this study.

References

[1] Ferraris CF, De Larrard F. Testing and modelling of fresh concrete rheology. NISTIR 6094, 1998.

[2] Donev A, Cisse I, Sachs D, Variano EA, Stillinger FH, Connelly R, Torquato S, Chaikin PM. Improving the density of jammed disordered packing using ellipsoids. Science, 2004;303(990):990-993.

[3] Weisstein EW. Sphere Packing. MathWorld A Wolfram. 2009; http://mathworld.wolfram.com/SpherePacking.html

[4] Weisstein EW (2009b) Kepler Conjecture. MathWorld A Wolfram. 2009; http://mathworld.wolfram.com/KeplerConjecture.html
[5] Fuller WB, Thompson SE. The laws of proportioning concrete. Proc Am Soc Civil Engr 1907;33:222-298
[6] Andreasen A, Andersen J. Über die Bezieung zwischen Kornabstufung und Zwischenraum in Produkten aus losen Körnern (mit einigen experimenten). Kolloid-Zeitschrift 1930;50:217-228
[7] Dinger DR. Particle Packing and Pore Size Distributions. 1980;1,9. www.dingerceramics.com update 2003.
[8] Kwan AKH, Wong HHC. Effects of packing density, excess water and solid surface area on flowability of cement paste. Adv Cem Res 2008;20(1):1-1.
[9] Edmeades RM, Hewlett PC. Cement admixtures. Lea's Chemistry of Cement and Concrete. 5th ed. Arnold; 1998.
[10] Wong HHC, Kwan AKH. Packing density of cementitious materials: part 1-measurement using a wet packing method. Mater Struct: 10.16177s11527-007-9274-5; 2007.
[11] Fung WWS, Kwan AKH, Wong HHC. Wet packing of crushed rock fine aggregate. Mater Struct 2008;42(5):631-643.
[12] Kwan AKH, Fung WWS. Packing density measurement and modelling of fine aggregate and mortar. Cem Concr Comp 2009;31:349-357.
[13] Kwan AKH, Wong HHC. Packing density of cementitious materials: part 2-packing and flow of OPC+PFA+CSF. Mater Struct 2007; 10.617/s11527-007-9281-6
[14] UNE-EN 459-1. Cales para la construcción. Parte 1: Definiciones, especificaciones y criterios de conformidad. AENOR, Madrid, 2002.
[15] ASTM D854-92. Standard test method for specific gravity of soils; 1993.
[16] UNE-EN 1015-3. Métodos de ensayo de los morteros para albañilería. Parte 3: Dterminación de la consistencia del mortero fresco (por la mesa de sacudidas). AENOR, Madrid; 1998.
[17] Martín Ramos JD. XPowder. A software package for powder X-ray diffraction analysis, Lgl. Dep. GR 1001/04; 2004.
[18] UNE-EN 1015-11. Metodos de ensayo de los morteros para albañileria. Parte 11: Determinación de la resistencia a flexión y a compresión del mortero endurecido. AENOR, Madrid; 2000.
[19] Yu AB, Feng CL, Zou RP, Yang RY. On the relationship between porosity and interparticle forces. Powder Technology, 2003;130(1-3):70-76.
[20] Arizzi A, Hendrickx R, Cultrone G, Van Balen K. Differences in the rheological properties of calcitic and dolomitic lime slurries: influence of particle characteristics and practical implications in lime-based mortar manufacturing. Mater Construcc 2011;60(0), DOI: 10.3989/mc.2011.00311.
[21] Boletín AFAM. Morteros Guía General; 2003. www.afam-morteros.com.
[22] Arandigoyen M, Alvarez JI. Pore structure and mechanical properties of cement–lime mortars. Cem Concr Res 2007;37:767–775.

[23] Arizzi A, Martinez-Martinez J, Cultrone G, Benavente D. Mechanical evolution of lime mortars during the carbonation process. Key Engin Mater 2011;465: 483-486.
[24] Arandigoyen M, Pérez Bernal JL, Bello López MA, Alvarez JI. Lime-pastes with different kneading water: pore structure and capillary porosity. Appl Surf Sci 2005;252:1449-59.
[25] Lanas J, Alvarez JI. Masonry repair lime-based mortars: Factors affecting the mechanical behavior. Cem Concr Res 2003;33:1867–1876.

Concluding Remarks

None of the methods studied in this part of the thesis can be considered totally suitable for the design of repair lime-based mortars. However, this study leads to important considerations that are tackled below.

Firstly, this investigation has clearly shown the superiority of the "wet" methods compared to the "dry" ones for the establishment of the correct water dosage.

Secondly, the flowability test shows a low adaptability to aerial lime-based mortars, because the range of flow values settled in the standard is inaccurate for aerial lime mortars. Therefore, defining a new range of flowability for aerial lime-based mortars could be crucial for a correct design of these materials. For example, *chapter II.1* has shown that the approximate range of consistence for a packed mixture of lime and fine aggregate stays between 140 and 170 mm, which is narrower than the range defined in the standards for cement mortars and concrete (140-200 mm).

Finally, the "wet packing method" is not adopted in the following studies of this thesis, although it has shown to be the most realistic method among the others we have considered. This decision derives from the fact that the achievement of the highest packing density resulted in a discontinuous pore system between the interior and the surface of the samples, which cannot be a positive aspect for the mortar quality.

PART III

Additives and admixtures: a study of their influence on mortar hardening properties and an assessment of the most suitable proportions.

Objectives

Once established the main components of mortars (calcitic lime and calcareous aggregate) and studied the properties during hardening of the basic mixes elaborated in part I and II, new components are taken into account in the third part of this thesis, with the aim of improving or modifying some of the most undesired properties of the aerial lime-based mortars.

As general overview, shrinkage is the most negative aspect observed in the mortars mixes studied up to here [(*)]. This phenomenon is due to the big water amount absorbed by the lime during mortar preparation and, at the same time, to a high water evaporation rate. This leads to a rapid volume reduction, with the formation of many shrinkage fissures and high porosity.

The studies presented in *chapters III.1* and *III.2* claim to find out a way of decreasing the water dosage, with the objective of reducing shrinkage and porosity in lime mortars, thus improving their final performances. With this aim, blended mortars will be studied in this part of the thesis.

Firstly, a white Portland cement is added to the lime in order to find out whether it can be a favourable component when used in low amounts in repair mortars (*chapter III.1*). The use of cement has been considered since this material suffers lower plastic shrinkage than the aerial lime.
Secondly, different types of additives and admixtures are added, alone or blended together, to the lime mortars (*chapter III.2*). The additive used is a pozzolan, chosen because it confers good properties to lime mortars in fresh and hardened state. The admixtures used are known to indirectly reduce shrinkage, by acting in a physical or chemical way. The main proposal of this study is to discover in which way these components affect the properties of the lime-based mortars once hardened.

In both researches, a mineralogical, morphological and physical-mechanical study has been carried out, in order to verify the compatibility of these materials with the general conditions established for repair mortars.

Moreover, the selection of the appropriate dosages of additions and aggregate is tackled in *chapter III.2*.

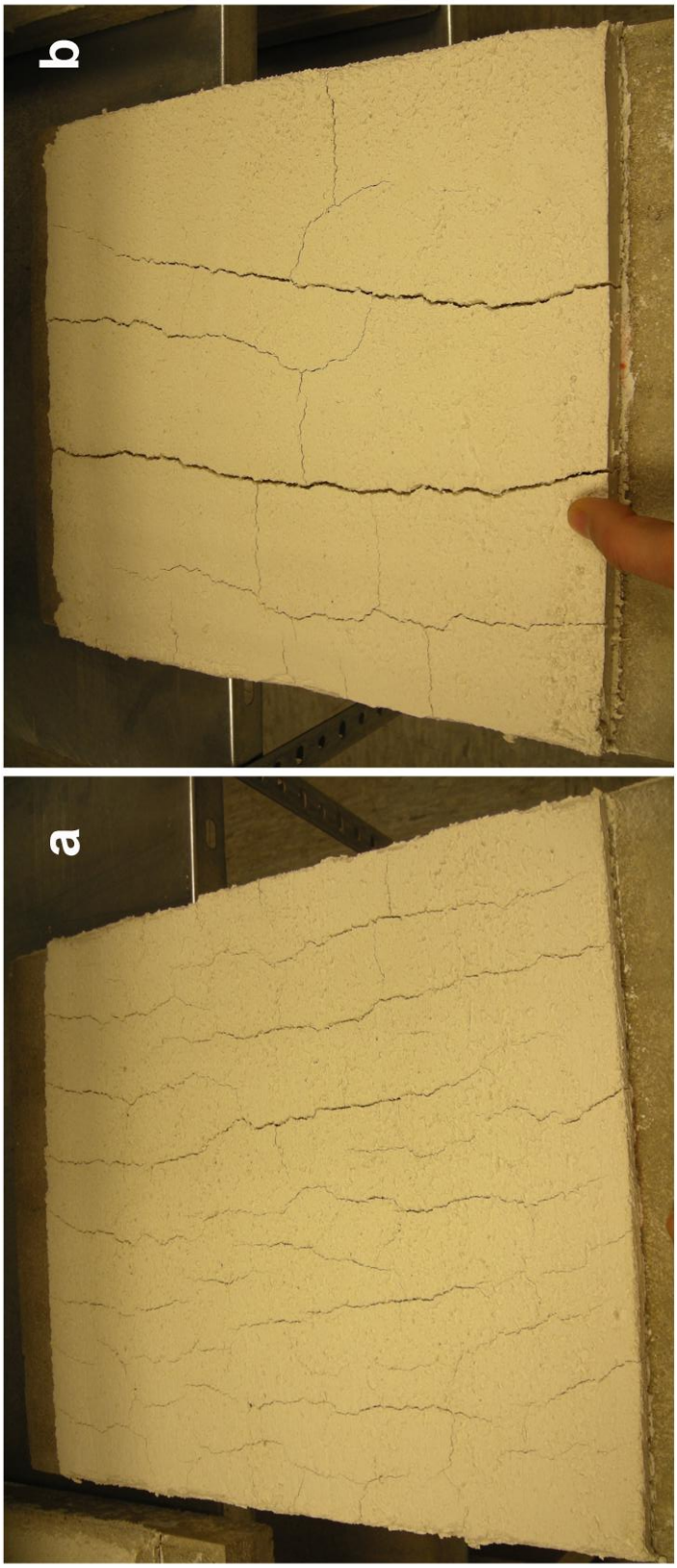

(*)Photos of the shrinkage fissures formed during 24 hours in lime mortar layers of 1 (a) and 2 (b) cm applied on a concrete substrate and left drying under atmospheric conditions (T ~ 20 ºC; RH ~ 60%).

Chapter III.1

Negative effects of the use of white Portland cement as additive to aerial lime mortars set at atmospheric conditions: a chemical, mineralogical and physical-mechanical investigation

Arizzi A., Cultrone G.
Chapter in *Bricks and Mortars Research* book,
ISBN: 978-1-61942-927-7

Abstract

In recent years the use and study of lime mortars are being improved because lime shows a high compatibility with the ancient materials of the Architectural Heritage. On the other hand, the scarce knowledge of the fabrication techniques, the application methods used in the past and the long time of setting have driven scientists and restorers to add other binders (i.e. cement, pozzolans) to the lime, which claim to obviate the inconveniences of the use of this material alone. The use of Portland cement as additive in lime-based mortars seems to be an easy and diffused solution for the industrial production of repair mortars. In this work, we have compared the chemical-mineralogical and physical-mechanical properties of mortars prepared with calcitic lime and a calcareous aggregate, with mortars in which a white Portland cement (WPC) has been used in substitution of a 25 wt.% of the lime. This chapter shows that mortars prepared with Portland cement do not provide satisfactory results after two months since their elaboration. From mineralogic data and porosimetric analyses no improvements were observed by the addition of cement. In fact, even if this percentage of cement produced lower shrinkage than lime mortars, it did not improve the hydric and mechanical properties. Most importantly, the WPC caused the formation of ettringite that provoked fissures in mortars samples. This chapter demonstrates that the use of cement, even if only as additive in lime mortars, would impair the longevity of the masonry that encloses it.

1. Introduction

After its discovery in 1824, Portland cement, a binder of high mechanical resistances and workability, has replaced lime in the great majority of new construction and restoration works. The rapid diffusion of this material all over the world was promoted by the low costs and times of production that, in turn, were favoured by the standardization of the cement properties. Due to these economic advantages, in the last century Portland cement has been used in many historic buildings as repair material, where it has caused serious and irreversible damages. The reasons of that stay in the high stiffness, low permeability and content of soluble salts of this binder, which make it non-compatible with the traditional construction materials [1,2]. Because the application of Portland cement in the Architectural Heritage has demonstrated to be counterproductive, its use in this field has been drastically reduced in the last decades whilst, in contrast, the production of lime mortars is being improved.

On the one hand, lime is the binder that better performs in ancient buildings, because of its high permeability and porosity that allow the materials to "transpire", its low mechanical strengths that allow the materials to "move", and its high reversibility that allows the repair materials to be removed without damaging the original ones. On the other hand, there exists a scarce knowledge of the methodologies used in the past for its production and application, as well as there is a lack of standards that prevents its production at an industrial level, especially if ones consider the wide functional and constructive versatility of lime mortar (i.e. renders, plasters, structural and pointing mortars, etc.).

These problems have pushed manufacturers and architects to the use of other materials blended to the lime in the mortar mix, with the function of second binders or additives. This halfway solution is being achieved with the use, for example, of the Portland cement. It has been found that, by blending cement to the lime, it is possible to reduce cracking, to quicken the application and hardening of the mortar, thus providing protection from rain before carbonation has been completed, and to ensure reliability and predictability of its properties [3]. Moreover, new types of cement have been developed to obtain better performances with the lime, such as the white Portland cement (WPC). This material is manufactured from materials virtually free of iron oxide and other impurities, which impart the grey colour to the normal Portland cement. However, because of the different manufacturing processes (the absence of iron causes a temperature increase), it is much more expensive (i.e. twice the price) than the equivalent grey product. Typical applications of WPC are architectonical elements, such as rendering, cast stone, precast and in-situ structural concrete and pointing, and ornamental elements that require a white colour for eventual pigment addition.

The main interest of this work is to find out whether and how the addition of white Portland cement improves the physic-mechanical

properties of an aerial lime-based mortar cured at atmospheric conditions, by checking the mineralogical and textural changes induced by it. In this research, the WPC is used as an additive rather than as a real binder, therefore it seems reasonable to expose the mortars to a non-moist environment, at which aerial lime mortars are normally cured. In this way, it is possible to know if the cement is still effective in the mortar hardening and, consequently, in the improvement of its physical characteristics (i.e. water absorption, shrinkage), without developing excessive high strength and low porosity. This study claims to verify if the use of cement as additive in repair lime mortars is a really good halfway point or, instead, represents a solution that has to be definitively discarded in restoration works.

2. Materials and Methods

2.1 Mortars elaboration

CC mortar was prepared with a calcitic dry hydrated lime, (named CL, CL90-S [4]) produced by ANCASA (Seville, Spain) and a calcareous aggregate (named CA) with a continuous grading from 0.063 to 1.5 mm. A white Portland cement (named WPC, BL II/A-LL 52.5 R [5]), produced by CEMEX commercial (Valencia, Spain), was used in substitution of 25 wt.% of lime in the elaboration of a new mortar named CPC. The binder-to-aggregate (B/A) ratio used in both mortars is 1:3 by weight. The amount of water, established in order to obtain mortars with a plastic consistency, was 31% and 27% of total mass, for CC and CPC mortars, respectively. The flow was calculated as the average of the spread diameter (in mm) measured on three fresh samples during the flowability assay [6], in the range of 140-160 mm. After preparation [7], mortars were cured for 7 days in standard steel moulds (4×4×16 cm) at RH = 60±5% and T = 20±5 °C and, after removal from the moulds, were cured for a further 21 days in the same laboratory following the modification of the UNE-EN 1015-2 standard [7] proposed by Cazalla [8]. Mortars were conserved at the same conditions throughout the study.

2.2 Characterization of the mortars components

The chemical composition (major and minor elements) of the components of mortars was studied using a Bruker S4 Pioneer X-ray fluorescence spectrometer (XRF), with wavelength dispersion equipped with a goniometer that analyzes crystals (LIF200/PET/OVO-55) and a Rh X-ray tube (60 kV, 150 mA). Semiquantitative scanning spectra were obtained using Spectraplus software. Mortar powders (ca. 5g) were dispersed in KBr, deposited in an aluminium cup and then pressed at 10 ton to obtain a pressed pellet (40 mm sample disc). Measurements were performed in a vacuum with a rotating sample.

The mineralogical phases of binders and aggregate were determined by X-ray diffraction (XRD) and thermogravimetric (TGA) analyses. In the first

case, a Philips PW-1710 (disoriented powder method) was used. Analysis conditions were: radiation CuKα (λ=1.5405 Å), 3 to 60 º2θ explored area, 40 kV voltage, 40 mA current intensity and goniometer speed of 0.1 º2θ/s. The interpretation and quantification of the mineral phases was performed using the X-Powder software package [9]. Thermal measurements were made with a Shimadzu TGA-50H analyzer. Approximately 50 mg of sample was heated in an alumina crucible, in a flushed-air atmosphere (100 mL/min), at a heating rate of 5º/min over a range of 25-950 ºC. TGA data treatment was carried out according to the UNE-EN ISO 11358 [10] standard.

2.3 Mortars characterization

Both inner (core) and outer (1 cm from the core to the surface) parts of the mortars samples were analyzed after 28 and 60 days since mortars elaboration.

The mineralogical phases of the mortars were determined by TGA using the same analytical device described above. Mortar phases were determined by measuring the weight loss resulting from the stoichiometric reactions of:

1. gypsum decomposition (110<T<170 ºC);
2. calcium silicate hydrates decomposition (100<T<125 ºC);
3. portlandite dehydroxylation (450<T<550 ºC);
4. calcite decomposition (700<T<900 ºC).

The decrease in portlandite content was taken as reference to estimate the carbonation degree of mortars (I_{CD}, %).

The textural characteristics of mortars were studied by means of field emission scanning electron microscopy (FESEM), using a Carl Zeiss Leo-Gemini 1530 microscope on previously dried, carbon-coated mortar fragments.

Open porosity (P_o, %) and pore size distribution (PSD, in a range of 0.002<r<200 μm) were determined using a Micrometics Autopore III 9410 mercury intrusion porosimeter (MIP). Mortar fragments of ca. 2 cm^3 were oven-dried for 24 h at 60 ºC before the analysis.

The capillary imbibition test was performed only after 60 days since mortars elaboration, on three samples per mortar type of 4×4×16 cm that were oven-dried at 100 ºC for 24 h before measurements were taken. Two imbibition coefficients (A and B) were determined from the mass uptake per surface unit and the height over time, according to the Beck et al. [11] procedure.

Flexural and compressive strength (R_f and R_c) were measured by means of a hydraulic press INCOTECNIC-Matest. According to the UNE-EN 1015-11 [12] standard, flexural assays were carried out at 28 days of carbonation, on three samples per mortar (of 4×4×16 cm). The six samples obtained after the flexural rupture were used for the compressive assays.

Shrinkage of hardened mortars was determined after 60 days measuring the variation of the dimensions (expressed as percentage) on three perpendicular directions: a, parallel to the compaction plane; b, parallel to the compaction plane along the largest face of the sample; c, perpendicular to the compaction plane. Measurements were carried out on three samples per mortars.

3. Results and discussion

3.1 Characterization of the mortars components

The chemical analysis (XRF, Tab. III.1.1) of the white Portland cement shows high contents of CaO and SiO_2. These elements (Ca and Si) correspond to the calcium silicates C_3S (tri-calcium silicate, or alite) and C_2S (di-calcium silicate, or belite), found by XRD (Tab. III.1.1). The TiO_2 proceeds from a pigment added to white Portland cement to further enhance the whiteness.

Chemical composition (XRF)	
(Oxides %)	WPC
SiO_2	14.98
CaO	70.49
SO_3	5.58
MgO	0.61
Fe_2O_3	0.26
Al_2O_3	4.22
TiO2	0.08
Mineralogical composition (XRD)	
Mineral phases (%)	WPC
CC	20.9
CH	16.8
Gyp	2.3
C_2S	29.9
C_3S	30.1
Mineralogical composition (TGA)	
Mineral phases (%)	WPC
CC	22.2
CH	2.2
Gyp	2.4

Table III.1.1 *Chemical (X-ray fluorescence analysis, XRF) and mineralogical (X-ray diffraction, XRD and thermogravimetric analysis, TGA) composition of white Portland cement (WPC). CC=calcite; CH=portlandite; Gyp=gypsum; C_2S=dicalcium silicates; C_3S=tricalcium silicates*

The presence of Al in WPC was detected only by XRF and this indicates that aluminate phases are present in amounts not detectable by XRD (Fig. III.1.1, Tab. III.1.1).

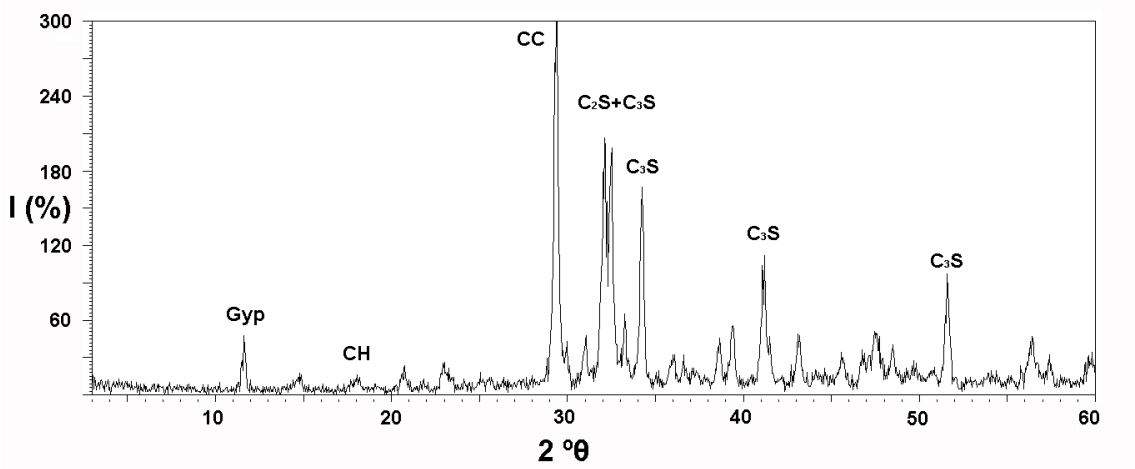

Figure III.1.1 *X-ray diffraction pattern of white Portland cement (WPC). CC = calcite; CH = portlandite; Gyp = gypsum; C_2S = dicalcium silicates; C_3S = tricalcium silicates.*

By means of thermogravimetric analysis only calcite (CC), portlandite (CH) and gypsum (Gyp) phases were identified (Fig. III.1.2, Tab. III.1.1).

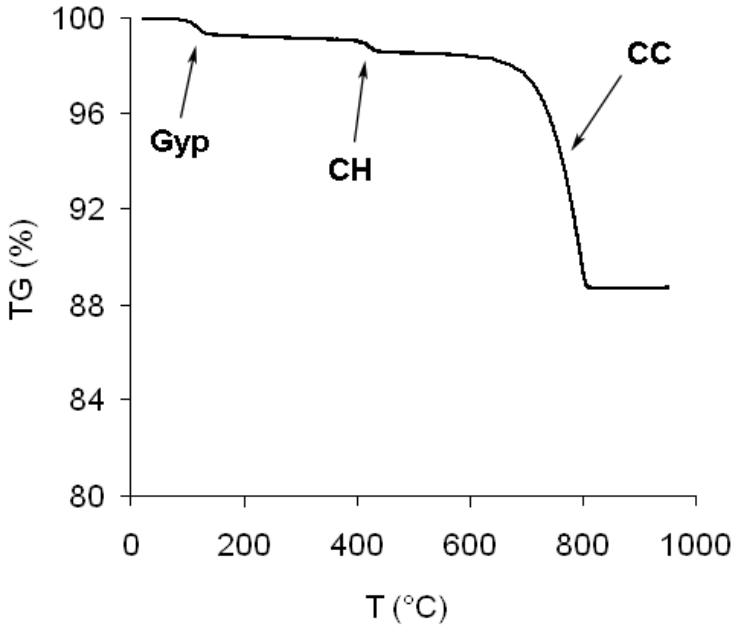

Figure III.1.2 *Thermogravimetric curve of white Portland cement (WPC) where the weight loss (TGA, expressed in %) is represented as function of temperature (T, in ºC). CC = calcite; CH = portlandite; Gyp = gypsum.*

3.2. Evaluation of the hardening processes in lime and cement-lime mortars

3.2.1 Carbonation Degree

An important question to consider is whether and how the cement takes part in the hardening of mortars at these curing conditions. According to Cizer et al. [13], in cement-lime mortars there is no competition between hydration and carbonation under atmospheric conditions because cement hydration always takes place initially and evolves before carbonation becomes effective. This means that in CPC mortars, which have been cured at atmospheric conditions (*cf.* Section 2.1), both processes took place, although it is likely that this happens at different degrees in the surface and in the core of the mortars.

After 2 months since the elaboration, CC and CPC mortars show the same carbonation degree (expressed as I_{CD}, in %, Tab. III.1.2) in the external part (-ex) of the samples, whilst the interior of mortars (-in) presents always a lower degree of carbonation than the surface. Moreover, this difference in the degree of carbonation between the surface and the core is much higher in CPC mortars (about 55%) than in CC ones (about 23%).

We remember that the carbonation degree index (I_{CD}) is calculated for each mortar considering the variation in the amount of portlandite obtained between the beginning of mortar life and the end of the study. This determination does not consider the amount of portlandite liberated during the hydration reactions in cement-lime mortars, so that the I_{CD} is not an accurate value in this case, although it is useful for estimating the progress of carbonation and hydration of mortars. Thus, a lower I_{CD} value, which indicates a higher amount of calcium hydroxide, is due to a slower consumption of the lime during time (i.e. formation of a smaller amount of calcite) in CC mortars; whilst, in CPC mortars, it indicates the formation of more CSH phase (*cf.* Tab. III.1.2) that, during the hydration reaction, liberates $Ca(OH)_2$ [14], thus increasing its amount in the internal samples. Both options can be attributed to the fact that the interior of mortars dries slower than the exterior and this might result in a more moist ambient in the core than in the surface. In the smallest pores, water condensation is likely to occur and this would hinder the diffusion of CO_2 [15], thus slowing down carbonation in this zone. Moreover, the formation of calcium silicate hydrates would be enhanced by the alkaline ambient created due to the dissolution of calcium hydroxide in the pore water [16].

This result confirms our initial assumption that carbonation and hydration happens at different degrees in the exterior and the interior of cement-lime mortars: in the surface, the carbonation process takes place at the same degree than in lime mortars whilst, in the core, carbonation is less favoured and hydration reaction enhanced.

Carbonation degree index (I_{CD})		
Mortar sample	Zone	
	Ex	In
CC	71.67	49.04
CPC	71.77	17.12
Open porosity (P_o)		
Mortar sample	Time (days)	
	28	60
CC	32.5±2.74	35.0±1.10
CPC	36.2±1.80	37.3±1.00
Imbibition coefficients		
Mortar sample	A	B
CC	0.08	9.95
CPC	0.09	10.79
Mechanical resistances		
Mortar sample	R_f	R_c
CC	1.03±0.03	1.43±0.16
CPC	2.59±0.09	1.62±0.23
Shrinkage		
Mortar sample	a	b	c
CC	3.6±1.41	3.8±0.03	6.8±0.00
CPC	3.3±0.71	0.0±0.00	6.0±0.35

Table III.1.2 *Physical parameters of CC (CL+CA) and CPC (CL+WPC+CA) mortars: Carbonation degree index (I_{CD}, in %) of the surface (ex) and the core (in) after 60 days since the elaboration; Open porosity (P_o, in %) values and standard deviation after 28 and 60 days since the elaboration; Imbibition coefficients (A, in g/cm^2 min$^{1/2}$ and B, in cm/min$^{1/2}$) after 60 days since the elaboration; Flexural (R_f, in Mpa) and compressive (R_c, in Mpa) resistances and standard deviation after 28 days, according to the UNE-EN 1015-11 (2000); Shrinkage values (in %) and standard deviation along a, b and c directions of mortars samples after 60 days since their elaboration.*

3.2.2 Identification of the Hydrated Phases in Cement-Lime Mortars

The CSH phase in cement paste is amorphous or semicrystalline and it gives powder patterns very similar to those of the calcium silicates present in cement (C_2S and C_3S) [17]. However, the X-ray diffraction analysis was not able to detect the presence of hydrated phases in CPC mortars, because their peaks were marked by other mineral phases (calcite and portlandite) with higher cristallinity and reflecting power. The thermogravimetric analysis, in turn, allows the identification of CSH that

decomposes at a temperature between 100 and 125 ºC. However, this range of temperature coincides partially with that in which gypsum decomposes (*cf.* Section 2.3 and Fig. III.1.2), so the quantification of CSH and gypsum phases in the carbonated mortars by means of TGA can be a difficult task.

The electron microscopy, in turn, is effective in the identification and characterisation of the hydrated phases morphologies [18] although not in their quantification. Both upper and inner zones of mortars were observed by FESEM after two months since their elaboration. After this period of time, the CPC external samples presented some CSH phases in form of small fibres (only 200 nm long, Fig. III.1.3a), which have been recognised elsewhere as an early hydration structure [17], and many unhydrated or partially hydrated phases (Fig. III.1.3b) in form of particles with a rough surface. Internal samples of CPC showed some flattened particles of CSH (Fig. III.1.3c), which are typically present in samples with twenty-eight days of hydration [17].

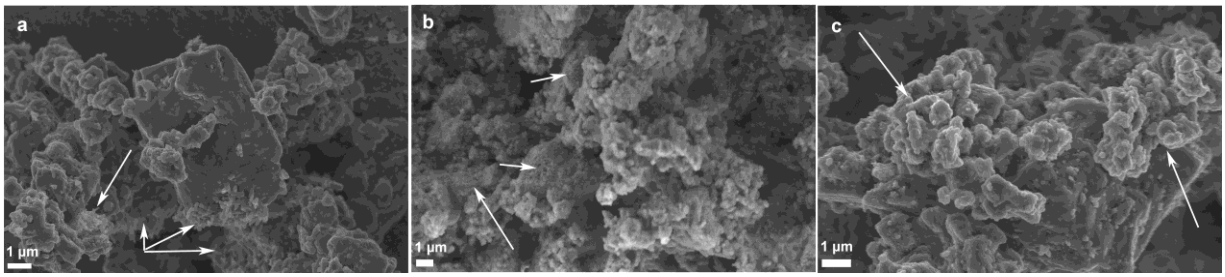

Figure III.1.3 *FESEM images of CPC mortar: upper part of the mortar, in which there are small fibres of CSH (a) and partially hydrated or unhydrated particles (CS_2 and CS_3) with rough surface (b); internal part of mortar (c), in which small and flattened particles of CSH are observed.*

The morphologies observed in Figure III.1.3 suggest that a poor hydration takes place in the exterior of CPC mortars, whilst this process is more extended in the interior. Once again, it is shown that carbonation and hydration processes take place at different degrees in the mortar zones.

3.2.3 Pore System

The pore system is another textural aspect that helps to understand the progress of the hydration and carbonation processes. Two main types of pores typical of cement mortars have been obtained here (Fig. III.1.4): the gel pores, of radius comprised between around 0.01 and 0.05 µm, and the capillary pores, in the range of 0.1-1 µm. The former do not depend to the water amount but to the production of hydrated phases, as also observed by other authors in lime [19] and cement [20] mortars. The latter depend to the water-to-cement ratio and decrease as the hydration reaction progresses; they are responsible for the water transfert properties and the mechanical behaviour of cement mortars [21]. One of the advantages of adding cement to lime-based mortars is that the hydrated phases give place to a segmentation of the capillary pores, which

reduces importantly the water absorption in mortar [21]. Here, this effect was not obtained, since CPC mortar presents only slight lower volume of capillary pores compared to CC mortar (Fig. III.1.4), and this little difference has to be attributed only to the lower amount of water used for the preparation of CPC mortar (*cf.* Section 2.1).

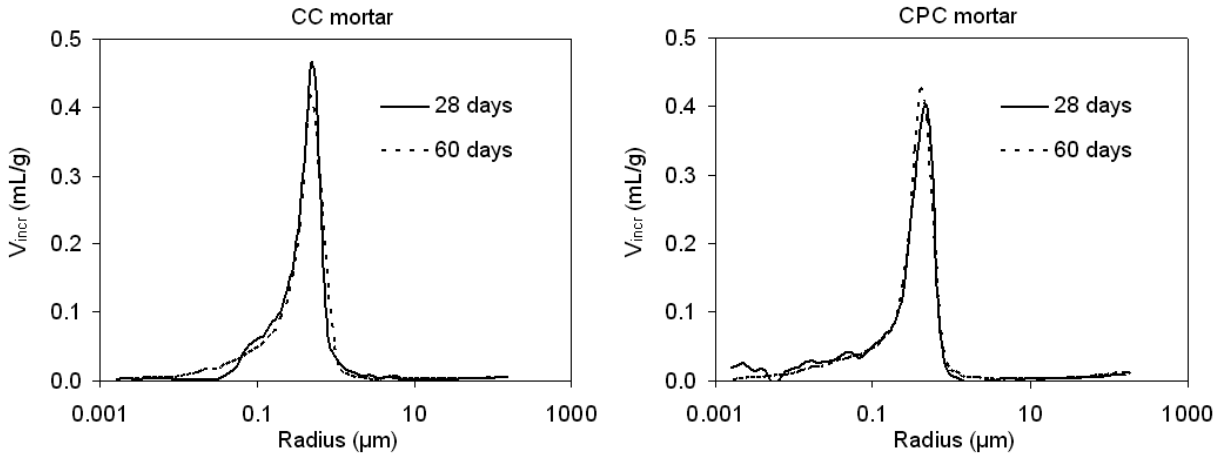

Figure III.1.4 *Pore size distribution curves of CC (CL+CC) and CPC (CL+WPC+CA) mortars after 28 and 60 days of curing.*

A volume of pores with radius smaller than 0.06 μm was registered in the CPC 28 days-old sample (Fig. III.1.4b), and it remained almost unvaried in the 60 days-old sample, although a lower volume might be expected, since the hydrated phases change their morphology in this period of time and occupy the pores left by the cement phases and the CSH gel [17].

In turn, in CC mortar, an increase of the volume of pores in the 0.01 - 0.06 μm size range was registered from 28 to 60 days (Fig. III.1.4a), and it is responsible for the porosity increase registered after 2 months (Tab. III.1.2). This phenomenon is attributed to the formation of agglomerates of small calcite particles at the interfacial transition zone (ITZ) between aggregate grains and matrix [22], which is also expected to occur in presence of cement.

The final consequence of these two opposite mechanisms (decrease of the pore gel volume and increase of the pores at the ITZ) is that the volume of small pores remains unvaried in CPC mortars, as well as the open porosity value determined at 28 and 60 days (Tab. III.1.2).

3.3. Physical-Mechanical Properties of Mortars

3.3.1 Capillary Uptake

Figure III.1.5 shows the capillarity curves obtained for CC and CPC mortars after 2 months of curing. It can be noticed that, although CPC mortar presents slightly higher values of open porosity (Tab. III.1.2), it does not absorb the highest amount of water. This fact, related with the

pore size distribution of mortars, indicates that only pores of radius ranging between 0.1 and 1 μm, whose volume is bigger in CC samples at every curing age, are responsible for the water capillary uptake in mortars. However, this difference in the amount of water absorbed and the rate of absorption is not big between the two mortars, as reflected in the similar values of open porosity and imbibition coefficients (P_o, A and B, Tab. III.1.2).

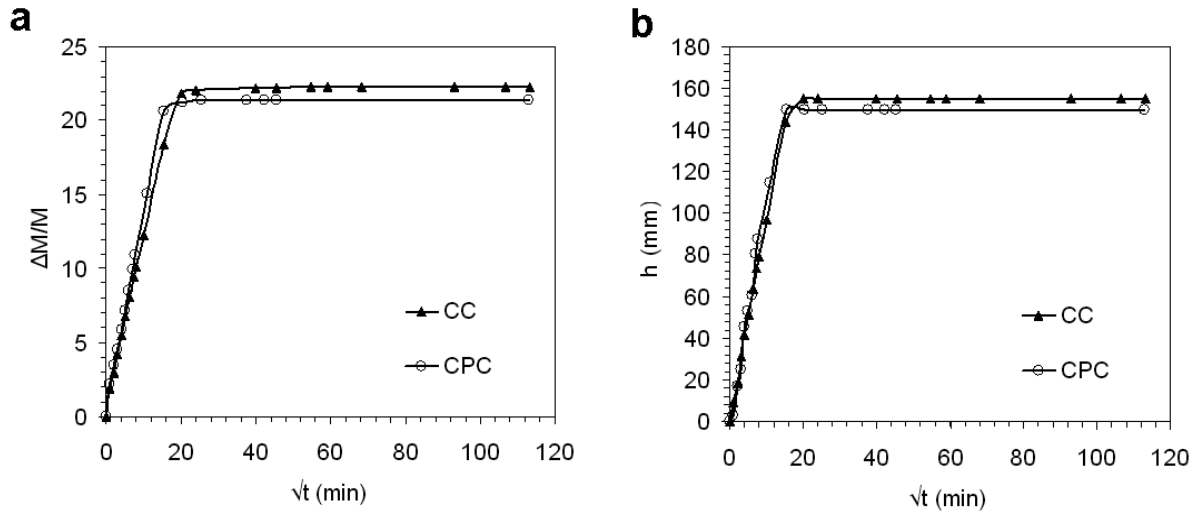

Figure III.1.5 *Capillarity curves of CC (CL+CA) and CPC (CL+WPC+CA) mortars after 60 days since their elaboration. Time (in minutes) is plotted versus the weight increase (ΔM/M, in %) (a) and the water uptake level (h, in mm) (b).*

During the capillary test, some fissures appeared on the three samples of CPC, mainly between the dry and the wet zones of samples, and spread out, causing even important fractures in some points, as shown in Figure III.1.6.

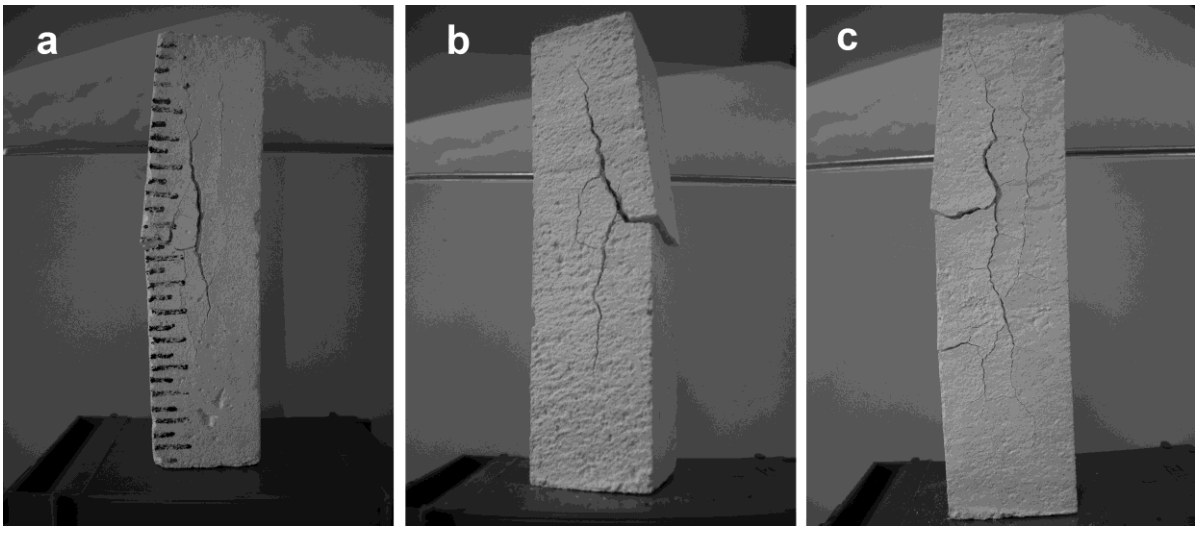

Figure III.1.6 *Development of fissures on the three samples of CPC (CL+WPC+CA) mortar after the capillary assay.*

Once the capillary assay was finished, CPC samples were broken and the internal parts, in which the fissures had propagated, were analysed by means of X-ray diffraction to find out the cause of these fractures. XRD pattern (Fig. III.1.7) shows the presence of small amount of ettringite, in addition to the original phases initially detected in this mortar.

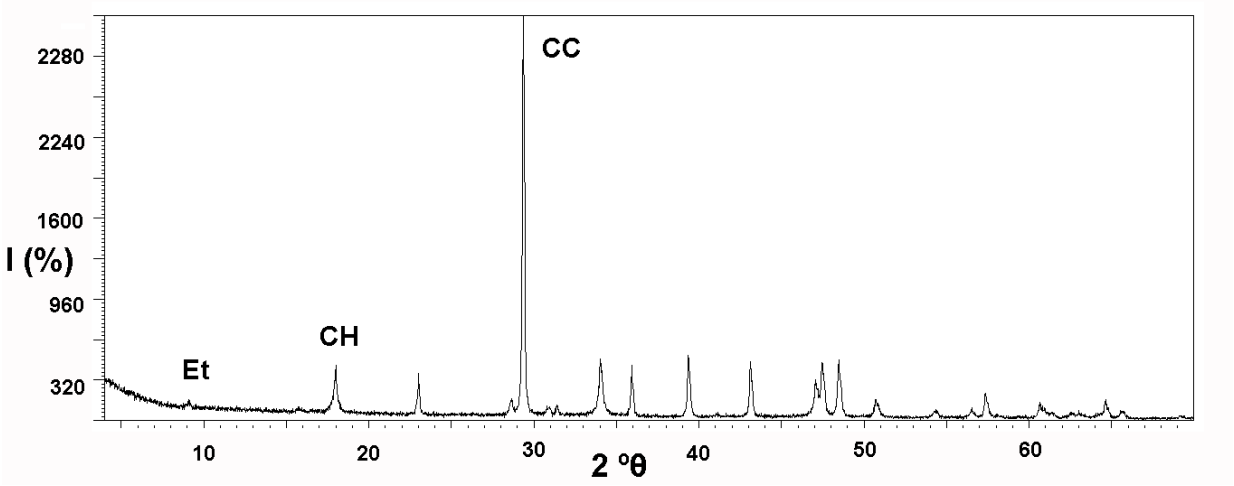

Figure III.1.7 X-ray diffraction pattern of CPC mortar after the water capillary uptake. Et = ettringite; CH = portlandite; CC = calcite.

Ettringite ($Ca_6Al_2(SO_4)_3(OH)_{12}\cdot 26H_2O$) derives from the reaction between the aluminates phases and the SO_4^{2-} ions present in cement.

The moist conditions created during the water imbibition test may have induced this reaction between the gypsum and the few aluminate phases of cement (*cf.* Section 3.1), which had remained unhydrated in the cement matrix until this moment, given that no traces of aluminate hydrates were found during this study. Then the ettringite precipitated at the interface between the dry and wet zones of the samples, where the fissures had been initially observed. In fact, drying-wetting cycles contribute to a slight acceleration of the reaction although they are not necessary for the occurrence of ettringite [23].

3.3.2 Mechanical Strength

CPC mortar shows the highest values of mechanical resistances (especially R_f, Tab. III.1.2), as expected for the presence of cement, although this increase was not high, due to the low percentage of cement replacing the lime [24] as well as to the atmospheric conditions to which the CPC mortar was exposed during the curing [21].

3.3.3 Shrinkage

The shrinkage values (in %) measured on the hardened samples (after 60 days) in three perpendicular directions (a, 4 cm; b, 16 cm; c, 4 cm) are shown in Table III.1.2.

In CPC mortar, shrinkage is smaller than in CC, especially in the longest direction (b), where is equal to zero. The highest value of shrinkage has been measured in both mortars along the c direction. This is caused by the fact that the surface perpendicular to direction c is the most exposed to the air when the sample is in the mould (first 7 days of curing) and, consequently, faster water evaporation occurs in this face at early age.

4. Conclusions

This study shows that at the curing conditions applied for aerial lime mortars (T=20 ºC and RH=60%), the phases of Portland cement do not undergo to complete hydration so that only few changes in the microstructure and physical-mechanical properties are produced in the blended mortars. It was observed that the progress of the carbonation and hydration processes occurs at different degrees in the interior and the surface of mortars but few hydrated phases are formed in both cases. This is the reason of the scarce reduction of the capillary pores volume, which has resulted in no improvement of the water transfer properties (i.e. no reduction of the capillary uptake).

On the contrary, the little hydration occurred gave place to similar mechanical resistances between the lime and cement-lime mortars, which may represent a positive aspect for the whole masonry. The addition of cement presented also the advantage of reducing importantly the shrinkage in one of the three dimension of mortar sample. Notwithstanding, these benefits of using white Portland cement in lime-based mortars are totally countered by the occurrence of soluble salts, such as the ettringite found here.

In summary, the white Portland cement has demonstrated to be harmful and not very effective when mixed to lime mortars, even if only as additive. In view of these results, we recommend using and producing repair mortars without cement and, at the same time, we encourage researchers to improve the study of other alternative and more effective materials to be added to the lime.

Acknowledgement:

This study was financially supported by Research Group RNM179 of the Junta de Andalucía and by Research Project P09-RNM-4905. We are grateful to Argos Derivados Del Cemento S.L. (Granada) for providing the raw materials used in this study.

References

[1] Veniale, F., Setti, M., Rodriguez-Navarro, C., Lodola, S., Palestra, W., Busetto, *A. Cem. Concr. Compos*. 2003, 25, 1123-1129.

[2] Callebaut, K., Elsen, J., Van Balen, K., Viaene, W. *Cem. Concr. Res*. 2001, 31, 397-403.

[3] O'Hare, G. (1995) Lime mortars and renders: the relative merits of adding cement. www.buildingconservation.com/articles/cement/cement.htm.
[4] UNE-EN 459-1. Cales para la construcción. Parte 1: Definiciones, especificaciones y criterios de conformidad. *AENOR*, Madrid; 2002.
[5] UNE-EN 197-1. Cemento. Parte 1: composición, especificaciones y criterios de conformidad para los cementos comunes. *AENOR*, Madrid; 2000.
[6] UNE EN 1015-3. Métodos de ensayo de los morteros para albañilería. Parte 3: Determinación de la consistencia del mortero fresco (por la mesa de sacudidas). *AENOR,* Madrid; 1998.
[7] UNE EN 1015-2. Métodos de ensayo de los morteros para albañilería. Parte 2: Toma de muestra total de morteros y preparación de los morteros para ensayo. *AENOR*, Madrid; 1999.
[8] Cazalla, O. Morteros de cal. Aplicación en el Patrimonio Histórico. *Ph.D. Thesis*, Universidad de Granada; 2002.
[9] J. D. Martín Ramos, XPowder. A software package for powder X-ray diffraction analysis. *Lgl. Dep. GR* 1001/04; 2004.
[10] UNE-EN ISO 11358. Plásticos. Termogravimetría (TG) de polimeros. Principios generales. *AENOR*, Madrid; 1997.
[11] Beck, K., Al-Mukhatar, M., Rozenbaum, O., Rautureau, M. *Build. Environ*. 2003, 38, 1151-1162.
[12] UNE-EN 1015-11. Metodos de ensayo de los morteros para albañileria. Parte 11: Determinación de la resistencia a flexión y a compresión del mortero endurecido. *AENOR*, Madrid; 2000.
[13] Cizer, O., Van Balen, K., Van Gemert, D., Elsen, J. Building materials and building technology to preserve the built heritage. ISBN: 978-3-937066-15-8; WTA-Schriftenreihe Heft 33 VII-XIV: *Leuven (BE),* 2009; Vol. 2, pp. 353-368.
[14] Giraldo, M., Manuel Alejandro. *Dyna. Rev. fac. Nac. Minas*. 2006, 73 (148), 69-81. ISSN 0012-7353.
[15] Houst, Y. F.; Wittmann, F. H. *Cem. Concr. Res*. 1994, 24 (6), 1165-1176.
[16] Cizer, O. Competition between carbonation and hydration on the hardening of calcium hydroxide and calcium silicate binders. *PhD Thesis*; Katholieke Universiteit Leuven, 2009.
[17] Ramachandran, V. S., Feldman, R. F. *Concrete Admixtures Handbook, Properties, Science and Technology, Noyes Publications*, New Jersey (US), 1995; Ch. 1, pp.1-36.
[18] Varas, M. J., Alvarez de Buergo, M., Fort, R. *Cem. Concr. Res*. 2005, 35, 2055-2065.
[19] Arandigoyen, M., Alvarez, J. I. *Appl. Surf. Sci*. 2006, 252, 8077-8085.
[20] Pandey, S. P., Sharma, R. L. *Cem. Concr. Res*. 2000, 30, 19-23.

[21] Fernandez Luco, L. Valoración de técnicas no destructivas para el control de la eficiencia de curado del hormigón. *PhD Thesis*, Universidad de Alicante; 2008, pp. 33-64.
[22] Lawrence, R. M., Mays, T. J., Rigby, S. P. Walker, P., D'Ayala, D. *Cem. Concr. Res.* 2007, 37, 1059-1069.
[23] Escadeillas, G., Aubert, J. E., Segerer, M., Price, W. *Cem. Concr. Res.* 2007, 37, 1445-1452.
[24] Arandigoyen, M., Alvarez, J. I. *Cem. Concr. Res.* 2007, 37, 767-775.

Chapter III.2

Aerial lime-based mortars blended with a pozzolanic additive and different admixtures: a mineralogical, textural and physical-mechanical study

Arizzi A., Cultrone G.
Construction and Building Materials
31 (2012) 135-143

Abstract

This work deals with the effects of a lightweight aggregate, plus water-retaining and a water-reducing agents on the hardened properties of mortars in which the aerial lime is replaced by a 10% and 20% metakaolin content. The influence of different binder-to-sand ratios (1:3, 1:4, 1:6, 1:9 by weight) is also investigated here. A tight relationship between metakaolin content and mortar physical-mechanical properties (compressive strength and pore system) has been found. This study is especially helpful for the establishment of the adequate proportions of additives and admixtures to be used in aerial lime mortars designed for restoration works.

1. Introduction

The addition of inorganic or organic substances to artificial materials such as mortars and bricks is an ancient practice in the field of construction. There are evidences that many organic materials, especially proteins-based (i.e. blood, hair, straw, milk, eggs) [1] were used in the elaboration of historic mortars, in order to improve their workability, resistance and hardening.

Nowadays, although practices and materials have changed and new performances are required in modern constructions, additions are essential components of masonry materials, especially concrete. These additions are divided in two groups: *additives* (i.e. pozzolans, mineral fillers, ceramic powder) that are used in lime based mortars with the aim to improve certain properties or obtain special performances mainly related to the increase of mortar strength, and *admixtures*, added in low amounts (i.e. not higher than a 5% of the total mass) in order to produce a permanent modification in the fresh or hardened mortar, such as density decrease, workability improvement or waterproofing.

The use of lime as binder in mortars involves well-known inconveniences (i.e. slow setting and carbonation times, high drying shrinkage, low mechanical strength) [2] that, in the last fifty years, have been overcome with the use of Portland cement. On the other hand, the ill-omened effects of the use of Portland cement in the Architectural Heritage [3-4] have forced workmen, restorers and scientists to find out alternative materials apt to improve the performances of lime-based mortars. In this sense, it is opportune to use specific admixtures, such as air-entraining and water-retaining agents and pozzolans, which improve workability in the fresh state, and mechanical strength, water permeability and frost resistance in the hardened state of lime-based mortars.

The effects that some admixtures (i.e. water-retaining agents, air-entraining agents and water repellents) have on fresh and hardened performances of air lime-based mortars were almost unknown until the last decades, because the research on these substances was limited to concrete and cement mortars [5]. Only recently, researchers have demonstrated interest in highlighting the advantages and disadvantages of the use of admixtures on aerial lime pastes [6] and aerial lime mortars [7-10]. Nevertheless, none of these studies deals with the effect that those admixtures have on mortars in which a pozzolan is blended to the binder (aerial lime). There exist many evidences of the use of pozzolanic materials, such as brick pebbles or dust and calcined clays [11,12], in ancient mortars. Pozzolans were used in combination with lime to improve the resistance to moisture of rendering mortars, the compactness of floor bedding mortars and the mechanical strength of structural mortars [13,14]. Nowadays, the addition of pozzolanic additives (i.e. fly ashes, silica fumes and calcined clays) to aerial lime mortars is recommended because they confer good properties in the early age, high values of

mechanical strength, low water permeability, good cohesion between binders and aggregates and durability [15-20].

Our aim is to study the changes in mineralogical, textural and physical-mechanical characteristics caused by the addition of different admixtures (both organic and inorganic) in mortars composed by a calcareous aggregate and an aerial lime blended with metakaolin. Three types of admixtures have been considered and blended together or individually in mortars: a lightweight aggregate (perlite), a water-retaining agent (cellulose derivative) and a plasticiser (polycarboxylate). The study of the fresh properties of mortars is not considered here, since the effectiveness of these admixtures in exerting their function is already known within the scientific community [5, 8,10,21,22]. On the other hand, there is a lack in the petrophysical characterization of partially carbonated mortars with such mixtures. For this reason, the characteristics of mortars will be investigated after 60 days since their elaboration.

Perlite is an obsidian derivative that is transformed into a very light, porous and fire resistant material, after a rapid heating at temperatures between 900 and 1100 °C. It has a low density, due to the formation of bubbles inside it that cause an expansion up to 15-20 times its original volume. Perlite is used as additive in mortars, concrete and bricks because it provides thermal insulation, reduces fissures and improves long-term mechanical performances [21] and durability [22].

The cellulose derivative increases the adhesion power of mortar and controls the water retention capacity in the fresh state [23], thus lowering the shrinkage during drying and the water film formation. It confers an initial high consistence to the mortar, although this is not maintained during the mortar application phase (consistence changes from very high to moderate).

On the other hand, the polycarboxylate is a synthetic polymer that, by dispersing the lime particles, supplies a high maintenance of the mortar workability and reduces the voids content [24].

This study deals with the morphological, textural, mineralogical and physical-mechanical modifications that the addition of these admixtures produces in mortars, when added alone or blended together. One part of the study refers to mortars in which these admixtures are blended in different combinations whilst the binder-to-aggregate ratio is maintained fix. Another part focuses otherwise on the modifications that occur in mortars prepared with fixed amount of the same admixtures but different binder-to-aggregate ratios.

2. Materials and Methods

All mortars were prepared with a calcitic dry hydrated lime (CL90-S, [25]) produced by ANCASA (Seville, Spain) and a calcareous aggregate (CA) with a continuous grading from 0.063 to 1.5 mm. The pozzolan used is a metakaolin (MK) (CLASS N POZZOLAN, [26]), produced by Burgess Pigment Company (USA).

The chemical composition (major and minor elements) of these components (CL, CA and MK) was studied by means of a Bruker S4 Pioneer X-ray fluorescence spectrometer (XRF) (with wavelength dispersion equipped with a goniometer that analyzes crystals (LIF200/PET/OVO-55) and Rh X-ray tube (60 kV, 150 mA)), as it is shown in Table III.2.1. The mineralogy of metakaolin was also characterised by means of X-ray diffraction, using a Philips PW-1710 (disoriented powder method, analysis conditions: radiation CuKα (λ=1.5405 Å), 3 to 60 º2θ explored area, 40 kV voltage, 40 mA current intensity and goniometer speed of 0.1 º2θ/s), and its X-ray pattern is shown in Fig. III.2.1.

(Oxides, %)	CL	CA	MK
SiO_2	0.35	0.16	50.84
CaO	78.01	59.59	0.22
SO_3	1.39	0.03	0.09
MgO	0.70	0.87	0.66
Fe_2O_3	0.10	0.04	0.44
Al_2O_3	0.18	0.06	45.26
K_2O	0.05	0.01	0.24
P_2O_5	0.04	0.01	0.17

Table III.2.1 *Chemical composition of the calcitic lime (CL), calcareous aggregate (CA) and metakaolin (MK).*

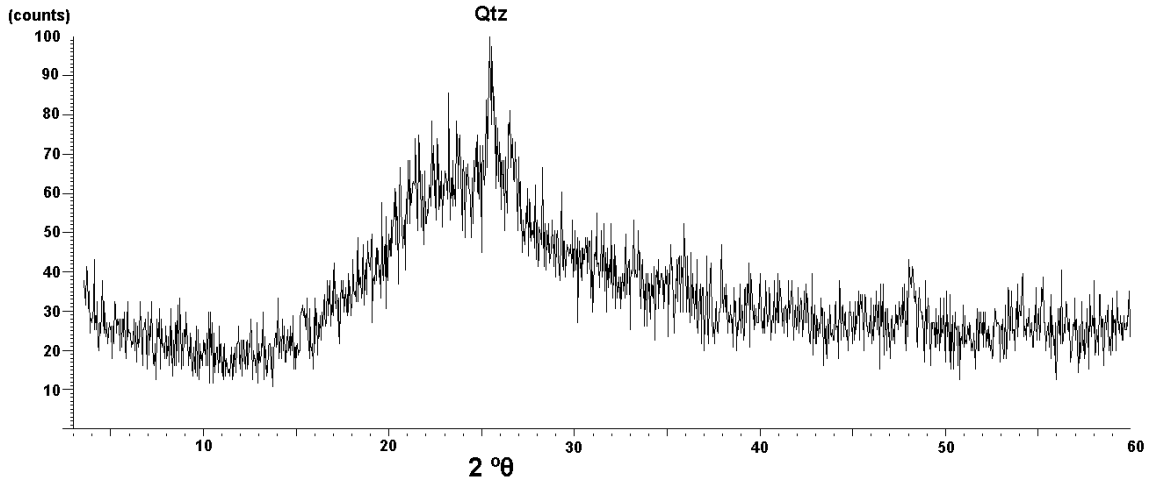

Figure III.2.1 *X-ray diffraction pattern of the metakaolin. Qtz = quartz.*

Eight mixtures were prepared with different binder/sand (B/S) ratios, metakaolin-to-binder proportions and admixtures amounts, as shown in Table III.2.2.

The flow of the fresh mortar pastes, determined according to the European Standard EN 1015-3 [27], is comprised between 120 and 150 mm. Mortars were conserved during 7 days in normalized steel moulds (4×4×16 cm) at T = 20±5 °C and RH = 60±5%, instead of being cured at

a RH of 95%, following the modification of the standard EN 1015-11 [28] proposed by Cazalla [2]. Despite the presence of metakaolin, the mortars studied here are not hydraulic mortars but aerial ones, hence the preference of curing them at conditions that favour carbonation more than hydration. After desmoulded, they were cured at the same conditions of T and RH for 60 days in total. Then, mineralogical, morphological and textural characteristics of mortars were determined.

Mortars name	Components name and proportions					Water
	B/S	MK	P	C	R	
CCM	1:3	20	-	-	-	31.5
CCMP	1:3	20	X	-	-	30.5
CCMPC	1:3	20	X	X	-	27.5
CCMPCR	1:3	20	X	X	X	29.0
CCMPCR3	1:3	10	X	X	X	28.0
CCMPCR4	1:4	10	X	X	X	26.5
CCMPCR6	1:6	10	X	X	X	21.5
CCMPCR9	1:9	10	X	X	X	20.0

Table III.2.2 Proportions of components used in the elaboration of the eight mortar types. Abbreviations indicate: binder-to sand ratio (B/S, by weight); metakaolin (MK, in % of the total weight of the binder); perlite (P); cellulose derivative (C); polycarboxylate (R). The symbols - and X indicate the absence and presence of the corresponding phase, respectively. The total amount of admixtures does not exceed the 2% of the total mass. The amount of kneading water (as % of the total mass) was determined in order to obtain a paste with a flow comprised between 120 and 150 mm (EN 1015-3 [27]).

The mineralogical phases of both internal and external zones of mortar samples were determined by means of two different techniques: thermogravimetry (TGA) and X-ray diffraction (XRD). In the first case, it was employed a Shimadzu TGA-50H thermogravimetric analyser, working in air in a temperature range of 25-950 ºC, with a heating speed of 5 ºC/min. For the XRD analysis, it was used a Panalytical X'Pert PRO MPD diffractometer, with automatic loader and X´Celerator detector, 4 to 70 º2θ explored area. The identification of the mineral phases was performed by using the X-Powder software package [29].

For the textural study, mortars fragments were metalized with a carbon layer and the microstructure analyzed by using a Carl Zeiss Leo-Gemini 1530 field emission scanning electron microscope (FESEM).

Open porosity (P_o, %) and pore size distribution (PSD, in a range of $0.002<r<200$ μm) were determined using a Micrometics Autopore III 9410 porosimeter (mercury injection porosimetry, MIP). Mortar fragments of ca. 1 cm^3 were oven-dried for 24 h at 60 ºC before the analysis.

Flexural and compressive strength were measured by means of a hydraulic press INCOTECNIC-Matest. According to the EN 1015-11 [28] standard, flexural assays were carried out on three samples per mortar (of 4×4×16 cm). The six samples obtained after the flexural rupture were used for the compressive assays.

3. Results and discussion

3.1 Mineralogical phases of mortars

The XRD patterns of the core (IN) and the surface (EX) of mortars are shown in Fig. III.2.2. The main phase formed in mortars is calcite (CC, Fig. III.2.2) because of the high presence of calcium carbonate as aggregate and also because of the carbonation of lime. The portlandite amount found in mortars after only 28 days of carbonation is low compared to the quantity that is likely to be found in aerial lime-based mortars without admixtures. This is because a part of the portlandite dissolved in water transforms into calcite (i.e. carbonation) whilst another part is involved in the lime-pozzolan reactions (i.e. hydration) favoured by the alcaline environment. The fact that mortars prepared with a lower amount of metakaolin (CCMPCR3-9 with 10% of MK on the total binder) show slightly higher peaks of unreacted lime (i.e. portlandite) in their X-ray diffraction patterns (Fig. III.2.2) confirms that a faster lime consumption does not indicate a quicker carbonation but only the development of hydrated phases.

Calcium aluminate and silicate hydrates of variable steichiometry are formed after activation of the aluminate and silicate phases of metakaolin, in presence of calcium hydroxide (i.e. portlandite) and water [30]. By means of XRD analysis, three general hydrated phases were detected: CSH, ($CaO\text{-}SiO_2\text{-}H_2O$) or calcium silicate hydrates; CASH, ($CaO\text{-}Al_2O_3\text{-}SiO_2\text{-}H_2O$) or calcium alumina silicate hydrate; and CAĈH, ($Ca_4Al_2(CO_3)(OH)_{12} \cdot 6H_2O$) or monocarboaluminate. The latter is one of the mono-phase calcium hydrates and derives from the reaction between the reactive aluminates of metakaolin and the CO_3^{2-} ions present in mortars [31]. In mortars with fixed amount of admixtures, lower metakaolin content and different B/S ratios (i.e. CCMPCR3-9), CAĈH phases have precipitated in very low amounts compared to the other mortars, and they have been detected only in the internal part of the mortars (Fig. III.2.2). Calcium silicate hydrates (CSH) and calcium alumina silicate hydrate (CASH), which are among the main hydrated phases formed at room temperature after pozzolanic reaction of metakaolin [30,32,33], were detected in very low amounts by means of X-ray diffraction because of their low crystallinity and reflecting powder.

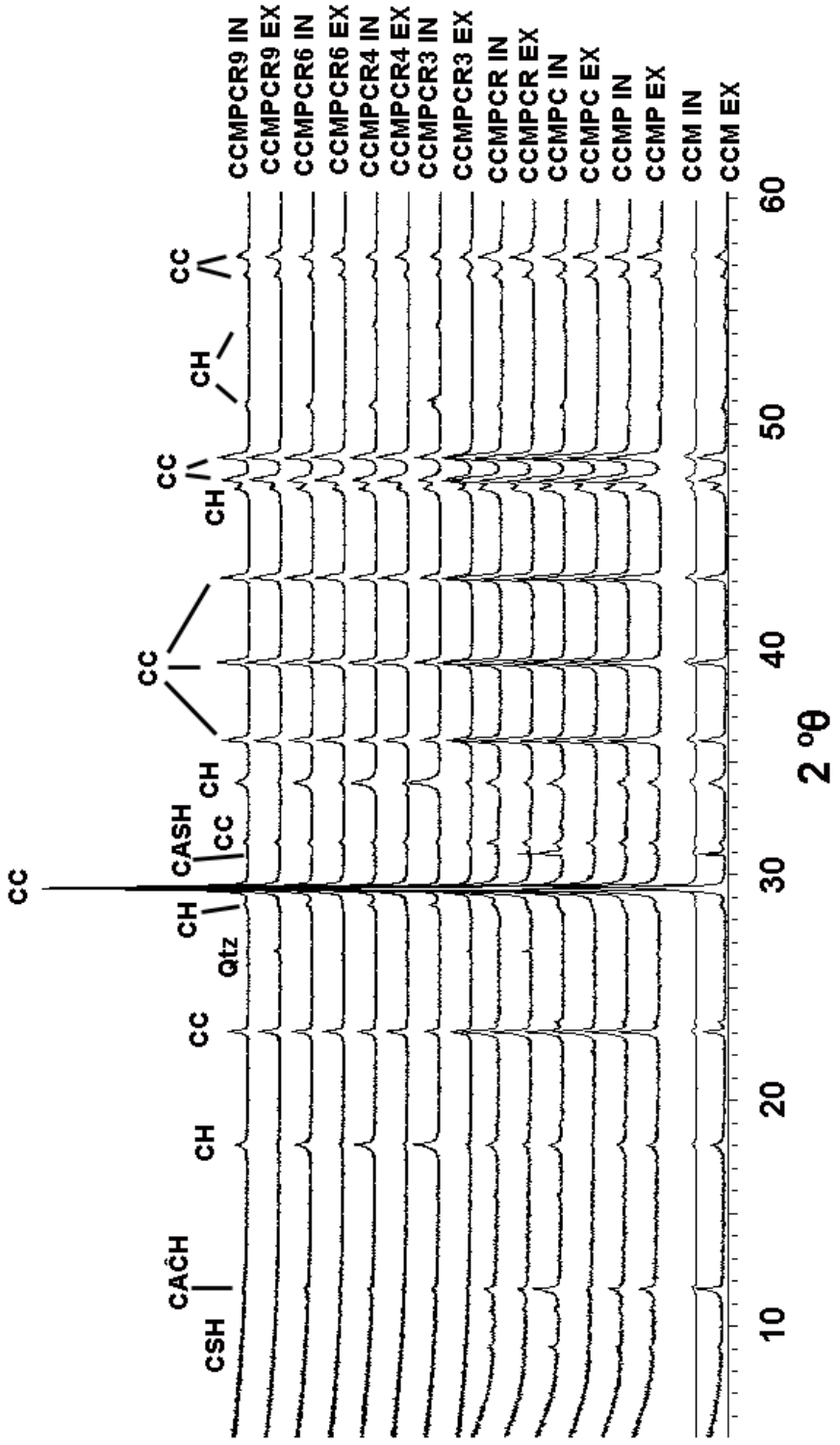

Figure III.2.2 X-ray diffraction pattern of external (EX) and internal (IN) zones of mortars with different amounts of admixtures and fixed B/S ratio and mortars with different B/S ratios and fixed amount of admixtures. CC = calcite, CH = portlandite, CAĈH: monocarboaluminate; CSH: calcium silicate hydrate; CASH: calcium alumina silicate hydrate; Qtz: quartz.

CSH and different calcium aluminate hydrates (CAH) were also detected by means of thermogravimetric analysis (TGA). The thermal decomposition of CSH occurs at temperature comprised between 100 and 125 ºC, whilst CAH decompose in a temperature range equal to 150-310 ºC. According to Saikia et al. [34], in the latter range of temperature both CAH and CASH decompose. Also portlandite and calcite were determined in the ranges of temperature of 350-480 and 650-900 ºC, respectively.

As it was expected, carbonation is more extended in the surface than in the core of mortar as indicated by the higher peaks of portlandite obtained in the internal samples.

3.2 Textural characteristics of mortars

The textural aspect of mortars (porosity, compactness, cohesion between aggregate grains and matrix, amount of the different phases) is shown in Fig. III.2.3. In general, the core of mortars appears more porous than the surface, and this is due to the fact that carbonation proceeds from the exterior to the interior of mortar (see differences between EX and IN, in the FESEM images of Fig. III.2.3).

Mortars with fixed B/S ratio show a similar cohesion and porosity (Figs. III.2.3a-d), whilst some differences of compactness were found in mortars with different B/S ratios (Figs. III.2.3e-h). In CCMPCR mortars with bigger lime content (1:3 and 1:4 B/S ratios, Figs. III.2.3e and f) the aggregate grains are not easily distinguished at low magnification because they appear completely recovered by the matrix. Whereas, in mortars with bigger amount of sand (1:6 and 1:9 B/S ratios, Figs. III.2.3g and h), this cohesion is worse and isolated grains of aggregate can be observed. This indicates that the latter mortars are characterised by a lower compactness.

3.3 Morphology of the hydrated phases

Aluminates (as CAĈH) crystallise as hexagonal platelets similar to those of portlandite but normally larger and thinner [30] (Figs. III.2.4a-f). Generally, they appear tangled in the mortar matrix, in some cases randomly oriented (Figs. III.2.4a and b) and in others in form of overlapping sheets oriented perpendicularly to the basal plane, along the [001] direction (Figs. III.2.4c-e). Bigger quantity of aluminates was found in CCM at higher magnifications (Fig. III.2.4a and c). On the other hand, few aluminate phases were found in mortars with different B/S ratios (i.e. CCMPCR3-9). As shown in Fig. III.2.4f, they have smaller size (almost 2 μm) and they occasionally share one plane. The common morphologies that calcium silicate hydrate ($CaO\text{-}SiO_2\text{-}H_2O$, i.e. CSH) phases adopt after precipitation are: fibres (Fig. III.2.4g), flakes (Fig. III.2.4h), honeycomb structure (Fig. III.2.4i), and reticular network (Fig. III.2.4j). In CCMPCR3 and CCMPCR4 mortars all the calcium silicate morphologies were observed (Fig. III.2.4i and j) whilst in the other mortars only fibres (Fig. III.2.4g) and flakes (Fig. III.2.4h) of CSH were recognised.

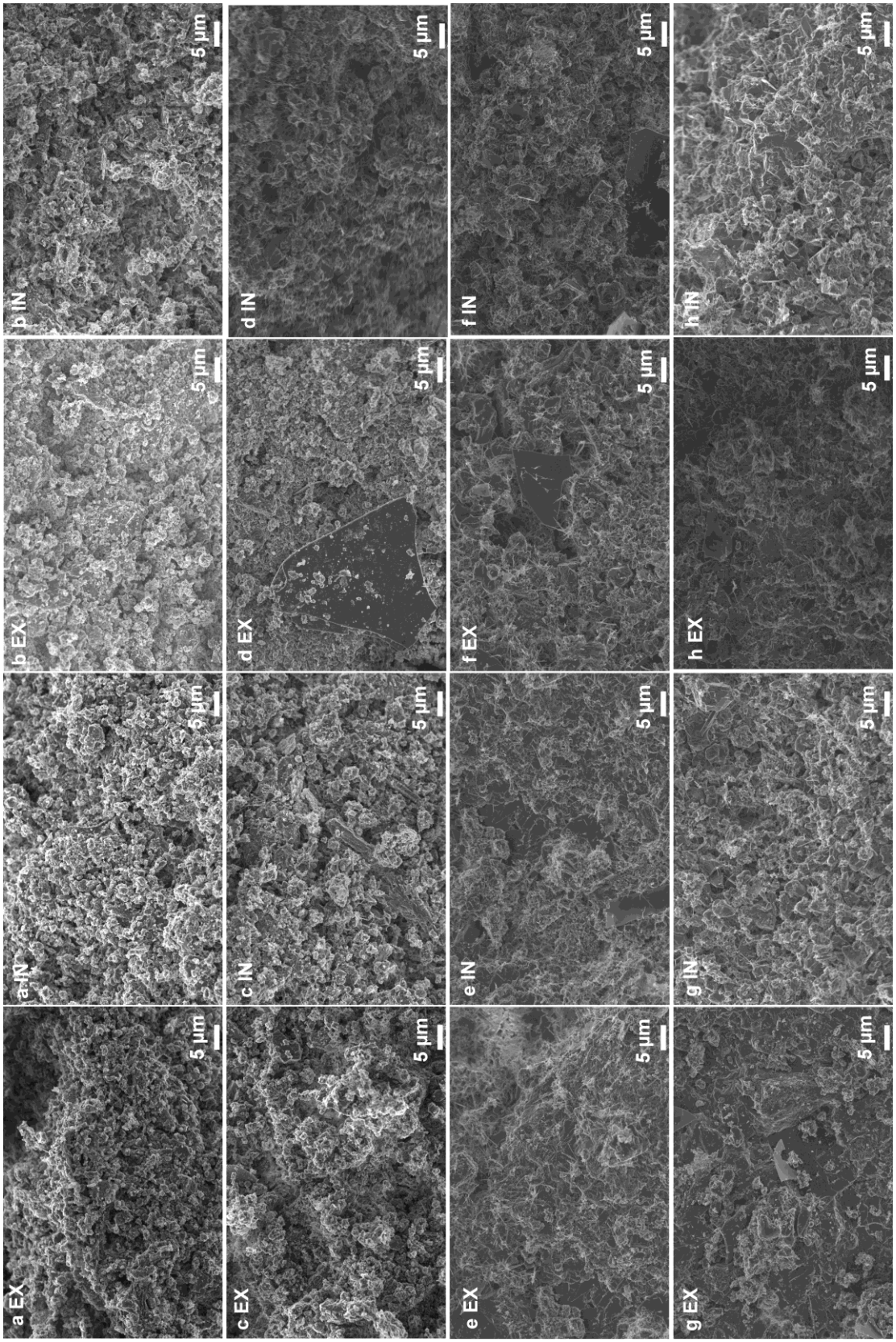

Figure III.2.3 *FESEM images of the eight types of mortars: differences in mortars texture between the surface (EX) and the core (IN) of CCM (a), CCMP (b), CCMPC (c), CCMPCR (d), CCMPCR3 (e), CCMPCR4 (f), CCMPCR6 (g) and CCMPCR9 (h).*

CSH phases do not appear in CCM at the magnification of 5000 X (Fig. III.2.3a EX and IN), whilst they are visible in CCMP (Fig. III.2.3b) and in lower quantity in CCMPC (Fig. III.2.3c) and CCMPCR (Fig. III.2.3d), always in the internal zone (IN) of the samples. This is an unexpected finding, given that these mortars were prepared with the highest quantity of metakaolin (Tab. III.2.2). On the other hand, a much bigger amount of CSH was observed in CCMPCR3-9 mortars at the same magnification (Fig. III.2.3e-h) and few evidences of aluminates were found. The amount of CSH phases seems to decrease with decreasing the lime content of mortars, being the biggest in CCMPCR3 (Fig. III.2.3e) and CCMPCR4 (Fig. III.2.3f), and the lowest in CCMPCR6 (Fig. III.2.3g) and CCMPCR9 (Fig. III.2.3h).

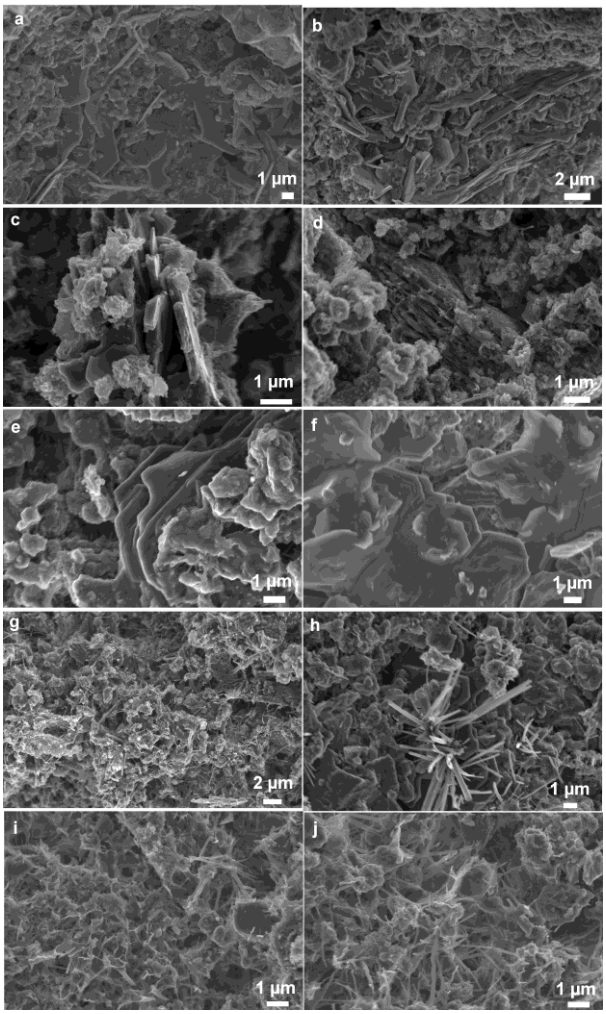

Figure III.2.4 *FESEM images of the hydrated phases (aluminate and silicate) formed after pozzolanic reaction in mortars: hexagonal AFm platelets randomly oriented observed in CCM (a) and CCMPCR (b); overlapping sheets of aluminate observed in CCM (c) and CCMPC (d); aluminate crystals oriented along the [001] direction in CCMPC (e); smaller AFm crystals precipitated in the matrix with hexagonal habit and identical orientation in CCMPCR3-9 mortars (f); CSH fibres in CCMP (g) and CSH isolated flakes in CCMPCR (h); honeycomb structure (i) and reticular network (j) of silicate hydrates in CCMPCR3-9 mortars.*

3.4 Morphology of the organic and inorganic admixtures

Perlite has a peculiar empty structure formed by big and ordered circular cavities (around 10-20 μm in size) (Fig. III.2.5a-c) that confers lightness to the mortar. Notwithstanding, it appears as a very fragile structure that is broken in many big fragments dispersed in the matrix (Fig. III.2.5d).

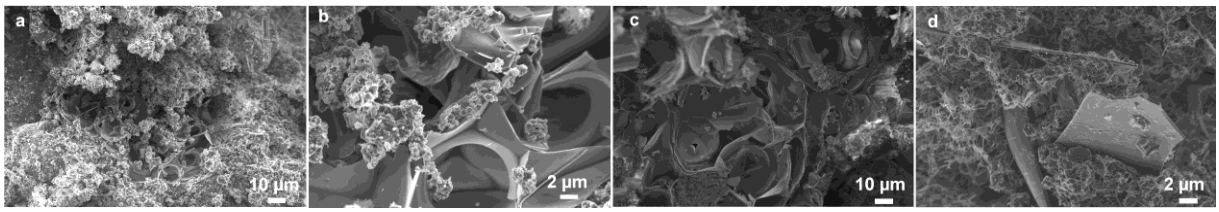

Figure III.2.5 *FESEM images of perlite in mortars: porous structure of this admixture observed in CCMP (a and b (detail)) and CCMPCR (c); fragments of perlite within the matrix of CCMPCR3-9 mortars (d).*

In CCMPCR mortars the porous structure of perlite was not observed in any sample, and only its fragments were found in the matrix. It is likely that the processes of mixing and kneading of the mortar, as well as the mechanical tensions produced during carbonation and hydration processes, cause the rupture of the perlite structure.

No evidences of the presence of the other admixtures (C and R, *cf.* Tab. III.2.2) were found by means of FESEM observations.

3.5 Characteristics of the pore system of mortars

3.5.1 Open porosity value

The values of open porosity of the surface and the core of mortars are presented in Table III.2.3. Mortars that present the highest porosity values (CCM, CCMP, CCMPCR) were prepared with the highest amount of kneading water (from 29 to 31.5%, *cf.* Tab. III.2.2). The porosity is lowered by about 3% in CCMPC mortar, because of the effect of the cellulose derivative (C) that retains the water longer in the matrix, like this preventing a rapid evaporation and the porosity formation. The introduction of the polycarboxylate causes the porosity to be higher in the interior than in the surface of mortars (see all CCMPCR and CCMPCR3-9 mortars compared to the others, Tab. III.2.3) that, in this case, indicates a normal behaviour of lime mortars, in which carbonation reduces porosity at the surface more than in the interior. This fact may indicate that the lime particles dispersion induced by the polycarboxylate gives place to an improvement of the lime reactivity towards CO_2. This difference of porosity between the surface and the core is constant in CCMPCR3-9

mortars, where the external samples showed a reduction of porosity by about 2% with respect to the internal ones.

CCMPCR and CCMPCR3 mortars, which differ only for the metakaolin and water dosage, show a porosity difference of about 4%. This suggests that in lime-based mortars an amount of metakaolin above 10% of the total binder gives place to a porosity increase. This is not in agreement with Frías and Cabrera'statement [35], who found that MK contents have no effect on the total porosity of metakaolin-cement pastes. On the other hand, the decrease of porosity found from mortar 1:3 to 1:9 must be related only with the different amounts of water used according to the initial lime content, since the MK proportion on the total binder is the same in these mortars.

Mortar name	MIP analysis		Mechanical assays	
	Zone	P_o	R_f	R_c
CCM	Ex	43.3±0.6	0.38±0.3	7.18±1.1
	In	34.2±6.6		
CCMP	Ex	42.7±0.4	2.72±0.3	8.57±0.7
	In	40.7±0.6		
CCMPC	Ex	39.1±0.1	3.04±0.2	8.27±0.2
	In	33.5±2.5		
CCMPCR	Ex	41.1±0.8	3.44±0.1	11.96±0.4
	In	44.1±1.3		
CCMPCR3	Ex	37.8±4.1	1.41±0.2	3.35±0.1
	In	39.9±6.2		
CCMPCR4	Ex	33.1±0.1	1.69±0.2	3.48±0.1
	In	35.9±0.3		
CCMPCR6	Ex	30.9±0.1	1.86±0.1	3.63±0.3
	In	32.7±0.2		
CCMPCR9	Ex	30.4±1.3	0.07±0.1	3.05±0.2
	In	32.2±0.5		

Table III.2.3 *Results of the mercure intrusion porosimetry (MIP) analysis and the mechanical assays on the eight types of mortar: open porosity (P_o, in %) of the external (Ex) and internal (In) zones of samples, flexural (R_f, in Mpa) and compressive (R_c, in Mpa) strengths.*

3.5.2 Pores size distribution curves (PSD)

The main peak obtained in all samples corresponds to pores whose radius is comprised between 0.1 and 1 μm and whose volume is the most influent on the total porosity of mortars (Fig. III.2.6). This is a structural peak, typical of lime pastes, whose height and width normally depend on the amount of kneading water [36]. Here, the presence of metakaolin makes the dependence between water content and pore size distribution not as clear as in lime mortars, since a part of the water is consumed during the pozzolanic reaction. In CCMPC and CCMPCR the main peak is

wider because a new small peak appears, contiguous to the main one and corresponding to bigger radius (around 0.6 μm). This peak has been observed also in MK-OPC pastes with MK contents up to 10% after 28 days of curing [35] and it is produced by the presence of metakaolin. Here, the peak at 0.6 μm is only evident in CCMPC and CCMPCR, perhaps because in the other mortars it is hidden by the peak at 0.1 and 1 μm.

In all mortars a second minor peak of pores whose radius is comprised between 0.01 and 0.1 μm is present. The presence of metakaolin results in the development of these smaller pores [35] normally formed by the network of hydrated calcium silicates (the range of these pores is $0.01<r<0.04$ μm, according to Pandey and Sharma [37]). The volume of these pores is much higher in mortars with 20% of metakaolin. Among these mortars, this peak is slightly bigger in CCMP, CCMPC and CCMPCR, in which more CSH phases were observed. In general, it appears slightly shifted to smaller radius in the internal samples. Mortars with only a 10% of metakaolin present a significant reduction of the volume of these pores. This suggests that the degree of hydration in CCMPCR3-9 mortars is lower with respect to the others, even if a bigger quantity of CSH phases has been observed during FESEM observations. Moreover, by comparing CCMPCR3-9 mortars PSD curves (Fig. III.2.6), one can notice that the volume of these pores is slightly bigger in CCMPCR3 and CCMPCR4, which were prepared with a higher content of binder (i.e. lime + metakaolin).

These findings confirm that pores with radius in the range of 0.01 and 0.1 μm are formed because of the presence of metakaolin and they indicate that these pores constitute a significant part of the pore system only when metakaolin is added to the binder in proportions bigger than 10%. Another important deduction that must be made according to the PSD curves obtained for CCMPCR3-9 mortars is that their pore system is similar to that of mortars with only calcitic lime and calcareous aggregate (i.e. without the addition of pozzolans and admixtures) which are almost exclusively characterised by pores in the range of 0.1 and 1 μm in size [38]. In addition to have the same pore system, CCMPCR mortars are characterised by a much lower porosity, which is a positive aspect in relation with their durability.

The presence of perlite does not affect the pore size distribution, which is similar to that obtained for CCM samples (Fig. III.2.6). The pores of the unbroken structure of perlite observed in some zones by means of FESEM (Fig. III.2.5a-c), whose main size is 20 μm, do not appear in these curves probably because the pressure of mercury during the MIP analysis destroys this structure, which seems to be very fragile, as discussed in section 3.4.

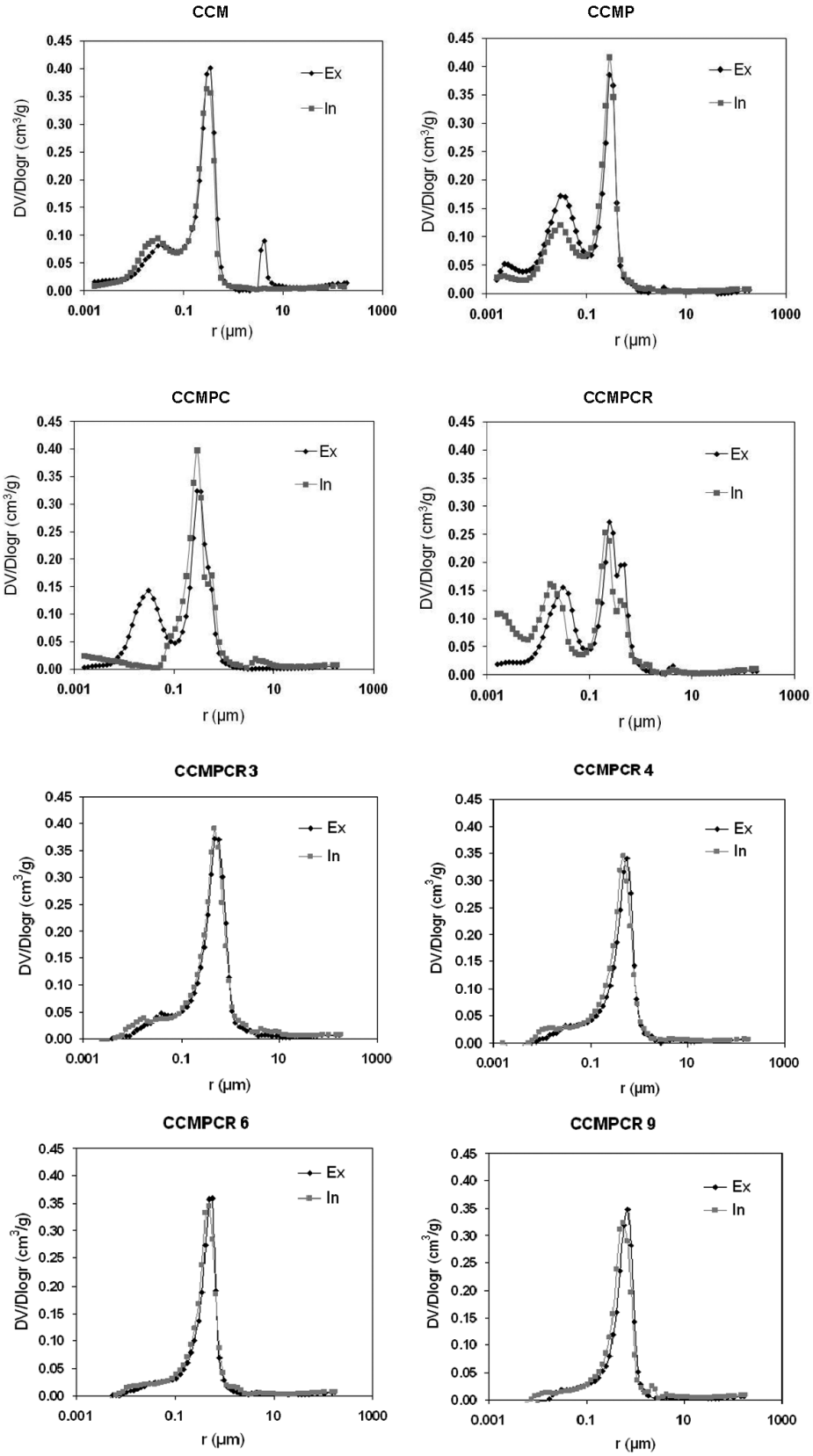

Figure III.2.6 *Pore size distribution curves of external (Ex) and internal (In) zones of mortars. The radius of pores (r, in µm) is represented in function of the incremental volume of mercury intruded (DV/Dlogr, in cm^3/g).*

3.6 Mechanical properties of mortars

As shown in Table III.2.3, mechanical strengths (both R_f and R_c values) of mortars with a pozzolan and other admixtures are much higher than those of aerial lime-based mortars composed by only lime and aggregate (up to 2 MPa) [39,40].

We have obtained increasing values of compressive and flexural strengths with increasing aggregate proportions, except for the mortar with the lowest B/S ratio (CCMPCR9). The function of the aggregate in a mortar stays in conferring volume stability to the lime paste and in improving its mechanical resistance. Notwithstanding, a too high content of aggregate may result in a mortar with poor cohesion between the grains (low binding ability) and, consequently, with lower mechanical resistances.

The values of mechanical strengths of mortars also indicate that a 20% of metakaolin content produces a larger enhancement of the mechanical strengths, compared to a 10% metakaolin content, which has produced values of compressive strength between twice and three times lower. This finding is in agreement with a previous study carried out by Wild et al. [41] on metakaolin-cement pastes, in which the optimum amount of metakaolin in replacement of OPC for the strength enhancement was found to be about 20%.

The presence of admixtures affects strongly the compressive resistance of the mortars prepared with 20% of metakaolin. An increase of R_f and R_c is obtained with the addition of perlite and, mainly, of the polycarboxylate because of its ability in dispersing the lime particles and thus reducing the quantity of voids in the matrix [24]. On the other hand, the cellulose derivative decreases slightly the mortar compressive strength, as also found by other authors [5,7].

4. Conclusions

This study aimed to find out differences in the mineralogical, morphological and textural characteristics and in the mechanical properties of aerial-lime based mortars induced by the addition of a pozzolanic additive (metakaolin) and inorganic (perlite) and organic (cellulose derivative and polycarboxylate) admixtures.

It has been observed that the pozzolan leads to the formation of hydrated phases such as CSH, CASH and CAĈH, whilst the perlite, the cellulose derivative and the plasticiser do not produce any mineralogical and morphological change in mortars. The amount of the hydrated phases was found to be small according to the X-ray diffraction analysis, whilst many non-crystalline CSH phases have been observed by means of scanning electron microscopy, especially in samples with 10% of metakaolin.

Important variations of the open porosity values have been found in all mortars, as consequence of the amount of water used for their preparation, which in turn is affected by the presence of the organic

admixtures. On the other hand, the only additional component that affects the pore size distribution is the pozzolan, which leads to the formation of pores with radius comprised between 0.01 and 0.1 μm. It is fundamental to point out that this family of pores is only present in mortars prepared with 20% of metakaolin content on the total binder, whilst the pore system of mortars with 10% of metakaolin is closer to that of aerial lime mortars without additives.

The addition of 20% of metakaolin also causes a bigger strength enhancement. Among the mortars prepared with the lowest metakaolin content (10%), those with higher content of binder (i.e. lime + metakaolin) are characterised by higher porosity values and lower mechanical strength. Notwithstanding, it has been found that the use of a binder-to sand proportion higher than 1:6 does not lead to any change in the pore system (open porosity value and pore size distribution) but instead produces a decrease in the mechanical strength of mortar.

This paper demonstrates that, by establishing adequate proportions of pozzolanic additives and admixtures, it is possible to improve mortars properties without modifying excessively the original characteristics of the aerial lime mortar. This aspect is crucial in the design of aerial lime-based mortars that have to be applied in restoration works. In this sense, we have demonstrated that it is possible to overcome the inconveniences of the application of an aerial lime based mortar (for example, slow hardening process and high porosity) by means of the use of additives in adequate proportions, at the same time avoiding undesired modifications of the hardened properties (for example, an excessive improvement of the mechanical strength), which might cause incompatibility with the original materials.

In view of these results, we consider that a metakaolin content of 10% on the total binder, a B/S proportions between 1:4 and 1:6 and a total amount of admixtures lower than 2% on the total mass can be the appropriate dosages for the obtaining of compatible and durable repair mortars with good workability in the fresh state, low shrinkage and low mechanical strengths, which can be used, for example, as rendering materials.

Acknowledgements:

This study was financially supported by Research Group RNM179 of the Junta de Andalucía and by Research Project P09-RNM-4905. We are grateful to ARGOS DERIVADOS DEL CEMENTO S.L. (Granada) for providing the raw materials used in this study.

References

[1] RILEM TC 203-RHM: Repair mortars for historic masonry. Testing of hardened mortars, a process of questioning and interpreting. Mater Struct 2009; 42:853-65.

[2] Cazalla O. Morteros de cal. Aplicación en el Patrimonio Histórico. Ph.D. Thesis. Universidad de Granada; 2002.

[3] Veniale F, Setti M, Rodriguez-Navarro C, Lodola S, Palestra W, Busetto A. Thaumasite as decay product of cement mortar in brick masonry of a church near Venice. Cem Concr Compos 2003; 25:1123-29.
[4] Callebaut K, Elsen J, Van Balen K, Viaene W. Nineteenth century hydraulic restauration mortars in the Saint Michael's Church (Leuven, Belgium). Natural hydraulic lime or cement?. Cem Concr Res 2001; 31:397-403.
[5] Edmeades RM, Hewlett PC Cement admixtures. Lea's Chemistry of Cement and Concrete. 5th ed.: Arnold; 1998.
[6] Ruiz-Agudo E, Rodriguez-Navarro C. Effects of additives on lime putty rheology: applications in the design of mortars for conservation purposes. In: proceedings 1st Historical Mortars conference, Lisbon; 2008. p. 24-26.
[7] Paiva H, Esteves LP, Cachim PB, Ferreira VM. Rheology and hardened properties of single-coat render mortars with different types of water retaining agents. Constr Build Mater 2009; 23:1141-46.
[8] Seabra MP, Paiva H, Labrincha JA, Ferreira VM. Admixtures effect on fresh state properties of aerial lime based mortars. Constr Build Mater 2009; 23:1147-53.
[9] Izaguirre A, Lanas J, Alvarez JI. The use of water-repellent admixtures on the behaviour of aerial lime-based mortars. Cem Concr Res 2009; 39:1095-104.
[10] Izaguirre A, Lanas J, Alvarez JI. Aging of lime mortars with admixtures: durability and strength assessment. Cem Concr Res 2010; 40:1081-95.
[11] Baronio G, Binda L, Lombardini N. The role of brick pebbles and dust in conglomerates based on hydrated lime and crushed bricks. Constr Build Mater 1997; 11(1): 34-40.
[12] Baronio G, Binda L. Study of the pozzolanicity of some bricks and clays. Constr Build Mater 1997; 11(1): 41-46.
[13] Papayianni I. The longevity of old mortars. Appl Phys A-Mater 2006; 83:685-8.
[14] Papayianni I, Stefanidou M. Durability aspects of ancient mortars of the archeological site of Olynthos. J Cult Her 2007; 8:193-6.
[15] Khatib JM, Wild S. Sulphate resistance of metakaolin mortar. Cem Concr Res 1998; 28(1):83-92.
[16] Malhotra SK, Dave NG. Investigations into the effect of addition of fly ash and burnt clay pozzolana on certain engineering properties of cement composites. Cem Concr Comp 1999; 21:285-91.
[17] Sabir BB, Wild S, Bai J. Metakaolin and calcined clays as pozzolans for concrete: a review. Cem Concr Comp 2001; 23:441-54.
[18] Blanco F, Garcia MP, Ayala J, Mayoral G, Garcia MA. The effect of mechanically and chemically activated fly ashes on mortars properties. Fuel 2006; 85:2018-26.
[19] Al-Akhras NM. Durability of metakaolin concrete to sulfate attack. Cem Concr Res 2006; 36:1727-34.
[20] Siddique R, Klaus J. Influence of metakaolin on the properties of mortar and concrete: A review. Appl Clay Sci 2009; 43:392-400.

[21] Lanzón M, García-Ruiz PA. Lightweight cement mortars: advantages nand inconveniences of expanded perlite and its influence on fresh and hardened state and durability. Constr Build Mater 2008; 22:1798-806.
[22] Topçu IB, Isikdag B. Manufacture of high conductivity resistant clay bricks containing perlite. Build Environ 2007; 42:3540-46.
[23] Patural L, Marchal P, Govin A, Grosseau P, Ruot B, Devès O. Cellulose ethers influence on water retention and consistency in cement-based mortars. Cem Concr Res 2011; 41:46-55.
[24] Kwan AKH, Wong HHC. Effects of packing density, excess water and solid surface area on flowability of cement paste. Adv Cem Res 2008; 20 (1):1-11.
[25] EN 459-1. Building lime. Part 1: Definitions, specifications and conformity criteria; 2001.
[26] ASTM C618-08. Standard Specification for Coal Fly Ash and Raw or Calcined Natural Pozzolan for Use in Concrete. Annual Book of ASTM Standard, 4.02; 2008.
[27] EN 1015-3. Methods of test for mortar for masonry - Part 3: Determination of consistence of fresh mortar (by flow table); 1999.
[28] EN 1015-11. Methods of test for mortar for masonry. Part 11: Determination of flexural and compressive strength of hardened mortar; 1999.
[29] Martín Ramos J.D. XPowder. A software package for powder X-ray diffraction analysis. Lgl. Dep. GR 1001/04; 2004.
[30] Cizer O. Competition between carbonation and hydration on the hardening of calcium hydroxide and calcium silicate binders. PhD Thesis. Katholieke Universiteit Leuven; 2009.
[31] Matschei T, Lothenbach B, Glasser FP. The role of calcium carbonate in cement hydration. Cem Concr Res 2007; 37:551-8.
[32] De Silva PS, Glasser FP. Phase relations in the system CaO-Al_2O_3-SiO_2-H_2O relevant to metakaolin-calcium hydroxide hydration. Cem Concr Res 1993; 23:627-39.
[33] Rojas MF, Cabrera J. The effect of temperature on the hydration rate and stability of the hydration phases of metakaolin-lime-water systems. Cem Concr Res 2002; 32:133-8.
[34] Saikia N, Kato S, Kojima T. Thermogravimetric investigation on the chloride binding behaviour of MK-lime paste. Thermochim Acta 2006; 444:16-25.
[35] Frías M, Cabrera J. Pore size distribution and degree of hydration of metakaolin-cement pastes. Cem Concr Res 2000; 30:561-9.
[36] Arandigoyen M, Pérez Bernal JL, Bello López MA, Alvarez JI. Lime-pastes with different kneading water: pore structure and capillary porosity. Appl Surf Sci 2005; 252:1449-59.
[37] Pandey SP, Sharma RL. The influence of mineral additives on the strength and porosity of OPC mortar. Cem Concr Res 2000; 30:19-23.
[38] Lanas J, Alvarez JI. Masonry repair lime-based mortars: factors affecting the mechanical behaviour. Cem Concr Res 2003; 33:1867-76.

[39] Lanas J, Sirera R, Alvarez JI. Study of the mechanical behaviour of masonry repair lime-based mortars cured and exposed under different conditions. Cem Concr Res 2006; 36:961-70.
[40] Arizzi A, Martínez-Martínez J, Cultrone G, Benavente D. Mechanical evolution of lime mortars during the carbonation process. Key Eng Mater 2011; 465:483-6.
[41] Wild S, Khatib JM, Jones A. Relative strength, pozzolanic activity and cement hydration in superplasticised metakaolin concrete. Cem Concr Res 1996; 26 (10):1537-44.

Concluding Remarks

The idea of using a white Portland cement as additive has been discarded since it has a deleterious effect on the durability of mortars. Even if, as expected, the cement has been effective in reducing shrinkage, its use cannot be considered in the design of repair mortars (*chapter III.1*).

A great step forward has been taken with the study carried out in *chapter III.2*.

Firstly, it has been pointed out that the metakaolin content plays an important role both in the pore system and in the mechanical resistances of the lime mortars. When the proportion is the 20% of the lime, mortars with high mechanical strengths and porosity are obtained. Since these characteristics are not the most suitable for rendering mortars, only the 10% proportion is kept for the following investigations, whilst the 20% one is no longer considered in this thesis.

Secondly, the use of three admixtures together seems to be an efficacious way to reduce the water dosage and, consequently, porosity. Interestingly, this has been possible with a small amount of admixtures (less than the 2%). In this way, the mortar composition is still very close to that of the mortar prepared only with lime, metakaolin and aggregate, which is a benefit in terms of compatibility.

Further researches are needed to settle the most suitable binder-to-aggregate content to be employed.

PART IV

The durability of mortars: a study of their behaviour for rendering applications.

Objectives

Part IV arises as a continuation of the mineralogical, morphological, textural and mechanical studies performed in part III, and it tackles another essential aspect of mortars quality: the durability.

The study presented in *chapter IV.1* concentrates on the assessment of the behaviour of mortars towards water movements. The relationship between the mortars hydric parameters and microstructure is also considered, thus linking the results achieved in *chapter III.2* to this last part of the thesis.

Moreover, the shrinkage of mortars is also measured in *chapter IV.1*, in order to consider its potential influence on the hydric properties and final performances of each mortar.

Chapter IV.2 deals with the study of the different factors that affect mortars durability, by performing new laboratory ageing tests that have been designed specifically for rendering mortars and include a wide range of atmospheric conditions and ageing agents (e.g. water and salt).

This study rises especially from the perplexity about the adoption of standardized methods for evaluating the durability of mortars. Standards are often not very specific, with the consequence that they are used in an indiscriminate way on a wide materials range. In the specific case of rendering mortars, only a general recommendation about performing freezing-thawing cycles exists [(*)]. Therefore, the durability study presented in *chapter IV.2* claims to supply a reference for the assessment of mortars longevity.

To conclude, part IV has the final aim of defining the most suitable rendering mortar among those designed in this thesis.

[(*)]UNE EN 998-1 (2003). Specification for mortar for masonry - Part 1: Rendering and plastering mortar. AENOR, Madrid.

Chapter IV.1

The water transfer properties and plastic shrinkage of aerial lime-based mortars: an assessment of their quality as rendering materials

Arizzi A., Cultrone G.
Submitted to *Journal of Cultural Heritage*

Abstract

Water (in the solid, liquid and vapour state) is one of the main factors that drive construction materials to deterioration. To assess the quality and durability of a rendering mortar, thus ensuring its protective function in the masonry structure, it is fundamental to study the behaviour of this mortar towards water. Mortars were elaborated with a calcitic dry hydrated lime, a calcareous aggregate, a pozzolan, a lightweight aggregate, a water-retaining agent and a plasticiser.

The effect of different binder-to-aggregate proportions on the mortars hydric behaviour was assessed, by performing free water absorption and drying, capillary uptake, hydraulic conductivity and water vapour permeability tests. Another aspect that was considered in the assessment of mortar quality was the plastic shrinkage that was measured by means of a non-standardized device. It has been found that higher amount of water are absorbed by mortars with higher lime content, whilst faster drying and higher permeability to water and water vapour are obtained in mortars with higher aggregate content. The hydric behaviour, as well as the plastic shrinkage of mortars have been interpreted taking into account the differences in microstructure and pore system between mortars.

1. Introduction

In the last decades, many investigations have been carried out to understand the mechanisms of deterioration driven by water in building materials [1-5]. Processes like moisture gas diffusion [6], rising damp [6-7], draining rain [8], freezing-thawing phenomena [9], salts transport and crystallization [10] and biodeterioration [11] occur in the majority of the historic and modern buildings all over the world.

The practice of rendering, i.e. covering a wall or a building façade with one or more layers of mortar, has the main aim to protect the masonry structure against the processes above mentioned, which are all driven by water [7,8,12]. Repair mortars, in general, are considered "sacrificial" materials because, as explained by Maurenbrecher [13], "it is easier to repair mortar joints than replace masonry units". In the same way, a rendering mortar is a "sacrificial layer" that fulfils a protective function towards the substrate (stone, brick, concrete). Therefore, to evaluate the quality and durability of a rendering mortar, thus ensuring its protective function in the masonry structure, it is fundamental to assess the behaviour of this mortar towards water.

In the case of structural (with a "joining" function) or rendering mortars, the water absorption should be not very different to that of the existing masonry materials [13,14], in order to ensure a homogeneous flow of water through different materials, to avoid the localisation of water in certain zones of the masonry (which would lead it to a faster deterioration). In addition, water vapour transmission rates should be higher so as to encourage drying through the mortar [15]. In practice, the drying of a porous surface occurs in two stages: the early stage, which depends mainly on the conditions of temperature, relative humidity and ventilation, and the later stage, which is determined primarily by the water transfer properties of the material [16]. This explains the importance of ensuring a fast drying kinetics in a rendering mortar.

The aim of this work is to assess the water transfer properties of aerial lime-based mortars designed for rendering purposes. Four types of mortars of the same composition but different binder-to-aggregate ratios have been compared, in order to determine which proportions give place to a mortar with the best hydric behaviour and, consequently, the highest durability. Mortars were elaborated with a pozzolanic additive and different admixtures. The study was carried out by performing hydric assays on laboratory samples, which allowed assessing water absorption and drying, capillary uptake, hydraulic conductivity and water vapour permeability in mortars. By means of these tests, we were able to establish a relationship between the hydric behaviour of mortars and their microstructural characteristics. Indeed, the water transfers through a mortar are influenced by its pore system; in particular main pore size and tortuosity are the factors that most determine the amount of water absorbed and the kinetics of absorption/desorption [17].

However, there is another factor that is not taken into account during the hydric assays but which plays an important role in the water transfer properties of a rendering mortar: the shrinkage. This process, caused by the rapid evaporation of the kneading water (i.e. water added to the mortar mixture) with the final formation of cracks, is especially strong in aerial lime-based mortars, which need more water for their mixing. On the one hand, shrinkage is a negative aspect for mortar durability since it gives place to open ways of access through which water can entry and diffuse easily. On the other hand, the presence of shrinkage fissures allows maintaining water moisture diffusion from the substrate to the surface [18]. These factors are rarely taken into consideration during the hydric assays performed in laboratory, since mortar samples of 4×4×16 or 4×4×4 cm in size do not undergo to such degree of shrinkage. For this reason, the mortar shrinkage in large samples was also studied here and then considered in the final assessment of mortars hydric properties.

2. Materials and Methods

2.1 Mortars preparation

Four mortars types were elaborated with the following components: a calcitic dry hydrated lime (CL90-S [19]; ANCASA, Seville, Spain), a calcareous aggregate (CA, 0.063<ø<1.5 mm), a pozzolanic additive (CLASS N POZZOLAN, [20]; Burgess Pigment Company, USA), and three different admixtures: a lightweight aggregate (perlite), a water-retaining agent (cellulose derivative) and a plasticiser (polycarboxylate) (additional detail of these components can be found at www.argosdc.com). The mortars have been labelled CCMPCR3, CCMPCR4, CCMPCR6, CCMPCR9, according to their binder-to-aggregate (B/A) ratio (1:3, 1:4, 1:6 and 1:9 by weight); the pozzolan was kept at 10% of the total binder (by mass) and the total admixtures proportion was less than 2% of the total mass. The fresh mortar pastes had a flow comprised between 120 and 150 mm [21]. The components and dosages used in each mortar are shown in Table IV.1.1.

Mortars name	Components name and proportions			Water
	B/S	MK	P+C+R	
CCMPCR3	1:3	10	1.7	28.0
CCMPCR4	1:4	10	1.7	26.5
CCMPCR6	1:6	10	1.7	21.5
CCMPCR9	1:9	10	1.7	20.0

Table IV.1.1 *Proportions of components used in the elaboration of the four mortar types. Abbreviations indicate: binder-to sand ratio (B/S, by weight); metakaolin (MK, in % of the total weight of the binder); perlite (P); cellulose derivative (C); polycarboxylate (R). The total amount of admixtures (P+C+R) is in % of the total weight of mortar. The amount of*

kneading water (as % of the total weight) was determined in order to obtain a paste with a flow comprised between 120 and 150 mm.

Mortars were conserved during 7 days in normalized steel moulds (4×4×16 cm) at T = 20±5 °C and RH = 60±5%, instead of being cured at a RH of 95%, following the modification of the standard EN 1015-11 [22] proposed by Cazalla [23]. After desmoulded, they were cured at the same conditions of T and RH for 60 days in total. The pore system of these mortars was determined in a previous study [24].

2.2 Hydric assays

Free water absorption, drying, capillary imbibition, hydraulic conductivity and water vapour permeability tests were performed to study the hydric properties of mortars. Hydric tests were not performed until the mortars had been cured for 60 days, because "younger" mortars are less compact and lime may dissolve in water. Mortar samples were oven-dried at 100 ºC for 24 h before measurements were taken.

2.2.1 Free water absorption and drying

The absorption and drying kinetics were evaluated on three samples (4×4×4 cm) per type by measuring the changes in the mass of mortar samples over time, due to the movements of water in the pore system. The absorption coefficient (C_a) was determined as the slope of the curve representing the weight increase as a function of the square of time 4 minutes after the beginning of the test [25]. The drying index (I_d) was measured according to the NORMAL 29-88 standard [26].

2.2.2 Capillary uptake

Capillary rise was performed on three samples of 4×4×16 cm, according to the UNI EN 1925 [27]. Two imbibition coefficients (A and B) were determined from the mass uptake per surface unit and the height over time, following the Beck et al. [6] procedure.

2.2.3 Hydraulic conductivity

The hydraulic conductivity (or permeability to water) of mortars was determined with the falling head method, by means of the experimental apparatus performed by Domenico and Scwartz [28].

Previous to the experiment, prismatic samples 2×4×4 cm in size were polished to reduce as much as possible the roughness in the surface and their edges were rounded off (Fig. IV.1.1a). This was necessary for the next preparation step, in which samples were wrapped in a single length PTFE tape (plumber's thread sealing tape) to create at least ten overlapping layers that completely cover the largest surface of the sample (Fig. IV.1.1b). To compress the tape-layer into the surface of the mortar and produce a watertight sleeve, samples were then encapsulated with electrician's heat shrinkable sleeving (Fig. IV.1.1c). The heat shrinkable sleeving was shrunken with a hot-air gun to its minimum diameter. The water flow during the permeability test would be possible only in one direction, through two parallel surfaces of the samples. Samples were

stored underwater for one day and then completely saturated under vacuum before the test. After this, each sample was connected to the standpipe of the falling head permeameter (Fig. IV.1.1d) using a rubber bung that was pushed into the sleeving of the prepared sample (Fig. IV.1.1e). The height was recorded from the water level in the trough, in which the samples were kept submerged.

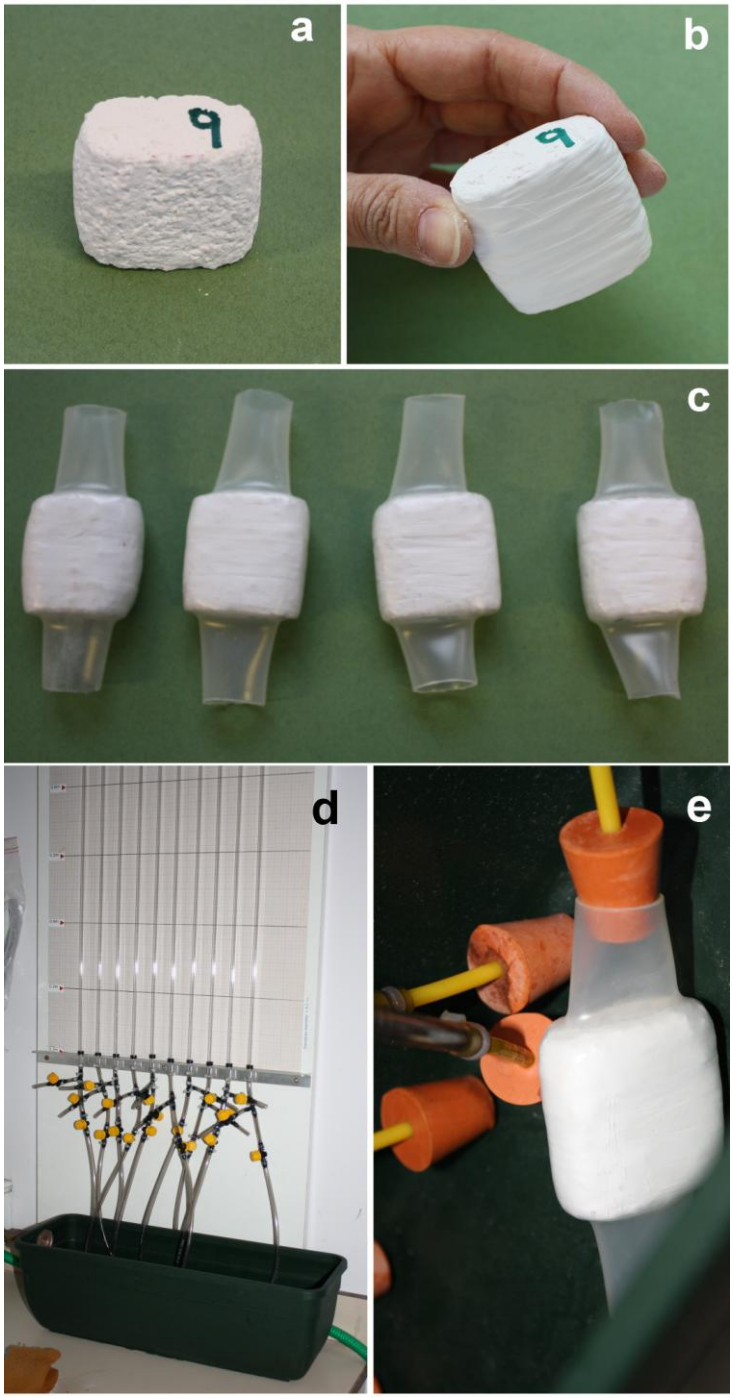

Figure IV.1.1 *Falling head water permeability test. (a) polishing and smoothing of the sample; (b) covering of the sample surface with PTFE tape; (c) aspect of the samples after being encapsulated with electrician's heat shrinkable sleeving; (d) falling head permeameter; (e) connection of the sample to the standpipe using a rubber bung.*

The time required for a given change in head at different intervals was noted manually and used in the Eq. IV.1.1 to determine hydraulic conductivity. This equation is derived from equating flow through the tube with flow through the sample:

$$K_h = \frac{aL}{At} \ln\left(\frac{h_1}{h_2}\right) \qquad [IV.1.1]$$

where K_h is the hydraulic conductivity (in ms^{-1}), *a* is the cross sectional area of the tube (in m^2), *L* is the length of core (in m), *A* is the cross sectional area of cores (in m^2), *t* is the time (in s) taken for head fall from initial head h_1 to final head h_2.

2.2.4 Water vapour permeability

The water vapour permeability (K_v, in $gm^{-2}h^{-1}$) was determined on three samples (1.5×4×4 cm) per mortar type, oven-dried at 90 ºC for 24 hours before the measurement. Afterwards, they were placed in experimental permeameters (Fig. IV.1.2) filled with deionised water, avoiding the contact of water with the sample surface. Permeameters were then sealed by using dishes of silicon rubber. The water vapour permeability assay was performed for 5 days in total, at controlled conditions of temperature (T = 25 ºC). The whole mass (permeameter + sample + water) was recorded every day and a lineal trend curve was obtained from the mass drop over time.

Figure IV.1.2 Image of a water vapour permeameter.

The water vapour permeability was calculated according to the following equation:

$$K_v = \frac{\frac{\Delta M}{S}}{t} \cdot 0.7378 \cdot e \qquad [IV.1.1]$$

where *ΔM/S* is the mass variation of the permeameter + sample + water per surface unit (surface of the sample exposed to vapour), *t* is the duration time of the assay, *0.7378* is a correction factor applied to determine the hydraulic conductivity value at T = 20 ºC, as established in the NORMAL 21/85 [29] standard and *e* is the sample thickness.

2.3 Samples dimensional variations (shrinkage)

A SWG-H-400 shrinkage-measuring device (ARGOS Derivados del Cemento S.L., Granada, Spain) was used to measure the initial shrinkage of mortars. This apparatus measures the horizontal dimensional variations of a fresh mortar, by means of two sensors connected to a PC.

The internal surfaces of the apparatus were covered with a polyethylene film to easy the mortar removal after the measurement. The fresh mortar mixture (~ 3 kg) was poured into the apparatus and the sensors were connected to the two extremities. These sensors recorded the length of the mortar sample each 30 minutes during 7 days and data were collected simultaneously by a computer. This allowed obtaining a curve of shrinkage over time, the slope of which corresponded to the shrinkage coefficient (C_{shr}, mm/h). In addition, the shrinkage percentage on the length of the sample measured was determined.

3. Results and discussion

3.1 Hydric behaviour of mortars

The possible alteration of mortars microstructure due to the reactions with water should be taken into account in the interpretation of the hydric behaviour of mortars.

3.1.1 Free water absorption and drying

The water absorption curves (Fig. IV.1.3a) show a first section with sharp slope, which indicates fast water absorption within the first hour, and by a second section with a very slight, almost plane, slope, which suggests that mortars continued absorbing water at a much lower rate during the following 15 days, until reaching a constant weight. Trapped water might have been present in the mortars pore network, thus producing a very slow final absorption rate [16]. The absorption coefficients (Tab. IV.1.2) values indicate that mortars with higher lime content presented a higher water absorption. As shown in the inset of Fig. IV.1.3a, CCMPCR3 mortars samples absorbed water slower than CCMPCR4 during the first 4 minutes and this is reflected in the C_a value of this mortar. This different absorption rate at the beginning of the test might be due to the fact that CCMPCR3 is characterized by a higher amount of metakaolin, i.e. of reactive phases that turn into hydrated phases if they react with water; this would produce little changes in the microstructure, thus giving place to an initial water absorption slightly slower than the expected. This fact confirms the modifications of microstructure produced

by the formation of hydrated phases [24]: if further hydration occurs, this would increase the volume of smallest pores (in the range between 0.01 and 0.1 μm), with a consequent decrease of mortar water absorption rate [16,30,31]. This is, in fact, what occurred in CCMPCR3 samples. However, after the first minutes, the water uptake is the highest in CCMPCR3 that, indeed, is characterized by the highest volume of pores (Tab. IV.1.2).

During the water absorption test, a small quantity of material was lost from the mortars samples, especially CCMPCR9. In general, this occurred because mortars were only partially carbonated after two months and the lime was likely to dissolve in water. In the specific case of CCMPCR9 mortar, however, the loss of material was more likely because of the low cohesion between the aggregate grains and the matrix [24].

Interestingly, the highest value of drying index was obtained in CCMPCR9 mortar, whilst the other mortars present similar values among them (Tab. IV.1.2). This should indicate that, in this mortar, water evaporates slightly faster than in the others. In reality, all mortars showed a very similar drying behaviour, as reflected in the similar slopes of the drying curves (Fig. IV.1.3b). The only difference between these curves is that the weight variation in CCMPCR9 samples reached zero (that corresponds to the initial weight) at the end of the test, whilst the other mortars did not. Their curves, in fact, remained asymptotical to the x-axis. Theoretically, also CCMPCR9 would have given a similar curve to the other samples, if it had not loose material, then weight, during the water absorption test.

Mortar name	MIP analysis*		Hydric assays			
	Zone	P_o	C_a	I_d	A	B
CCMPCR3	Ex	37.8±4.1	9.61	0.49	0.04	6.80
	In	39.9±6.2				
CCMPCR4	Ex	33.1±0.1	9.84	0.49	0.04	7.47
	In	35.9±0.3				
CCMPCR6	Ex	30.9±0.1	7.95	0.46	0.03	5.13
	In	32.7±0.2				
CCMPCR9	Ex	30.4±1.3	6.89	0.53	0.03	-
	In	32.2±0.5				

* values according to Arizzi and Cultrone [24]

Table IV.1.2 *Open porosity* (P_o, in %) of the external (Ex) and internal (In) zones of samples; absorption coefficient (C_a, in g/min$^{1/2}$); drying index (I_d); imbibition coefficients (A, in g/cm^2 min$^{1/2}$ and B, in cm/min$^{1/2}$). – B value was not calculated for CCMPCR9 mortar.*

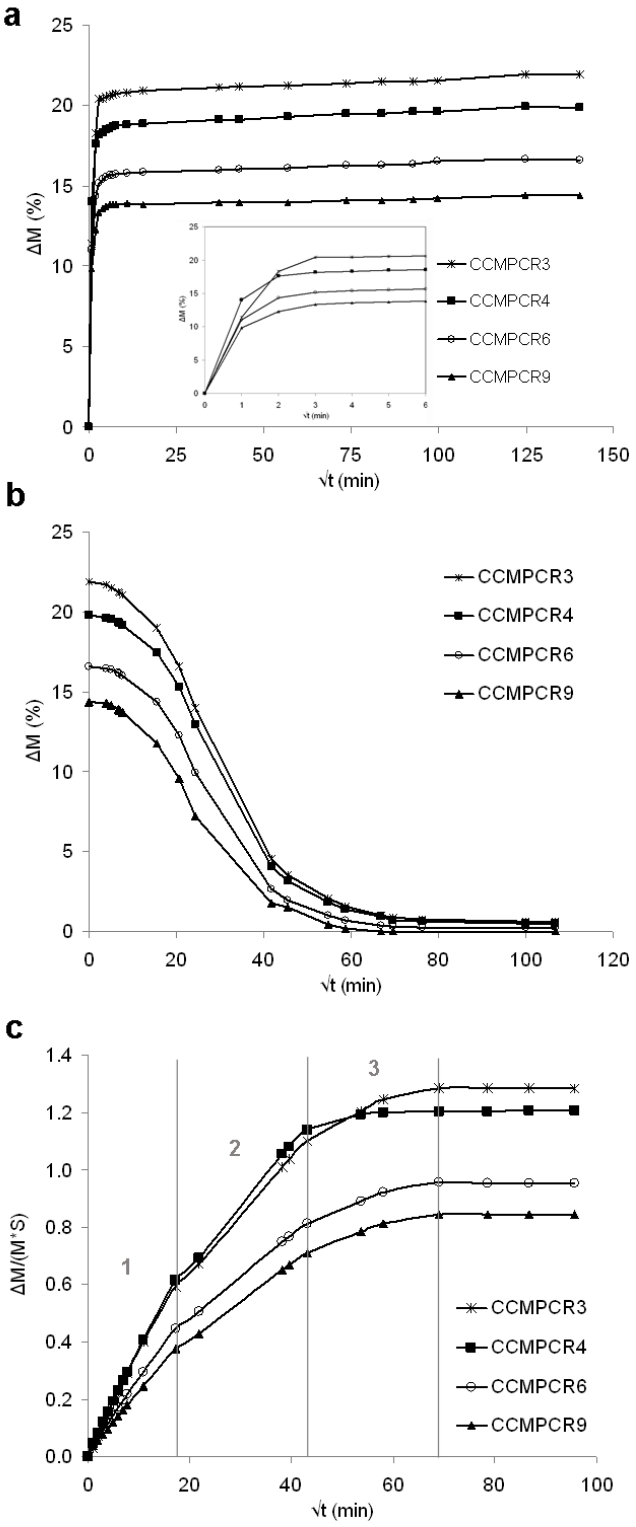

Figure IV.1.3 *Free water absorption (a), drying (b) and capillary uptake (c) curves of mortars after 60 days of carbonation. In the water absorption and drying curves, the weight variation (ΔM, in g) is represented as function of the square of time (√t, in $min^{-1/2}$).The inset in (a) shows the first section of the water absorption curves. In the capillary uptake curve, the weight increase (ΔM, in g) per surface unit (S, in m^2) (c) is represented as function of the square of time (√t, in $min^{-1/2}$).*

3.1.2 Capillary uptake

The four mortars showed the same behaviour towards the capillary uptake as toward the water absorption, being the mortars with the highest lime content those which absorbed the highest amount of water for capillarity. Moreover, a similar trend between the water absorption and capillary uptake curves can be recognized in CCMPCR3 and CCMPCR4 mortars (Figs. IV.1.3a and IV.1.3c). During the first five hours (section 1 in the capillary curves, Fig. IV.1.3c), these two mortars showed the same capillary uptake (*cf.* A values, Tab. IV.1.2); then, within the following day (section 2, Fig. IV.1.3c), CCMPCR4 absorbed water faster than CCMPCR3 although, at the end of the test (section 3, Fig. IV.1.3c), the latter absorbed more water. As mentioned above, the little difference observed in the capillary kinetics of these two mortars maybe the result of bigger changes in the microstructure of CCMPCR3, after the formation of more hydrated phases due to the contact of this mortar with water.

A considerably lower (Fig. IV.1.3c) and slower capillary uptake (A values, Tab. IV.1.2) occurred in CCMPCR6 and CCMPCR9 mortars, because of their lower porosity (Tab. IV.1.2).

Determining the position of the capillary front in mortars have been a difficult task because the white colour of the mortars samples did not enable a precise lecture, especially in CCMPCR9, where the presence of more aggregate grains made this determination harder; in this mortar, in fact, the B value could not be determined (Tab. IV.1.2). The B value can be linked to the value of sorptivity, a parameter that is widely considered to characterize the microstructure and durability of cement-based mortars [16]. The lime-based mortars studied here present a value of sorptivity that approaches quite well that of other building materials, such as limestones, sandstones and plasters [16].

3.1.3 Hydraulic conductivity

The range of permeability values obtained for the four mortars is comprised between 10^{-6} and 10^{-5} m/s, which is between three and six orders of magnitude higher than the permeability of concrete and cement mortars [16,32-35]. When the measurement was repeated many times on the same sample, the K_h value decreased, because of the action of water that, passing through a partially carbonated mortar, dissolved the portlandite still present in it; the dissolution of portlandite in water probably modified mortars pore system when portlandite precipitated again. The same occurred due to the formation of more hydrated phases, as discussed above (*cf.* Sections 3.1.1 and 3.1.2). The dependence of the hydraulic conductivity on time was already observed by other authors [16].

According to the final values of hydraulic conductivity found for the four mortar types ($K_{h\ exp}$, Tab. IV.1.3), the water permeability decreases exponentially with the B/A ratio of the mortar (Fig. IV.1.4a), which means that there is an exponential increase for increasing volume of the aggregate. This is in agreement with the general observation that concrete presents higher permeability values than the corresponding

cement paste (i.e. without aggregate) [32] and it also confirms the importance of the interfacial transition zone (zone between the grain surface and the matrix) on the permeability of a mortar [34].

Mortar name	Hydraulic conductivity		Water vapour permeability
	$K_{h\ exp}$	$K_{h\ theo}$	K_v
CCMPCR3	1.2×10^{-6} (7.0×10^{-8})	1.7×10^{-6}	2.65 (0.10)
CCMPCR4	5.1×10^{-6} (6.9×10^{-7})	3.2×10^{-6}	2.87 (0.09)
CCMPCR6	7.5×10^{-6} (6.8×10^{-7})	11.0×10^{-6}	2.69 (0.08)
CCMPCR9	21.8×10^{-6} (4.9×10^{-6})	20.6×10^{-6}	3.09 (0.18)

Table IV.1.3 *Results of the permeability tests on mortars: experimental ($K_{h\ exp}$, in ms^{-1}) and theoretical ($K_{h\ theo}$, in ms^{-1}) values of hydraulic conductivity (water permeability); water vapour permeability (K_v, in $gm^{-2}h^{-1}$). Standard deviation is shown in square brackets.*

The exponential function presented in Fig. IV.1.4a was used to recalculate the K_h values of the four mortars. As shown in Table IV.1.3, experimental (K_h exp) and theoretical ($K_{h\ theo}$) permeability values are very similar and small differences maybe attributed to the strong dependence of the permeability on the heterogeneity of the mortar samples.

On the other hand, the relationship obtained between permeability and porosity of mortars is not very clear. As shown in Fig. IV.1.4b, the permeability value increases for decreasing porosity from CCMPCR3 to CCMPCR6 mortars. Notwithstanding, this trend is not followed by CCMPCR9 mortar, since it presents the same porosity as CCMPCR6 but a permeability value three times higher; moreover, CCMPCR9 is the only mortar that presented such a high dispersion of values. This finding confirms that the permeability of a material cannot be correctly determined on the basis of its porosity [36] especially if we consider that K_h is measured on saturated samples whilst porosity is determined after drying [34].

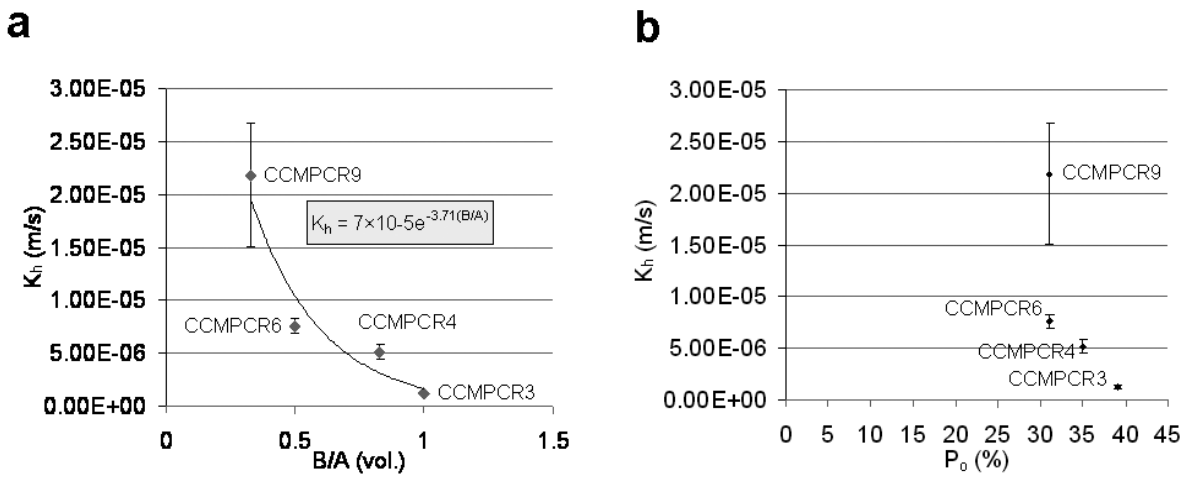

Figure IV.1.4 Hydraulic conductivity values (K_h, in m/s) are plotted against the binder-to aggregate ratio (B/A, by volume) (a) and the open porosity (P_o, in %) (b) of each mortar. In (a), the continuous line represents the exponential function found between hydraulic conductivity (K_h, in m/s) and B/A. Error bars represent the standard deviation determined on three samples per each mortar.

3.1.4 Water vapour permeability

Figure IV.1.5 shows the lineal weight drop of the samples subject to the water vapour permeability test. All mortars showed a very similar behaviour to water vapour, with some exception for CCMPCR9, whose curve has a sharper slope with respect to the others.

The water vapour permeability values measured in the four mortar types (Tab. IV.1.3) did not show a tight relationship neither with the aggregate content nor with the open porosity of each mortar (Tab. IV.1.2). In fact, although K_v seems to increase for increasing aggregate volume, as for the hydraulic conductivity (K_h), there is some discrepancy in the case of CCMPCR6, whose K_h value is too low if compared with the apparent trend followed by the other mortars. In fact, a very close behaviour to water vapour is observed in the curves of CCMPCR3, CCMPCR4 and CCMPCR6 mortars (Fig. IV.1.5).

It is known that the vapour diffusion through a material (i.e. stone, brick, mortar) depends on its microstructural characteristics, especially the pore system (main pore size and tortuosity) [37-39]. Since the pore size of the four mortars is almost the same (the main pore radius is comprised between 0.1 and 1 μm [24]), it is likely that the most relevant factor on the water vapour permeability of aerial lime-based mortars is the pore tortuosity, which is indeed increased by the presence of the aggregate. Here, in fact, the low cohesion between matrix and aggregate in CCMPCR9 mortar generated a higher porosity in the interfacial transition zone that gave place to a much higher permeability compared to the other mortars. In the same way as found here for water vapour, it is known that the CO_2 diffusion is higher (and the carbonation enhanced) at the interface between the surface of the grains and the matrix (at the interfacial transition zone) than in the matrix itself [40].

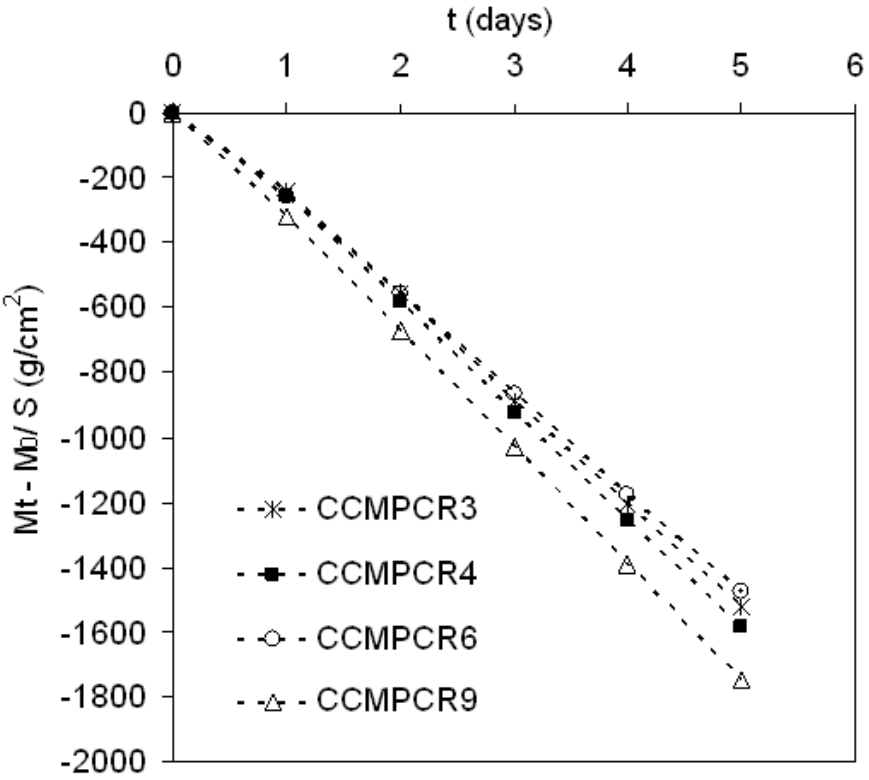

Figure IV.1.5 *Mass variation per surface unit (M_t - M_0/ S, in g/cm^2) of the four mortar types as function of time (t, in days) during the water vapour permeability test.*

3.2 Shrinkage of mortars

Figure IV.1.6 shows the shrinkage curves of the four mortars studied, determined within a week, whilst the inset in Figure IV.1.6 shows the shrinkage occurred during the first 24 hours.

The shrinkage is almost the same (0.5 mm) in all mortars within the first 4 hours; after this period, CCMPCR3 mortar presents a much higher volume reduction (4 mm) compared to the other mortars (1.3-1.9 mm), as reflected in the shrinkage coefficients (Tab. IV.1.4). This high volume reduction, which was expected in CCMPCR3 since it is the mortar with the highest lime content, achieved a quite constant value after 12 hours. However, CCMPCR3 showed a completely different shrinkage curve, with respect to CCMPCR4, 6 and 9 mortars (Fig. IV.1.5). Perhaps, the sharp slop of its curve is indirectly related to the effectiveness of the cellulose derivative as water-retaining agent. As shown in Table IV.1.1, the same amount of admixtures was added in each mortar, independently on the binder amount. It is likely that, in CCMPCR3 mortar, due to the high lime content, the amount of cellulose derivative is not enough to improve the water-retention capacity of the lime, then it is not able to counteract shrinkage. In the other mortars, instead, the water-reducing agent seems to be able to reduce the water evaporation rate but within a limited period of time (approximately 10 hours). In fact, CCMPCR9 reached the highest shrinkage after one day, CCMPCR6 showed a continuous increase until the fifth day, reaching a value of shrinkage similar to CCMPCR9 and higher

than CCMPCR3, and the volume reduction in CCMPCR4 still increased during the next days but it achieved a lower value than in the other mortars (Tab. IV.1.3).

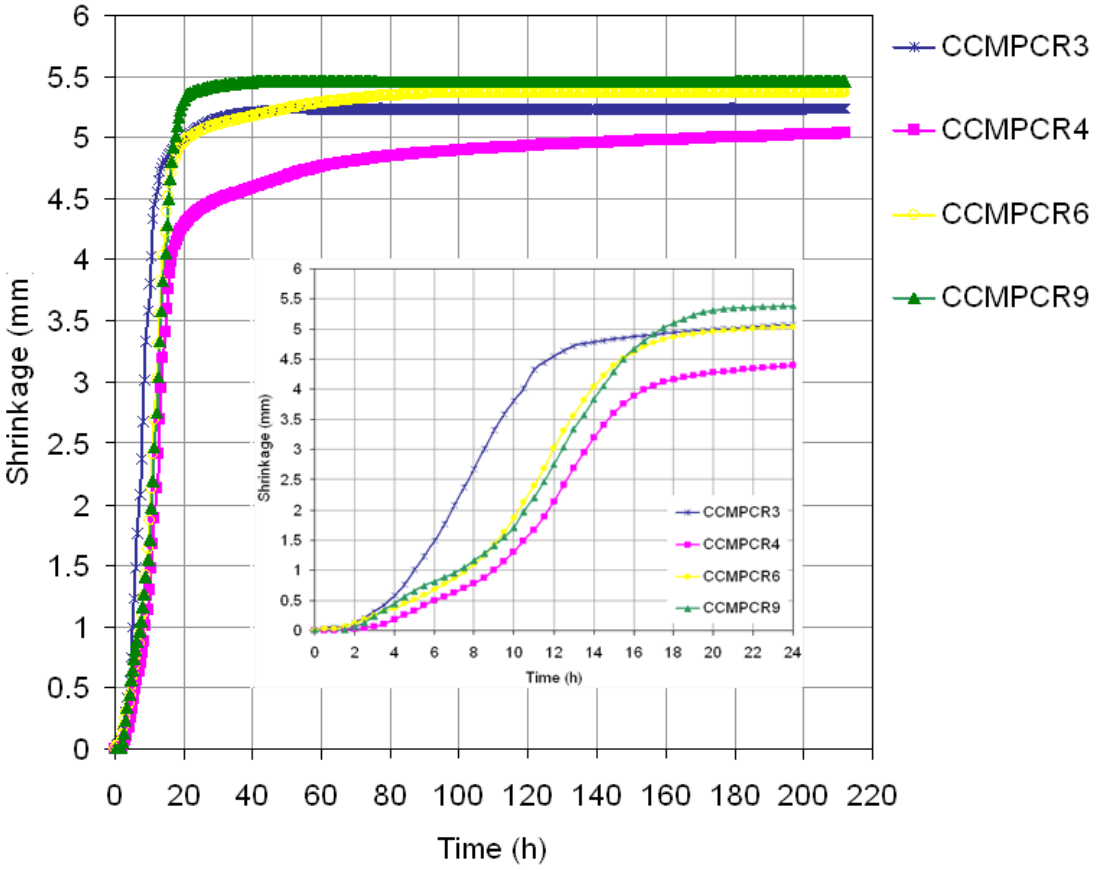

Figure IV.1.6 *Shrinkage curves of mortars samples during 7 days. The inset shows the shrinkage curves within the first 24 hours.*

Considering these results, we interpret that different factors contribute the development of shrinkage fissures in these types of mortars. The most important one is related to the amount of kneading water needed for the elaboration of mortars and it shows its effect during the first hours of drying. Mortars with higher water content undergo a much higher shrinkage in the first hours, such as the case of CCMPCR3 mortar. A secondary factor is probably related with the degree of cohesion exhibited between aggregate and matrix, during the first days of hardening. A very low cohesion is likely to develop in CCMPCR9 since the first days of its life and this would explain the slightly highest shrinkage achieved in this mortar at the end of the test.

However, the differences between the shrinkage values of these mortars are very little, considering that the final dimensional variations of the samples are almost equal (between 1.3 and 1.4 % of the total length of the sample, Tab. IV.1.4).

Mortar name	C_{shr}	Final shrinkage (%)
CCMPCR3	0.34	1.31
CCMPCR4	0.12	1.26
CCMPCR6	0.18	1.34
CCMPCR9	0.17	1.36

Table IV.1.4 *Shrinkage measurements in mortars: shrinkage coefficient (C_{shr}, in mm/h) determined after 12 hours and values of the final shrinkage (in %) measured on the length of the samples.*

4. Conclusions

The assessment of the hydric properties of the four mortars studied have contributed to a wider understanding of their performances during hardening, apart from giving an idea of their durability.

The mortars here considered had the same composition but different binder-to-aggregate proportions. Although the values obtained by testing their hydric properties are very similar among these mortars, differences have been found according to the microstructure, lime content and aggregate content of mortars.

Firstly, it has been found that the mortar with the highest lime content (CCMPCR3) was more susceptible to the water uptake by free immersion and capillarity; it generally showed a higher water content at the end of these tests. On the other hand, the mortar with the highest aggregate content (CCMPCR9) presented a faster drying and a higher permeability to water and water vapour. Both findings are related to the microstructure and pore network of these mortars. In the first mortar, the open porosity of the matrix is high and this explains the higher water content absorbed. In the second one, the porosity at the interface between the matrix and the aggregate grains is responsible for the behaviour shown.

Secondly, it has been considered that the microstructure of "young" (i.e. partially carbonated) mortars can be subject to slight modifications, due to the dissolution of portlandite in water and also to the occurrence of hydration reactions between the reactive phases of metakaolin and water.

Finally, the shrinkage of mortars turned out to be quite different to the expected, being the highest in the CCMPCR9 and not in CCMPCR3, which was prepared with the highest amount of lime and water. This has been related mainly to the scarce cohesion of this mortar.

Furthermore, it has been positively observed that these mortars present similar sorptivity values than the majority of limestones and sandstones, in agreement with one of the requirements initially established for rendering mortars. As a general conclusion, the CCMPCR6 seems to present the most suitable hydric behaviour among the other mortars, and then a better durability is envisaged in the masonry.

Acknowledgements:

This study was financially supported by Research Group RNM179 of the Junta de Andalucía and by Research Project P09-RNM-4905. We are grateful to Dr Mona Edwards (University of Oxford, UK) for her assistance in the use of the falling head permeameter.

References

[1] Rose D.A. Water movement in porous materials: Part 1-Isothermal vapour transfer. Brit J Appl Phys 14 (1963) 256-262.
[2] Rose D.A. Water movement in porous materials: Part 2-The separation of the components of water movement. Brit J Appl Phys 14 (1963) 491-496.
[3] Vos B.H. Hydric methods for the determination of the behaviour of stones. UNESCO-RILEM International Symposium, Paris (1978).
[4] Scherer G.W. Theroy of drying. J Am Cer Soc 73 (1990) 3-14.
[5] Rojo A., Alonso F.J., Esbert R.M. Hydric properties of some iberian ornamental granites with different superficial finishes: a petrophysical interpretation. Mater Constr 53 (269) (2003) 61-72.
[6] K. Beck, M. Al-Mukhatar, O. Rozenbaum, M. Rautureau, Characterization, water transfer properties and deterioration in tuffeau: building material in the Loire valley-France, Build Environ 38 (2003) 1151-1162.
[7] Hall C, Hoff WD. Rising damp: capillary rise dynamics in walls. Proc Roy Soc 463 (2007) 1871–1884.
[8] Groot C, Gunneweg JTM. The influence of materials characteristics and workmanship on rain penetration in historic fired clay brick masonry. Heron 55 (2) (2010) 141–54.
[9] Ingham J.P. Predicting the frost resistance of building stone. Q J Eng Geol Hydroge (2005) 38:387-399.
[10] Ruiz-Agudo E, Lubelli B, Sawdy A, van Hees R, Price C, Rodriguez-Navarro C. An integrated methodology for salt damage assessment and remediation: the case of San Jerónimo Monastery (Granada, Spain). Environ Earth Sci 63 (7) (2011) 1475-1486.
[11] Warscheid Th., Braams J. Biodeterioration of stone: a review. Int Biodeter Biodegr 46 (2000) 343-368.
[12] Wood C. Understanding and controlling the movement of moisture through solid stone masonry caused by driving rain. MSc Thesis; University of Oxford (2010).
[13] Maurenbrecher A.H.P. Mortars for repair of traditional masonry. Practice Periodical on Structural Design and Construction 9 (2004) 2, 62-65.
[14] Hughes J.J. The role of mortar in masonry: an introduction to requirements for the design of repair mortars. International Workshop on "Repair mortars for historic masonry". RILEM TC 203-RHM, Prague (2010).
[15] Groot C.J.W.P. Performance and repair requirements for renders and plasters. International Workshop on "Repair mortars for historic masonry". RILEM TC 203-RHM, Prague (2010).

[16] Hall C., Hoff W.D. Water transport in brick, stone and concrete. Ed. Taylor and Francis, London and New York (2002), p.73.
[17] De La Torre M.J. Caracterización de las propiedades hídricas de los materiales lapídeos. Cuadernos Técnicos. Metodología de diagnóstico y evaluación de tratamientos para la conservación de los edificios históricos. Villegas R., Eduardo M., Sebastian P. eds, (2003) 104-111.
[18] Benavente D., Cañaveras J.C., Cuezva S., Laiz L., Sanchez-Moral S. Experimental definition of microclimatic conditions based on water transfer and porous media properties for the conservation of prehistoric constructions: Cueva Pintada at Galdar, Gran Canaria, Spain. Environ Geol (2009) 56:1495-1504.
[19] UNE EN 459-1 (2002). Description Building lime - Part 1: Definitions, specifications and conformity criteria. AENOR, Madrid.
[20] ASTM C618-08. Standard Specification for Coal Fly Ash and Raw or Calcined Natural Pozzolan for Use in Concrete. Annual Book of ASTM Standard, 2008; 4.02.
[21] UNE EN 1015-3 (1999). Methods of test for mortar for masonry. Determination of consistence of fresh mortar (by flow table). AENOR, Madrid.
[22] UNE EN 1015-11 (1999). Methods of test for mortar for masonry. Part 11: Determination of flexural and compressive strength of hardened mortar. AENOR, Madrid.
[23] Cazalla O. Morteros de cal. Aplicación en el Patrimonio Histórico. Ph.D. Thesis. Universidad de Granada; 2002.
[24] Arizzi A., Cultrone G. Aerial lime-based mortars blended with a pozzolanic additive and different admixtures: a mineralogical, textural and physical-mechanical study. Constr Build Mater, 31 (2012) 135-143.
[25] UNI-EN 13755. Metodi di prova per pietre naturali. Determinazione dell'assorbimento d'acqua a pressione atmosférica. CNR-ICR, Rome (2008).
[26] NORMAL 29-88. Misura dell'indice di asciugamento (drying index). CNR-ICR, Rome (1988).
[27] UNI EN 1925 (2000). Natural stone test methods — Determination of water absorption by capillarity. CNR-ICR, Rome.
[28] Domenico P.A., F.W. Schwartz. Physical and Chemical Hydrogeology, John Wiley & Sons, New York, (1990), 824 p.
[29] NORMAL 21/85 (1985). Permeability to water vapour. CNR-ICR, Rome.
[30] Mamillan M. Connaissances actuelles des problemes de remontées d'eau par capillarite dans les murs. The conservation of stone II. Cent per la Conservazione delle Sculture all'aperto. Bologna (1981) 59–72.
[31] Benavente D., Lock P., García del Cura M.A., Ordóñez S. Predicting the capillary imbibition of porous rocks from microstructure. Transport Porous Med. 49 (2002) 59-76.
[32] Halamickova P., Detwiler R.J. Water permeability and chloride ion diffusion in Portland cement mortars: relationship to sand content and critical pore diameter. Cem Concr Res 25 4 (1995) 790-802.

[33] Ganjian E., Claisse P., Tyrer M., Atkinson A. Factors affecting measurement of hydraulic conductivity in low-strength cementitious materials. Cem Concr Res 36 (2006) 2109-2114.
[34] Scherer G.W., Valenza II J.J., Simmons G. New methods to measure liquid permeability in porous materials. Cem Concr Res 37 (2007) 386-397.
[35] Wongpa J., Kiattikomol K., Jaturapitakkul C., Chindaprasirt P. Compressive strength, modulus of elasticity, and water permeability of inorganic polymer concrete. Mater Des 31 (2010) 4748-4754.
[36] Anderson E. Relation between water permeability and water absorption of concrete. Industrial and Engineering Chemistry (1926).
[37] Dondi M., Principi P., Raimondo M., Zanarini G. Water vapour permeability of clay bricks. Constr Build Mater 17 (2003) 253-258.
[38] Johannesson B.F. Prestudy on diffusion and transient condensation of water vapor in cement mortar. Cem Concr Res 32 (2002) 955-962.
[39] Quenard D., Sallee H. Water vapour adsorption and transfer in cement-based materials: a network simulation. Mater Struct 25 (1992) 515-522.
[40] B. Bourdette, E. Ringot, J.P. Ollivier, Modelling of the transition zone porosity, Cem Concr Res 25 (4) (1995) 741-751.

Chapter IV.2

Experimental testing of the durability of lime-based mortars used for rendering historic buildings

Arizzi A., Viles H., Cultrone G.
Construction and Building Materials
28 (2012) 807-818

Abstract

To find out which render mortar mix shows the best durability properties, we have designed four ageing tests that aim to simulate water movements, ice formation and salt crystallization in lime mortars exposed to an extreme, but realistic, range of temperature and humidity. It has been found that the response of individual mortar mixes differs according to the mechanism and the agent of attack. These findings suggest that in order to provide useful data both the experimental testing approach and the types of mortar tested need to be tailored for the particular circumstance in which the render will be applied.

1. Introduction

Rendering mortars have always been considered the sacrificial layers of walls and building facades because their main purpose, as well as an aesthetic one, is to protect the masonry structure against weathering, slowing its decay. To ensure this function, renders need to be maintained and repaired or substituted by other compatible mortars when damaged. The major benefit achieved by covering a building with a render is the reduction of moisture present inside the masonry structure [1]. The presence of water and its movement inside the pore network of mortars are among the biggest causes of their degradation [1-3]. In fact, depending on the conditions of temperature and humidity, water in both vapour and liquid state can allow freezing-thawing phenomena, can favour the entry of salts which crystallize inside the matrix, and can cause the reduction of mortar mechanical strengths and adhesion to the masonry. As a general rule, a render should be characterised by low water absorption and high water vapour permeability, so that the water which enters the mortar can easily and quickly evaporate [4], as well as by high flexibility, good adhesion and compatibility with the support (i.e. stone, brick) [5,6]. Adequate design of the masonry materials and good knowledge of their characteristics (pore system, hygric and physic-mechanical properties) are required to predict and, consequently, minimise their decay.

Accelerated weathering tests are the easiest, quickest and most commonly used way to study the resistance of a construction material exposed to certain environmental conditions as well as to know which factors are involved in its decay and in which way the material properties are affected [7]. However, one must bear in mind that natural weathering is a combination of conditions (i.e. temperature, relative humidity, solar radiation, wind, rain, salts and pollutants) which are hard to reproduce faithfully by a laboratory test. Moreover, the layer of mortar (1-3 cm thick) applied on the surface of a wall may show different textural characteristics (such as pore systems) to a laboratory sample (the standard size is 4×4×16 cm) and consequently, it may be affected in a different way by weathering. However, the performance of accelerated ageing tests is still the most useful tool for understanding the mechanisms of decay occurring in rocks and masonry structures.

Freeze-thaw cycles, mechanical stress and salt crystallization are the most effective causes of degradation of mortar used in renders. According to some authors [8,9], decay due to freezing-thawing cycles, rainfall and salts attack is more noticeable in mortars with high porosity and low strength.

Good understanding of the growth mechanisms of salts in porous materials has been achieved by many salt crystallization tests performed during the last 20 years [9-21].

In mortars, sulphate attack consists of a sequence of three sub-processes: firstly, sulphate ions diffuse into the pores of the mortar, more

or less easily depending on its permeability; secondly, the sulphate ions react with calcium hydroxide, thus enhancing further penetration of sulphates into the matrix; finally, gypsum or ettringite precipitates, depending on the composition of the binder (lime or cement) [21]. Gypsum and ettringite are responsible for the development of cracks and spalling, respectively [9]. In cement mortars, further deterioration is due to the degradation of calcium silicate hydrates with consequent leaching of calcium hydroxide [9]. The presence of thaumasite, which is similar to ettringite but derives from the reaction between calcium silicate hydrates and sulphate ions, has also been reported in cement, lime and gypsum-based mortars [22,23].

Magnesium (epsomite and hexahydrite) and sodium (thenardite and mirabilite) sulphates are the most dangerous salts for building material durability, because they normally crystallize inside the material [24] often only a few millimetres below the surface, depending on the salt viscosity and the drying rate of the material [25]. Due to their high crystallization pressure [26], these salts cause cracks, sanding and spalling.

Karatasios et al. [11] described the degradation of calcitic lime mortars due to sodium sulphate crystallization and demonstrated how the addition of barium hydroxide enhances the resistance to salts, by blocking Ca^{2+} dissolution and further precipitation of salts. The use of industrial residues (such as blast furnace slag) as additives in mortars has proved to be effective in reducing the damage caused by salt crystallization and freezing-thawing cycles [27].

The objective of this work is to study the durability of lime-based mortars to be used as rendering materials in restoration interventions. To study the effect of ageing on the properties of these mortars, they have been subjected to accelerated weathering, by simulating the extreme atmospheric conditions (of temperature and relative humidity) which occur during 1 year in the city of Granada (Andalusia, South of Spain) (Tab. IV.2.1).

The damage caused by rain and freezing-thawing cycles has also been studied by simulating rainfall (that mostly occurs in winter time in Granada).

Two further tests have also been carried out to study the impact of salt crystallization on mortars: the salt solution was applied during the weathering cycles as a "salt fog" on the surface of mortars, whilst other samples were placed in contact with a combination of sand and salt and periodically activated by water. In the first case, previous studies have found that fog enhances stone decay by salt because it is a source of moisture [20] and it controls the rate of breakdown, whilst salt controls timing [17]. In the second case, simulations of hyper-arid environments (such as deserts) previously performed on stone samples have demonstrated that salt weathering can operate quickly on samples not fully immersed in saline solutions but in contact with a combination of salt and sand [20].

The effect of these four weathering cycles on mortar samples has been monitored by means of visual and photographic observations, as well as by using weight loss and microscopic techniques.

1.1 Atmospheric conditions of the city of Granada (Andalucía, Spain)

Granada is located at the foot of Sierra Nevada Mountains in Spain at an elevation of 738 m above the sea level and at a distance of 60 km from the Mediterranean coast. Due to this particular geographic location, the city is characterised by extremely hot summers, during which temperatures can reach 40 °C (and about 50 ºC in the sun), and quite cold winters when temperatures sometimes fall below 0 °C (Tab. IV.2.1). Moreover, a temperature range of 30 ºC can be registered between night and day.

Year 2009	T_{max} (°C) / average	T_{min} (°C) / average	HR_{max} (%) / average
January	15.0 / 10.0	-6.0 / 1.0	99 / 87.9
February	19.3 / 14.4	-3.0 / 1.5	90 / 77.3
March	24.0 / 18.7	-0.2 / 4.5	97 / 71.3
April	24.8 / 18.6	-1.8 / 4.2	85 / 64.7
May	34.0 / 27.0	3.6 / 9.3	67 / 52.2
June	38.0 / 31.8	9.4 / 14.5	70 / 45.5
July	39.7 / 35.8	11.7 / 16.0	47 / 37.3
August	37.0 / 34.4	11.3 / 15.6	57 / 46.1
September	35.7 / 27.3	7.5 / 12.8	90 / 65.1
October	32.8 / 26.3	5.5 / 9.2	85 / 64.4
November	27.0 / 19.0	-0.7 / 4.3	96 / 69.3
December	19.4 / 13.8	-4.1 / 3.0	95 / 85.4

Table IV.2.1 *Atmospheric conditions occurred in Granada in 2009. Data were taken from the Meteorological station 84190 (LEGR) of Granada Airport (latitude: 37.18°; longitude: -3.78°; altitude: 567m). The most extreme conditions were registered in July and January.*

Granada is one of the most polluted cities of Spain, especially because of the high amount of particulate matter produced by traffic. The amount of PM_1, PM_{10}, and NO_2, recorded in 2009 and 2010 in many areas of the city [28,29], was higher than the legal limit. On the other hand, the lowest values of contamination were registered for SO_2 and CO gas in 2009 [28]. However, the accelerating effects of suspended particles on mortar decay caused by the interaction with SO_2 gas and the formation of deleterious sulphate salts should be taken into account [30-33]. The main sources of sulphate ions which give rise to these salts are thought to be traffic and industries, as only a small portion of SO_4^{2-} ion incorporated into the atmospheric aerosol originates in sea spray [34]. Moreover, the most

deleterious damage found in stones and composite materials of ancient buildings of Granada has been caused by the crystallization of magnesium salts [35,36]. Sulphate and magnesium ions are likely to come from the soil (ground water) and/or from adjacent lime or gypsum mortars, often prepared with dolomitic aggregates because dolostones commonly outcrop near Granada. In modern repair works, dolomitic lime and aggregate have been substituted by calcite due to the harmful effect of magnesium ions [24-26,30]. However, the high abundance of these elements is still a big cause of deterioration of the materials present in the historic buildings of Granada [36].

2. Materials and Methods

The following components were used in the production of the test mortars: a calcitic dry hydrated lime (CL90-S [37]) produced by ANCASA (Seville, Spain), a calcareous aggregate (CA) with a continuous grading from 0.063 to 1.5 mm, a pozzolan (CLASS N POZZOLAN, [38]), produced by Burgess Pigment Company (USA) as additive, and three different admixtures: a lightweight aggregate (perlite), a water-retaining agent (cellulose derivative) and a plasticiser (polycarboxylate) (additional detail can be found at www.argosdc.com). Four types of lime mortars were prepared, in which the binder-to-aggregate (B/A) ratios were 1:3, 1:4, 1:6 and 1:9 by weight, whilst the pozzolan was kept at 10% of the total binder (by mass) and the total admixtures proportion was less than 2% of the total mass, as shown in Table IV.2.2. The mortars have been labelled M3, M4, M6, M9, according to their B/A ratio. Mortars were stored for 7 days in normalised steel moulds (4×4×16 cm) at RH = 60±5% and T = 20±5 °C following a modification of the standard UNE-EN 1015-2 [39] proposed by Cazalla [40]. After being removed from the moulds, they were cured at the same conditions of T and RH until the beginning of the study.

Mortars name	Components name and proportions			
	CL	MK	CA	admixtures
M3	450.0	50.0	1500.0	34.0
M4	360.0	40.0	1600.0	34.0
M6	257.1	28.6	1714.3	34.0
M9	180.0	20.0	1800.0	34.0

Table IV.2.2 *Proportions (expressed in g) of components used in the elaboration of the four mortar types. Abbreviations indicate: calcitic lime (CL); metakaolin (MK); calcareous aggregate (CA); admixtures (perlite + cellulose derivative + polycarboxylate).*

The weathering experiments were carried out three months later in order to ensure good carbonation, because the standard time of 28 days was considered too short for ensuring carbonation and properties improvement on these materials. Four different tests were performed: 1)

weathering cycles with T, light and RH variations (WS); 2) weathering cycles and rain simulation (WS+R); 3) weathering cycles and salt resistance by capillary absorption (WS+SS); and 4) weathering cycles and salt resistance by surface deposition (WS+SD). Samples were weighed and photos taken every day in order to record any morphological change in mortars.

2.1. Weathering study (WS)

To study the effect of ageing process on mortar properties, the four different types of mortar were subjected to accelerated weathering, by simulating the atmospheric conditions that occur during one year in the city of Granada (Tab. IV.2.1). In this simulation the annual temperature and relative humidity range was repeated every 12 hours. The simulation was carried out on three samples per mortar type, in a Sanyo-FE 300H/MP/R20 environmental cabinet (internal dimensions of 675W 630D 650H mm) (School of Geography and the Environment, Oxford University, UK) which can operate at temperature range of -20 to +100°C and can be programmed with different conditions of temperature, relative humidity and light. Three samples (each of 2×4×4 cm) per mortar were placed on a sand layer (ca. 4 cm thick) in a tray, in the same way as in Goudie et al. [17] and Goudie and Parker [20]. The smaller surface (2×4 cm) was put in contact with the sand and the larger surface (4×4 cm) perpendicular to it. In this way, samples reproduce the real situation of a render (1-3 cm thick) on a wall.

Thirty cycles were performed in total. Each climatic cycle lasted 12 hours, and consisted of 4 steps, of 3 hours duration each step, with a cooling and warming rate of 25 °C/hour, as shown in Table IV.2.3. Temperature and relative humidity trends were checked with a data logger (ibutton® Hygrolog which records temperature and RH) to ensure that the programmed cycle was reproduced accurately.

2.1.1 Weathering study and rain simulation (WS+R)

Under the same weathering conditions (of T, RH and light) described in 2.1., rain was simulated by spraying both the sand (water level of 2 mm) and the mortar surface with around 25 mL of tap water, which was applied every 4 cycles just before the step at -10 °C (Tab. IV.2.3). The water absorbed by the samples (by capillary rise from the sand and by absorption from the wetted surface) froze when temperature decreased below 0 °C and dried when temperature increases up to 40 °C, with the consequence that freeze-thaw cycles were also simulated in this test. Thirty cycles were performed in total.

2.1. Salt resistance tests

As in most of the accelerated decay tests performed on mortars [9,11,14,21] and as recommended in standards regarding the estimation of the durability of building materials [41-42], a sodium sulphate solution

was used instead of a magnesium sulphate or a sodium chloride one. In fact, if Cl^- ions accumulation decreases with the increase of the distance from the sea [34], chlorides should be scarce in Granada, although an influx of marine particles can be expected when the wind direction is southerly [36]. Moreover, the damage caused by Cl^- salts is less noticeable than the deterioration by thenardite and mirabilite, because halite always crystallizes at the material surface (as efflorescences) [10,24].

2.2.1 Weathering study and salt attack by capillary absorption (WS+SS)

The experimental design proposed by Goudie et al. [17] was used, with some modifications, to evaluate the damage caused by the capillary uptake of a saline ground water within the mortar. Samples were placed on sand 4 cm thick, in which sodium sulphate was dispersed. Among the different conditions of weathering established by Goudie et al. [17], we chose the 1:10 salt to sand ratio by weight and a water level of 1 mm applied in each tray, in order to produce observable breakdown. Ten cycles were performed in total. Tap water was applied over the tray for around 60 s, using a spray every four cycles before the step at the highest temperature (40 °C, Tab. IV.2.3). Ion chromatography analysis (Dionex IC DX500) (School of Geography and the Environment, Oxford, UK) was performed on mortar samples before and after the salt resistance tests, in order to determine and quantify the concentration of soluble ions.

2.2.2 Weathering study and salt attack by surface deposition (WS+SD)

To analyse the damage caused by the deposition of a salt fog on the mortar surface, a sodium sulphate solution (14% w/w) was sprayed on the surface of the mortar samples, every two cycles before the step at the highest temperature (40 °C, Tab. IV.2.3). Thirty cycles were performed in total. Also after the WS+SD test, ion chromatography analysis (Dionex IC DX500) was performed on mortar samples.

2.3 Carbonation degree and porosity of the mortar samples

Carbonation degree and open porosity of both internal and external zones of mortar samples were determined before and after the weathering study.

The mineralogical phases and the degree of carbonation were determined by X-ray diffraction (XRD), by means of a Panalytical X'Pert PRO MPD diffractometer (Dept. of Mineralogy and Petrology, University of Granada, Spain), with automatic loader and X´Celerator detector, 4 to 70 º2θ explored area. The interpretation and quantification of the mineral phases was performed using the X-Powder software package [43]. The

decrease in portlandite content was taken as a reference to estimate the carbonation degree index (I_{CD}, expressed in %), according to the equation:

$$I_{CD} = \frac{CH_0 - CH_x}{CH_0} \times 100 \qquad \text{(Eq. IV.2.1)}$$

where CH_x is the amount of portlandite at time x and CH_0 is the initial content of portlandite (at time 0), determined by XRD. This method of quantification is not totally accurate since it does not take in account the small amount of portlandite consumed during the hydration of metakaolin phases. For this reason I_{CD} is considered as an approximate estimation of the carbonation degree of mortars.

Open porosity (P_o, %) and pore size distribution (PSD, in a range of 0.002<r<200 μm), were determined using a Micrometics Autopore III 9410 porosimeter (mercury injection porosimetry, MIP) (Dept. of Mineralogy and Petrology, University of Granada, Spain). Mortar fragments of ca. 2 cm^3 were oven-dried for 24 h at 60 ºC before the analysis.

2.4 Micro-scale crystallization cycles

Environmental scanning electron microscopy (ESEM) (Scientific Instrumentation Center, Granada, Spain) allows the detailed observation of the crystalline phases of a salt at different degree of hydration. A Philips Quanta 400 was used to analyse small mortar fragments (~2 mm^3), which did not need to be previously dried and sputter coated. Before observation, the microscope chamber was purged at a temperature of 10 ºC and a range of pressures between 0.9 and 5 torr, corresponding at this temperature to about 8 and 40% of relative humidity. Once equilibrium was achieved, temperature and pressure were fixed at 2 ºC and 2.5 torr (RH~36%), respectively. These conditions were established for the observation of the anhydrous phases in mortar samples. A low temperature ensures good working conditions and reliable results. Hydration and dehydration cycles of the salt crystals were performed with a fixed temperature of 2 ºC and a range of pressure of 2 to 6 torr, which reproduces relative humidities of 29 to 87%. Three cycles were performed in total. Chemical analyses were performed by means of an EDX microanalysis system, with Si(Li) detector of SUTW type.

T_{init} (h:min)	T_{fin} (h:min)	T (ºC)	RH (%)	Light	WS	WS+R	WS+SD	WS+SS
00:00	03:00	40	40	yes	-	-	-	-
03:00	06:00	15	70	not	-	water spraying	-	-
06:00	09:00	-10	--	not	-	-	-	-
09:00	12:00	15	70	not	-	-	water spraying	Sodium sulphate solution spraying

Table IV.2.3 *Scheme of the exposure conditions used in the tests, which represents one cycle of 12 hours duration, as indicated by the initial (T_{init}, in hours) and final (T_{fin}, in hours) time of each step. Temperature (T, in ºC), relative humidity (RH, in %) and light (40W Crompton reflector lamp) are the conditions used in all tests. "Yes" and "not" refers in which step the light was applied; "--" indicates that the relative humidity was not programmable in this step. WS: weathering study; WS+R: weathering study and rain simulation; WS+SS: weathering study and salt resistance by capillary absorption; WS+SD: weathering study and salt resistance by surface deposition. "-" indicates that no additional conditions were applied in this step.*

3. Results and discussion

The response of mortars (i.e. mass variation, deterioration forms and decay speed) to the weathering cycles was different depending on the type of attack produced in the four experimental runs by temperature and humidity changes, alternation of wet and dry periods and presence of salts. The climatic cycles reproduced by the environmental cabinet were monitored to ensure reproducibility during each test. Sample weights are shown in Figure IV.2.1 as a function of cycle number. Changes in mortar appearance observed during the weathering cycles are shown in Figure IV.2.2. An accurate description of the different deterioration forms developed in mortar samples during WS+R, WS+SS and WS+SD is given in Table IV.2.4 and the most representative images of those are shown in Figures IV.2.3, IV.2.4 and IV.2.5, respectively. Finally, the soluble ion content (anions, as SO_4^{2-}, and cations, as Na^+ and Ca^{2+}) determined on the mortar samples before and after the WS+SS and WS+SD tests is given in Figure IV.2.6. In the following sections, we present a detailed description of the results obtained in each test.

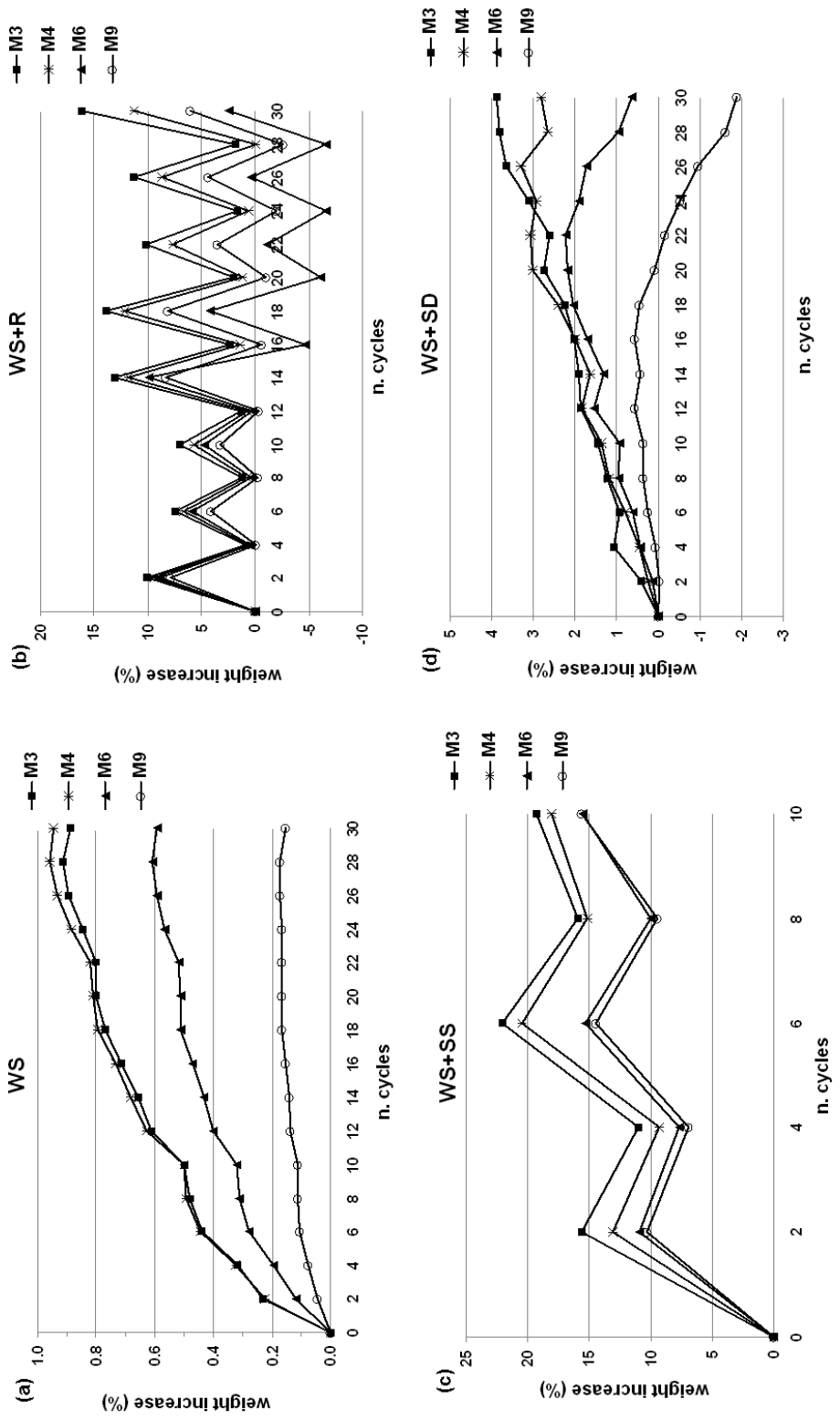

Figure IV.2.1 Representation of the weight variations (in %) as a function of the number of cycles of the following tests: WS (weathering study) (a); WS+R (weathering study and rain simulation) (b); WS+SS (weathering study and salt resistance by capillary absorption) (c); WS+SD (weathering study and salt resistance by surface deposition) (d).

Figure IV.2.2 *Samples aspect at the beginning and during the tests. (WS): normal weathering; (WS+R): weathering study and rain simulation; (WS+SS): weathering study and salt resistance by capillary absorption; (WS+SD): weathering study and salt resistance by surface deposition. The cycle number is indicated on each image.*

After WS+R	Mortars name			
Deterioration forms	M3	M4	M6	M9
Fissures	*i*,30	*i*,26	*i*,10/ *ii*,26	*i*,30
Fragments loss	-	*i*,20/ *ii*,30	*i*,14/ *iii*,20	*iii*,20
[a] Sanding	*i*,26/ *ii*,30	*i*,20/ *ii*,26	*i*,20/ *iii*,30	*iii*,20
[b] Spalling	*i*,26	*ii*,26	-	-
After WS+SS	Mortars name			
Deterioration forms	M3	M4	M6	M9
Fissures	*i*,2/ *ii*,4	*ii*,2	*i*,6	*i*,2
Efflorescences	*i*,4	*i*,6	*i*,6	-
Spalling	*i*,6	-	-	-
Cracks	*iii*,6	*iii*,6	*ii*,6	*ii*,6
Fragments loss	*iii*,8	*i*,6	*ii*,6/ *iii*,8	*iii*,10
Samples breaking	*ii*,8/ *iii*,10	*i*,8/ *iii*,10	*i*,8/ *iii*,10	*iii*,10
Sanding	*iii*,10	*iii*,10	*iii*,10	*iii*,10
After WS+SD	Mortars name			
Deterioration forms	M3	M4	M6	M9
Efflorescences	*ii*,18/ *iii*,30	*ii*,18/ *iii*,30	*iii*,18	*ii*,18
Spalling	*iii*,30	*ii*,20/ *iii*,30	*iii*,20	*ii*,20
Cohesion loss and sanding	*i*,30	*i*,20/ *ii*,30	*ii*,20/ *iii*,30	*iii*,20

[a] *Sanding refers to the loss of material in form of powder from the sample surfaces.*
[b] *Spalling refers to the detachment of layers from the sample surfaces.*

Table IV.2.4 *Deterioration forms observed in mortars during the following tests: WS+R (weathering study and rain simulation); WS+SS (weathering study and salt resistance by capillary absorption) and the WS+SD (weathering study and salt resistance by surface deposition). The indexes used represent the number of samples (i: one; ii: two; iii: three) of each mortar showing the corresponding deterioration form and the number of cycles after which the deterioration form appears.*

3.1 WS

All mortars samples presented a slow and constant increase in weight during the WS test (Fig. IV.2.1a), especially M3 and M4, where the final weight is about a 1% higher than the initial one (Fig. IV.2.1a). On the other hand, the lowest weight increase has been registered in M9, of only +0.1%.

This fact may indicate that the mortar samples are still undergoing carbonation under these conditions, since carbonation produces a weight increase in mortars [44], and this is clearly higher in mortars with higher amount of lime. Before the weathering study, the mortars presented different carbonation degree indexes (Tab. IV.2.5), with higher values in M3 and M4.

After WS, M4 was still the most carbonated mortar and this may explain the biggest increase in weight registered in this mortar at the end of the weathering cycles. Notwithstanding, this correspondence between weight increase and carbonation degree is not found in M3. In fact, the amount of portlandite found in this mortar after WS is the highest and this results in the lowest carbonation degree index at the end of the test. On the other hand, the weight of M3 samples recorded after 30 cycles of WS is one of the highest (Fig. IV.2.1a). This discrepancy can be explained by considering the differences found in the X-ray diffraction patterns of M3 and M4 (Fig. IV.2.7). In both patterns, calcite and portlandite are present but in M3 about 5% of the total amount of mineral phases is represented by the CAĈH phase ($Ca_4Al_2(CO_3)(OH)_{12} \cdot 6H_2O$, or monocarboaluminate). As shown in Fig. IV.2.7, the amount of this phase is the highest in M3 mortar. The CAĈH is one of the mono-phase calcium hydrates (AFm) that derives from the reaction between the reactive aluminates of metakaolin and the CO_3^{2-} ions [45]. According to Cizer [46], this monocarboaluminate replaces progressively its precursor (hemicarboaluminate) in the presence of excess calcite and this leads to the liberation of calcium hydroxide (i.e., portlandite) and thus to an increase in its amount. If 5% of CAĈH has been formed in M3 after the WS cycles, it is likely that calcium hydroxide is liberated during CAĈH formation and precipitates as portlandite, with the consequence that the amount of this phase is higher than expected. On this basis and according to the higher weight increase registered in M3 after WS, we can believe that M3 is still one of the most carbonated mortars at the end of this test.

Calcium silicate hydrates (CSH) and calcium alumina silicate hydrate (CASH) detected in some of the samples (Fig. IV.2.7) are among the major phases formed after pozzolanic reaction of the metakaolin [46].

Mortar samples did not show any visible change (i.e. deterioration) during the WS cycles, as shown in Figure IV.2.2a. The only modification was found at microscopic scale and concerns the pore size distribution of mortar samples (Fig. IV.2.8a). In the unaltered samples, the main peak obtained in the PSD curves corresponds to pores with radii between 0.1 and 1 μm and whose volume is the most influential on the open porosity of mortars (P_o, Tab. IV.2.5). Another range of smaller pores ($0.01<r<0.04$ μm) is present in the unaltered samples and their volume is bigger in M3 and M4, which were prepared with a higher content of binder (i.e. lime+metakaolin). After the WS test, M3, M4 and M6 show a decrease in the amount of pores in the main range ($0.1<r<1$ μm). Since MIP analysis only detects interconnected pores, the volume reduction of pores of the same size indicates that the interconnection among these pores

decreases. This occurs due to calcite crystallization during the carbonation process [47].

Mortar name	I_{CD} (%)		P_o (%)				
	Unaltered	After WS	Unaltered	After WS	After WS+R	After WS+SS	After WS+SD
M3	33	55	38.9±5.0	36.3±2.0	36.2±4.0	38.5±0.3	37.5±0.7
M4	34	85	34.5±0.2	34.1±0.4	35.4±1.1	42.0±5.0	32.9±0.3
M6	28	75	31.8±0.2	32.0±0.1	32.7±1.0	38.2±5.6	30.2±1.3
M9	30	65	31.3±0.9	32.5±0.1	33.1±0.5	37.1±2.0	30.0±0.8

Table IV.2.5 *Carbonation degree index (I_{CD}, in %, measured according to Eq. 1) and open porosity (P_o, in %) of mortars before (unaltered) and after the different weathering processes: WS (weathering study); WS+R (weathering study and rain simulation); WS+SS (weathering study and salt resistance by capillary absorption) and the WS+SD (weathering study and salt resistance by surface deposition).*

3.2 WS+R

In this test, besides the moisture uptake in mortars caused by the alternation of wet and dry periods, decay is also driven by the formation of ice inside them when temperature goes below 0 ºC (*cf.* Section 2.1). Figure IV.2.1b shows the influence of this alternation of wet and dry periods on the weight of samples: a weight increase (between 5 and 14%) was registered two cycles after the water application (i.e. simulation of rainfall). At the end of the test, the only increase in final weight was recorded in M3 samples (by about 2%) whilst M4 samples recovered their initial weight and M6 and M9 samples lost weight. These differences in sample weight as well as the changes observed in the appearance of samples during the WS+R test (Fig. IV.2.1b) indicate that the application of water, both on the sand and the surface of the samples, produced a much more pronounced response than the temperature and relative humidity cycles alone and that this response is different according to the mortar type.

The most rapid deterioration was observed in M6, where in one sample the development of a long fissure led after a few cycles to the detachment of a large fragment parallel to the surface (Tab. IV.2.4). The consequent mass loss suffered by this sample is responsible for the great decrease in weight registered for M6 at the end of the test (Fig. IV.2.1). However, given that this decay only occurred in one sample, it is likely to be initiated to a stress produced when the sample was cut before the test instead of being driven entirely by the test conditions.

In M4 and M6 the development of fissures on the bottom face of the samples led to the loss of small fragments from the same surface, whilst in M9 no fissures were detected before the loss of fragments (Tab. IV.2.4 and Fig. IV.2.3a). M3 did not show any loss of fragments unlike the other samples, but the development of a fissure in the bottom face of one of the M3 samples (Tab. IV.2.4 and Fig. IV.2.3a) after 30 cycles, allows us to

expect a similar decay for this mortar, even if slower. The loss of small fragments also occurred from the side surfaces of samples M4, M6 and M9 but later than from the bottom (Fig. IV.2.3b). This deterioration form (i.e. loss of fragments) was observed only on the surfaces in direct contact with water.

The decay of the bigger surface of samples differed according to the mortar type. In M3 and M4 spalling occurred first (Tab. IV.2.4) and, after the total detachment and fall of the superficial layers due to the volume increase (9%) caused by the ice formation, the surface below, already damaged by the previous process, was furthermore exposed to the water sprayed on the surface, which formed a film that froze and deteriorated the sample surface, with the consequence that sanding appeared (Figs. IV.2.3c and d). On the other hand, spalling did not occur in any samples of M6 and M9 and sanding directly occurred on the bigger surface (Tab. IV.2.4 and Fig. IV.2.3d), suggesting that in this case the most aggressive agent was the frozen water present on the surface of these mortars.

Surface flaking and internal damage are the two types of cracking recognised in mortars subjected to freezing-thawing phenomena in previous studies [48].

To explain the observed differences in the modifications of samples' appearance it is useful to study the modifications of the pore system of the mortars after the WS+R test. In M3 and M4 PSD curves, the main peak is shifted to smaller pore radius and the volume of these pores is lower (Fig. IV.2.8a). Moreover, the volume of pores with radius lower than 0.1 μm increases slightly. This indicates that water freezing has caused a shift of the maximum peak, with a smaller radius than the original one. The water movements within the mortar are responsible for the precipitation of calcite in the pores, as well as for the rearrangement of phases in the matrix system, which cause the observed pore network. At the same time, few pores with radius around 4 μm appear. This is probably due to a partial destruction of the pore system caused by freeze-thaw mechanism. On the other hand, in M6 and M9 the only change found in the PSD curves is the volume reduction or increase of the original pores. Particularly, the increase of the pore volume obtained in M9 is caused by the bad cohesion existing between matrix and aggregate grains that characterises mortars with high aggregate contents [49].

3.3. Salt resistance tests

3.3.1 WS+SS

Here, the mechanism of attack consists in the salt dissolution in water and in the following absorption of the salty solution by capillary rise. Due to the weathering cycles to which the samples are submitted in the meantime, the sulphate undergoes cycles of precipitation (at higher T) and dissolution (at lower T) processes inside the samples, leading to observable decay, which occurred after 10 cycles.

The WS+SS weight curves shown in Figure IV.2.1c present the alternation of positive and negative peaks (as obtained in the WS+R test, Fig. IV.2.1b) which indicates how sensitive the weight of mortar samples is to the activation of the salt with water, which was performed every 4 cycles. About 5% of weight is lost between a wet and a dry cycle but more than 10% of weight is gained after the salt activation, with the consequence that the combined action of wet/dry periods and salt results in a general weight increase in all mortar samples. At the end of the test, M3 samples showed the biggest weight increase (almost 20%), followed by M4 which recorded a weight increase only 1% lower than M3. M6 and M9 behaved in a very similar way, with the same final increase in weight, equal to 15%. The weight increase is related to salt uptake by the mortar. However, the final weight recorded is lower than expected because of the many fragments lost at the end of the test which could not be weighed, because they were very fragile and reduced to powdered fragments after being handled (Fig. IV.2.2c).

During the WS+SS test, the first deterioration form that appeared in mortars was the formation of fissures which developed perpendicularly to the upper face and along the bigger face of the samples (Tab. IV.2.4 and Fig. IV.2.4a). This deterioration was followed by the precipitation of sulphate on the side faces of the samples. In some cases, the salt precipitated on the surface in the form of efflorescences and in other cases as subflorescences, very close to the surface, causing the detachment of thin layers (i.e. spalling) (Tab. IV.2.4 and Fig. IV.2.4b). As the test continued, fissures spread and widened until they became large cracks in the form of a cross on the bigger face, already evident after six cycles (Tab. IV.2.4 and Fig. IV.2.4c). These cracks caused the total breaking of the samples after 10 cycles (Tab. IV.2.4 and Fig. IV.2.2). All samples presented this decay although to different degrees, more pronounced in M3 samples.

The salt detected by XRD in mortar samples after WS+SS is thenardite (Na_2SO_4), which is the anhydrous phase of sodium sulphate which precipitates from solution at temperatures higher than 32.4 ºC, below which mirabilite is stable ($Na_2SO_4 \cdot 10H_2O$). This means that, during the temperature and humidity cycles established in this study, mirabilite is also present in mortar samples. Ettringite and gypsum have not been detected by means of XRD, although the morphology of cracks (Fig. IV.2.4c) developed in mortars may indicate their formation. This can be explained knowing that the decay caused by sodium sulphate is big if thenardite crystals are formed due to heterogeneous nucleation in small fractures or micropores smaller than 1 μm [26]. At the same time, it might be possible that colloidal ettringite has formed in mortars with the highest content of lime [27,50].

From the pore size distribution curves of the altered samples it is clear that a strong reduction in the volume of pores of radius between 0.1 and 1 μm has occurred, and that a new family of pores with radius comprised between 3 and 50 μm has been produced (Fig. IV.2.8b). This is because the precipitation of mirabilite from the supersaturated solution, produced

at room temperature by the dissolution of thenardite, creates a crystallization pressure [15,51] high enough to break the original pores and generate others with bigger radius.

As found by other authors [52,53], mortar porosity is higher after the absorption of salt (Tab. IV.2.5).

3.3.2 WS+SD

In this test, the absorption of sprayed salt solution by the samples' surface led to a general increase in weight until the 16th cycle in M9 and up to the 22nd for M6; after that, these two mortars lost weight strongly whilst M3 continued to gain weight and M4 remained quite stable until the end of the test (Fig. IV.2.1d).

After 30 cycles, the mortar samples did not show any fissures or breaking and the only changes were in their superficial appearance (Fig. IV.2.2d).

The salt absorbed by the surface precipitates in form of efflorescences on the upper and side surfaces of samples and in some cases it is followed by spalling (Tab. IV.2.4 and Fig. IV.2.5a). In the bigger face a loss of cohesion between the mortar matrix and the sand grains occurs, leading the sample surfaces to become much rougher and less compact (Tab. IV.2.4 and Fig. IV.2.5b), especially after the 10 last cycles (Fig. IV.2.2d). The biggest consequence of this deterioration was the loss of aggregate grains and binder (i.e. sanding) from the external surfaces of the samples, in a more pronounced way in M9 and M6 samples, which were characterised by notable weight loss (Fig. IV.2.1d). As both weight variation (Fig. IV.2.1d) and sample appearance (Fig. IV.2.2d) indicate, the degree of alteration is inversely proportional to the lime content of mortars, being the highest in M9 and the lowest in M3 and M4. This type of decay is related with the cohesion between mortar sand grains and matrix, which is much poorer in M9, due to the high content of aggregate in this mortar [49].

The total porosity of mortars after the salt deposition test is lower compared to that of unaltered samples. PSD curves of mortars after WS+SD are very similar to those obtained after the rain simulation experiment (WS+R), showing the main peak centered at 0.5 μm and a small peak centered at 4 μm. This type of PSD curve suggests that the original pores have been blocked by the precipitation of salts inside them. The fact that no cracks or smaller fissures have been generated by salt deposition, indicates that the salt intake from the mortars surface is lower and that precipitation only occurs at superficial level.

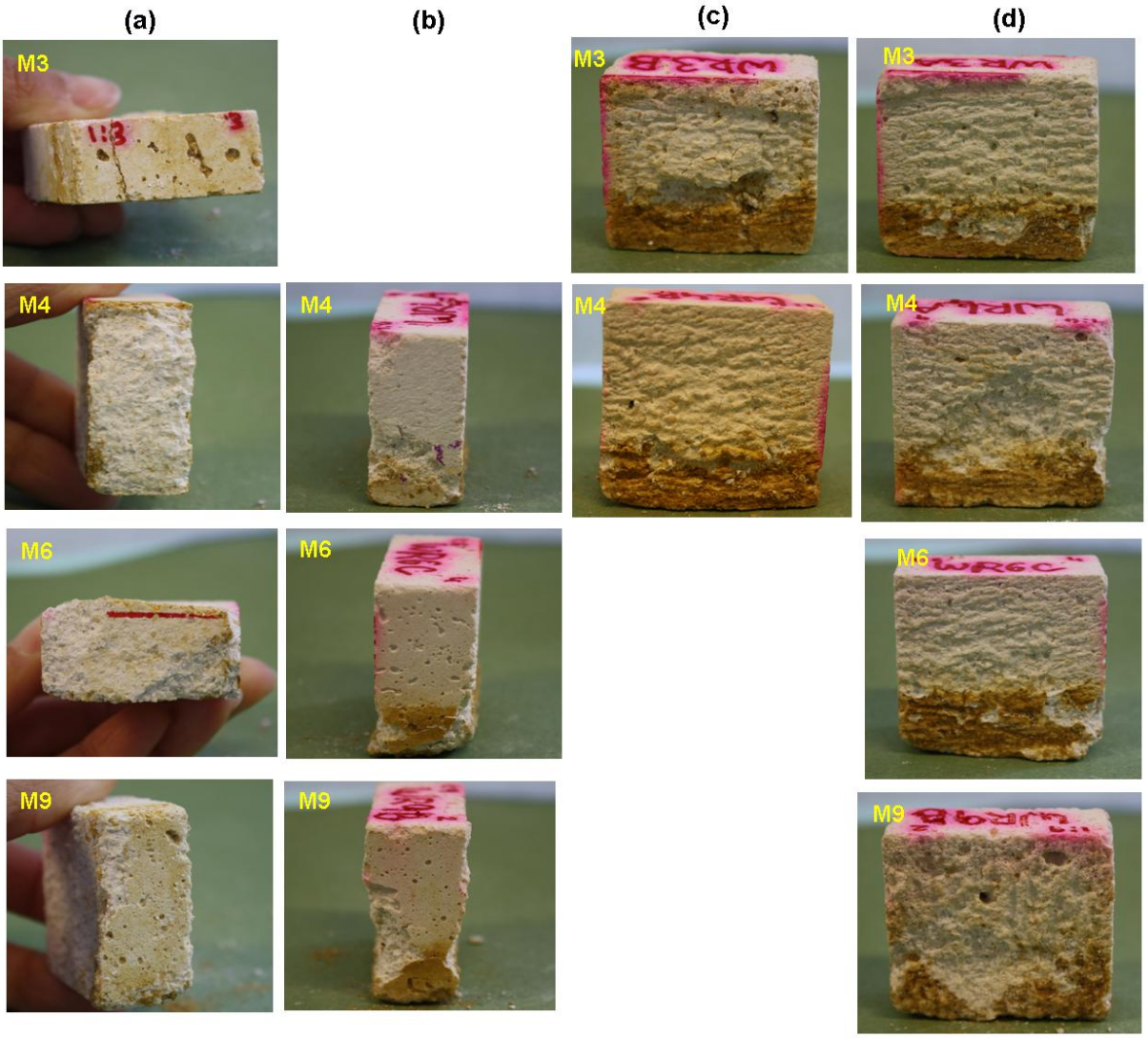

Figure IV.2.3 *Images of the different deterioration forms appeared in the mortars samples submitted to the WS+R test (weathering study and rain simulation): Fissures and fragment loss in the bottom (a) and the side (b) surfaces at the end of test; (c) spalling on the bigger surface, developed only in M3 and M4 samples after 30 and 26 cycles, respectively; (d) sanding on the bigger surface of samples at the end of the test.*

Figure IV.2.4 *Images of the different deterioration forms appeared in the mortars samples submitted to the WS+SS test (weathering study and salt resistance by capillary absorption): (a) Fissures developed after 4 cycles in samples M3, M4 and M9. (b) Efflorescences appeared after 6 cycles on the side surfaces of samples M3, M4 and M6; spalling also appears on sample M9. (c) Fractures in form of cross developed in all samples after 6 cycles.*

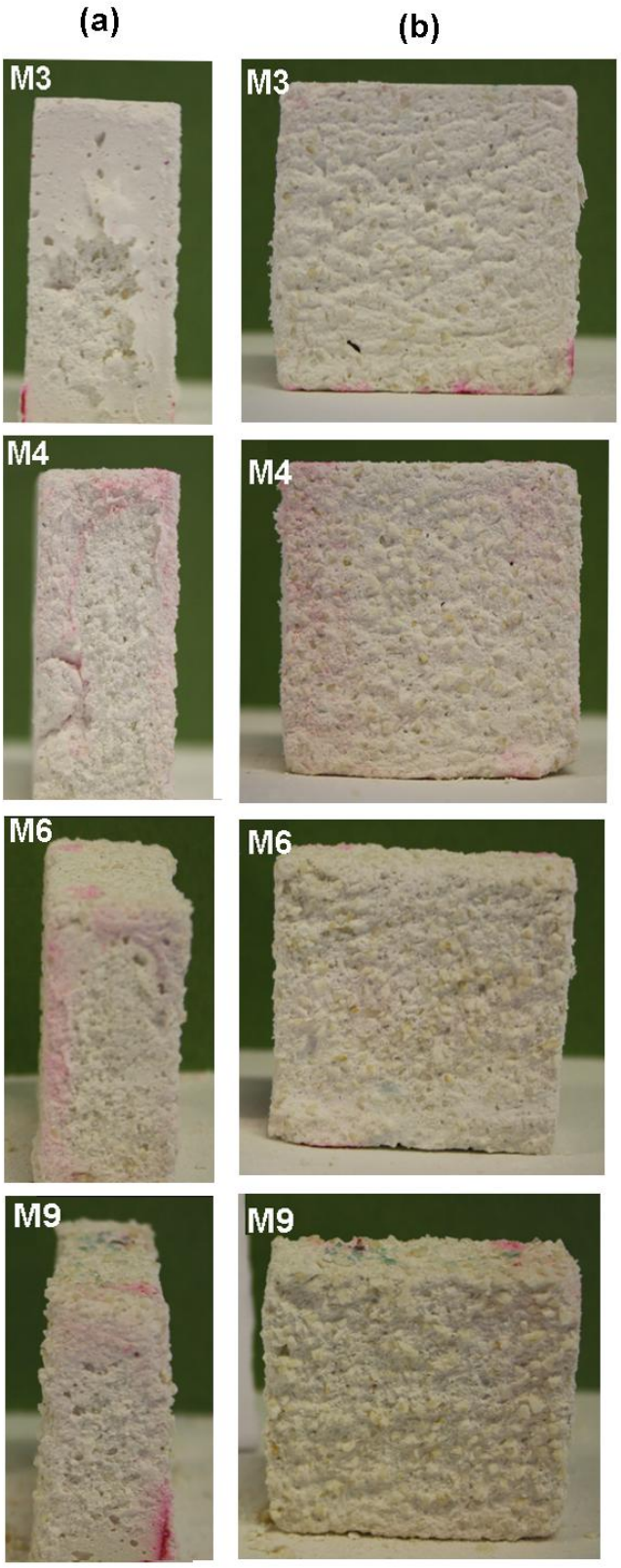

Figure IV.2.5 Images of the different deterioration forms appeared in the mortars samples submitted to the WS+SD test (weathering study and salt resistance by surface deposition). (a) Efflorescences and spalling observed on the side surfaces of the same samples, at the end of the test. (b) Surface aspect of the different mortars samples at the end of the test.

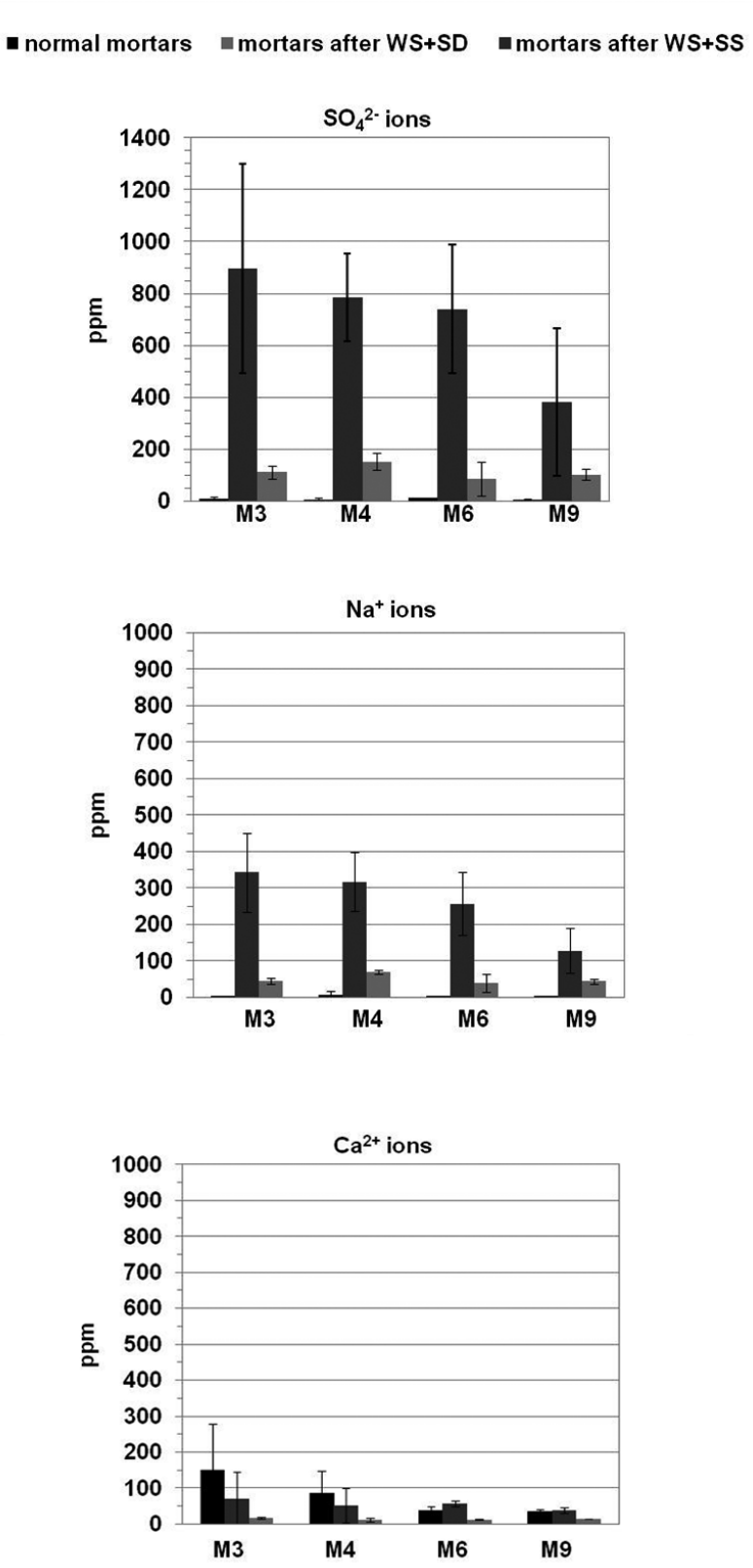

Figure IV.2.6 *Soluble ions (sulphates, SO_4^{2-}; sodium, Na^+; calcium, Ca^{2+}) concentration (in ppm) determined on M3, M4, M6 and M9 samples before (normal mortars) and after the WS+SS (weathering study and salt resistance by capillary absorption) and WS+SD (weathering study and salt resistance by surface deposition) tests. Error bars represent the standard deviation determined on three samples per mortar.*

3.3.3 Soluble ions

The soluble ions (Fig. IV.2.6) determined in mortar samples after the WS+SS test shows that both the sulphate (Fig. IV.2.6a) and the sodium (Fig. IV.2.6b) content is proportional to the lime content of the original mortars (Ca^{2+}, Fig. IV.2.6c). This indicates that the amount of salts is higher in mortars with higher lime contents, for two main reasons: on the one hand lime may react with sodium sulphate to form calcium sulphate, so that a higher lime content would produce a higher gypsum content; on the other hand, the porosity of mortars with high lime content is higher and the capillary uptake is more favoured, with the consequence of larger uptake of salts.

After the WS+SD test, a much lower content of sulphates has been found in mortar samples (Fig. IV.2.6a) and this agrees with the smaller decay they showed, compared to WS+SS. Nevertheless, a lower correlation has been found between the lime content of the original mortars and the sulphate and sodium content after the test. This is because water uptake does not occur in this test, so that there cannot be a correlation between mortar porosity and superficial decay.

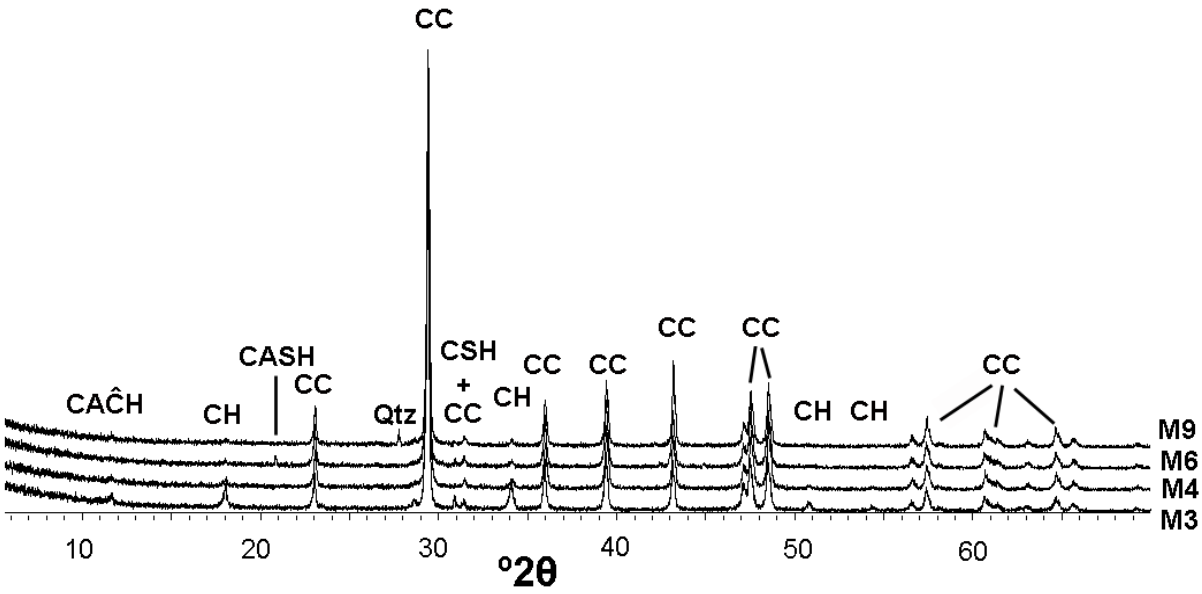

Figure IV.2.7 XRD pattern of mortars after the weathering study (WS). CC: calcite; CH: portlandite; CAĈH: monocarboaluminate; CSH: calcium silicate hydrate; CASH: calcium alumina silicate hydrate; Qtz: quartz.

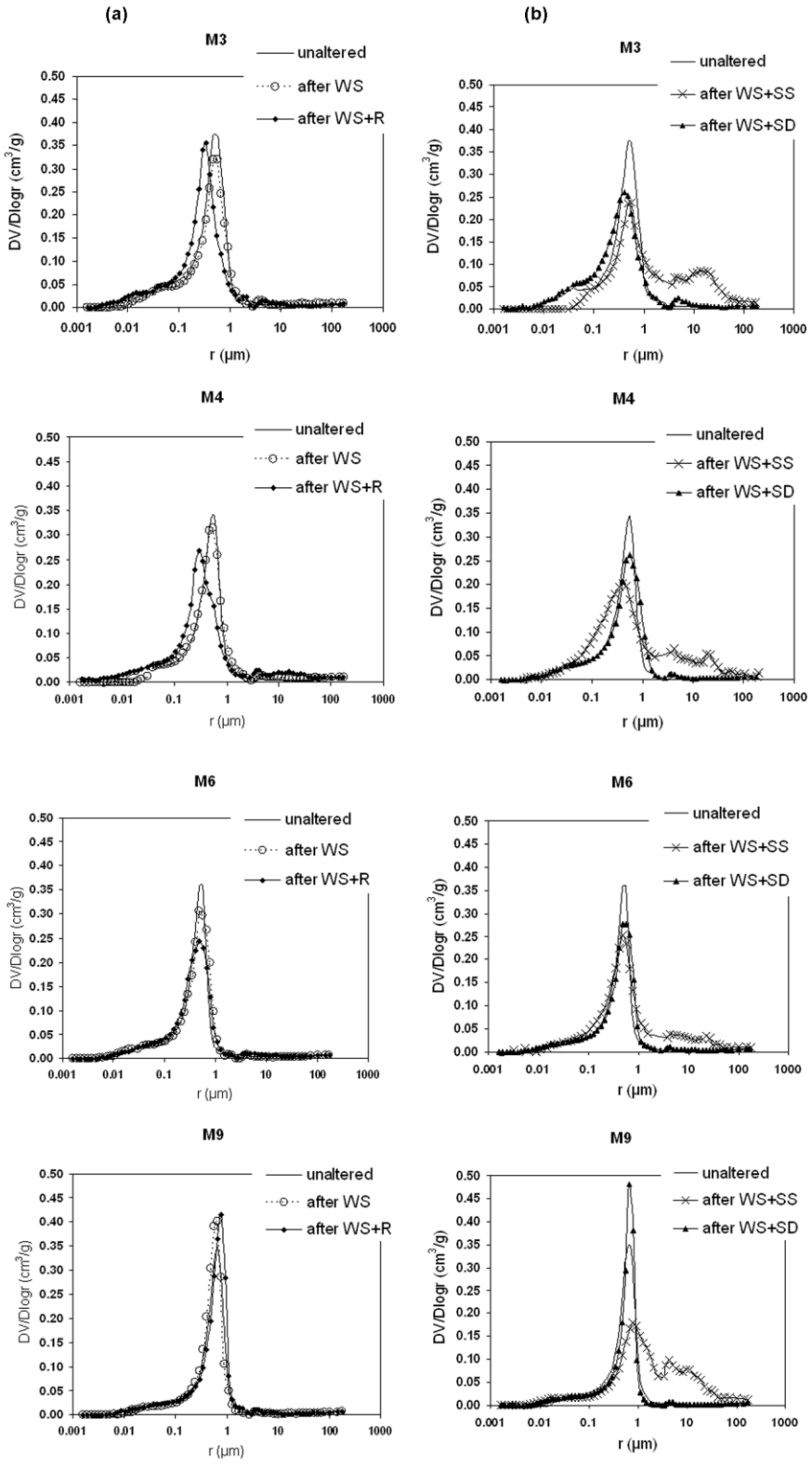

Figure IV.2.8 *Pore size distribution curves of mortars samples before (unaltered) and after the different weathering processes: WS (weathering study); WS+R (weathering study and rain simulation); WS+SS (weathering study and salt resistance by capillary absorption) and the WS+SD (weathering study and salt resistance by surface deposition).*

3.3.4 Crystallization at microscopic scale

By means of ESEM, we carried out a dynamic study of the crystallization process at microscopic scale. This allowed us to observe the morphology and size of salt crystals formed at different conditions of temperature and relative humidity. The only salt found in mortars at anhydrous conditions (T=10ºC and RH=20%) is thenardite (Fig. IV.2.9a and inset), which appeared as fibrous agglomerates (Fig. IV.2.9b) with high brightness. The hydration of this phase started at RH=72.5% when the typical fibres of thenardite (Fig. IV.2.9b) started to expand (Fig. IV.2.9c) until forming the first mirabilite crystals. The inverse process (dehydration, Figs. IV.2.9d-f) started at RH=37.7% and achieved equilibrium at RH=34.8%.

Mirabilite crystals precipitated on the surface have sizes between 20 and 50 μm. Even if limited by the size and the pore entrance [16], the maximum crystallization pressure of this salt is still able to overcome the physical constraint of the pore wall (defined by the tensile strength of the material) [15], so that bigger pores of similar size to the mirabilite crystals are generated (Fig. IV.2.8b). Moreover, the volume expansion (314% [51]) of the hydrated sodium sulphate is responsible for the big cracks obtained at the end of the WS+SS test in all samples (Tab. IV.2.4 and Fig. IV.2.2).

By means of the ESEM it was possible to observe how the performance of continuous hydration/dehydration cycles causes the loss of compactness in the matrix (Fig. IV.2.10), with a consequent reduction of the sample weight when the salt crystallizes near the surface (as found in M9 after WS+SD, Fig. IV.2.5).

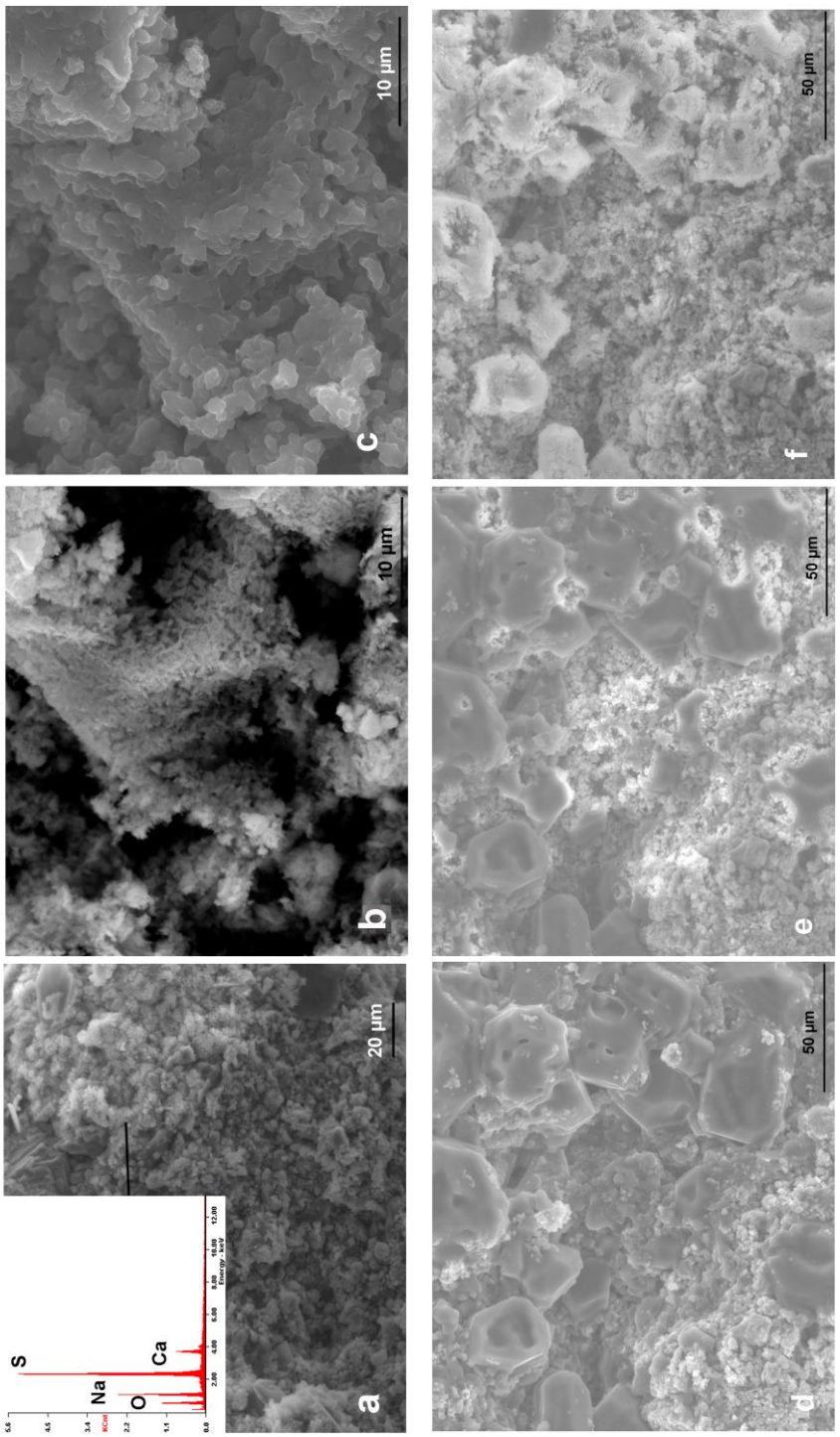

Figure IV.2.9 *ESEM images of one of the mortars after the WS+SS test: (a) aspect of the sample at anhydrous conditions (T=10ºC and RH=20%). The inset shows the EDX analysis of the salt, indicating that it is a sodium sulphate (thenardite, Na_2SO_4); (b) fibrous morphology of the surface of thenardite crystals at anhydrous conditions; (c) beginning of the hydration and expansion of the thenardite crystals; (d) mirabilite ($Na_2SO_4 \cdot 10H_2O$) crystals with size comprised between 20 and 50 µm, formed at T=2 ºC and RH=58%; (e) beginning of the dehydration process in some mirabilite crystals, at T=2 ºC and RH=37.7%; (c) thenardite crystals formed at T=2 ºC and RH=34.8%.*

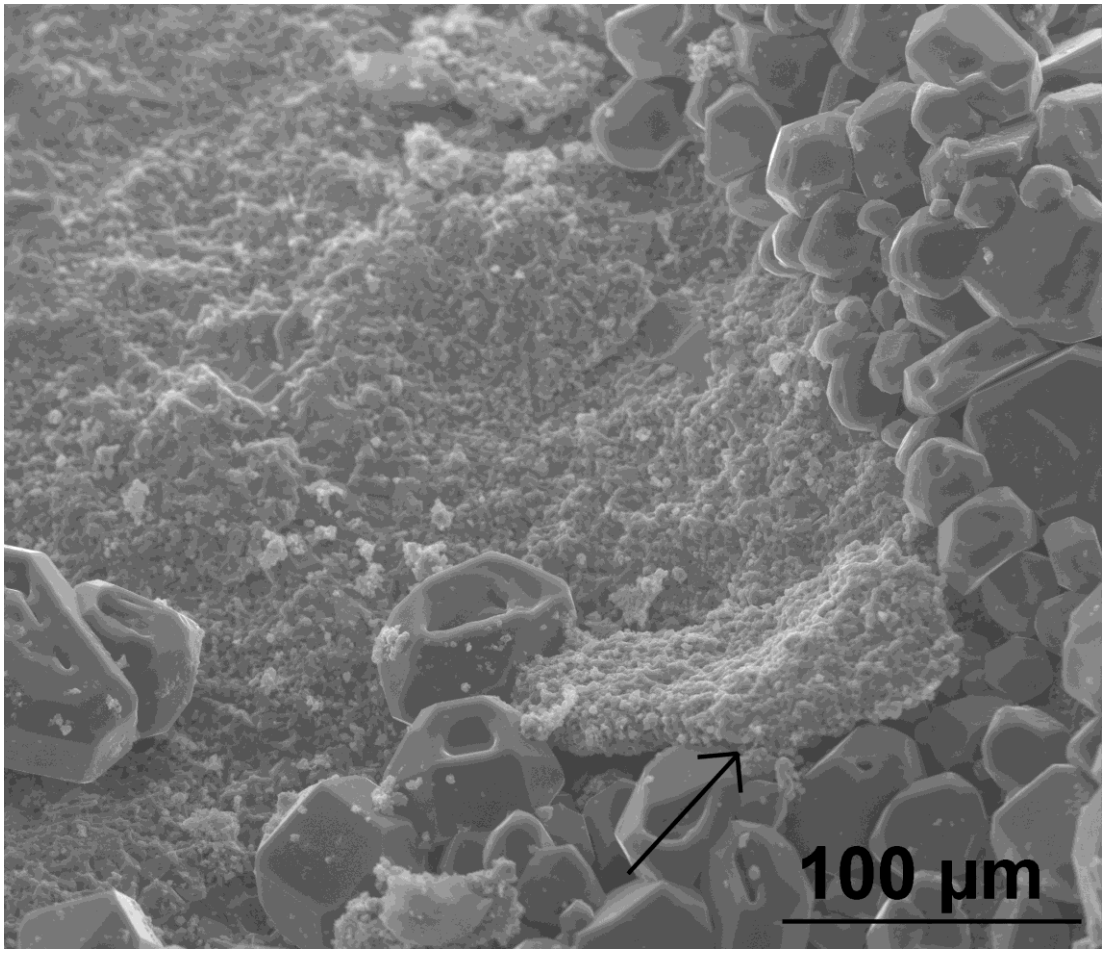

Figure IV.2.10 *ESEM image of mirabilite crystals grown within the mortar matrix, which has lost compactness and is progressively pushed by the salt crystals.*

4. Conclusions

This study has shown how differently mortars used to render historic buildings behave according to the mechanism and the agent of attack. It has been found that mortars are much more resistant to salt deposition than to salt capillary uptake because the former only produces superficial decay whilst the latter generates internal cracks.

It has been demonstrated that in mortars with higher contents of binder water uptake is more favoured and drives harmful decay, in the form of spalling, sanding and cracks. In particular, layer detachment can cause a lack of adhesion between the mortar surface and the material (brick, stone) in joints or on the surface. On the other hand, it has been found that the use of high proportions of aggregate can worsen the mortar cohesion, with the main consequence that the mortar suffers a larger amount of superficial decay.

These findings demonstrate, on the one hand, how important is the choice of a correct methodology to determine the durability of

construction materials; on the other hand, how controversial is the selection of a good mortar to be used as rendering materials. Both choices must be made considering the decay produced by weathering cycles that most reproduce the climate of the particular location of the historic building as well as the final function of the material in the masonry structure. For example, the salt deposition test (WS+SD) carried out in this study aimed to investigate the superficial decay of mortars caused by the deposition of a salt solution. In this sense, it accurately defines the decay of rendering mortars, whose surface is constantly exposed to external conditions, whilst the salt absorption test (WS+SS) is more representative of the damage caused by capillary rise uptake in ancient buildings where rain accumulation and high phreatic levels occur.

The question that arises is which binder-to-sand ratio is appropriate for a render, whether the one that might give place to slow decay in terms of water/salt solution absorption by capillarity or the one that might be more resistant to the superficial attack of a salt solution.

In our opinion, the surface properties of a render should be preserved as long as possible, especially when this render has an artistic, historic or cultural value. We must not forget that a render is frequently not only the sacrificial layer of a wall, but also the support of a stucco, a wall painting or a similar decoration. In this sense, its aesthetic function has to be preserved. For this reason, we would avoid the use of a mortar with high aggregate proportions because, as seen here, its original superficial appearance appears to become very damaged after weathering.

Among the mortars studied here, we consider that the one with 1:4 binder-to-sand proportion represents the halfway point between two bad extremes. In fact, M4 is the most carbonated mortar and one of the two mortars which presented the lowest superficial decay after salt deposition.

Regarding the methodology proposed in this study, it is fundamental to point out that although the tests have been performed simulating the climatic conditions of the city of Granada, they can certainly be taken as good reference for other Mediterranean areas and those with milder climate, since they cover a wide range of temperature and relative humidity.

Further studies should concentrate on the application of the tests performed in this work on other types of mortars, in order to consider the importance of the variability of the materials (i.e., grain size of the aggregate, proportions of metakaolin, other admixtures).

Acknowledgements:

This study was financially supported by Research Group RNM179 of the Junta de Andalucía and by Research Project MAT2008-06799-C03-03. We are grateful to Dr Mona Edwards for her assistance in the programming of the environmental cabinet and the use of the Dionex.

References

[1] Wood C. Understanding and controlling the movement of moisture through solid stone masonry caused by driving rain. MSc Thesis; University of Oxford; 2010.
[2] Hall C, Hoff WD. Rising damp: capillary rise dynamics in walls. In: proceedings of the Royal Society 2007; 463:1871-84.
[3] Groot C, Gunneweg JTM. The influence of materials characteristics and workmanship on rain penetration in historic fired clay brick masonry. Heron 2010; 55(2):141-54.
[4] Groot C. Performance and repair requirements for renders and plasters. RILEM TC203-RHM, ITAM, Prague; 2010.
[5] Rossi-Doria PR. Mortars for restoration: basic requirements and quality control. Mater Struct 1986; 19(114):445-8.
[6] Maurenbrecher AHP. Mortars for repair of traditional masonry. ASCE Practice Periodical on Structural Design and Construction 2004. p. 62-5.
[7] Charola AE. Stone deterioration in historic buildings and monuments. In: proceedings of the 10th international congress on deterioration and conservation of stone, Stockholm; 2004. p. 3-14.
[8] Lanas J, Sirera R, Alvarez JI. Study of the mechanical behaviour of masonry repair lime-based mortars cured and exposed under different conditions. Cem Concr Res 2006; 36:961-70.
[9] Cavdar A, Yetgin S. Investigation of mechanical and mineralogical properties of mortars subjected to sulfate. Constr Build Mater 2010; 24:2231-42.
[10] Lubelli B, Nijland TG, van Hees RPJ, Hacquerbord A. Effect of mixed in crystallization inhibitor on resistance of lime-cement mortar against NaCl crystallization. Constr Build Mater 2010; 24:2466-72.
[11] Karatasios I, Kilikoglou V, Theoulakis P, Colston B, Watt D. Sulphate resistance of lime-based barium mortars. Cem Concr Compos 2008; 30:815-21.
[12] Cardell C, Benavente D, Rodríguez-Gordillo J. Weathering of limestone building material by mixed sulfate solutions. Characterization of stone microstructure, reaction products and decay forms. Mater Charact 2008; 59:1371-85.
[13] Silva MAG, Silva ZCG, Simao J. Petrographic and mechanical aspects of accelerated ageing of polymeric mortars. Cem Concr Compos 2007; 29:146-56.
[14] Cultrone G, Sebastian E, Ortega Huertas M. Durability of masonry systems: a laboratory study. Constr Build Mater 2007; 21:40-51.
[15] Steiger M. Crystal growth in porous materials-I: The crystallization pressure of large crystals. J Cryst Growth 2005a; 282:455-69.
[16] Steiger M. Crystal growth in porous materials-II: Influence of crystal size on the crystallization pressure. J Cryst Growth 2005b; 282:470-81.
[17] Goudie AS, Wright E, Viles HA. The role of salt (sodium nitrate) and fog in weathering: a laboratory simulation of conditions in the northern Atacama Desert, Chile. Catena 2002; 48:255-66.

[18] Rodríguez Navarro C, Doehne E. Salt weathering: Influence of evaporation rate, supersaturation and crystallization pattern. Earth Surf Processes Landforms 1999; 24:191-209.
[19] Scherer GW. Crystallization in pores. Cem Concr Res 1999; 29:1347-58.
[20] Goudie AS, Parker AG. Experimental simulation of rapid rock blosk disintegration by sodium chloride in a foggy coastal desert. J Arid Environ 1998; 40:347-55.
[21] Ouyang C, Nanni A, Chang WF. Internal and external sources of sulfate ions in Portland cement mortar: two types of chemical attack. Cem Concr Res 1988; 18:699-709.
[22] Tesch V, Middendorf B. Occurrence of thaumasite in gypsum lime mortars for restoration. Cem Concr Res 2006; 36:1516-22.
[23] Crammond N. The occurrence of thaumasite in modern construction – a review. Cem Concr Compos 2002; 24:393-402.
[24] Benavente D, Garcia del Cura MA, Garcia-Guinea J, Sanchez-Moral S, Ordoñez S. Role of pore structure in salt crystallisation in unsaturated porous stone. J Cryst Growth 2004; 260:532-44.
[25] Ruiz-Agudo E, Mees F, Jacobs P, Rodriguez-Navarro C. The role of saline solution properties on porous limestone salt weathering by magnesium and sodium sulphates. Environ Geol 2007; 52:269-81.
[26] Rodríguez-Navarro C, Doehne E, Sebastian E. How does sodium sulphate crystallize? Implications for the decay and testing of building materials. Cem Concr Res 2000; 30:1527-34.
[27] Cerulli T, Pistolesi C, Maltese C, Salvioni D. Durability of traditional plasters with respect to blast furnace slag-based plaster. Cem Concr Res 2003; 33:1375-83.
[28] Horemans B, Cardell C, Bencs L, Kontozova-Deutsch V, De Wael K, Van Grieken R. Evaluation of airborne particles at the Alhambra monument in Granada, Spain. Microchem J 2011; 99:429-438.
[29] Lyamani H, Bravo Aranda JA, Alados Arboledas L. Informe de Calidad del Aire de Granada: Año 2009. Grupo de Física de la Atmósfera, Centro Andaluz del Medio Ambiente, Universidad de Granada, 2010.
[30] Cultrone G, Arizzi A, Sebastian E, Rodriguez-Navarro C. Sulfation of calcitic and dolomitic lime mortars in the presence of diesel particulate matter. Environ Geol 2008; 56:741-52.
[31] Sabbioni C, Zappia G, Ghedini N, Gobbi G, Favoni O. Black crusts on ancient mortars. Atmos Environ 1998; 32:215-23.
[32] Martinez-Ramirez S, Puertas F, Blanco-Varela MT, Thompson GE. Studies on degradation of lime mortars in atmospheric simulation chambers. Cem Concr Res 1997; 27(5):777-84.
[33] Zappia G, Sabbioni C, Pauri MG. Mortar damage due to airborne sulphur compounds in a simulation chamber. Mater Struct 1994; 27:469-73.
[34] Hossain KMA, Lachemi M, Sahmaran M. Performance of cementitious building renders incorporating natural and industrial pozzolans under aggressive airborne marine salts. Cem Concr Compos 2009; 31:358-68.

[35] Ruiz-Agudo E, Lubelli B, Sawdy A, van Hees R, Price C, Rodriguez-Navarro C. An integrated methodology for salt damage assessment and remediation: the case of San Jerónimo Monastery (Granada, Spain). Environ Earth Sci 2011; DOI 10.1007/s12665-010-0661-9.
[36] Kontozova-Deutscha V, Cardell C, Urosevic M, Ruiz Agudo E, Deutsch F, Van Grieken R. Characterization of indoor and outdoor atmospheric pollutants impacting architectural monuments: the case of San Jerónimo Monastery (Granada, Spain). Environ Earth Sci 2011; DOI 10.1007/s12665-010-0657-5.
[37] UNE-EN 459-1. Cales para la construcción. Parte 1: Definiciones, especificaciones y criterios de conformidad. AENOR, Madrid; 2002.
[38] ASTM C618-08. Standard Specification for Coal Fly Ash and Raw or Calcined Natural Pozzolan for Use in Concrete. Annual Book of ASTM Standard, 2008; 4.02.
[39] UNE EN 1015-2. Métodos de ensayo de los morteros para albañilería. Parte 2: Toma de muestra total de morteros y preparación de los morteros para ensayo. AENOR, Madrid; 1999.
[40] Cazalla O. Morteros de cal. Aplicación en el Patrimonio Histórico. Ph.D. Thesis. Universidad de Granada; 2002.
[41] RILEM. Recommended tests to measure the deterioration of stone and to assess the effectiveness of treatment methods (V-1a, V-1b, V-2). Mater Struct 1980; 75:175–253.
[42] CEN, EN 12370. Natural stone test methods—determination of resistance to salt crystallisation. Bruxelles; 1999.
[43] Martín Ramos J.D. XPowder. A software package for powder X-ray diffraction analysis. Lgl. Dep. GR 1001/04; 2004.
[44] Moorehead DR. Cementation by the carbonation of hydrated lime. Cem Concr Res 1986; 16:700-8.
[45] Matschei T, Lothenbach B, Glasser FP. The role of calcium carbonate in cement hydration. Cem Concr Res 2007; 37:551-8.
[46] Cizer O. Competition between carbonation and hydration on the hardening of calcium hydroxide and calcium silicate binders. PhD Thesis. Katholieke Universiteit Leuven; 2009.
[47] Cultrone G, Sebastián E, Ortega Huertas M. Forced and natural carbonation of lime-based mortars with and without additives: mineralogical and textural changes. Cem Concr Res 2005; 35:2278-89.
[48] Menéndez E, de Frutos J, Andrade C. Internal deterioration of mortars in freeze-thawing: non-destructive evaluation by means of electrical impedance. Adv Mater Res 2009; 68:1-11.
[49] Arizzi A, Martínez-Martínez J, Cultrone G, Benavente D. Mechanical evolution of lime mortars during the carbonation process. Key Eng Mater 2011; 465:483-6.
[50] Metha PK. Mechanism of expansion associated with ettringite formation. Cem Concr Res 1976; 3:1-6.
[51] Tsui N, Flatt RJ, Scherer GW. Crystallization damage by sodium sulfate. J Cultural Heritage 2003; 4:109-15.

[52] Bochen J, Gil S, Szwabowski J. Influence of ageing process on porosity changes of the external plasters. Cem Concr Compos 2005; 27:769-75.
[53] Bochen J. Study on the microstructure of thin-layer facade plasters of thermal insulating system during artificial weathering. Constr Build Mater 2009; 23:2559-66.

Concluding Remarks

In this part of the thesis a deeper knowledge into the performances of the mortars during hardening has been attained.

The assessment of the hydric properties has been crucial to understand more in deep the susceptibility of these materials to the decay caused by water. In particular, the study performed in *chapter IV.1* has allowed to select the most suitable binder-to-aggregate proportion in terms of hydric behaviour, which is the 1:6 one.

At the same time, the measurement of the plastic shrinkage has allowed to understand the factors that influence the volume reduction of mortars due to water evaporation, which are not only related to the lime and water contents. However, it should be born in mind that the plastic shrinkage measured on laboratory samples cannot correspond exactly to that occurring in mortars exposed to the environment. Moreover, the suction capacity of the substrate, which affects strongly the formation of fissures, is not considered in this type of measurement. Therefore, the values of shrinkage determined by means of the non-standardized device used should be merely regarded for comparative purposes.

A deep assessment of the factors affecting the durability of the four mortars has been achieved in *chapter IV.2*. By means of this study, it was also possible to select the most durable mortars among those designed in this thesis, which seemed to be M4 and M6.

4. CONCLUSIONS

4.1. General conclusions

The aim of this thesis has been to design ready-to-use rendering mortars to be employed in both ancient and modern buildings. To this end the research has tackled some of the most important aspects of the design of repair mortars:

1) the selection of mortar components such as binders, aggregates and additions that meet the requirements of compatibility and suitability;
2) the selection of the correct amounts of water and additions and lime-to-aggregate ratios to design mortars with optimum performances in both their fresh and hardened states;
3) the selection of suitable preparation, curing and testing methods to be able to characterize mortars accurately and exhaustively.

The main results and concluding remarks of this research have already been highlighted in the four sections of the previous chapter (*cf.* Results and Discussion). The general conclusions that can be drawn from these results are commented upon below.

4.1.1 Mortar components

Dolomitic lime mortars were more workable due to the higher water-retention capacity of the nanoparticles of the dolomitic lime and its plastic behaviour in suspension. Nevertheless, the use of a calcitic lime in mortars cured under dry conditions led to a higher degree of carbonation and better mechanical performances (*cf.* Section 4.1.3). These results suggest that dry hydrated calcitic lime is to be recommended in mortars that will be exposed to dry areas with low humidity. However, in practice, the performances of dolomitic mortars can be improved by humidifying the surface of the render and by keeping it wet.

The type of aggregate used influenced considerably the textural properties of mortars and their behaviour during hardening. The use of a siliceous aggregate produced brittle mortars due to a lower degree of compactness and carbonation. A calcareous aggregate, on the other hand, led to higher cohesion and mechanical strength. Furthermore, calcareous aggregate favoured the carbonation of calcitic lime, due to the similar composition of these two materials.

The use of white Portland cement in lime-based repair mortars resulted in irreversible damage when they came into contact with water and on the whole this study concludes that white Portland cement is a deleterious material for ancient masonries and should never be used for repair interventions in the same way that the classic grey one should be avoided.

The addition of metakaolin afforded a better approach to improving the quality and durability of aerial lime-based mortars. The enhancement of mechanical resistance and the effect on the pore system of the mortar, however, were influenced to a greater or lesser degree depending upon the amount of metakaolin used, and so it is important to control its

content according to the final performance required (*cf.* Section 4.1.2). The curing conditions also influenced the outcome of the use of metakaolin (*cf.* Section 4.1.3).

The inclusion of admixtures enhanced the performance of lime-based mortars considerably when fresh, especially by decreasing the water dosage and mortar density. Admixtures, however, did not modify the mineralogical and microstructural characteristics of mortars. In fact, perlite did not show its expected feeble-hydraulic behaviour, possibly because of the dry curing conditions to which the mortars were exposed (*cf.* Section 4.1.3). Cellulose derivative and polycarboxylate improved the water-retention capacity of the lime and particle dispersion respectively and consequently the reactivity of the lime towards CO_2 also increased.

4.1.2 Mortar dosages

Large quantities of kneading water were necessary in mortars composed only of lime and aggregate. This resulted in high shrinkage during drying and considerable porosity during and after hardening. Different attempts were made to reduce the water dosage, particularly by adopting non-standardized methods and using specific admixtures. The latter was definitely the best way of decreasing water content and porosity *(cf.* Section 4.1.1*)*, especially bearing in mind the small amount of total admixtures used for this purpose (2% of the total weight). In some specific situations, however, such as in summer period, the amount of water-retaining agent should be slightly increased to better counteract shrinkage.

Mortar properties showed different responses according to the amount of metakaolin used. For rendering mortars, a proportion of 10% turned out to be the most suitable since it gave rise to moderate changes in mechanical strength and porosity.

The binder-to-aggregate ratio had great influence on the hydric and mechanical behaviour of mortars: in general, those with a high lime content (weight ratios of 1:3 and 1:4) showed a higher water uptake by total absorption and capillarity and lower mechanical resistance, as was to be expected. Nevertheless, the improvement in strength reached a limit, after which any further increase in aggregate content resulted in a loss of compactness and resistance (as with a weight ratio of 1:9, for example). This inverted trend was caused by a lower cohesion at the interface between the aggregate grains and the matrix. For the same reason, higher hydraulic conductivity and permeability to water vapour, as well as higher shrinkage, were measured in mortars with a higher aggregate content (with mass ratios of 1:6 and 1:9). Furthermore, different responses to weathering were registered according to the binder-to-aggregate ratios. In view of these results, both the lowest and the highest amounts of aggregate (corresponding to weight ratios of 1:3 and 1:6) should be discarded for rendering purposes, since the former resulted in higher than acceptable porosity and water absorption and the latter gave rise to poor cohesion and significant surface decay. According to the

specific requirements established for a render (*cf.* Section 1.2.2), the mortar with a 1:6 binder-to-aggregate ratio performed the most adequately:

- The water dosage used was one of the lowest (21.5 % of the total weight), as was the open porosity (P_o~31%) and water absorption (C_a~7.95 g/min$^{1/2}$ and A~0.03 g/cm^{2}min$^{1/2}$). Permeability to water vapour was similar in all the mortars with different ratios and in this mortar it was only 0.4 lower than the highest one (K_v~2.69 g/m^{2}h).
- This mortar presented the highest mechanical resistances (R_f~1.86 MPa and R_c~3.63 MPa) without being too strong for a rendering repair mortar.
- It showed medium resistance to the damage caused by capillary salt uptake and freeze-thaw cycles and only slight surface decay due to salt deposition.
- Finally, the carbonation degree in this mortar was among the highest when exposed to the environmental conditions settled upon during the weathering study.

4.1.3 Preparation, curing and testing methods

All the standards for cement mortars were lacking when applied to aerial lime-based mortars. One of the most controversial problems that had to be addressed during the research for this thesis concerned the way of choosing the correct water dosage for making the mortar. In particular, the consistency values set out in the UNE EN1015-3:1999 standard turned out to be unsuitable for the lime-based mortars designed, for which we established a much narrower range of flowability of between about 120 and 150 mm.

The dry curing conditions selected in this thesis strongly influenced the final quality of the mortar. Dolomitic lime mortars showed considerable plastic shrinkage when cured under these conditions, with the consequence that their final quality was irreversibly worsened. For the same reason, metakaolin did not hydrate completely, although this proved to benefit the mortars' properties since it induced only a slight increase in their mechanical strengths. Similarly, perlite did not show its potential hydraulic character.

The ultrasound technique turned to be more useful for the characterization of mortars than was expected. Ultrasound did in fact play a part not only in measuring the dynamic-mechanical parameters of mortars, but also provided an additional tool for characterizing the texture of mortars during hardening; similar results were obtained by means of commonly used destructive analytical techniques, such as X-ray diffraction, electron microscopy and mercury intrusion porosimetry, and non-destructive ultrasonic measurements. Furthermore, studying mortars by means of ultrasound has been crucial to understand the importance of the water dosage for the microstructure of lime mortars.

The design of new laboratory tests to investigate the durability of rendering mortars contributed to a deeper understanding of the

mechanisms of decay occurring in these types of mortar. Due to the particular environmental conditions, weathering agents and sample sizes allowed for, these methods can be taken as a reference to assess the longevity of mortars intended for application in other areas with similar or milder climates. Moreover, the results of this study may serve to facilitate the choice of the correct amounts of aggregate according to the main role of the mortar in the masonry structure.

4.2 Original contributions

This thesis represents a step forward in research into lime-based mortars and at the same time contributes to the survival of our architectural heritage by describing suitable new repair mortars. The originality of this research lies in its attempt to provide a solution for both the current lack of compatible and durable mortars, which are required to avoid the damage caused to our architectural heritage by the frequent use of unsuitable repair materials, and the high demand for ready-to-use mortars due to low manufacturing costs and times and the ease of use of mortars produced and marketed on an industrial scale. This thesis has successfully tackled the difficult task of ensuring a beneficial combination between restoration and industrial requirements and the results achieved represent a crucial starting point for other similar research.

4.3 Future perspective works

The possibilities for further research are manifold: in particular, the guidelines proposed in this research for the design of repair mortars should be tested on a broader basis. For example:

- Moist curing conditions should be adopted in order to investigate their influence on the final performance of mortars. Under these conditions the degree of shrinkage of dolomitic lime mortars, the outcome of the hydration and carbonation processes in lime-metakaolin blended mortars and the hydraulic character of perlite should be studied to corroborate the conclusions arrived at here.
- Natural hydraulic limes should also be taken into consideration in the design of repair mortars, especially those that are to be applied in high-moist areas.
- To improve the quality of mortars still further, more types of admixtures should be tested, paying special attention to natural organic and inorganic substances such as starch, Nopal juice and mucilage, fibres and diatomaceous earth among others.
- Applying the testing methods to a wider variety of mortars would lead to a deeper knowledge of their limits and, on this basis, new standards specific for aerial lime-based mortars could be developed.

- The empirical equations obtained to assess mortar porosity and its degree of carbonation should be corroborated by developing a micro-mechanical model based on ultrasound data.

Finally, a long-term study *in* situ of the rendering mortars designed in this thesis would complete this research and add to our knowledge of the quality and durability of the renders in question.

APPENDIXES

Appendix I

Admixtures specifications

Rheomix GT205 MA® (BASF Construction. Chemicals España, S.L.)									
Density (at 20 ºC, g/cm^3)				**pH**			**Cl$^-$**		
0.690 – 0.790				8 ± 1			< 0.1%		
Otaperl® (Otavi Iberica SLu.)									
Real density (g/cm^3)	**Bulk density** (g/cm^3)	**pH**	***K*** (W/mºK)	**Chemical composition** (%)					
				SiO_2	Al_2O_3	Na_2O_3	K_2O	MgO	Fe_2O_3
~2.2	0.05±0.01	~7	0.045	74.0±2.0	12.8±0.8	3.0±0.7	4.1±0.8	0.2±0.1	0.7±0.2
Tylose® MHS 10012 P6 (SE Tylose GmbH&CO.KG)									
Viscosity (at 20 ºC, in %)				**Particle size**					**Cl$^-$**
				<0.100 mm		<0.063 mm			
1.9				85 %		60 %			1.5%

Appendix II

A study of the behaviour of lime mortars applied as rendering materials in the Vargas Palace in Granada (Spain)

Application of mortars and long-term natural ageing

The rendering mortars designed at the end of this thesis were applied in the "Vargas Palace" (16th century, Granada). Six mortars panels were applied. Four panels were prepared with the same mortar mix in both the first and the second layer. The other two panels were prepared using a higher content of aggregate in the first layer and a higher content of lime in the second layer. The application was performed following the steps indicated below and shown in Fig. 1:
a) the wall was brushed to eliminate the looser and weaker parts of the surface and to leave it more compact and smoother (Fig. 1a);
b) then it was wetted with water to eliminate rests of mortars and powder (Fig. 1b);
c) whilst the wall was drying, the dry mortar was mixed with water to prepare a mortar mixture with a workable consistence (Fig. 1c);
d) the first layer of render was applied (Fig. 1d) and then spread with a plastic trowel (Fig. 1e).
The use of a metal trowel was avoided since this material leaves the surface of the render too smooth and it attracts the water towards the exterior.
This first layer of the render had the only function of filling voids and irregularities of the wall surface. For this reason, this layer did not have a specific thickness.
e) The second layer, with a thickness of 0.5±0.2 cm, was applied with a steel trowel (Fig. 1f). The surface was left smooth until it started drying;
f) finally, the surface was trowelled with a sponge trowel (Fig. 1g). This operation had the function of taking the aggregate grains out (on the surface) and thus, reducing the shrinkage in the surface. Moreover, by trowelling, the surface becomes more porous and carbonation is favoured within the mortar.

Characteristics of the mortars during mixing and application

M3 mortar showed high plasticity and workability. However, many shrinkage fissures (in form of X) formed after only 15 minutes since the application of the first rendering layer.
M4 and M6 were stickier and less workable than M3 but they presented less shrinkage.
M9 was a workable mortar but it showed less adhesion, due to the least lime content.

The mortars changes are followed by visual inspection and by studying the textural and mineralogical characteristics of pieces of samples at different intervals of time. The environmental conditions (T and RH) are controlled by means of a data logger EL-USB-LCD-2 (Omni-Instruments).

Figure 1 *Steps of the application of the rendering mortars in the Vargas Palace (Granada): brushing (a) and wetting (b) of the wall surface; mortar mixing (c); application of the mortar (d); spreading of the first layer (e); application and spreading of the second layer (f); trowelling of the surface (g).*

List of publications

International journal articles:

Cultrone G., Arizzi A., Sebastián E., Rodriguez-Navarro C. Sulfation of calcitic and dolomitic lime mortars in the presence of diesel particulate matter. *Environmental Geology*, 56, 741-752 (2008).

Arizzi A., Martínez Martínez J., Cultrone G., Benavente D. Mechanical evolution of lime mortars during the carbonation process. *Key Engineering Materials*, 465; 483 (2011).

Arizzi, A., Viles H., Cultrone G. Experimental testing of the durability of lime mortars used for rendering purposes. *Construction and Building Materials*, 28 (2012) 807-818.

Arizzi, A., Cultrone G. Aerial lime-based mortars blended with a pozzolanic additive and different admixtures: a mineralogical, textural and physical-mechanical study. *Construction and Building Materials*, 31 (2012) 135-143.

Arizzi, A., Hendrickx, R., Cultrone, G., & Van Balen, K. Differences in the rheological properties of calcitic and dolomitic lime slurries: influence of particle characteristics and practical implications in lime-based mortar manufacturing. *Materiales de Construcción*, 60(0): DOI: 10.3989/mc.2011.00311, (2012).

International book chapters:

Arizzi A., Cultrone G. Negative effects of the use of white Portland cement as additive to aerial lime mortars set at atmospheric conditions: a chemical, mineralogical and physical-mechanical investigation. Brick and Mortar Research, Ed. S.M. Rivera and A.L. Pena Diaz. ISBN: 978-1-61942-927-7 (2012).

Conference proceedings:

Arizzi A., Belfiore C.M., Cultrone G., Rodriguez-Navarro C., Sebastian Pardo E., Triscari M. Citric acid as salts nucleation inhibitor: new hints for the prevention and conservation of calcarenites and a potential application to Barocco's monuments. *Epitome* (Geoitalia, Rimini, Italia - FIST). 2, D09B- 25 (2007).

Arizzi A., Cultrone G., Sebastián E. Evolución de la carbonatación de morteros de cal calcítica y dolomítica. *X Congreso Internacional Rehabilitación del Patrimonio Arquitectónico y Edificación CICOP,* Sevilla (Spain). I, pp. 3-8 (2008).

Arizzi A., Cultrone G., Sebastián E. Influence of the aggregate composition on textural properties of calcitic lime mortars. *1st Historical Mortars Conference*, Lisbon (Portugal). p.115 (2008).

Arizzi A., Cultrone G., Sebastián E. Estudio de las fases minerales de neoformación en morteros de cal aérea tras la adición de metacaolín y sulfoaluminato cálcico. SEM, Salamanca (Spain). *Macla*, 11; 29-30 (2009).

Arizzi A., Martínez-Martínez J., Cultrone G., Benavente D. Mechanical evolution of lime mortars during the carbonation process. *6th International Conference on Materials Structure and Micromechanics of Fracture*, Brno (Czech Republic) (2010).

Arizzi A., Hendrickx R., Cultrone G., Van Balen K. Differences in the flow behaviour of calcitic and dolomitic lime slurries: influence of particles characteristics. *International Soft Matter Conference*, Granada (Spain). p.262 (2010).

Arizzi A., Cultrone G. Comparison of different methods to measure the packing density of fresh mortars. *2nd Historic Mortars Conference HMC10*, Prague (Czech Republic). pp. 863-870 (2010).

Luque A., Vázquez P., Arizzi A., Cultrone G., Sebastián E., Alonso J. Cambios de permeabilidad observados en mármoles tratados térmicamente, SEM, Madrid (Spain). *Macla*, 13; pp. 139-140 (2010).

Romero J., Ramos J., Arizzi A., Sebastian E. Restauración-Rehabilitación y Puesta en Valor de la Madraza Yusufiyya (Granada, España). *X Congreso Internacional Rehabilitación del Patrimonio Arquitectónico y Edificación CICOP,* Santiago de Chile (Chile) (2010).

Kudlacz K., Ruiz-Agudo E., Arizzi A., Rodriguez-Navarro A., C. Rodriguez-Navarro A. The mechanism of thermal decomposition of dolomite and its implications in pyrotechnology: new insights from 2D-XRD and TEM analyses. *IMA,* Budapest (Hungary) (2010).

Arizzi A., Cultrone G. Properties of calcitic and dolomitic lime mortars used for rendering purposes. *EGU General Assembly*, Vienna (Austria) (2011).

Arizzi A., Cultrone G. Testing the hardened properties of mortars prepared according to the Wet Packing Method: is this model truly successful? *EGU General Assembly*, Vienna (Austria) (2011).